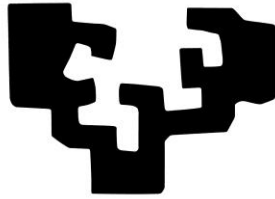


eman ta zabal zazu



Universidad  
del País Vasco

Euskal Herriko  
Unibertsitatea

# **Modern advances in glass-coated microwires: A significant distinction as a soft magnet**

By

**Ahmed Talaat**

Departamento de Física de Materiales

Facultad de Química

San Sebastián, **2015**



## Overview

The introduction of a metallic glass (or ferromagnetic amorphous metal) covered by a glass sheath have turned out to be a promising new soft magnetic material with outstanding magnetic properties. These are the so-called "Glass-coated microwires" which are known as a composite material made of a metallic glassy nucleus covered by a glass-coating layer. One of the most appealing features of these microwires is their fabrication technique and the simultaneous fast solidification of a composite microwire consisting of ferromagnetic metallic nucleus and glass coating quenched from the molten alloy. Therefore, considerable differences between thermal expansion coefficients of either the glass or/and the metal result in appearance of large internal stresses. In addition, this fabrication technique allows considerable wire diameter reduction that is one of the most interesting features for magnetic sensors applications.

In the absence of magnetocrystalline anisotropy, the magnetic properties of an amorphous glass-coated microwire are predominantly determined by the magnetoelastic coupling energy between the spontaneous magnetization (local magnetic moments) and internal stresses. Consequently, the main attention to engineer the magnetic properties of glass-coated microwires is oriented to the magnetoelastic anisotropy,  $K_{me}$ . Herein, the main possibilities to tailor magnetic properties of amorphous microwires are either the internal stresses or a proper selection of the chemical composition of the metallic nucleus (the magnetostriction).

This dissertation attempts to demonstrate the progresses of magnetically soft glass-coated microwires from three enclosed perspectives:

- Controlling the internal stress strengths through the modification of the ratio between the metallic nucleus diameter and the glass thickness.
- Achieving nanocrystalline state with two-phases of nanoscaled crystallites embedded in an amorphous matrix.
- Controlling the heat treatment conditions prior to any participation of crystalline phases, i.e. relaxing the internal stresses frozen-in post the fabrication process.

## Part I

Fundamentals

- Chapter 1:** Introduction & literature survey
- Chapter 2:** Glass-coated microwires: A research tool
- Chapter 3:** Glass-coated microwires: Technological applications
- Chapter 4:** Experimental techniques

## Part II

Results & discussion

- Chapter 1:** Optimized giant magneto impedance effect (GMI) in thin microwires composed of Finemet-like alloys
- Chapter 2:** Nanocrystalline Hitperm alloys: A structural investigation and magnetization process
- Chapter 3:** Engineering of Co-based amorphous microwires by annealing
- Chapter 4:** Magnetic hyperthermia of Fe-based alloys
- Chapter 5:** Conclusions

## References

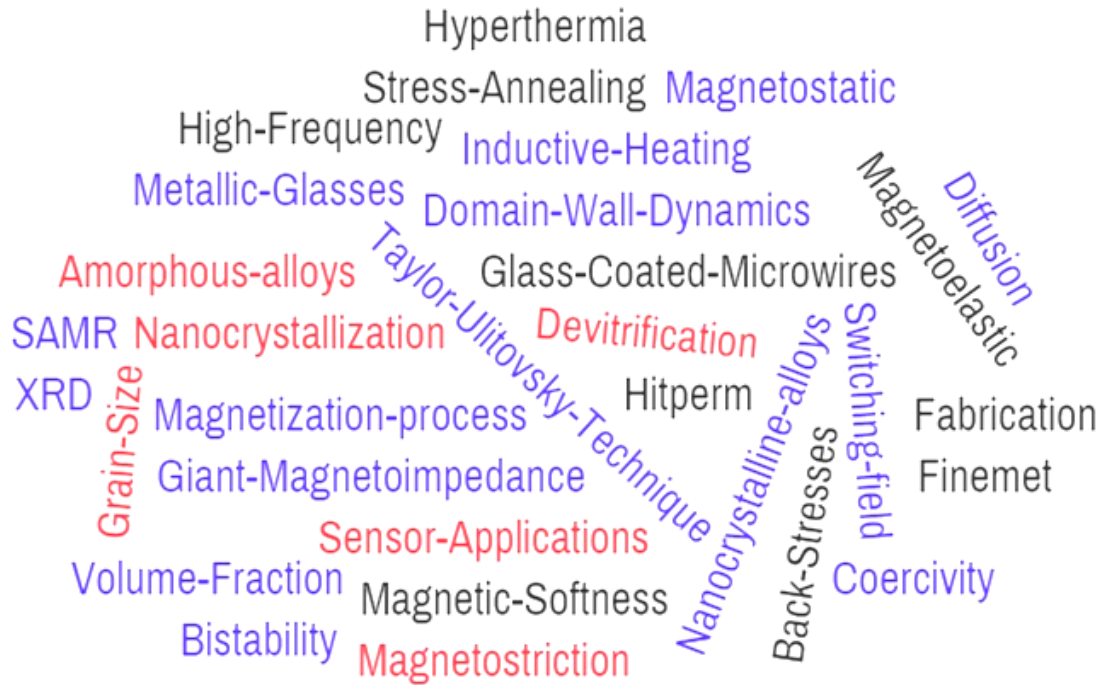
As shown in above-drawn diagram, the dissertation encompasses two main parts: part I, fundamentals, and part II, results and discussion. Each part splits into several chapters.

Chapter 1 deals with the big picture of soft magnetic materials as well as a historical perspective about amorphous metallic glassy alloys and first instances of fabrication of glass-coated microwires. Chapter 2 sets the basic magnetic and structural properties of glass-coated microwires under a magnifying glass in order to understand the main origin of their magnetic softness. Chapter 3 looks into the most interesting areas of the technological applications of these composite microwires. Further, in the same chapter, some limitations will be addressed and more insights for this current research motivations will be given. The last chapter of part I, chapter 4, provides a description of different experimental techniques and procedures carried out in this work.

Through part II, we systematically describe our experimental results beyond 4 chapters. Chapter 1 involves an optimization of giant magnetoimpedance effect (GMI) of thin *Finemet*-like glass-coated microwires by means of nanocrystallization. Chapter 2 continues with the nanocrystallization phenomena in new *Hitperm*-like glass-coated microwires and their magnetization processes. Chapter 3 revolves around engineering the magnetic properties of amorphous Co-based glass-coated microwires by annealing. Chapter 4 includes the first

investigation of Fe-based microwires for advanced magnetic hyperthermia treatment. Finally, chapter 5 resumes up and concludes the major findings of this dissertation.

## Keywords





# Contents

<b>Part I: Fundamentals</b> .....	<b>1-68</b>
<b>Chapter 1: Introduction &amp; literature survey</b> .....	<b>3-11</b>
1.1 Opening remarks .....	4
1.2 Amorphous metallic glass alloys.....	5
1.3 Early development: A historical theme .....	7
<b>Chapter 2: Glass-coated microwires: A research tool</b> .....	<b>13-32</b>
2.1 Glass-coated microwires as a research tool.....	14
2.2 Internal and residual stress distribution of glass-coated microwires.....	15
2.3 Magnetic characterizations of glass-coated microwires.....	16
2.3.1 Local and exchange anisotropy .....	16
2.3.2 Magnetoelastic/shape anisotropy and magnetostriction .....	18
2.3.3 Domain structure and hysteresis loops .....	19
2.3.4 Magnetic bistability and Barkhausen effect .....	21
2.3.5 Structural relaxation and induced magnetic anisotropies .....	22
2.4 Nanocrystalline glass-coated microwires and crystallization phenomena .....	25
2.4.1 On the origin of magnetic softness .....	26
2.4.2 Alloy design and microstructural consequences.....	28
2.4.3 Methods of preparation: A final word .....	31
<b>Chapter 3: Glass-coated microwires: Technological applications</b> .....	<b>33-46</b>
3.1 Glass-coated microwires for technological interest .....	34
3.2 Fundamental aspects of GMI.....	34
3.2.1 Early advances and research growth.....	34
3.2.2 Major principles.....	35
3.2.3 GMI in glass-coated microwires and sensing technologies.....	38
3.3 Oriented applications based on magnetic bistability of glass-coated microwires .....	41
3.4 Simplified model of DW in glass-coated microwires .....	43
3.5 Closing remarks.....	45
<b>Chapter 4: Experimental technique</b> .....	<b>47-68</b>
4.1 Fabrication technique of glass-coated microwires .....	48
4.2 Microstructural characterization techniques.....	51
4.2.1 Scanning Electron Microscopy (SEM).....	51
4.2.2 Imaging with Axio Scope A1 microscopy.....	52
4.2.3 X-ray diffraction .....	53
4.2.4 Bragg's law .....	53
4.2.5 Powder X-ray diffraction (XRD).....	55
4.3 Magnetic characterization techniques .....	56
4.3.1 Hysteresis loops .....	56
4.3.2 The induction flux-metric method for hysteresis loops measurements .....	58
4.3.3 Annealing processes .....	59
4.3.4 Giant magneto-impedance (GMI) measurements.....	61
4.3.5 Vector network analyzer (VNA) .....	62
4.3.6 Domain wall (DW) propagation measurements .....	63
4.3.7 Small angle magnetization rotation (SAMR) for magnetostriction measurements .....	65
4.3.8 Magnetic hyperthermia measurements .....	66

<b>Part II: Results and discussion</b> .....	<b>69-136</b>
<b>Chapter 1: Optimized giant magnetoimpedance effect (GMI) in thin microwires composed of Finemet-like alloys</b> .....	<b>71-86</b>
1.1 Finemet alloys .....	72
1.2 Alloy chemical compositions and microwires dimension .....	72
1.3 Microstructure investigation .....	74
1.4 Beyond the magnetic properties .....	79
1.5 Giant magnetoimpedance (GMI) .....	81
1.6 Concluding remarks .....	85
1.7 Further reading: Publications related to this chapter .....	86
<b>Chapter 2: Nanocrystalline Hitperm alloys: A structural investigation and magnetization process</b> .....	<b>87-102</b>
2.1 Hitperm alloys .....	88
2.2 Samples preparation and microstructure investigation .....	88
2.3 Magnetic characteristics .....	94
2.4 Domain wall propagation .....	99
2.5 Concluding remarks .....	101
2.6 Further reading: Publications related to this chapter .....	102
<b>Chapter 3: Engineering of Co-based amorphous microwires by annealing</b> .....	<b>103-117</b>
3.1 The main objective .....	104
3.2 As-prepared state .....	104
3.3 Engineering of magnetic properties by heat treatment .....	105
3.3.1 Conventional annealing: A manipulation between annealing time and temperature ..	105
3.3.2 Stress annealing .....	108
3.3.3 Simultaneous detection of DW and GMI in the same annealed microwire samples...	111
3.4 Concluding remarks .....	116
3.5 Further reading: Publication related to this chapter .....	116
<b>Chapter 4: Magnetic hyperthermia of Fe-based alloys</b> .....	<b>119-136</b>
4.1 Magnetic hyperthermia .....	120
4.2 Fundamental principles .....	120
4.3 Nanostructured magnetic materials for hyperthermia treatment .....	122
4.4 Influence of geometry and varying number of microwires .....	123
4.5 Heating mechanism of glass-coated microwires .....	126
4.6 Effect of microwire orientation respect to the magnetic field direction on SAR .....	131
4.7 Separation between two microwires: Role of magnetostatic anisotropy .....	133
4.8 Concluding remarks .....	135
<b>Chapter 5: Conclusions</b> .....	<b>137-141</b>
<b>References</b> .....	<b>143-163</b>
<b>Publications</b> .....	<b>164-167</b>
<b>Resume in Spanish</b> .....	<b>168-172</b>
<b>Acknowledgments</b> .....	<b>173-174</b>



# Part I

## *Fundamentals*

- 
- Chapter 1: Introduction & literature survey
  - Chapter 2: Glass-coated microwires: A research tool
  - Chapter 3: Glass-coated microwires: Technological applications
  - Chapter 4: Experimental techniques
-



# Chapter 1

## Introduction & literature survey

---

**W**e initiate this dissertation by a general overview of the big picture of soft magnetic materials and trends of their applications. Behind this picture we highlight amorphous metallic glass alloys as an important class of soft magnets. We critically discursive, where possible, a historical perspective about the discovery of amorphous metallic glasses and their breadth of progress until the so-called glass-coated microwires.

---

## 1.1 Opening remarks

Our understanding of magnetism has drastically changed over the past few decades. In our modern society, the recent technological and scientific innovation of soft magnetic materials have already led to many steps forward to decent advancements in the field of material science and applied physics. When we first begin experimenting with the basic characteristics of soft magnetic material: our choice is a trade-off between excellent magnetic properties and cost effectiveness, however, we soon found that like many other things in life, it was not quite that simple.

Soft magnetic materials are those materials that are easily magnetized and demagnetized. They typically have an intrinsic coercivity less than of  $1000 \text{ A/m}$ . They are used primarily to enhance and/or channel the flux produced by an electric current. The main parameter, often used as a figure of merit for soft magnetic materials, is the relative permeability ( $\mu_r$ ), which is a measure of how readily the material responds to the applied magnetic field. Initial permeabilities of all magnetic materials range from ( $\mu_r \approx 1.000.000$ ) [1, 2] in soft magnetic materials such as amorphous alloys down to as low as ( $\mu_r \approx 1$ ) in some of the permanent magnets. It is known that initial permeability and coercivity have in broad terms a reciprocal relationship, so that materials with high coercivity necessarily have a low initial permeability and vice versa. The other main parameters of interest are the saturation magnetization and the electrical conductivity. The highest saturation magnetization available in bulk magnetic materials is ( $\mu_0 M_s \approx 2.43 \text{ T}$ ) which is achieved in Fe-Co alloys containing 35% of cobalt. The possible values of saturation magnetization then range downward continuously to effectively zero. There has been a little progress in improving the range of saturation magnetization of materials for about hundreds years.

The types of applications for soft magnetic materials fall into two main categories: *AC* and *DC*. In *DC* applications the material is magnetized in order to perform an operation and then demagnetized at the conclusion of the operation. In *AC* applications the material will be continuously cycled from being magnetized in one direction to the other, throughout the period of operation. A high permeability will be desirable for each type of application but the significance of the other properties varies. For *DC* applications the main consideration for material selection is most likely to be the permeability. This would be the case, for example, in

shielding applications where the flux must be channeled through the material. In addition, the material is used to generate a magnetic field or to create a force then the saturation magnetization may also be significant. For AC applications the important consideration is how much energy is lost in the system as the material is cycled around its hysteresis loop. A quick guide for application of soft magnets can be found in [2, 3].

Three 3-*d* metal elements and their respective alloys are naturally magnetic: iron (Fe), cobalt (Co), and nickel (Ni). The ferromagnetic and electrical properties of these materials can be classified into two main categories: those that are structure sensitive and those are structure insensitive. Structure insensitive refers to properties not remarkably affected by small changes in gross composition, small amounts of certain defects, heat treatment or plastic deformation. Several generally accepted structure insensitive properties are the saturation magnetization  $M_s$ , and resistivity  $\rho$ . These properties are largely dependent on the composition of the particular alloy and are not changed substantially in the process of manufacturing a component from the alloy. Structure sensitive properties are those that are drastically affected by impurities, residual stress, grain size, defects, coercivity  $H_c$ , hysteresis losses, magnetic remanence  $M_r$ , and magnetic stability are all considered to be structure sensitive. Methods of controlling all aforementioned properties can be achieved throughout the manufacturing processing of the alloy and/or by the proper use of heat annealing treatment. One alloy, of course, does not suit all needs, but there are few widely used grades, which have been optimized over the years.

## 1.2 Amorphous metallic glass alloys

Amorphous metallic glasses are alloys consisting of metals and metalloid which share the properties of both metals and glasses without long-range atomic order. They have also been called glassy alloys, metallic glasses, non-crystalline alloys, or amorphous metals/alloys. They are made by a variety of techniques all of which involve the rapid solidification of an alloy constituents from the gas or liquid phases. The solidification occurs so rapidly that the atoms are frozen in their liquid configuration. This class of materials has shown extremely unique magnetic, mechanical, electrical, and corrosion behaviors which basically result from their amorphous nature, and therefore, make them very attractive candidates for lots of applications.

In general, the big picture of metallic glasses can be divided into two main portions: metal-metal alloys and metal-metalloid alloys. They are commonly presented as:  $TL_{1-x}(TE, R, M)_x$  and that is why they are typically made up of  $1-x = 60-90$  at.% of late transition metal (TL: i.e., Fe, Co, Ni) with the balance  $x$  being some combination of early transition elements (TE: i.e., Cr, Mo, Nb), rare earths (R: i.e., Gd, Tb, Sm), and metalloids (M: i.e., B, Si, C). These are the approximate compositional limitations defining the ambient temperature ferromagnetism. The presence of the metalloids is necessary to lower the melting point making it possible to quench the alloy through its glass temperature rapidly enough to form an amorphous phase. Once it made, the metalloids stabilize the amorphous phase but their presence drastically alters the magnetic, mechanical and electrical properties of the alloy by donating electrons to the  $d$ -band. These alloys, again, lack long-range atomic order and consequently exhibit: high metallic resistivity, no macroscopic magnetocrystalline anisotropy, and no microstructural discontinuities i.e. grain boundaries and defects, on which either magnetic domain walls or mechanical dislocations can be pinned. As a result, ferromagnetic metallic glasses based on  $3-d$  transition metals are generally good soft magnetic materials with both low  $DC$  hysteresis loss and high permeabilities. All these properties are of technological significance for application as soft magnets.

Though there are several excellent general reviews of metallic glasses and their technological importance, each to some extent reflects the authors' personal research interests and expertise. Due to the pace of development and breadth of research, a truly comprehensive review is probably impossible, and certainly beyond the scope of this current topic. Generally speaking, William Johnson, one of the pioneering scientists who has a prominent figure in the field of metallic glasses has been interviewed earlier with Nature on June 2015 [4]. He mainly summarized the general historical aspects of metallic glasses and gave a quick shortcut about the importance of such class of materials as well as their role in the global market. Now, with that in mind, the forthcoming section will give a quick anecdote and historical perspective about the discovery of metallic glasses and the materials' growth until the up-to-date progress of special class of metallic glasses, the so-called glass-coated microwires.

### 1.3 Early development: A historical theme

Although glass science is quite old, the history of metallic glasses and of amorphous alloys is comparatively young. Various researchers appear to have stumbled across non-crystalline metallic alloys in their research for new materials. Examples include the early observations of Brill-1930 et al. [5], the Ni-P electrodeposits of Brenner-1946 et al. [6], and the superconducting films studied by Buckel and Hilsch-1952 et al. [7]. However, it is generally accepted that until Pol Duwez began his extensive research on metastable and amorphous alloys at Cal Tech in the late 1950's [8], the intrinsic scientific interest and the technological potential of such materials were not appreciated. Duwez pointed out that small amounts of liquid alloys can be quenched rapidly enough to forestall the normal nucleation and growth processes, and therefore solid solution can be obtained. Concurrently with the discovery of Duwez, in the USSR, Miroshnichenko and Salli et al. [9] reported on the rapid solidification method for preparing an amorphous alloys produced at high cooling rates. In this technique, a droplet of liquid metal alloy is propelled on to a cold surface where it spreads into a thin film and is thus rapidly solidified.

An amorphous alloy of a controlled composition which was stable at room temperature was obtained by Klement-1960 (Duwez's group) et al. [10] throughout rapid quenching of the melt. This technique was developed with an initial intention of finding new metastable phases of metallic crystalline alloys. Nevertheless, the investigation of this new material was actively pursued by Duwez's group, by replacing a non-magnetic element of one of the amorphous alloys with a magnetic element, where they found that Pd-Fe-Si alloy shows ferromagnetism as reported by Tsuei and Duwez-1966 et al. [11]. Then a strongly magnetic amorphous alloy,  $\text{Fe}_{80}\text{P}_{13}\text{C}_7$  with soft magnetic properties of relatively low coercivity of about 240 A/m and large saturation magnetization of 0.7 T was reported by Duwez and Lin-1967 et al. [12], and Duwez-1967 et al. [13]. The main concept of these observations was to achieve a complete solid solubility in the equilibrium state as predicted by Hume-Rothery rules [14] (set of basic rules that describe the conditions under which an element could dissolve in a metal, forming a solid solution.). To explore the physics behind the equilibrium phase diagram, thermal kinetics were used to suspend the laws of thermodynamics [10]. In accordance, a successful amorphous alloys was achieved by rapid solidification.

A prodigious development in the racetrack of preparation of amorphous alloys was elaborated by Pond and Maddin et al. [15] in a series of related patents from 1958-1961 (US Patent Nos. 2825108, 2910744, and 2976590) for the preparation of continuous long lengths of ribbons (the current concept of the melt spinner technique). Thus, they opened up the possibility of large scale production and set the stage for the explosive growth of research on amorphous alloys since it was already, and hitherto, clear that these alloys could be prepared in large quantities at low cost. Later on 1976, Liebermann and Graham et al. [16] further developed the process as a continuous casting technique by this time on the drum's outer surface, producing an amorphous alloy made of Fe-Ni-P-B. This method was adopted by the Allied Chemical Corporation (now Allied Corporation) to commercially produce amorphous alloy ribbons named as *Metglas* alloys. Such alloy was successfully commercialized in the early 1980 and was used for low-loss power distribution transformers (amorphous metal transformer). *Metglas*-alloys is Fe-B base composition with some addition of either Si or C, having a Curie temperature of  $373^{\circ}\text{C}$  and a room temperature saturation magnetization of about  $1.56\text{ T}$  [17]. Concurrently with the release of *Metglas*-alloys, Miroshnichenko et al. [18] came up with a product of an amorphous alloy of the composition  $\text{Fe}_{76}\text{C}_{15.5}\text{Si}_{2.5}$  in a form of glass-coated wires with a metallic core diameter of about 1 to 3 microns covered by a Pyrex-borosilicate glass-type. Such wire has been fabricated based on the rapid quenching method of direct casting from a soften melt introduced to a glass-like tube.

Actually, the technique of producing thin microwires directly from the melt was available long time before. In particular, in 1924 Taylor et al. [19] reported on producing thin glass-coated metal filaments with only few microns in diameter. On the fabrication method, which is known as "Taylor-wire process" [20], the metal produced in microwire form is held in a glass tube, typically a borosilicate composition, which is closed at one end of about  $2\text{ mm}$  in diameter. This end of the tube is then heated by a glass flame in order to soften the glass to a temperature at which the metal part is in a liquid state and the glass can be then drawn down to produce a thin glass capillary containing a metal core. A cooling device consisting of a water-cooled metal cylinder situated immediately after the heating zone, thus the produced continues filaments are rapidly cooled down. At that time, most of the produced metallic filaments were based on non-magnetic elements, i.e. Cu, Ag, Au [20, 21]. Interest in the commercial production of microwire in the USSR was reported by Ulitovsky along about 13 years from 1951-1964 in a serious of



patents [22-24] reporting on producing glass-coated metal microwires with core diameters in the range between 2-20 microns. Various alloys including Cu, Fe, and Mn-alloys were being produced as a microwire at that time on a commercial scale for the applications in electrical industry as resistors, coils for galvanometers and related electrical devices. Consequently, by the end of 1960-s and the beginnings of 1970-s, the technological parameters for preparing glass-coated microwires were well-established as critically reviewed by Badinter et al. [21].

The first recorded instance of the Taylor-wire process being used successfully to produce amorphous filaments was given by Wiesner and Schneider in 1974 [25] after Nixdrof et al. [26] by so-called "filament-winding technique". They prepared an amorphous  $\text{Fe}_{83-x}\text{P}_{17}\text{M}_x$  alloys, where  $\text{M} = \text{Ga}, \text{Ge}$  or  $\text{As}$  and  $x = 2-8\%$ , with diameters in the range of 10-20 microns by drawing the molten alloy in a fused quartz tubes at quenching speed of about 120 *m/min*. Some structural and magnetic properties of such alloys were reported indicating that the low coercivity of these rapidly quenched alloys are not representative for the structural disorder. Subsequently, many reports of further metallic glassy alloys using the Taylor-wire method were given by Goto et al. [27]. Amorphous metallic alloys like  $\text{Fe}_{80}\text{P}_{16}\text{C}_3\text{B}_1$  filaments of about 5 microns in diameter were reported. In addition, amorphous filaments of Fe-B, Fe-Si-B, Fe-Ni, and Fe-based alloys have been also reported by Goto et al. [28, 29] with diameters range between 4-12 microns. In as much as, the Taylor-wire process likely offers an ideal method for preparing a wide variety of amorphous metallic microwires of circular cross-section, cheap raw materials and low cost fabrication scheme. A number of works have evaluated the microstructure, as well as the mechanical, electrical and magnetic properties of several microcrystalline and amorphous alloys. A good review covering wide variety of alloy's compositions produced in a form of microwires was done by Donald-1987 et al. [30]. There were, however, a further issues to be considered for these concerns, one of the main obstacles related to this method at that time, was to find a sheath materials that possess a sufficient chemical inertness towards the molten metal used, as well as having a softening temperature consistent with the melting temperature of the metal. In addition, one problem arising in this technique is the contamination of the material by the glass sheath. It was necessary to find a glass compatible with the material in terms of its chemical properties, viscosity and melting temperature.

In 1993, an equally significant method of amorphous glass-coated microwires production was reported by Hagiwara et al. [31] throughout a glass-coated melt spinning technique. He achieved most of the limitations of rapid molten alloy quenching basics proposed by Inoue et al. [32]. Inoue previously outlined some basic features affect the microwires' production [32]. Some of which are related to accomplishing high super cooling capacity of the metallic melt stream without the precipitation of any crystalline phases in the temperature range between melting and glass transition. Such conditions strongly depend on the glass-forming ability of the metallic alloys, the diameter of the melt stream, and the cooling capacity of the cooling fluid. By the melt spinning technique, it was possible to control the microwire formation, since the ability of the metallic melt stream to be broken into droplets before solidification was drastically reduced by the presence of the glass, which in turn, prevents a direct contact between the molten metal and the cooling liquid. The glass layer also ensures a smooth cylindrical shape for the melt stream. Chiriac et al. [33] reviewed in detail about the technological parameters that affect amorphous glass-coated microwires with diameters of about 30 microns. He underlined the important role of maintaining a low level of vacuum of about 50–200 Pa inside the glass type or/and filing the tube by an inert gas atmosphere (i.e. argon) to avoid any occurrence of metal oxidation. Besides this, the glass tube should be displaced with a feeding speed of 0.5-7 mm/min.

Giant strides in the 2000s have revealed a renewed upsurge interest in glass-coated microwires with unique magnetic properties. Larin et al. [34] revived the method proposed by Taylor and Ulitovsky as discussed above, reporting on a modified production technique of composite glass-coated microwires with metallic nucleus diameter ranging between 1-30 microns, and glass-coating layer ranging between 2-10 microns. The main parameters of the modified fabrication process were systematically distinguished covering overall aspects as: the casting rate of microwire and its limits, the cooling rate of the metal core, the geometrical characteristics and alloy compositions. Some features based on the generated micro-structure either metastable, amorphous or supersaturated state phases were well-addressed. In addition, mixed structures consisting of micro- and nanocrystallites embedded into the amorphous matrix were perfectly attainable by varying the critical quenching rate ( $10^4$ – $10^7$  K/s) of this modified technique. The main advantages of this method are: the repeatability of microwire properties at mass production; wide range of variation in parameters (geometrical and physical); fabrication of continuous long pieces of microwire up to few Km; enhanced corrosion resistance; good

mechanical properties; and controlling of geometrical parameters (inner core diameter and glass thickness) during the fabrication process. Afterwards, Zhukov et al. [35] has fruitfully reviewed the most technological parameters of such microwires produced by the modified method which made them very attractive ferromagnetic tiny amorphous, nanocrystalline, and granular system of metallic glasses covered by an insulating glass coating.

Indeed, the literature review is still not completely dominant, but at least this survey has summarized the main aspects since the discovery of the first metallic glasses up to the latest methodology used up-to-date in a new class of metallic glasses: glass-coated microwires production process. As was shown, the fabrication conditions have a strong influence of the generated material.

The upcoming chapter of this dissertation will be in the scope of magnetic and structural properties of glass-coated microwires as a pioneering material for scientific research.



# Chapter 2

## Glass-coated microwires: A research tool

---

**I**n this chapter, we enlarge the magnetic and structural characteristics of glass-coated microwires as an important tool of research in the field of soft magnetic materials. We discuss the basic properties of either intrinsic or extrinsic fundamentals phenomena in order to draw out a roadmap for understanding the major physical and metallurgical approaches in different compositions of glass-coated microwires.

---

## 2.1 Glass-coated microwires as a research tool

Let us first recall again what glass-coated microwires mean. They are composite materials made of a metallic glass (amorphous metal) covered by a glass-coating layer (see Fig. 2.1). The variety of dimensions as well as chemical compositions are easily obtainable by the modified Taylor-Ulitovksy fabrication technique as discussed in the previous chapter [34, 35].

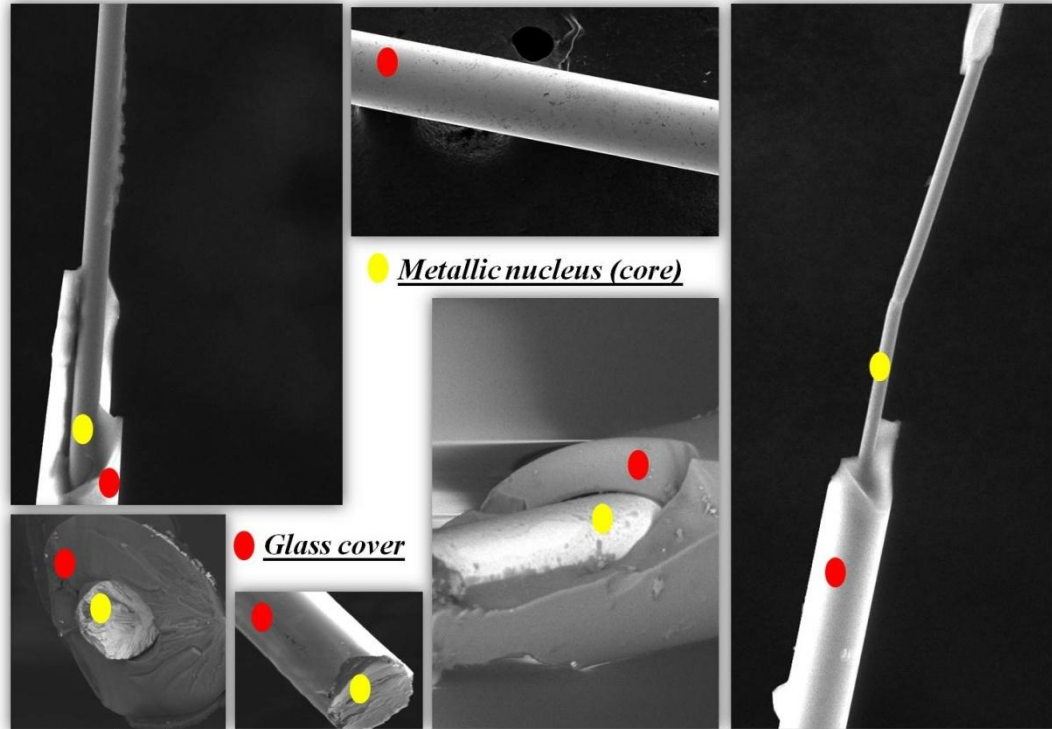


*Figure 2.1 SEM gallery of glass-coated microwire samples studied in this dissertation. The yellow spots show the metallic nucleus (core), and the red spots show the glass-coating cover.*

In accordance to the production methodology, a complex radial distribution of internal stresses with axial, radial, and circular component are often generated inside the metallic parts due to different quenching rates between the surface layer and the central region of the microwire. In addition, the difference in thermal expansion coefficients of either the glass sheath or the metallic nucleus always plays an additional role in the induced stresses of as-prepared microwires [34, 35]. Certainly, there is no shortage of disagreement within these distribution, which are of a significant influence on the magnetic properties of this category of materials giving them a combination of intrinsic characteristics never encountered before in another

metallic glasses. The next section is devoted to describing the origin of these internal stresses quenched-in glass-coated microwires that is then reflected by their magnetization process and their magnetic characterization.

## 2.2 Internal and residual stresses distribution of glass-coated microwires

The standard calculation of internal stress distributions in microwires [33, 36-39] involves two mechanism arising during the production process. First, is the glass transition of the metal that is assumed to take place simultaneously with the hardening of the glass at the glass temperature  $T_g$  [36]. The internal stresses in such case are introduced due to the solidification of metal as the solidification front proceeds radial inward to the centre of the wire. Such process creates the radial and circular stresses. Second, is the cooling of the metal-glass from  $T_g$  to room temperature. During the cooling process, axial, circumferential, and radial internal stresses are introduced due to the contraction of both materials (glass and metal) characterized by different thermal expansion coefficients obeying the following equation:

$$\sigma (T) = E_m (\alpha_g - \alpha_m) \Delta T \quad (2.1)$$

where  $E_m$  is the Young moduli of the metallic nucleus;  $\alpha_g$  and  $\alpha_m$  are the thermal expansion coefficient of glass-coating and metallic nucleus, respectively, and  $\Delta T$  the difference between molten alloy temperature and as-prepared microwire temperature.

Ordinarily speaking, it has been widely assumed in glass-coated microwires studies that axial tensile stress dominates in the center of metallic nucleus, whereas compressive axial and tensile radial stresses prevails just below the surface [33, 38, 39]. Proponents of researchers [37, 38] have also suggested that, the stretching of composite components during the fabrication process induces additional axial stresses. The resulting stress distribution is then evaluated by the superposition of all stresses originated by the progressive solidification of a microwire, and it has therefore a tensor character [37, 38]. The corresponding components of internal stress tensor can be evaluated by [38, 40]:

$$\sigma_{axial} (r) = 2vA - KT (r) \quad (2.2)$$

$$\sigma_{radial} (T) = -K (1-r^2) I(R) + A -B/r^2 \quad (2.3)$$

$$\sigma_{circular}(r) = K(1-r^2)I(r) + A - B/r^2 - KT(r) \quad (2.4)$$

being  $K = \alpha_m E_m / (1/\nu)$  where  $\nu$  is the Poisson's coefficient;  $A$  and  $B$  are integrating parameters determined by boundary conditions.

We notice here that axial stresses are linear function of the distance from wire centre. While the evolution of radial and circumferential stresses strongly depends on integrating parameters  $A$  and  $B$  determined by many factors: specifically the radius of metallic core (known as  $d$ ), the total diameters of the wire geometry (known as  $D$ ), and the ratio between the metallic core and glass thickness (known as  $\rho$  and is given by  $\rho = d/D$ ). The estimated values of internal stresses arising from the difference in thermal expansion coefficients of metallic nucleus and glass coating are in the order of 100-1000 MPa [39, 41] depending strongly on the ratio between the glass coating thickness and metallic core diameter,  $\rho$ . The latter increases with increasing the glass coating thickness. Such large internal stresses give rise to drastic change of the shape anisotropy-magnetoelastic anisotropy,  $K_{me}$ , even for small changes in the glass-coating thickness at fixed metallic core diameter as will be elucidated the forthcoming section.

## 2.3 Magnetic characteristics of glass-coated microwires

### 2.3.1 Local and exchange anisotropy

Before considering the anisotropic properties of glass-coated microwires, it is important to note that there are some fundamental questions related to the existence of the magnetic ordering in ferromagnetic materials. As a matter of fact, the ferromagnetic interactions of a magnetic material can be coherently considered as a ferromagnetic structure as predicted by Gubanov et al. [42]. However, the origin of magnetic anisotropy in structurally disordered materials is unclear. Magnetic moments tend to arrange their orientations parallel to each other via exchange interactions: thus they do align along a magnetic easy axis which is in the same direction at every point in the material. For all that, if the easy axis orientation fluctuates from site to site, a conflict between ferromagnetic coupling and anisotropy will be significant. As long as we imagine the lattice periodicity, a ferromagnetic structure is a consequence of ferromagnetic exchange interactions, therefore, the strength of the anisotropy is being irrelevant. In this situation we are assuming a major simplification, namely: the direction of the easy axis is uniform throughout the



sample. With this in mind, we present crucial questions related to the influence of an amorphous structure on the magnetic order.

Regarding to the magnetic ordering in an amorphous materials, it is assumed by most of researchers that it determines mostly by two anisotropies contributions: exchange and local anisotropy [43-45]. The exchange contribution arises from the electron-electron correlations. The mechanism of the electrostatic interactions between electrons has no relation to structural order and is to be only sensitive to overlapping of the electron wave functions. With respect to magnetic anisotropy is also originated by the interaction of the local electrical field with spin orientation, through the spin-orbit coupling. Therefore, magnetic anisotropy is, in fact, a local concept. Nevertheless, the structural configuration of magnetic solids exerts an important influence on the macroscopic manifestation of the local anisotropy. As a consequence, when the local axes fluctuate in orientation owing to the structural fluctuation (in amorphous or nanocrystalline materials as examples), the calculations of the resultant macroscopic anisotropy becomes quite difficult. In the case of amorphous alloys the usual approach when a magnetic order connected to a lattice periodicity is not applicable. The structure of amorphous materials should be considered as similar to the liquid, because in the first instance, the crystallization process can not develop because of high quenching rate of the liquid. Therefore these magnetic materials can be defined as solids in which the orientation of local symmetry axes fluctuate with a typical correlation length  $l = 1 \text{ nm}$ . The local structure can be characterized by few local configurations with icosahedral, octahedral, and trigonal symmetry. These structure units have randomly distributed orientation. The local magnetic anisotropy would be larger in these units with lower symmetry. It is remarkable that in these types of structures the correlation length,  $l$ , of such fluctuation is typically corresponds to the correlation length of the structure and ranges from  $1 \text{ nm}$  (amorphous) to  $10\text{-}20 \text{ nm}$  (nanocrystalline) and  $1 \text{ mm}$  (polycrystalline).

Fluctuations in the inter-atomic distances associated with the amorphous structure should also contribute to some degree of randomness in the magnetic interactions of the magnetic moments. In addition, such randomness is expected not to affect the magnetic behavior qualitatively [45-47]. Moreover, random distribution of the orientation of the easy axis drastically affects to the magnetic properties. Random anisotropy model developed by Alben et

al. [48] provides a successfully explanation that how the correlation length,  $l$ , exerts a relevant influence on the magnetic structure.

### 2.3.2 Magnetoelastic/shape anisotropy and magnetostriction

The prominent consequences of structural disorder and the no long-range order of amorphous alloys (glass-coated microwires as example), is that likely there is no magnetocrystalline anisotropy. For this reason, the main source of magnetic anisotropy appears in the interaction of local magnetic moments with applied mechanical stress induced during the microwire's production by drawing, quenching as well as due to different thermal expansion coefficients of metallic nucleus and glass-coating as mentioned above. This shape magnetoelastic anisotropy is regulated by:

$$K_{me} \approx 3/2 \lambda_s \sigma_{internal} \quad (2.5)$$

where is  $\lambda_s$  the saturation magnetostriction coefficient, and  $\sigma_i$  is the internal stresses induced during the fabrication process.

The magnetostriction depends not only on the chemical composition [49, 50] but also on structural relaxation process [51]; nanocrystallization [51, 52]; and external applied stresses [52, 53]. In all these cases the observed changes in magnetostriction constant are of an order of about  $10^{-6}$ , therefore glass-coated microwires are considered as low magnetostrictive materials. Herein, the sign and magnitude of magnetostriction coefficient determines the type of either the domain structure or the overall hysteresis loop character of glass-coated microwires. In addition, in low magnetostrictive compositions, the stress dependence of magnetostriction either applied or internal can be relevant [54, 55]. The dependence of the magnetostriction on stress is expressed as:

$$\lambda_s(\sigma) = \lambda_s(0) - B\sigma \quad (2.6)$$

where  $\lambda_s(\sigma)$  is the magnetostriction constant under stress;  $\lambda_s(0)$  is the zero-stress magnetostriction constant;  $B$  is a positive coefficient of order  $10^{-10} MPa$ , and  $\sigma$  stresses. This change of the magnetostriction can be associated with both either applied,  $\sigma_{applied}$ , or/and internal,  $\sigma_{internal}$ , stresses ( $\sigma_{total} = \sigma_{applied} + \sigma_{internal}$ ). In accordance, for the low-magnetostrictive

compositions (with  $\lambda_s(0) \approx 10^{-7}$ ) and internal stresses of the order of 1000 MPa, the second term of eq. 2.6 is almost of the same order as the first one. Correspondingly, the magnetostriction is one of the key factors to tune magnetic properties of glass-coated microwires as well as to bring out unexpected drastic changes of magnetic responses for the same alloy compositions but with different dimensional parameters.

Given the current high debate with regard to the magnetostriction, it is worth underlying that glass-coated microwires can be classified into three main groups [34, 56]: microwires with negative magnetostriction (i.e. Co-based alloys), microwires with positive magnetostriction (i.e. Fe-based alloys), and microwires with zero or small negative magnetostriction (i.e. Fe Co-based alloys). Evidences in support of these features will be systematically discussed in reach of the upcoming lines.

### 2.3.3 Domain structures and hysteresis loops

The domain structure of glass-coated microwires is always determined as a combination of magnetostriction value and internal stresses distribution during the fabrication process. These contributions result in different domain structures, likely based on the sign of magnetostriction constant as we described in the foregoing section. In a similar way, different hysteresis behaviors will vary for each certain case as will be demonstrated below.

For amorphous Co-based glass-coated microwires with negative magnetostriction typically in the range of ( $\lambda_s \approx -2$  or  $-3 \times 10^{-6}$ ) the easy axis of these microwires is found to circular [57]. As a consequence, they are characterized by a domain structure consisting of circular domains as was directly observed for thick wires [58] (see Fig. 2.2- upper/right). Magnetization process of these Co-based microwires are in due an easy axis direction perpendicular to the wire axis, therefore leading to an alignment of the magnetic moments in the direction which is perpendicular (circumferential) to the wire axis running through reversible rotation of magnetic moments inside domains. As a result, only small hysteresis is observed when an axial magnetic field is applied (Fig. 2.2- upper/left).

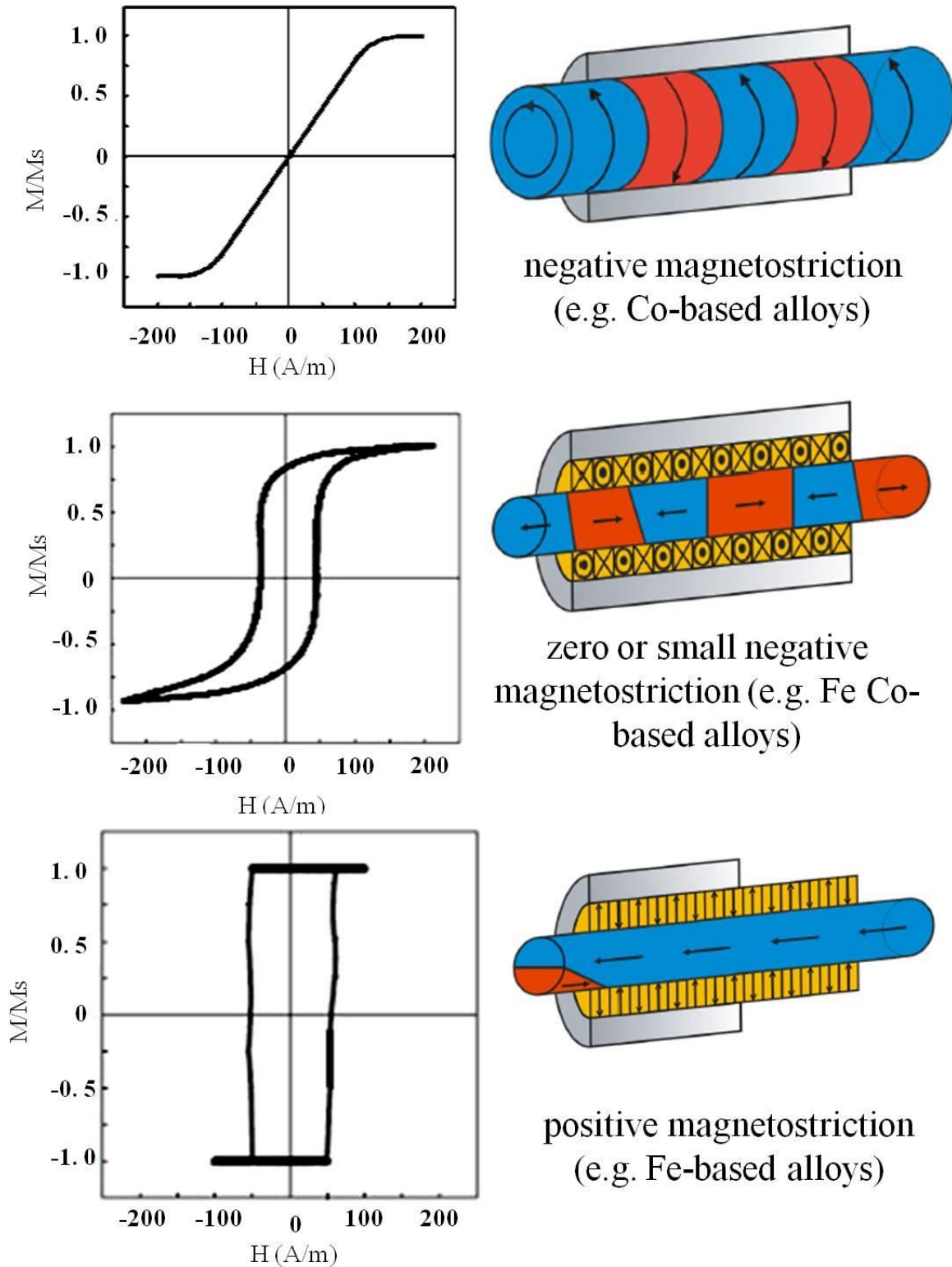


*Figure 2.2* Typical hysteresis loops of glass-coated microwires with negative, nearly zero, and positive magnetostriction-left sides (updated from [34]). Right sides corresponding schematic pictures of the domain structure of each value of magnetostriction (courtesy of Varga [56]).

For amorphous Co-Fe-based (3-8 at.% of Fe) glass-coated microwires with zero or low negative magnetostriction typically in the range of ( $\lambda_s \approx 1 \times 10^{-7}$ ), the domain structure of such microwires is characterized by circular domains just below the surface of metallic nucleus and axial domain structure in the center of the wire (Fig. 2.2- middle/right), as a result of small circular magnetoelastic anisotropy [59]. The latter leads to a compensation of induced anisotropies of either the magnetostatic or elastic anisotropy. Therefore, the hysteresis loop exhibits a *s*-like shape very low value of coercivity and high initial permeability (see Fig. 2.2- middle/left).

In the case of Fe-based glass-coated microwires with positive magnetostriction typically in the range of ( $\lambda_s \approx 2$  or  $3 \times 10^{-5}$ ), their domain structure consists of large single domain in the center of metallic nucleus that is covered by a radial domain structure (see Fig. 2.2- lower/right). In addition to small closure domains appear at the end of the wire in order to decrease the stray fields [56]. As a result of this peculiar domain structure, a well-defined shape anisotropy governs a perfectly rectangular hysteresis loop (Fig. 2.2- lower/left) where the magnetization process runs through two stable remnant states by depinning and subsequent propagation of closure domain along the entire microwire in a single large Barkhausen jump. The latter also is known as magnetic bistability which will be the case-study of the next section.

### 2.3.4 Magnetic bistability and Barkhausen effect

One of the most distinctive behavior of Fe-based glass-coated microwires relies on their spontaneous observation of magnetic bistability, characterized by single and Large Barkhausen Jump (LBJ) as a result of magnetization reversal runs in one single domain exists inside the microwire's inner core [60, 61]. Such phenomenon of square shaped hysteresis loop and LBJ take place under two main configurations. One is the amplitude of applied magnetic field, while the second contribution is the wire length.

The specific value of magnetic field for detection LBJ, is known as "The switching field-*H<sub>s</sub>*" below this field is not possible to reverse the magnetization, neither obtain rectangular hysteresis loop. Switching field of glass-coated microwires found to be strongly dependent on either the magnetoelastic anisotropy  $K_{me}$ , or the ratio between the glass coating thickness and metallic core diameter,  $\rho$  [61]. The rectangular hysteresis loop is interpreted in terms of nucleation or

depinning of the reversed domains inside internal single domain of Fe-based microwire and the consequent domain wall propagation [62] as well as the domain wall energy [56, 63].

On the other hand, the necessary critical length  $L_c$ , for obtaining magnetic bistability is a function of saturation magnetization, magnetoelastic energy, domain structure, and magnetostatic energy [60, 64]. The magnetostatic energy depends on the demagnetizing field,  $H_d$ , expressed as:

$$H_d = NM_s \quad (2.7)$$

where  $N$  is the demagnetizing factor given for the case of long cylinder with length,  $l$ , and the microwire diameter,  $D$ , as:

$$N = 4 \pi (\ln (2l/D) - 1) (D/l)^2 \quad (2.8)$$

The origin of this critical length has been explained considering that the closure end domains penetrate from the wire ends inside the internal axially magnetized core destroying the single domain structure. Detailed studies of amorphous wire geometries on magnetization profile and size of the edge closure domains have been performed [60]. In particular, critical length  $L_c$ , for magnetic bistability in conventional Fe-based wires (120 microns in diameter) is about 7 cm. While in the case of thin glass-coated microwires found to be as long as 2 mm for 10 microns metallic nucleus [60]. Below such length, LBJ is not achievable.

### 2.3.5 Structural relaxation and induced magnetic anisotropies

Amorphous nature of glass-coated microwires make them very sensitive to external parameters. Undoubtedly, the stress induced during the fabrication process, as mentioned before, defines well an important source of anisotropies. These anisotropies can be relaxed to a large extent by annealing. The compelling consequences of annealing processes require understanding of the origins of induced anisotropies. This, eventually, leads to partially relax the internal stresses induced by the production technique, and gives rise to additional sources of induced anisotropy. Controlling the anisotropy is extremely important for any technological application.

As a consequence of the rapid quenching, glass-coated microwires are metastable not only with respect to crystallization but also with respect to structural relaxation within an amorphous phase. Atomic redistributions within the glass tend gradually to reach the ideal amorphous

configuration. Accordingly, many physical properties are sensitive to structural relaxation and change with time [65, 66]. Although the rate of change is commonly negligible at room temperature it becomes faster at higher temperatures below the crystallization temperature. The dependence of the measured physical property on annealing time,  $t_{ann}$ , and temperature,  $T_{ann}$ , is a complex function of thermal history of the sample. The change of any magnitude with either  $t_{ann}$ , at a given,  $T_{ann}$ , depends on a number of factors.

The relaxation phenomena can be classified into at least two groups [67]. The first group shows irreversible and monotonic relaxation behavior except very close to and above the glass transition temperature  $T_g$ . This group of relaxation phenomena comprises of changes in the volume, and diffusivity or viscosity of a metallic glass. The second group includes relaxations in the anelasticity (creep-anisotropy), Curie temperature, field induced magnetic anisotropy, and thermal resistivity. This group of relaxation phenomena is characterized by a saturation of the change after prolonged annealing, indicating the attainment of a pseudo-equilibrium state [68]. The saturated state is called the pseudo-equilibrium state, since it is only metastable against crystallization. Usually the pseudo-equilibrium state is dependent upon the annealing temperature, so that when the annealing temperature,  $T_{ann}$ , is changed the system can move reversibly from one equilibrium state to another. Since this reversibility poses a striking difference compared to the first group, these relaxation phenomena are also known as reversible relaxation phenomena.

Annealing can be performed in lots of different ways: conventional annealing, stress annealing, field annealing, or annealing by electrical current (also known as Joule-heating). However, in case of glass-coated microwires, any single process of annealing can be considered as a twofold process ( $x$ -annealing + stress annealing). In other words, the presence of glass layer reinforces strong additional stresses, as a consequence, even only conventional annealing must be considered as conventional + stress annealing too [68, 69]. There are several proposed mechanisms for this induced anisotropy [70, 71] which include: atomic pair ordering resulting in directional order in the sample; induced texturing which line up easy axes; structural relaxation and rearrangement of free volume in amorphous materials; influence over the shape anisotropy of crystallites due to mechanical alignment. Thermal annealing at modest temperature and time affect the magnetoelastic anisotropy: after annealing the magnetoelastic anisotropy drastically



decreases. Hence, annealing at elevated temperature but below Curie temperature induces a macroscopic magnetic anisotropy with a preferential axis determined by the direction of magnetization during the annealing process [71, 72]. Field induced anisotropy found to be increased as high as the annealing temperature. This behavior has been experimentally observed in metallic glasses with different composition [71-74]. The microscopic origin of this field induced anisotropy has been successfully explained considering the directional ordering of atomic pairs mechanism developed by Néel et al. [75]. This model predicts a dependence of the field-induced anisotropy with the annealing temperature as:

$$K_u(T) = k (M_s)^n (T) \quad (2.9)$$

being  $n$  constant, the value of which can be assumed to be equal 2 if the microscopic origin is the directional ordering of atomic pairs. Theoretical predicted value of the index  $n$  was experimentally found in Fe-Ni based metallic glasses [75]. Nevertheless, deviations of such theoretical value have been obtained in Co-Fe based metallic glasses [76, 77]. In this case, an additional contribution coming from the single-ion (initially  $n = 3$ ) is considered. Moreover depending of the annealing temperature each contribution could be different according to the content of magnetic elements. Therefore macroscopically isotropic amorphous alloys can exhibit macroscopic magnetic anisotropy in the case if they are subjected to suitable annealing treatments at the presence of either a magnetic field (field annealing) or a mechanical stress (stress annealing).

A practical instance of such complex induced anisotropies in glass-coated microwires has been reported in Fe-based alloys [78]. Remarkable strong effect of stress annealing on overall shape of hysteresis loops and magnetic properties has been interpreted due to a drastic decrease in the longitudinal stress component and appearance of compressive longitudinal stresses, the so-called "back stresses" (Fig. 2.3). Such contribution of two different anisotropies induced by annealing, one by the mechanical load (longitudinal) and other by annealing (transversal) result in a redistribution of the internal stresses and/or local microstructure of the sample, and therefore, the net magnetoelastic energy in the stressed state was minimized.



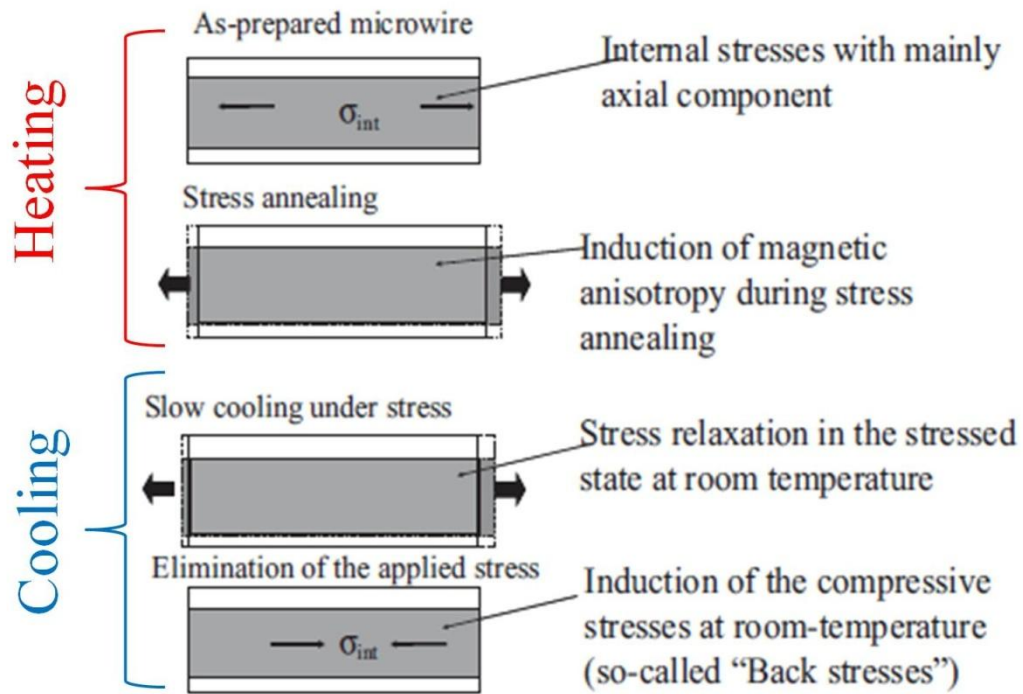


Figure 2.3 Schematic illustration of origin of back-stresses and effect of stress annealing in Fe-based glass-coated microwires (updated from [78] courtesy of Zhukov)

Having considered annealing to achieve desirable magnetic properties, in this way it is reasonable to control the annealing kinetics with the aim to avoid the crystallization, and therefore deteriorating the soft magnetic properties. Indeed, at certain cases the crystallization can improve magnetic softness even better than the amorphous state of glass-coated microwires. This is the so-called "nanocrystallization" and will be the spot topic of upcoming section.

## 2.4 Nanocrystalline glass-coated microwires and crystallization phenomena

An important group of soft magnetic materials is that consisting of nanocrystallites randomly nucleated in a soft amorphous matrix. This kind of soft two-phase materials can be obtained by crystallization of conventional Fe-Si-B amorphous alloys with small addition of Cu and Nb as a result of the important work carried out by Yoshizawa et al. [79]. So far, the crystallization of amorphous metals was rather known to significantly deteriorate the soft magnetic properties and to yield a relatively coarse microstructure with grain sizes of about 0.1–1 microns. However, Yoshizawa ultimately addressed that such unusual combination of this chemical design is a key for particular ultrafine grain structure and as a consequence superior

soft magnetic properties. The created microstructure possessed of small (around 10 nm grain size) nanocrystalites embedded in a residual amorphous matrix after annealing the amorphous precursor between 500-600°C for 1 hour. In this way, the devitrification process of these amorphous alloys came up with the basis features of excellent soft magnetic properties indicated by the high value of permeability about ( $1 \times 10^5$ ) and correspondingly, low coercivity. Nanocrystalline Fe-Si-B-Cu-Nb alloys have been patented under the trademark entitled *Finemet*, this name derives from the combination of "fine" and "metal" which indicates the material's features of being formed with fine crystal grains and having excellent magnetic properties. The next section will likely destined out the origin of this excellent magnetic softness as a unique advantage of nanocrystalline materials.

### 2.4.1 On the origin of magnetic softness

So far, the main concept of extremely magnetic softness character is thought to be originated because the magnetocrystalline anisotropy vanishes and very small magnetostriction value achieved when the grain size approaches 10 nm as theoretically estimated by Herzer [80, 81]. Herzer has successfully applied Alben model [48] to understand the origin of magnetic softness observed in the nanocrystalline state as sketched in Fig. 2.4. According to this model, low coercivity in the nanocrystalline state is ascribed to small effective magnetic anisotropy ( $K_{eff} \approx 10 \text{ J/m}^3$ ). The key to this property combination is the structural correlation length which is much smaller than the ferromagnetic correlation length. Somehow like in amorphous metals, the magnetocrystalline anisotropy is randomly averaged out by exchange interaction. While at the same time the averaging effect of exchange interaction in the small grain size regime allows to combine the individual properties of different structural phases which expands the variability of property tailoring over that of alloying single phases. In addition to the suppressed magnetocrystalline anisotropy, low magnetostriction values provide the basis for the superior soft magnetic properties observed in particular compositions. Low values of the saturation magnetostriction are essential to avoid magnetoelastic anisotropies arising from internal or external mechanical stresses. These findings make the essential difference to large grained materials where the magnetization follows the randomly oriented easy axes of individual grains and, accordingly, the magnetization process is controlled by the full magneto-crystalline anisotropy of the grains.

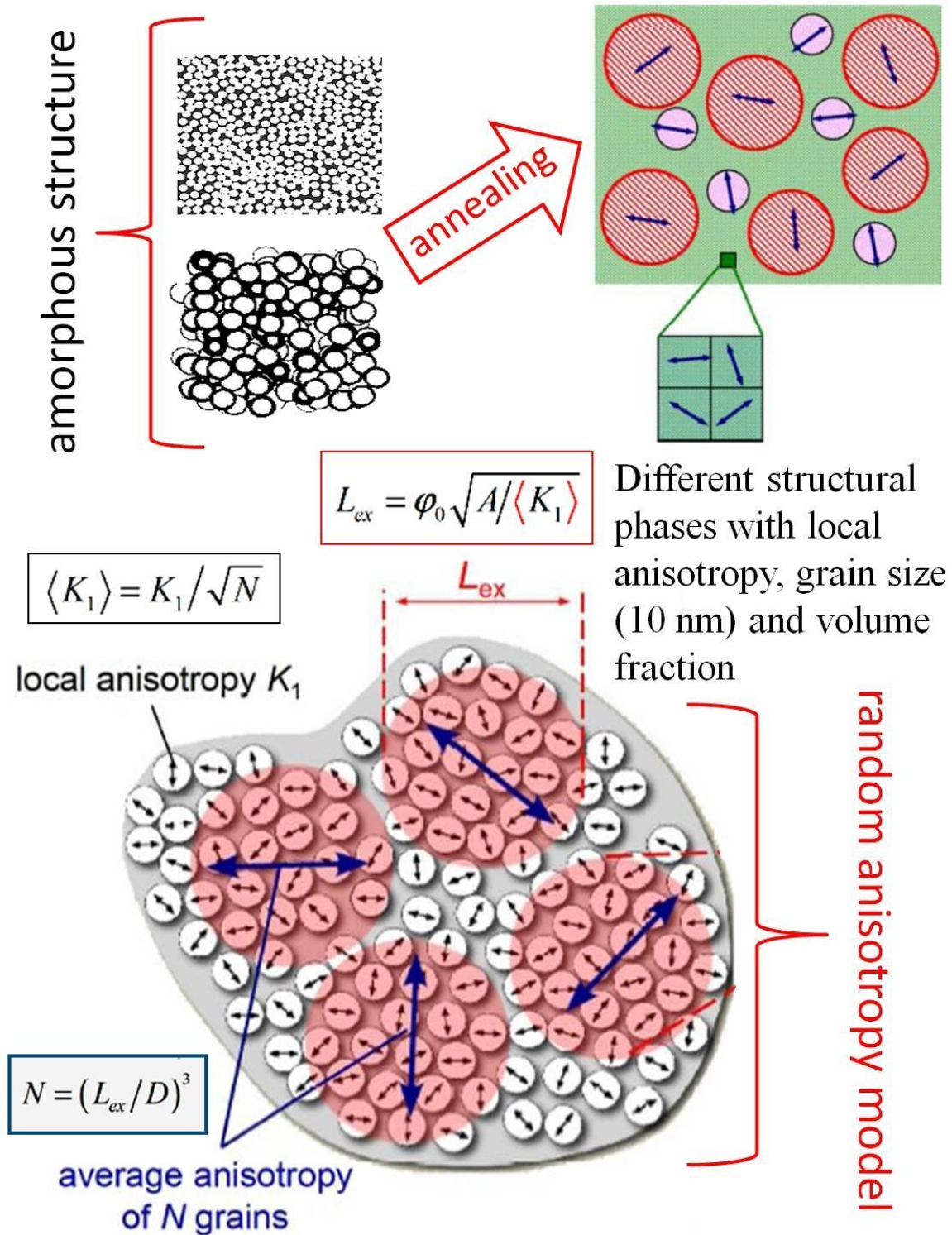


Figure 2.4 Schematic representation of the random anisotropy model developed by Herzer for nano grains embedded in an ideally soft ferromagnetic matrix. The figure is recreated based on Herzer's tutorials at the European school on magnetism held in Cargèse, France 2013.

This model later has been extended [82, 83] to better describe the average random anisotropy controlled by uniaxial anisotropies which are uniform on a scale much larger than the exchange length. In addition, if the grain size is sufficiently reduced, the most relevant contributions of either magnetoelastic or field induced anisotropies appear to be pretty much the same as in the case of amorphous alloys. However, there is still a competition between the random and uniform anisotropy contributions even in soft magnetically optimized nanocrystalline alloys. The latter mostly depends on the chemical alloy composition as will be argued in the next section where we basically deal with alternative choices of *Finemet* based alloys.

#### 2.4.2 Alloy design and microstructural consequences

Alloy design of nanocrystalline materials include issues of chemistry, processing of material's phase rule and their metallurgical behavior. Thus, it is very important to amend the chemical alloy design in order to optimize either magnetic or structural properties of created alloy. Let us first know the impact of these two elements Cu and Nb-addition to Fe-Si-B amorphous alloy. As initially shown by Yoshizawa et al. [79], Cu is introduced to increase the number of nucleation centers for the crystalline grain in order to get fine crystalline structure, while Nb impedes coarsening and, at the same time, inhibits the formation of boride compounds. Essentially, the Cu-addition alone is not sufficient, thus its effect is considerably promoted by the simultaneous presence of Nb. The latter enhances the crystallization temperatures and retards the grain growth by limiting diffusion. In particular, Nb-addition significantly increases the separation between the two crystallization stages which promotes the primary crystallization of BCC Fe-Si and stabilizes the residual amorphous matrix against the precipitation of Fe-B borides compounds. All together leads to an increased number of simultaneously growing and competing crystals resulting in the nanoscaled microstructure upon alloying at least about 2–3 at% of Nb with 1 at% of Cu.

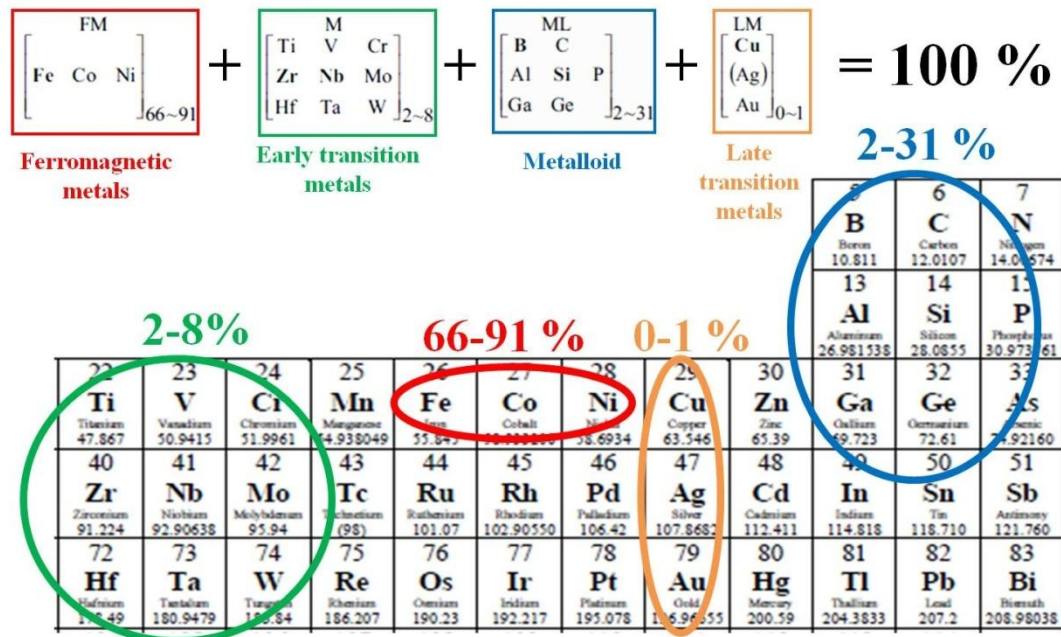
Looking at the periodic table of elements, Nb can be substituted by other refractory elements of group V or VI, like Cr, V, Mo, W or Ta, actually they act similarly on the crystallization process and on the magnetic properties of *Finemet* alloys [84]. Like for Nb, the atomic volumes of these refractory elements are larger than that of Fe which reduces the diffusion coefficients and, thus, stabilizes the amorphous matrix and slows down the kinetics of grain coarsening [85].

Accordingly, the efficiency of these elements for grain size refinement increases in the order of their atomic volumes (i.e.  $\text{Cr} < \text{V} < \text{Mo} \approx \text{W} < \text{Nb} \approx \text{Ta}$ ). Thus, finest grain structures and superior magnetic properties in practice require at least a certain amount of the elements Nb or Ta. On the other hand, substitution of Cu by other noble metal elements of group XI, like Au or Ag has been also reported [86]. Au-addition has been verified to have a comparable effect on the crystallization behavior, while Ag-addition could not be verified successfully because Ag is practically immiscible in Fe even in the liquid state. It is also worth mentioning that the B-ratio plays a significant role beside Cu and Nb. The B-content should be kept at a low or moderate level 8–10 at% of B in order to obtain an optimum nanoscaled structure. The optimum *Finemet* alloy composition originally proposed and subsequently not much changed is  $\text{Fe}_{73.5}\text{Cu}_1\text{Nb}_3\text{Si}_{13.5}\text{B}_9$ , having a good glass forming ability and is easily accessible by rapid solidification technique.

A major driving force in the search for further alloy compositions and alternative choices of *Finemet* alloys has been developed since the discovery of Yoshizawa. Similar alloy composition with the same features of *Finemet* has been commercially patented under the name *Vitroperm* -  $\text{Fe}_{73.5}\text{Cu}_1\text{Nb}_3\text{Si}_{13.5}\text{B}_7$  produced by Vacuumschmelze-Germany. Alternative compositions of Fe-Zr-B based alloys have been developed by Suzuki et al. [87, 88] known up to date as *Nanoperm* alloys, and more recently (Fe,Co)-M-B-Cu (M = Nb, Hf, or Zr) nanocrystalline alloys, called *Hitperm* developed by Willard et al. [89] with quite attractive inductions (1.6-2.1 T) combined with high permeabilities and high Curie temperatures. In *Finemet*-alloys  $\alpha$ -Fe-Si BCC structure has been observed, while  $\alpha$ -Fe BCC in *Nanoperm*-alloys and  $\alpha$ -Fe-Co BCC structure in *Hitperm*-alloys were observed, respectively. All these aforementioned alloys and their derivatives are currently made the basis line of research in regarding to nanocrystalline materials as have been comparatively revised in several reviews [90-92]. In summary, the behavior of each alloy and the onset of crystallization mainly depend on the chemical alloy composition as well as the crystallization kinetics of each alloy design. A schematic map of the periodic table of elements with almost all reported up-to-date alloy designs is sketched in Fig. 2.5. The mixture of each developed alloy inevitably governs their crystallization mechanism and their microstructural consequences. However, there are some basic principles which often control the driving forces for any transformation between the initial and final states of crystallization.



## The periodic table of elements



### “Chemical alloy design of nanocrystalline materials”

Figure 2. 5 Schematic map of the periodic table of elements shows the major reported up-to-date chemical alloy designs of nanocrystalline materials.

In fact, the earliest investigations into the crystallization sequence of metallic glasses suggested that the transformation proceeds through a series of progressively more stable phases until final equilibrium is reached, rather than directly to the equilibrium phases [93]. Depending on the chemical alloy composition and thermal treatment, a number of basic transformations are possible. The reaction that proceeds however, is not necessarily the one with the largest driving force but rather the one that can occur fastest under the imposed conditions. Phase transformations in condensed systems are fundamentally the same, irrespective of whether the initial state is liquid, crystalline or non-crystalline. The crystallization of metallic glasses has been shown to occur by nucleation and growth processes in a similar fashion to that observed in normal crystalline solids [93, 94], which may occur individually, in parallel or in succession, by three different means (modes):

- Polymorphous crystallization: In this mode of transformation the glassy alloy will transform into a single crystalline phase without any change in the composition. This is only

possible to form in the ranges where the glassy phase was formed in the composition range of a stable, metastable or an intermetallic phase.

- Eutectic crystallization: Contrary to the previous mode, the glassy phase transforms simultaneously into two or more phases by a discontinuous reaction. Eutectic crystallization can occur in the whole concentration ranges between two stable/metastable phases.
- Primary crystallization: This mode of crystallization is the main transformation method observed in metallic glasses. It consists in a supersaturated solid solution first formed from the glassy phase and consequently, the remaining glassy matrix will be enriched in solvent atoms until it will further transform later or at higher temperatures.

The growth of primary crystals, whether they are from liquid, glass, or crystalline solid solution, may be limited by either the rate of atoms transfer across the advancing interface (interface control related to grain growth) or the diffusion rate of atoms toward or away from the growing phase (diffusion control related to nucleation mechanism) [93, 94]. All the evidence up to date is that the crystallization of metallic glasses is diffusion controlled. Thus, the behavior of the onset of crystallization on temperature and composition of metallic glasses demonstrates that a basic condition for the formation of a typical nanocrystalline structure is given by a primary crystallization process before stable or metastable intermetallic phases are formed. The latter can be easily achievable by accomplishing two main concerns: firstly, alloy additions (control the chemical composition) which lead to clearly separated stages of crystallization at  $T_{x1}$  and  $T_{x2}$ ; and secondly, by annealing an amorphous precursor at  $T_{x1} < T_{ann} < T_{x2}$  such that only the phase forming at and above  $T_{x1}$  is crystallizing. The upcoming section will highlight these circumstances of how to prepare/obtain nanocrystalline alloy in a successful way.

### 2.4.3 Methods of preparation: A final word

In principle, crystalline phases embedded in an amorphous metallic matrix (nanocrystalline materials) can be obtained in two different ways either by controlling the crystallization kinetics throughout optimizing the heat treatment conditions (annealing temperature, annealing time, heating rate, etc.), or by decreasing the quenching rate velocity during the casting process. In this way, by adjusting the chemical alloy composition, the crystalline phase is precipitated directly from the melt during rapid cooling without performing any annealing processes.

Actually these abovementioned properties presented in this chapter provide the fundamental guidelines for studying magnetic glass-coated microwires being an important research tool. Thus, for example, even within a single piece of sample, they combine collections of phenomenal parameters either magnetic or structural with high scientific interest.

A final word is that this chapter reflects the basics concerning to physical properties which bear on the technical application of magnetic glass-coated microwires. Some of these applications are in the purview of the next chapter.



# Chapter 3

## Glass-coated microwires: Technological applications

---

**T**he preceding chapter would be incomplete without addressing some insights of technological applications raised by the interesting features of glass-coated microwires. We explain, where possible, the fundamental aspects of two highly major phenomena used in magnetic sensors applications: giant magneto-impedance (GMI) and magnetic bistability/domain wall (DW) propagation.

---

### 3.1 Glass-coated microwires for technological interest

In light of the compelling nature of these glass-coated microwires, having circular symmetry, outstanding magnetic properties, and produced by cheap-accessible fabrication method, all these characteristics make them truly attractive from any application's perspectives. Among very widely application trends in the field of magnetic materials: those related to sensing operations are nearly used in all engineering and industrial sectors. The basic concept of many magnetic sensors are tied up with the well-known phenomena giant magneto-impedance (GMI). In addition, also some of these applications are likely rooted to a fast and controllable domain-wall (DW) motion or propagation throughout magnetic bistability. So far, glass-coated microwires offer such existence of these two functionalities either GMI or magnetic bistability in a broad variety of compositions of each of two main families: Co-based or Fe-based alloys, respectively.

Undoubtedly, the use of any magnetic material (including glass-coated microwires) in a certain type of application needs first to cross many barriers and specific criteria. Herein, we discuss some basic features of these two abovementioned phenomena GMI and magnetic bistability of glass-coated microwires since apparently they are the two main application trends of this class of soft magnetic materials.

### 3.2 Fundamental aspects of GMI

#### 3.2.1 Early advances and research growth

Historically, the phenomena of giant magneto-impedance (GMI) was first investigated in Ni-Fe alloy in 1935 by Harrison et al. [95], however at that time, it did not attract so much attention until the rediscovery in 1994 by Panina and Mohri et al. [96] as well as by Beach and Berkowitz et al. [97]. GMI was analyzed that time more thoroughly in non-magnetostrictive soft magnetic Co-based amorphous wires of about 120 microns in diameter. The term "giant" was employed following the well-known giant magneto-resistance (GMR), which is a large variation of the material's resistance upon the application of an external magnetic field. While GMI defines the changes of the material complex impedance as a function of an external applied magnetic field. Although the first insights are very similar either GMI or GMR, for example, in both cases one observes a large variation of the voltage drop across the samples upon the

application of external magnetic field, however, the physical origin of both phenomena is completely different. From the very basic point of view, in the case of GMI, the overall effect of the magnetic field application is to induce strong modifications in the effective magnetic permeability, a factor that is relevant to determine the field and current distribution within a sample. When a soft magnetic material is used, the magnetic permeability can change orders of magnitude when a rather small field is applied, causing strong variations in the internal fields and electrical current density, and as a consequence, on the sample's impedance as was reported [96, 97]. The effect, therefore, is strongly dependent on the frequency of the applied current and the magnetic anisotropies present in the material, which generates a number of interesting new magnetic phenomena.

Currently, many ongoing scientific reviews have dealt with different aspects of GMI either as a research tool to investigate some intrinsic and extrinsic magnetic properties of novel artificially grown soft magnetic materials with different geometries [98, 99], or as a leading theory to assess deeper understanding of the mechanism behind GMI as well as to predict some expected behaviors under particular assumptions [100-103]. Each of these assumptions make an important contribution and peculiar properties, being interesting for several practical applications. It is worth saying that many of these applications are already proposed and tested in laboratory prototypes (i.e. portable digital display of the terrestrial magnetic field, brain tumor sensor, sensor for the induction motor control, car passing measurement and recording disk, finger-tip blood vessel pulsation, etc.) [98, 99]. In the next sub section we describe the major principles of GMI that will assist in understanding the GMI behavior of glass-coated microwires.

### 3.2.2 Major principles

As a matter of fact, when a soft ferromagnet is exposed to a small alternating current  $AC$ , a large change in the  $AC$  complex impedance of the material can be achieved under an applied magnetic field. The relative change of the impedance,  $Z$ , with applied field,  $H$ , denotes the GMI effect (also known as GMI ration), and is expressed by:

$$\Delta Z/Z (\%) = 100\% \times \frac{Z(H) - Z(H_{max})}{Z(H_{max})} \quad (3.1)$$

where  $H_{max}$  is usually the external magnetic field sufficient to saturate the sample magnetization.

The complex impedance of a linear electronic element,  $Z = R + j\omega L$  ( $R$  and  $L$  are the resistance and inductance, respectively) is given by the ratio of the voltage amplitude  $V_{ac}$ , measured on the element, to the current amplitude  $I_{ac}$  of a sinusoidal current  $I_{ac} \sin \omega t$ , passing through it. For a conductor with length,  $L$ , and uniform cross-section with area,  $q$ , the impedance can be expressed by the formula as reported in [101]:

$$Z = \frac{V_{ac}}{I_{ac}} = \frac{LE_z(S)}{q\langle j_z \rangle q} = R_{dc} \frac{j_z(S)}{\langle j_z \rangle q} \quad (3.2)$$

where  $E_z$  and  $j_z$  are the longitudinal components of electric field and current density, respectively, and  $R_{dc}$  is the dc electrical resistance.  $S$  is the value at the surface, and  $\langle j_z \rangle q$  is the  $j_z$  average value over the cross section  $q$ . The current density  $j_z(r)$  in eq. (3.2) of the conductor can generally be obtained within the framework of classical electrodynamics of continuous media, by solving simultaneously the reduced Maxwell equation (3.3) and the Landau-Lifshitz equation (3.4) for the motion of the magnetization vector as follows:

$$\nabla^2 \mathbf{H} - \frac{\mu_0}{\rho} \dot{\mathbf{H}} = \frac{\mu}{\rho} \dot{\mathbf{M}} - \text{grad div } \mathbf{M} \quad (3.3)$$

$$\mathbf{M} = \gamma \mathbf{M} \times \mathbf{H}_{eff} \frac{\alpha}{M_s} \times \mathbf{M} - \frac{1}{\tau} (\mathbf{M} - \mathbf{M}_0) \quad (3.4)$$

where  $\gamma$  is the gyromagnetic ratio;  $M_s$  the saturation magnetization;  $M_0$  the static magnetization;  $H_{eff}$  the effective magnetic field, and  $\alpha$  the damping parameter [101]. Analytically, it is difficult to obtain the exact solution of the problem by solving simultaneously either the Maxwell eq. (3.3) or the Landau–Lifshitz equation of motion eq. (3.4). However, at low frequency, the problem can be treated with a quasistatic approximation. In this case, using the simple material relation ( $B = \mu H$ ) in the Maxwell equations, the current density in an infinite film conductor can be easily calculated according to [101] and substituting for  $j_z(r)$  into eq. (3.2) the impedance of a cylindrical magnetic conductor is regulated as:

$$Z = R_{dc} K_r J_0(K_r) / 2J_1(K_r) \quad (3.5)$$

being  $J_0$  and  $J_1$  are the Bessel functions;  $K = (1 + j) / \delta_m$  where  $\delta_m$  denotes the skin penetration depth with imaginary unit  $j$ .  $\delta_m$ , and with circumferential permeability, and  $r$  is the wire's radius. This skin depth  $\delta_m$  in case of magnetic wires is given by:

$$\delta_m = \sqrt{\pi f \sigma \mu_\phi} \quad (3.6)$$

where  $\sigma$  is the electrical conductivity,  $f$  the frequency of the current along the sample, and  $\mu_\phi$  the circular magnetic permeability assumed to be scalar. The *DC* applied magnetic field introduces significant changes in the circular permeability,  $\mu_\phi$ . Therefore, the penetration depth,  $\delta_m$ , also changes through and finally results in a change of  $Z$ . It means that to large GMI responses, it is necessary to reduce skin depth by choosing magnetic materials that have large  $\mu_\phi$  and small  $\delta_m$  and  $R_{dc}$ .

Depending on the frequency  $f$  of the driving *AC* current  $I_{ac}$  flowing through the sample, different GMI regimes can be considered:

- Low frequency regime (1–10 *KHz*): The skin depth is usually larger than the radius or the sample (weak skin effect or negligible). The impedance changes, therefore, at these frequencies are of an inductive character due to a circular magnetization process exclusively and might not be considered properly as GMI effect since it has been mostly called magneto inductive effect.
- Intermediate frequency range (where the GMI effect has been first reported and described) from 10–100 *KHz* to 1–10 *MHz*: The GMI originates basically from variations of the magnetic penetration depth due to strong changes of the effective magnetic permeability caused by a *DC* magnetic field. It is widely believed that in this case, both domain walls movement and magnetization rotation contribute to changes of the circular permeability and consequently to the skin effect.
- High frequencies range from 1–10 to 100–1000 *MHz*: The GMI effect is also originated by the skin effect of the soft magnetic conductor, i.e. must be attributed to the GMI. At these frequencies the domain walls are strongly damped. Therefore the magnetization rotation must be considered as responsible for the magnetic permeability change induced by an external magnetic field [96-98].
- Elevated *GHz* band frequencies: The magnetization rotation in these ranges is strongly influenced by the gyromagnetic effect [103], where strong changes of the sample's impedance have been attributed to the ferromagnetic resonance FMR [103, 104]. Upon increasing the frequency, the GMI peaks are shifted to higher magnetic fields values for being the sample magnetically saturated. It is also predicted that the diameter reduction at *GHz* frequency range

must be associated with the increasing of the resonance frequency. Accordingly, optimizing GMI effect at these frequencies range is a tradeoff between dimension and frequency required in order to detect a maximum effect [103, 104].

### 3.2.3 GMI in glass-coated microwires and sensing technologies

So far, based on abovementioned fundamental features of GMI, a well-defined circumferential magnetic anisotropy in combination with a soft magnetic behavior is desirable for GMI, since it will provide a large permeability change for even small magnetic fields. Obtaining reasonable GMI effect lies in the dependence of  $\mu_\phi$  on an axial magnetic field which results in a change of  $\delta_m$ . The latter has to be close to the thickness of the conductor, and hence, the thinner a ferromagnetic conductor and the lower its permeability, the higher the operation frequency required. However, in ferromagnetic materials with high circumferential anisotropy (as the present case study of glass-coated microwires) the magnetic permeability always possesses a tensor nature and the classical form of impedance definition is not so much authenticated. In other words, the relation between electric field (which determines the voltage) and magnetic field (which determines the current) is defined through the surface impedance tensor [105, 106] to be:

$$e = \hat{\zeta} h \quad \text{or} \quad \left\{ \begin{array}{l} e_z = \zeta_{zz} h_\phi - \zeta_{z\phi} h_z \\ e_\phi = \zeta_{\phi z} h_\phi - \zeta_{\phi\phi} h_z \end{array} \right\} \quad (3.7)$$

The circular magnetic fields  $h_\phi$  is produced by the currents  $i_w$  running through the wire. At the wire surface  $h_z = i/2\pi r$ , where  $r$  is the wire's radius. The longitudinal magnetic fields  $h_z$  is produced by the currents  $i_c$  running through the exciting coil,  $h_z = N_l i_c$ , where  $N_l$  is the exciting coil number of turns. On the other hand, various excitation and measurement methods are required to reveal the impedance matrix elements. The longitudinal and circumferential electrical field on the wire surface can be measured as voltage drop along the wire  $v_w$  and voltage induced in the pickup coil  $v_c$  wound on it [105, 106].

$$v_w \equiv e_z l_w = (\zeta_{zz} h_\phi - \zeta_{z\phi} h_z) l_w \quad (3.8)$$

$$v_c \equiv e_\varphi l_t = (\zeta_{\varphi z} h_\varphi - \zeta_{\varphi\varphi} h_z) l_t \quad (3.9)$$

where  $l_w$  is the wire length,  $l_t = 2\pi r N_2$  the total length of the pickup coil turns  $N_2$  wound directly on the wire.

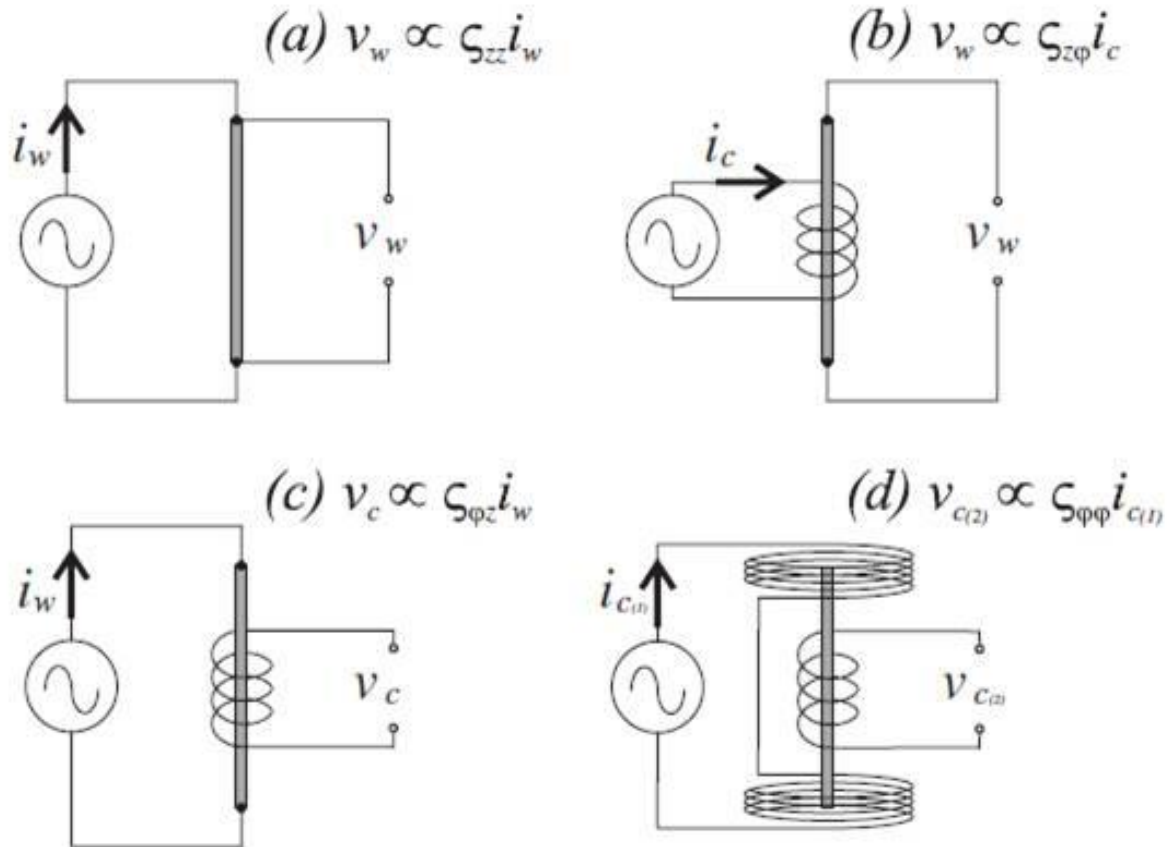


Figure 3.1 Methods for revealing the impedance matrix elements: (a)  $\zeta_{zz}$ , (b)  $\zeta_{z\varphi}$ , (c)  $\zeta_{\varphi z}$ , (d)  $\zeta_{\varphi\varphi}$  [107]

The methods for revealing the different elements of impedance tensor are shown in Fig. 3.1. The longitudinal diagonal component  $\zeta_{zz}$  is defined as the voltage drop along the wire and corresponds to impedance definition in the classical model described in the prior section as shown in Fig. 3.1a.

$$\zeta_{zz} \equiv \frac{v_w}{h_\varphi l_w} = \left( \frac{2\pi a}{l_w} \right) \left( \frac{v_w}{i_w} \right) \quad (3.10)$$

The off-diagonal components  $\zeta_{z\varphi}$  and  $\zeta_{\varphi z}$  (Fig. 3.1 b&c) and the circumferential diagonal component  $\zeta_{\varphi\varphi}$  (Fig. 3.1d) arose from cross sectional magnetization process ( $h_\varphi \rightarrow m_z$  and  $h_z \rightarrow m_\varphi$ ) [105-107]. Once the impedance is determined for each desired frequency and each value of the static longitudinal magnetic field, the GMI ratio can be calculated by substituting the real part of impedance,  $Z$ , into eq. (3.1).

In due the investigation of glass-coated microwires for high-frequency GMI effect, quite striking and prodigious observations have been investigated either in as-prepared states or after subjecting the microwires to a broad variety of annealing, the latter are performed in order to induce specific magnetic anisotropies, inducing magnetic permeability, and in turn, modifying GMI response. Up to 600% GMI ratio has been reported by optimizing the magnetic anisotropy of nearly zero magnetostrictive Co-based amorphous microwires [108, 109]. The value of the magnetic field at which maximum GMI ratio is obtained increases as the diameter of the magnetic nucleus decreases as compared to the diameter of glass coating. This is attributed to the different anisotropies induced by the stress from the coating as shown in the previous chapter.

Not long ago, the development of high-performance magnetic sensors has been arose based on GMI effect either diagonal (symmetrical) or off-diagonal (asymmetrical) in thin wires. A number of magnetic sensors based on GMI effect and stress-impedance (SI) effect with the CMOS IC circuitry and advantageous features comparing with conventional magnetic sensors have been reported by Aichi Steel Co. in Japan by Honkura and Morhi et al. [110, 111], and Cobeño et al. [112] which were in this case relevant for the detection of even low magnetic fields. Finally, a magnetic compass for cell phones and other portative devices utilizing off-diagonal GMI effect with linear response to external magnetic field has been developed and prepared for a mass production [113]. The key factor is the ultra high sensitivity of GMI effect and the linear response to external magnetic field. Further development of GMI wire-base magnetic sensor by Uchiyama et al. [114] has resulted in achieving a sensitivity of about  $1 \text{ pT}$ . In addition, a number of sensors based on gathering magnetoelastic properties and SI effect of microwires, such as GMI-magnetoelastic sensor, and temperature sensor based on GMI effect in



microwires with low Curie temperature,  $T_c$ , have been reviewed by Zhukova et al. [115] within the use of thin glass-coated microwires with different geometries and compositions. Biosensors [116-118], on the other hand, based on GMI effect in microwires have been developed and used to detect different types of biomolecules binding on magnetic particles. New type of free-space microwave sensing technique based on embedded short or long ferromagnetic glass-coated microwire inclusion into the composites also took part of these developments [119].

Whilst the discussion in the preceding paragraph is yet not complete, we will back again by the end of this chapter to close some limitations of these abovementioned findings. Now, we move on to smoothly stretch those applications of glass-coated microwires but on the bases of another phenomena, magnetization switching (bistability) and DW propagation.

### 3.3 Oriented applications based on magnetic bistability of glass-coated microwires

Magnetic bistability as we seen in the previous chapter is one of the most distinctive properties of glass-coated micowires. After achieving the two main configurations which are necessary to observe such property, the magnetic bistability is characterized by two sharp voltage peaks induced in the pick-up coil wound around the microwire. In other word, this property give rise to two-twin equal derivative peaks on the oscilloscope, one negative and another positive. The induced electro motive force, *emf*, is caused by an abrupt change of the magnetic flux during a large Barkhausen jump LBJ. This effect is potentially used in magnetic sensor technologies.

Anciently, the first sensor based on magnetic bistability were reported in the 1970s by Wiegand et al. [120]. Wiegand wires with rectangular hysteresis loops inducing sharp 20–30  $\mu$ s pulses in the secondary coil mounted on the sample subjected to AC magnetic field were widely applicable in automobile industry for the detection of motions and positions. However, the excitation field needed to trigger the sharp peaks was approximately high of about 4 *KA/m*. As a consequence, alternative choices of these wires were reported by Mohri et al. [121] throughout amorphous Fe-based ribbons with reduced excitation field (100 *A/m*) as compared to Wiegand's wires. Subsequently, the Matteucci effect, appeared in the twisted amorphous ribbon was also employed for the modified rotation speed sensor by Mohri et al. [122]. A number of magnetic sensors based on magnetic bistability and/or Matteucci effect of amorphous wires were

developed [123, 124] where they were commonly used for the distance sensor, revolution counter and position sensor. These technological developments in magnetic sensors have greatly expanded due to the existence of bistable character with reduced dimensionality of glass-coated microwires. Therefore, a successful magnetic sensor used in encoding/tags and magnetic codification were reported by Zhukov et al. [125] owing to plurality of coercivities and strong dependence of these microwires on geometric dimensions and heat treatment. In addition, the extended values of switching fields and high stress sensitivity made them pretty attractive to these perspectives. Thus, a magnetoelastic sensor of a level of liquid were designed by Zhukov et al. [126] using the stress dependence of the coercivity in nearly-zero magnetostriction Co-based microwires. Besides, a magnetoelastic pen consisting of ferromagnetic bistable amorphous wire with positive magnetostriction used for identification of signatures based on the strength of stress character of each person as was also developed by Zhukov et al. [127].

In as much as the magnetic bistability phenomena of glass-coated provides an immense application directions in the community of magnetic sensors, the bistable behavior found to be as a consequence of magnetization reversal inside one single domain. In accordance, the movement of this single domain and its dynamics are in a spate of technological interest. The speed at which a DW can travel in a wire has an impact on the viability of many proposed technological applications in magnetic logic devices, random access memory, integrated circuits, hard disks, and spintronic [128, 129], all of those are based on fast and controllable propagation of DW of a magnetic material. The first DW propagation instance in glass-coated microwires was reported by Zhukov et al. [62]. Numerous studies of DW propagation in amorphous glass-coated microwires have pointed to some unique aspects of this phenomena, which have been clearly linked to the special magnetic structures formed in positive and nearly zero magnetostrictive microwires. Thus, DW velocities reported in amorphous microwires are very fast of about 1 to well over 2  $Km/s$  [130] and in some particular cases are extremely fast up to 18.5  $Km/s$  as reported by Varga et al. [131]. Reported velocities of DW in either amorphous or nanocrystalline glass-coated microwires are actually much more faster than those reported in nanowires [132] even they are obtained at much smaller values of applied magnetic fields, in some cases down to 20  $A/m$  as was observed by Varga et al. [133]. In a similar way, the DW mobility values are also quite high in microwires, and both wall velocity and mobility depend on the type of magnetic structure from the near-surface region of the microwires. Three reasons were somehow

established for fast DWs in glass-coated microwires [56] first; low anisotropy and Gilbert damping; second, existence of two perpendicular anisotropies; and third, existence of radial domain structure below the surface of metallic nucleus which hinders the DW pinning on surface defects. In the forthcoming section we describe the main dynamics that control DW propagation in glass-coated microwires.

### 3.4 Simplified model of DW in glass-coated microwires

The response of a domain wall to a weak magnetic field in a viscous medium is described by a classical equation of motion [134]. This leads to the following expression for the steady-state wall velocity at the frequencies of interest:

$$v = S (H - H_0) \quad (3.11)$$

where  $H$  is the axial magnetic field;  $H_0$  is the critical propagation field in which below this value the DW propagation is not possible, and  $S$  is the DW mobility regulated by:

$$S = \frac{2 \mu_0 M_s}{\beta} \quad (3.12)$$

being  $\mu_0$  the magnetic permeability of vacuum;  $M_s$  the saturation magnetization, and  $\beta$  the viscous damping coefficient being the most relevant parameter that determine DW dynamics in glass-coated microwires.

Recently, three contributions to the DW damping are recognized [56]:

- Eddy-current damping,  $\beta_e$ : Basically, eddy currents arise in any conducting magnetic material as a result of the flux density change that occurs during the DW propagation. The exact calculation of the eddy-current contribution to the total DW damping must be performed with respect to either the wire geometry or the structure of moving DW. In the case of amorphous glass-coated microwires, the DW propagates in a cylindrical axial domain, which is surrounded by outer shell of radial domains. For such case, the eddy-current damping,  $\beta_e$ , is expressed as previously shown in [135]:

$$\beta_e = \frac{4 \mu_0^2 M_s^2 r_0}{\rho} \left( \ln \frac{r_0}{r_b} + \frac{8}{\pi^2} \right) \quad (3.13)$$

where  $r_o$  is the radius of the metallic nucleus;  $r_b$  is the axial domain radius, and  $\rho$  is the resistivity. However, the strong damping for highly insulated materials, such as ferrites, cannot be explained by the eddy current damping. Therefore, another damping mechanism, based on Landau-Lifshitz equation has been introduced.

- Magnetic relaxation damping,  $\beta_r$ : This damping arises from the fact that DW cannot move faster than the magnetic moments [136]. In other word, magnetic relaxation damping is related to the delayed rotation of electron spins which is basically related to Gilbert damping parameter and is found to be inversely proportioned to the DW width,  $\delta_w$  [137]:

$$\beta_r \approx \frac{\alpha M_s}{\gamma \delta_w} \approx M_s \sqrt{K/A} \quad (3.14)$$

where  $\gamma$  is the gyromagnetic ratio,  $A$  is the exchange stiffness constant, and  $K_{me}$  is the magnetoelastic anisotropy given by eq. 2.5 (page 18). Therefore, we can outline here the important correlation between the DW mobility and magnetoelastic anisotropy of glass-coated microwires.

- Structural relaxation damping,  $\beta_s$ : Due to the amorphous nature of these microwires, another damping is suggested to arise from the structural relaxation of mobile defects on atomic scale [134]. This instance was firstly approved in the case of amorphous glass-coated microwires by Varga et al. [138] to be as a consequence of the intrinsic metastable state of amorphous microwires. Therefore, the small displacements of mobile defects will increase the local anisotropy which are, in turn, governed by a relaxation time that is, consecutively, strongly temperature dependent [138]. By assuming that the thermal energy,  $KT$ , is higher than the splitting energy between two positions of the mobile defects [139] the damping term due to structural relaxation,  $\beta_s$ , is given by the following expression:

$$\beta_s(T, ) \propto \frac{\varepsilon_p^2 c_p}{f_r KT} (1 - e^{-f_r/2f}) \quad (3.15)$$

where  $c_p$  denotes the density of mobile defects;  $\varepsilon_p$  corresponds to the interaction energy with the local spontaneous magnetization;  $f$  is the frequency of the applied field; ( $f_r = f_0 e^{-Q/KT}$ ) is the relaxation frequency of the mobile defects;  $f_0$  is a pre-exponential factor, and  $Q$  is the activation energy.

In contrary to previous contributions (eddy current and magnetic relaxation) to DW damping, the structural relaxation component can be modified by either properly setting the experimental conditions or by controlling the thermal treatment [56, 140]. During a DW experiment, three time parameters are in operation:

- $\tau$ - the relaxation time of mobile defects that obeys Arrhenius law:  $\tau = \tau_0 \exp(Q/KT)$
- $t_1$ - the time necessary for DW to propagate across the position of atomic mobile defect giving by: ( $t_1 = \delta_w / v$ ) being  $\delta_w$  the DW width and  $v$  the DW velocity.
- $t_2$ - the time between two DW propagations (i.e. the period of the measurement that corresponds to the measuring frequency of applied magnetic field).

In the face of these findings, we must assume that by properly selecting the measurement frequency, the structural relaxation damping can be suppressed, and as a consequence achieving fast DW is easily doable.

### 3.5 Closing remarks

The endless of interesting features of glass-coated microwires actually made this closure quite difficult. As shown, intensive attempts for numerous potential applications have already crossed the laboratory barriers and being nowadays successfully implemented at mass production as recently epitomized [141].

However, the treatment of glass-coated microwires always comes up with new unexpected results, and therefore inspires new lines of research to be emerged. For example, in most cases either GMI or magnetic bistability are observed for microwires with completely different compositions of Co-based or Fe-based, respectively. Thus, fast magnetization switching and related fast DW propagation are typically observed in microwires with positive magnetostriction coefficient exhibiting rectangular hysteresis loops. The condition for achieving considerable GMI effect is the high circular magnetic permeability usually observed in Co-based microwires with low and negative magnetostriction coefficient. Accordingly, the creation of samples exhibiting both aforementioned properties is very attractive, and thus, opens up a new pathway to exploit new microwires for dual functional GMI and DW corresponding applications. In addition, the optimization of GMI effect in Fe-based microwires became a very competitive task due to the cost effectiveness of Fe as-compared to Co. The hysteresis observed in most GMI

studies also stands as one of the most obstacles that should be overcome. The complex DW dynamics of microwires made them a controversial problem that, in turn, seek further studies and deeper investigation.

All of these limits are in the scope of current investigations, and that is basically the main purpose of this dissertation as will be presented in the 4 chapters of the second part (results and discussion). The next chapter before results typically describes the experimental techniques used along the studies of glass-coated microwires.

# Chapter 4

# Experimental techniques

---

**T**he chapter provides a description of different experimental techniques procedures that have been employed to investigate glass coated microwires. We pay attention on addressing the fundamental background behind each technique as well as the experimental setup conditions that have been performed.

---

#### 4.1 Fabrication technique of glass-coated microwires

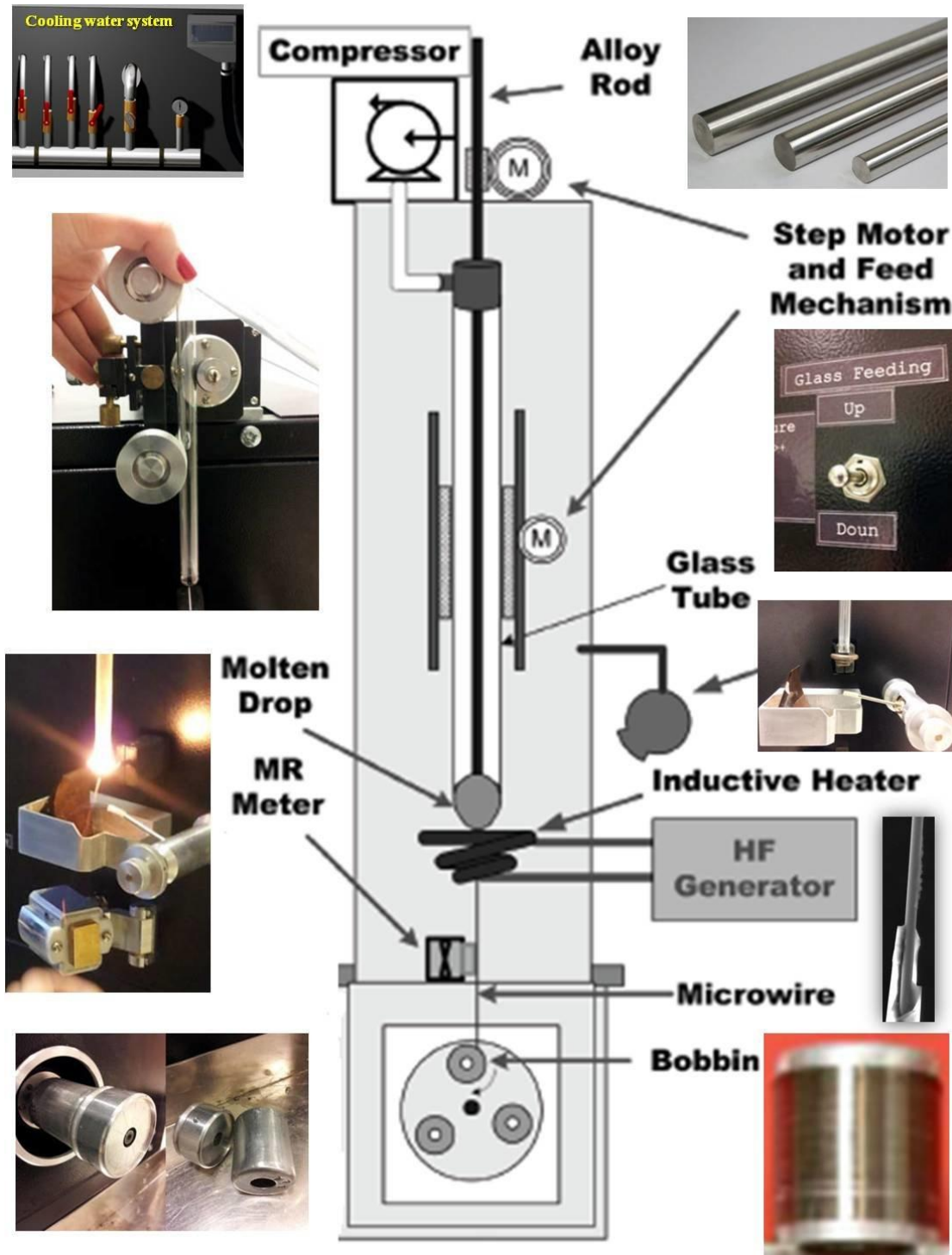


Figure 4.1 Schematic draw of the microwire fabrication process by Taylor-Ulitovsky methodology.



As has been contended along the literature review in chapter 1, the modified Taylor-Ulitovsky method is the technique used to fabricate all samples presented in this dissertation (Fig. 4.1). In short again, the technique based on the simultaneous rapid solidification of a glass capillary with metallic nucleus inside with diameter between 1-30 microns and an insulating glass sheath varies in diameter between 2-10 microns [34, 35].

The process of microwire production is qualified with bunch of high elevated levels of complexity. It presents joining of mechanical, thermal, electrodynamical, physical, and chemical interactions. In addition, those aforementioned interactions are not just a multiple mixing of technical proceedings, but also they are overlapped all together in a very sophisticated way during the time of casting. It can be supposed that a model of casting might be derived from the underlying properties of the process itself. However, even under various approximations, the final model unlikely will not be able to describe such assumptions in an adequate way. Having a high degree of complexity, the creation of either a mathematical complete model or a proper model for the automation and the optimization of the process of microwire casting, actually, faces highly difficult barriers [142]. We believe that pure physics or even a mathematical evaluation of such technique does not present any practical solution. Therefore, in many cases of controlling such casting process, the human eyes are more effective rather than any other automatic control. Thus, a lot of human experience in the field of microwire's production has been accumulated with the aim to optimize the control of this respective casting process.

In the laboratory process, an ingot containing a few grams of arc melted master alloys with the desired composition is put into a Pyrex-like glass tube and placed within a high frequency inductor heater as systematically drawn in Fig. 4.1. The alloy is heated up to its melting point, forming a droplet. While the metal melts, the portion of the glass tube adjacent to the melting metal softens, enveloping the metal droplet. A glass capillary is then drawn from softened glass portion and wound on a rotating coil. At suitable drawing conditions, the molten metal fills the glass capillary and a microwire is thus formed where the metal core is completely coated by a glass shell. The amount of glass used in the process is balanced by a continuous feeding of the glass tube through the inductor zone, whereas the formation of the metallic core is restricted by initial quantities of the master alloy droplet. The microstructure of a microwire and hence, its properties, mainly depends on the cooling rate, which can be controlled by a cooling mechanism

when the metal-filled capillary enters into a stream of cooling liquid water on its way to the receiving coil.

Regardless of the apparently simple fabrication method, the spinning process is quite complicated and the effective quenching rate is determined by large numbers of technological parameters like: the excess pressure inside the glass tube; the nozzle diameter; the gap between the nozzle and the cooling part; the quenching rate velocity; the bobbin rotation speed, the electromagnetic field from the inductor, the chemical interaction of the melt metallic alloy with the glass, the drawing stress and the temperature variance of the cooling liquid and quenching medium (gas/vacuum/air) etc [21, 34, 35, 142, 143]. In consequence, three types of microstructure have been established based on the crystallization degree and fabrication conditions [143]:

- Fully completed crystallization during the melt quenching, and obtaining single or multiphase microcrystalline structure.
- Partial or not complete crystallization during the melt quenching. As a result, an amorphous-nanocrystalline structure is formed with very unusual properties or,
- Melt quenching resulting in a complete amorphous state formation. In this case nanocrystals can be obtained by annealing under appropriate conditions.

Therefore, controlling the quenching process is ought to be roughly associated with the final structure of the produced microwire. In a similar way, the geometrical characteristics of a microwire depends on the physical properties of either the glass composition or the parameters of the heating inductor. The diameter of a microwire produced by Taylor-Ulitovsky method has both upper and lower limits depending on the speed of casting. Typical limits for the metallic core diameter are between 1-50 microns, while the thickness of the glass coating is in the range of 2-15 microns. It should be noted, that even during the stationary casting process, there is some variation in the metallic nucleus and, in turn, the glass coating thickness along the wire length. Depending on the required diameter, the precision can vary from 5% for wires in between 5-10 microns, to 10% for wires in the range between 10-50 microns [142, 143]. Therefore, we used either optical microscopy or scanning electron microscopy to estimate precisely the metallic nucleus diameter and the glass thickness of each produced sample.

## 4.2 Microstructural characterization techniques

### 4.2.1 Scanning Electron Microscopy (SEM)

The scanning electron microscope (SEM) uses a focused beam of high-energy electrons to generate a variety of signals at the surface of a solid specimens (Fig. 4.2) [144]. The signals that derive from electron-sample interactions reveal information about the sample including external morphology (texture), chemical composition, crystalline structure and orientation of materials making up the microwire.

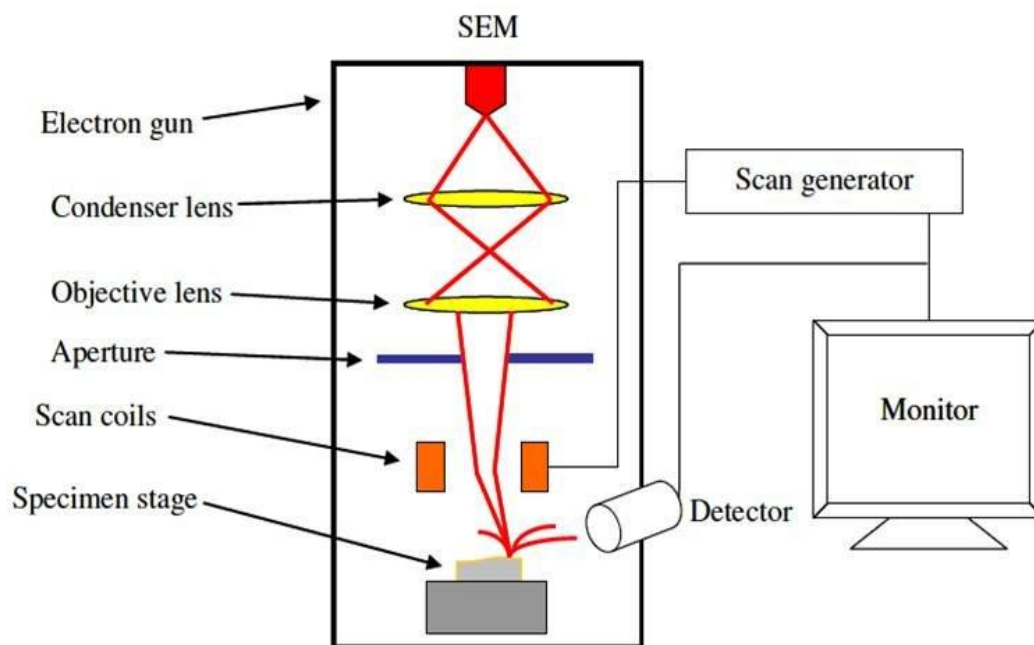


Figure 4.2 Scanning electron microscopy set-up.

A SEM picture presents the data which are collected over a selected area of the surface of the examined sample, and a 2-dimensional image is generated that displays spatial variations in these properties. SEM is also capable of performing analyses of selected point locations on the microwire: this approach is especially useful in qualitatively or semi-quantitatively determining chemical compositions using energy-dispersive X-ray spectroscopy (EDS).

The basic concept of SEM is based on the kinetic energy and accelerated electrons of a SEM beam. This energy is dissipated as variety of signals produced by electron-sample interactions when the incident electrons are decelerated in the sample. One of these signals produce SEM

image. The secondary and backscattered electrons are commonly used for imaging samples: secondary electrons are most valuable for showing morphology and topography of tested microwires, while backscattered electrons provide useful informations for illustrating contrasts in the chemical composition by EDS.

We used JEOL JSM-6390LV model for examining either the microwire geometries or chemical composition.

#### 4.2.2 Imaging with Axio Scope A1 microscopy

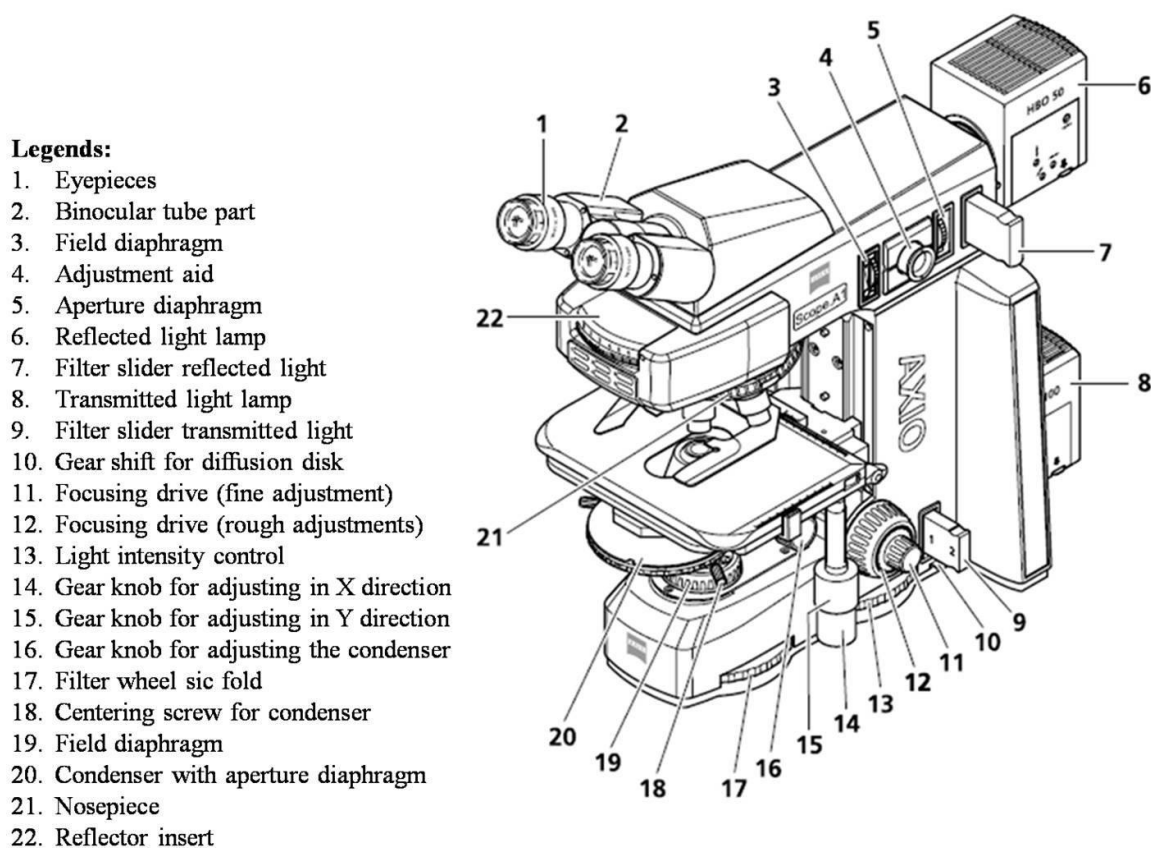


*Figure 4.3 Axio scope A1 microscopy*

Microscope Axio Scope A1 is an optical microscope which use visible light and system of lenses to magnify images of small (Fig. 4.3) [145]. In brief, two microscope components are of critical importance in forming the image: first, the objective lens, which collects light diffracted by the specimen and forms a magnified real image at the real intermediate plane near the eyepieces or oculars, and second, the condenser lens, which focuses light from the illuminator

onto a small area of the specimen. Since we want to have a closer look at the microwire geometry, a single wire is attached to a glass plate (worked as a sample holder) and placed under the microscope objective. The manipulation between different illumination sources as well as different microscope objectives, one can clearly obtain all desired information about the microwires diameters.

### 4.2.3 X-ray diffraction

X-rays are electromagnetic waves which, when incident on a material, interact with electrons inside the material and are scattered [146]. X-ray waves scatter from different electrons and interfere with each other. This interference gives the resulting diffraction pattern, the positions of diffraction peaks and their relative heights, in which the intensities vary with the scattering angle. Upon analysis of the diffraction pattern, information on the arrangement of atoms in a given lattice can be obtained: the shape and size of the unit cell are obtained directly from diffraction peak positions while the positions of atoms within the unit cell are related to the relative heights of the diffraction peaks. X-rays are useful in determining lattice structures because their wavelengths are on the order of 1 angstrom, that is the same order of magnitude as the interatomic distances in condensed matter.

X-rays scattered from the periodic repeating electron density of a perfectly crystalline material give sharp diffraction peaks at angles that satisfy the Bragg's relation (see below), whether the crystal consists of atoms, ions, small molecules, or large molecules. Amorphous materials will also diffract X-rays and electron, but the diffraction is a much more diffuse, low frequency halo the so-called amorphous halo. Analysis of the diffraction peaks from amorphous materials leads to provide information about the statistical arrangement of atoms in the neighborhood of another atom.

### 4.2.4 Bragg's law

When X-rays are scattered from a crystal lattice, observed peaks of scattered intensity, which correspond to the angle of incidence, should be equal to the angle of scattering while the path length difference is equal to an integer number of wavelengths. Bragg derived Bragg's law [147] for the distance  $d$  between consecutive identical planes of atoms in the crystal:

$$n\lambda = 2d \sin \theta \quad (4.1)$$

where the parameter  $n$  is the order of reflection, or the path difference in number of wavelengths of radiation scattered by adjacent planes of lattice atoms,  $d$  is the interplanar spacing for a given set of  $hkl$ ,  $\lambda$  is the wavelength, and  $\theta$  is the Bragg angle as shown in Fig. 4.4.

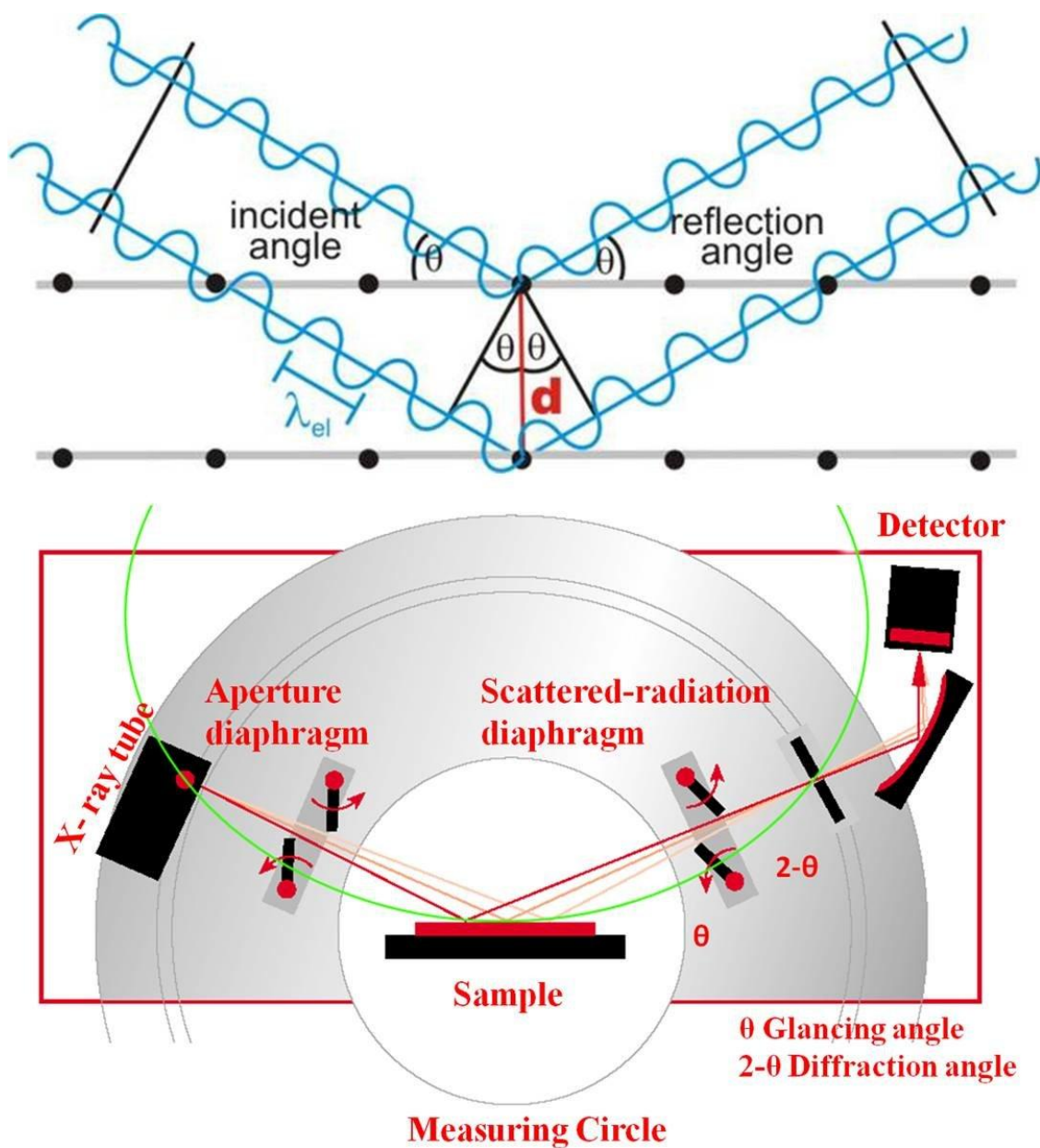


Figure 4.4 Geometrical illustrations of crystal planes and Bragg's law (above) and diffractometer beam path in  $\theta/2\theta$  mode (below).



Based on equation (4.1), the structure of the solid (i.e. the distance between the atoms) can be obtained if a monochromatic X-ray source is used (only at fixed value of  $\lambda$ ) and the intensity of X-rays are measured as a function of  $\theta$ . A schematic diagram of a diffractometer system is displayed in Fig. 4.4 where we see that the diffractometer consists of a main goniometer being:  $\theta$  the glancing angle;  $2\theta$  the diffraction angle, and  $\alpha$  the aperture angle [148, 149]. The process of reflection is described here in terms of incident and reflected (or diffracted) rays, each of which making an angle,  $\theta$ , with a fixed crystal plane. Reflections occurs from planes set at angle,  $\theta$ , with respect to the incident beam and generates a reflected beam at an angle,  $2\theta$ , from the incident beam. The  $2\theta$  values for the peak depend on the wavelength of the anode material of the x-ray tube. It is therefore reasonable to reduce the peak position to the interplanar spacing  $d$  that corresponds to the  $h, k, l$  planes that caused the reflection. The value of the  $d$ -spacing depends only on the shape of unit cell, and therefore, we get the  $d$ -spacing as a function of  $2\theta$  from Bragg's correlation (4.1).

#### 4.2.5 Powder X-ray diffraction (XRD)

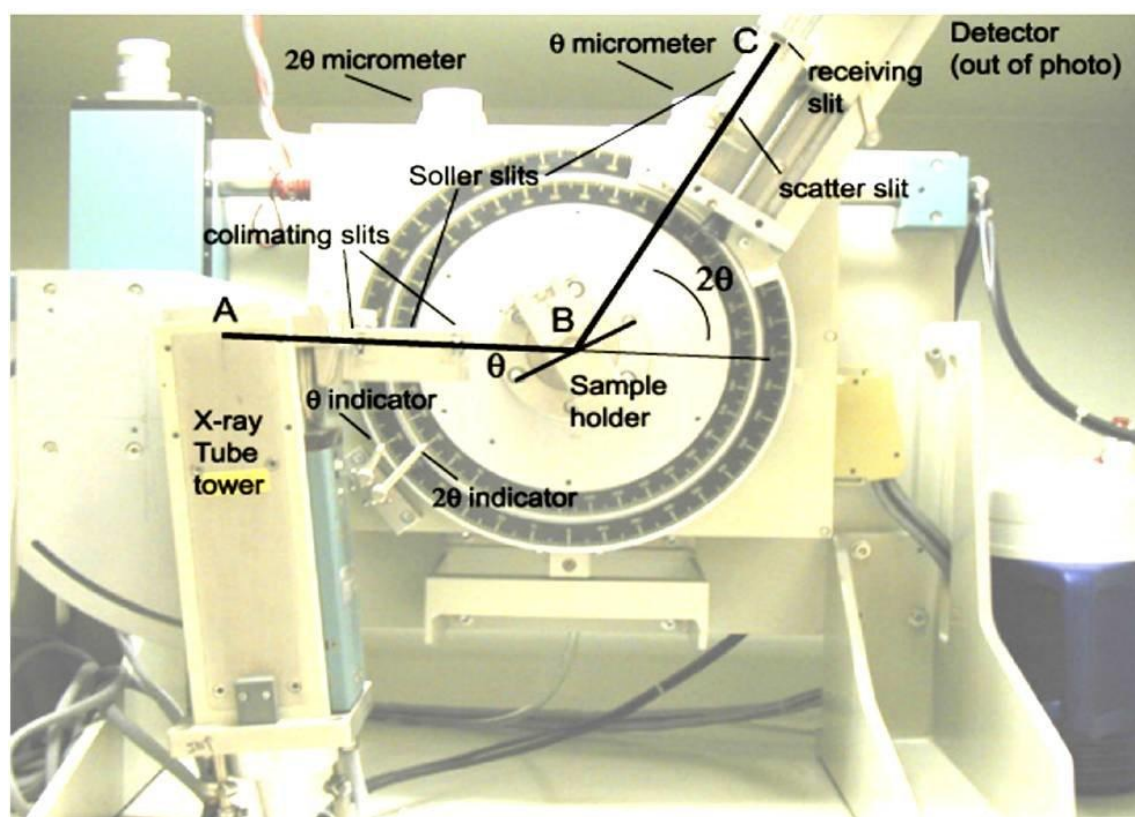


Figure 4.5 Powder X-ray diffractometer.

In our XRD, demonstrated in Fig. 4.5, the path  $AB=BC$  is the radius of the diffractometer circle. The tube position is fixed and the  $\theta$ - $2\theta$  geometry is maintained by rotating the sample holder at  $\frac{1}{2}$  the angular rate of the detector. There are soller slits on both the tube and detector side, and two collimating (that can be automatically changed in order to always illuminate the same area of the sample) and receiving slits. The detector in this system also includes a graphite monochromator adjacent to the scintillation detector eliminating the need for any filters in the system.

The X-ray powder diffraction technique was used to characterize both the crystal structures and phase compositions of most of studied microwires. The samples were attached to the diffractometer's sample holder at which each scan was made over the two theta angular range of 30 to 90 degrees, step size of  $0.05^\circ$  and a step time of 30 second for each step. The diffraction peaks were indexed using JCPDS (joint committee on powder diffraction standards) database. For all X-ray diffraction experiments presented, a BRUKER (D8 Advance) X-ray diffractometer with  $\text{CuK}\alpha$  ( $\lambda = 0.15406 \text{ nm}$ ) radiation was used and operated at applied voltage of 40 KV and filament current of 30 mA. The phase identification of all as-synthesized samples reported was performed by matching the peak positions and intensities in the experimental diffraction patterns to those patterns in the JCPDS.

## 4.3 Magnetic characterization techniques

### 4.3.1 Hysteresis loops

When a ferromagnetic material subjects to a magnetic field, their magnetization changes in a complex way [43, 45], which is described by a magnetization curve as depicted in Fig. 4.6. Starting from a demagnetized state ( $M = H = 0$ ), the magnetization increases with increasing the field along the curve  $OABC$  and finally reaches the saturation magnetization, which normally denoted by  $M_s$ . In the region  $OA$  the process of magnetization is almost reversible: that is, the magnetization returns to zero when the magnetic field removed. The slope of the curve  $OA$  called the initial susceptibility  $\chi_a$ . Beyond this region the processes of magnetization are no longer reversible. If the field is decreased from its value at point  $B$ , the magnetization comes back, but not along  $BAO$ . The slope at any point on the initial magnetization curve  $OABC$  called the differential susceptibility  $\chi_{diff}$ , and the slope of the line which connects the origin  $O$  and any



point on the initial magnetization curve is known as the total susceptibility  $\chi_{tot}$ . The maximum value of the total susceptibility, that is, the slope of the tangent line drawn from the origin  $O$  to the initial magnetization curve, called the maximum susceptibility  $\chi_{max}$ .

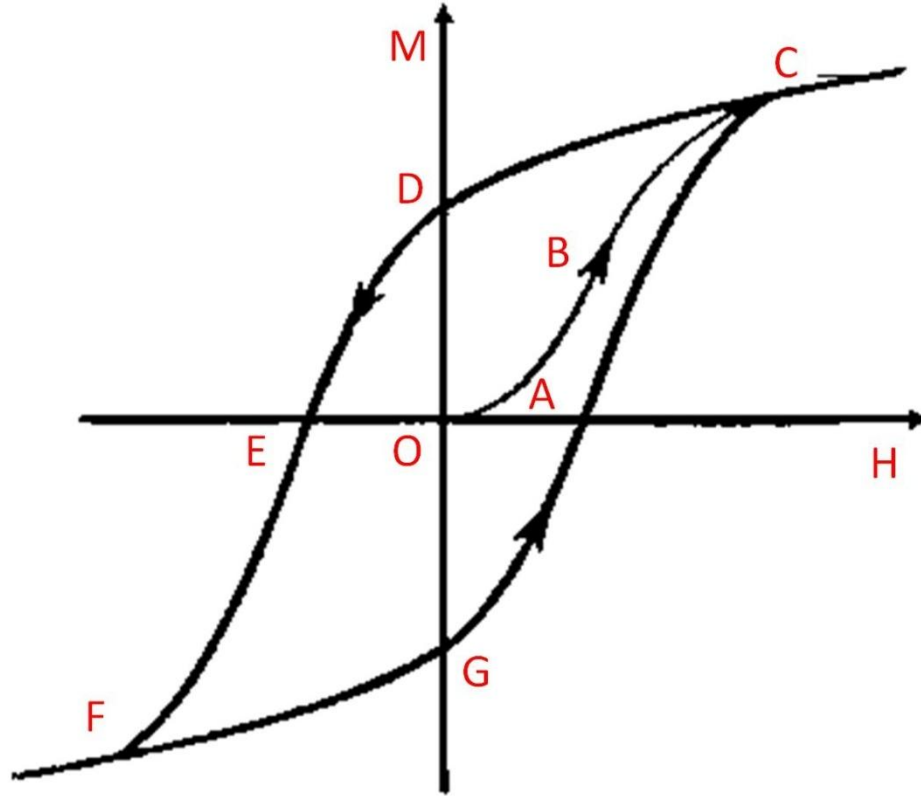


Figure 4.6 Typical hysteresis loop of soft magnet.

If the magnetic field is decreased from the saturated state  $C$ , the magnetization  $M$  gradually decreases along  $CD$ , not along  $CBAO$ , and  $H = 0$  it reaches the non-zero value ( $M_r = OD$ ), which called the residual magnetization or remanence. Further increase of the magnetic field in a negative sense result in a continued decrease in the intensity of magnetization, which finally falls to zero. The absolute value of the field at this point called the coercive field or the coercive force ( $H_c = OE$ ). This portion,  $DE$ , of the magnetization curve is often referred as the demagnetizing curve. Further increase of  $H$  in a negative sense results in an increase in the intensity of magnetization in a negative sense too and finally to negative saturation magnetization. If the field is then reversed again to the positive sense, the magnetization will change along  $FGC$ . The closed loop  $CDEFGC$  called the hysteresis loop.

### 4.3.2 The induction flux-metric method for hysteresis loops measurements

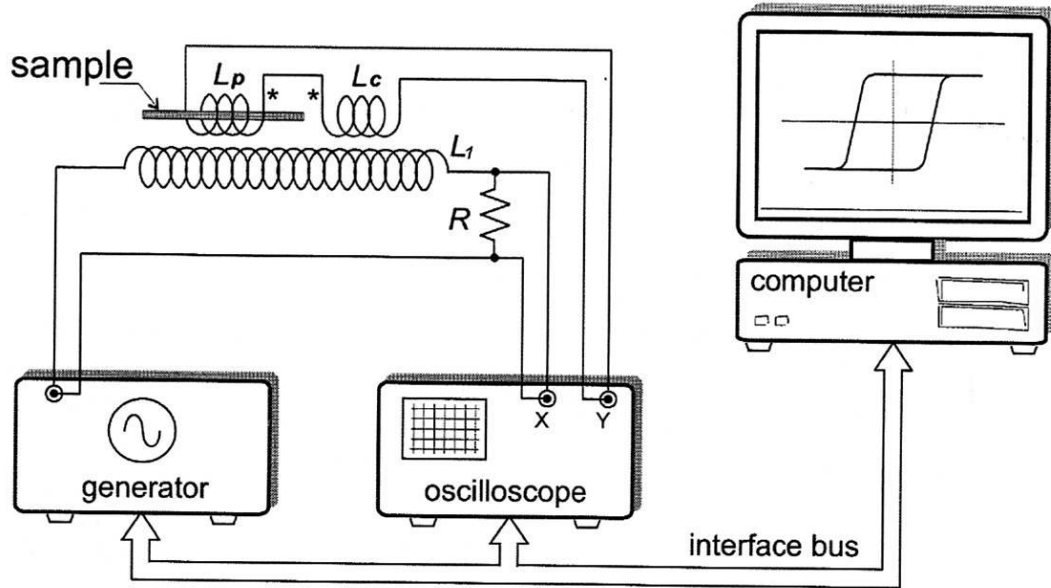


Figure 4.7 Connection scheme of the induction method for measuring hysteresis loops.

A sketch of a scheme set-up of hysteresis loop measurements is presented in Fig.4.7. The hysteresis loop can be obtained by induction method, according to Faraday's law [43, 45]:

$$\epsilon = -N \frac{d\phi}{dt} \quad (4.2)$$

where,  $\epsilon$  is the electromotive force and  $N$  is the number of turns in a coil through which the flux  $\phi$  is changing.

In the case of microwire, when the sample occupies a small part of the coil cross-section, the flux from the external field can be dominated. It is necessary to take into account the existence of both paths of magnetic flux originating from the sample magnetization  $M$  and from the magnetic field  $H$ :

$$\phi = \mu_0 [(A_c - A_s)H + A_s(H + M)] = \mu_0 [A_c H + A_s M] \quad (4.3)$$

where  $A_c$  and  $A_s$  are the coil and sample cross-section areas. Then the induced in pick-up coil voltage contains two components

$$\epsilon = -\mu_0 N \frac{d(A_c H + A_s M)}{dt} = -\mu_0 N \left[ A_c \frac{dH}{dt} + A_s \frac{dM}{dt} \right] \quad (4.4)$$

To eliminate the component  $A_c (dH/dt)$ , arising from the external magnetic field, the identical compensation coil is used. This second coil is connected in series- opposition with the pick-up coil, thus the electromotive force depends only on the sample magnetization change rate:

$$\epsilon = -\mu_0 N A_s \frac{dM}{dt} \quad (4.5)$$

and is zero in the absence of sample. The magnetization of the sample is obtained by integration of the induced voltage:

$$M = \frac{1}{N\mu_0 A_s} \int \epsilon dt \quad (4.6)$$

In all the hysteresis loops measurements have been performed at a fixed frequency (113 Hz). We represent the hysteresis loops as the normalized magnetization,  $M/M_s$  versus the applied magnetic field,  $H$ , where  $M_s$  is the magnetic moment of the sample at the maximum magnetic field amplitude,  $H_o$ .

### 4.3.3 Annealing processes

Mostly, the techniques used to perform thermal treatments involve the examined specimen heated in air/vacuum conventional furnace for a given time. The heating unit of the furnace as can be clearly seen in Fig. 4.8 is held by a stand and can be easily adjusted in two different positions either horizontally or vertically. Beyond the conventional annealing treatment, a single piece or bunch of microwires are placed inside the furnace in the horizontal position. The temperature and time of annealing are, then, to be regulated through a temperature/time control with the desired conditions. In most cases, the samples are cooled down slowly to room temperature inside the furnace. In addition to the classical way of annealing, we have performed another kind of annealing under tensile mechanical stress the so-called stress annealing. Stress annealing processes have been performed in the same conventional furnace but in such case the furnace is to be stand in the vertical position (Fig. 4.8). During the annealing process, a mechanical load has been introduced into one end of the microwire and axially placed via the

furnace nozzle. The final value of the applied tensile stress within the metallic nucleus and the glass layer has been calculated according to the following algorithms [150];

$$\sigma_m = \frac{K.P}{K S_m + S_{gl}}, \sigma_{gl} = \frac{K}{K S_m + S_{gl}} \quad (4.7)$$

where  $k = E_2/E_1$  are the Young moduli relations of the metallic nucleus and the glass cover, at the room temperature respectively.  $P$  is the applied mechanical load, and  $S$  is the microwire's cross sectional area ( $\pi r^2$ ).

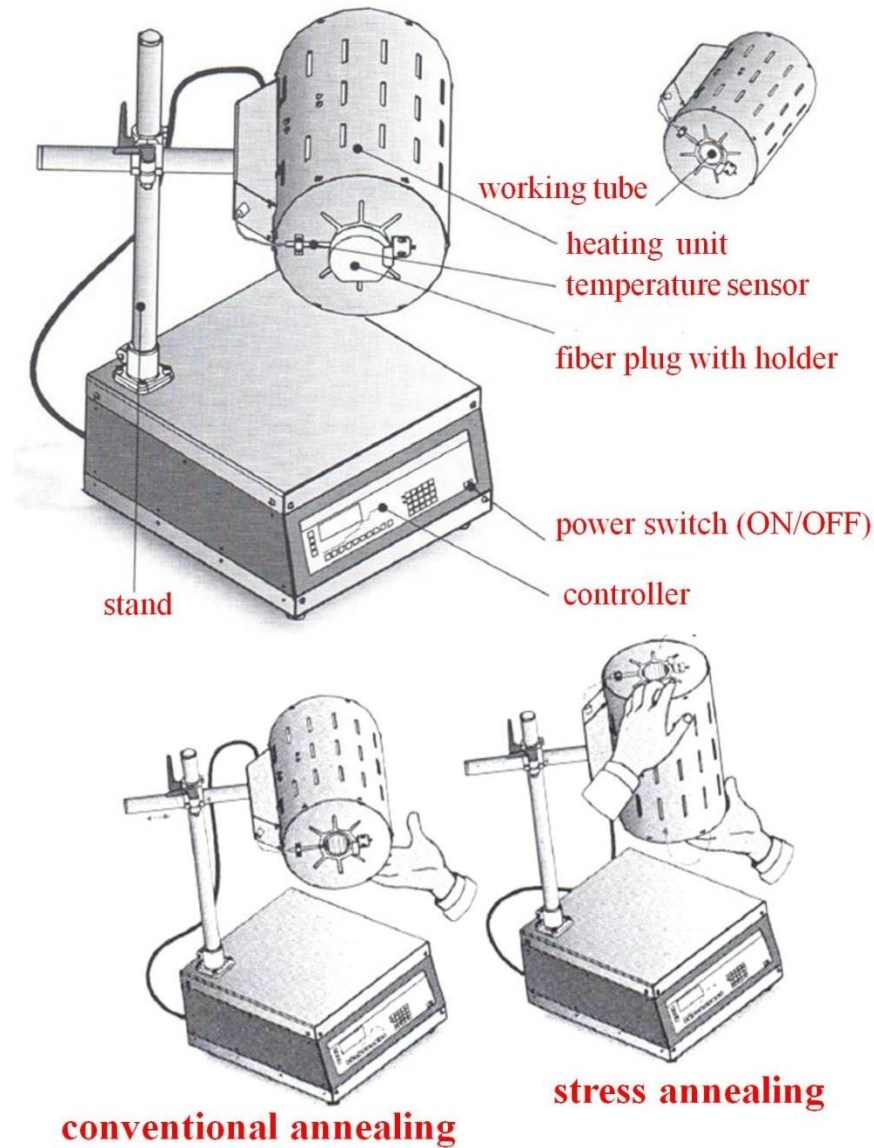


Figure 4.8 Conventional and stress annealing process.

We have also performed another kind of annealing in presence of current or so-called current annealing. In this case, the temperature increases by the Joule effect which has been produced by passing current onto the sample. Within this method, such current produce some temperature homogeneity within the sample as well as control the annealing time, exceeding the other traditional methods in various aspects. The heating process is released by an electrical current  $I$  passing into the microwire. The total power used to heat the wire is proportional to the electrical current  $I$  squared:

$$P = I^2 R \quad (4.8)$$

where  $R$  denotes an electrical resistance of the wire and  $P$  the total power released by electric current. The glass-coated layer was mechanically removed at both ends of small piece of the microwire (2 cm in length) in order to make an electrical contact. The microwire then was attached to a high-temperature resistive sample holder by the help of two screws plugged to a power supply.

#### 4.3.4 Giant magneto-impedance (GMI) measurements

The impedance measurements as a function of the applied magnetic field, that allow characterizing of GMI response in ferromagnetic materials, are usually performed using a four point technique (volt–amperometric measurements) at low frequencies range [151]. However, at high frequencies, the external inductance of the measuring set-up can greatly mask the effect [152]. This unwanted contribution to the measured impedance hinders the interpretation of the results in terms of proposed theories [153]. Besides, at higher frequencies, the wavelength of the electromagnetic field gets compared to the size of the test setup, and propagation phenomena must also be taken into account (non-quasi-static regimen). In order to overcome these limitations, vector network analyzer (VNA) technique is necessary. As a consequence, both low and high frequency regimes are very challenging by this technique obtaining an accurate impedance measurements at the microwave frequency range, and of course, avoiding the undesired contributions of such issues.

### 4.3.5 Vector network analyzer (VNA)

Network analysis is the process by which designers and manufacturers measure the electrical performance of the components and circuits used in more complex systems. When these systems are conveying signals with informative content, we are most concerned with getting the signal from one point to another with maximum efficiency and minimum distortion. Vector network analysis is a method of accurately characterizing such components by measuring their effect on the amplitude and phase of swept-frequency and swept-power test signals [154].

This technique is based on the  $S$ -parameters [155, 156], which consists in the measurements of the transmission and reflection coefficient of a dual-port device, the simplest measurement cell may be transmission-line whose inner conductor is made by the magnetic wire. In a transversal electromagnetic-line (TEM-line) both the electric and magnetic vectors are always orthogonal to the direction of the propagation which is coincident with the length of the magnetic sample. Mainly, there are two kinds of sample holders: coaxial transmission line and microstrip line depending on the measurements type desired [156, 157]. In both sample holder cases, a single piece of 6 mm length of microwire was fixed to the sample holder by the help of sliver loaded adhesive. A schematic diagram of the experimental set-up is shown in Fig. 4.9.

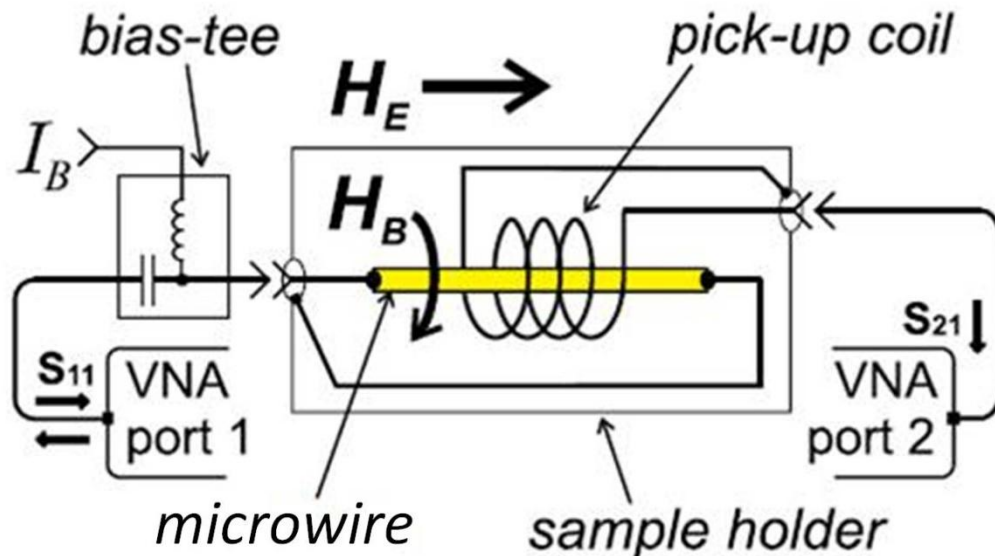


Figure 4.9 Set-up diagram of GMI measurements.

A single piece of 6 mm length of the microwire was placed in a specially designed microstrip sample holder, that is placed inside a long solenoid that creates a homogeneous magnetic field up to 15 kA/m along the microwire axis. The system allows the application of a circular/transversal bias field  $HB$  created by a DC bias current  $IB$  applied to the sample through a bias-tee element. The longitudinal (diagonal) impedance  $Z_{\phi z}$  is determined with an Agilent N5230A vector network analyzer (VNA) from the reflection coefficient  $S_{11}$  measurements, and the off-diagonal impedance can also be measured from the transmission coefficient  $S_{21}$  as a voltage induced in a 2-mm long pick-up coil wounded over the microwire. The frequency range for the off-diagonal component  $Z_{\phi z}$  was 10–300 MHz, while the diagonal impedance component has been measured until 7 GHz.

#### 4.3.6 Domain wall (DW) propagation measurements

Sixtus and Tonks were in between the first scientists who gave a trail to study the domain wall dynamics on the last century [158]. They built up a simple method to measure the domain wall velocity in magnetic wires. They did use an apparatus consisting of a primary coil with the aim to produce a homogenous magnetic field to facilitate the domain wall propagation and short nucleation coil needed to nucleate the domain wall.

In contrast to the classical method proposed by Sixtus-Tonks experiment, we used a system of three pick-up coils for estimation of the DW velocity as shown in Fig. 4.10. We do not need the nucleation coils since small closure domains are spontaneously appear at the end of the wire in order to decrease the stray field [159]. In addition, we placed one end of the sample (marked as 4 in Fig. 4.10) outside the magnetization solenoid in order to activate DW propagation always from the other wire end in our experimental setup. The microwire of 10 cm length is placed coaxially inside of the primary and three pick-up coil ( $p_1$ ,  $p_2$  and  $p_3$ ) so that one end is inside of the primary coil as depicted in Fig. 4.10. The magnetic field,  $H$ , is generated by a solenoid applying rectangular shaped voltage. More recently, it has been found that at high enough applied magnetic field the domain wall can nucleate in the middle of microwire on defects. Therefore we later modified once more the experimental setup adding the third pick-up coil [160]. We used 3 pick-up coils with distances  $d_{1-2}$  and  $d_{2-3}$  between coils of 27 mm mounted along the length of the wire. The detected voltage pulses in each pick-up coil are shown in Fig. 4.10 which represents screen-captured images displaying an averaged induction signal arising



during the DW propagation. The voltage pulses have a width that is a substantial fraction of their spacing, indicating qualitatively that the domain walls indeed are far from abrupt [159, 160]. The propagation DW induces electromotive force (*emf*) in the coil which are picked up at an oscilloscope upon passing the propagating wall.

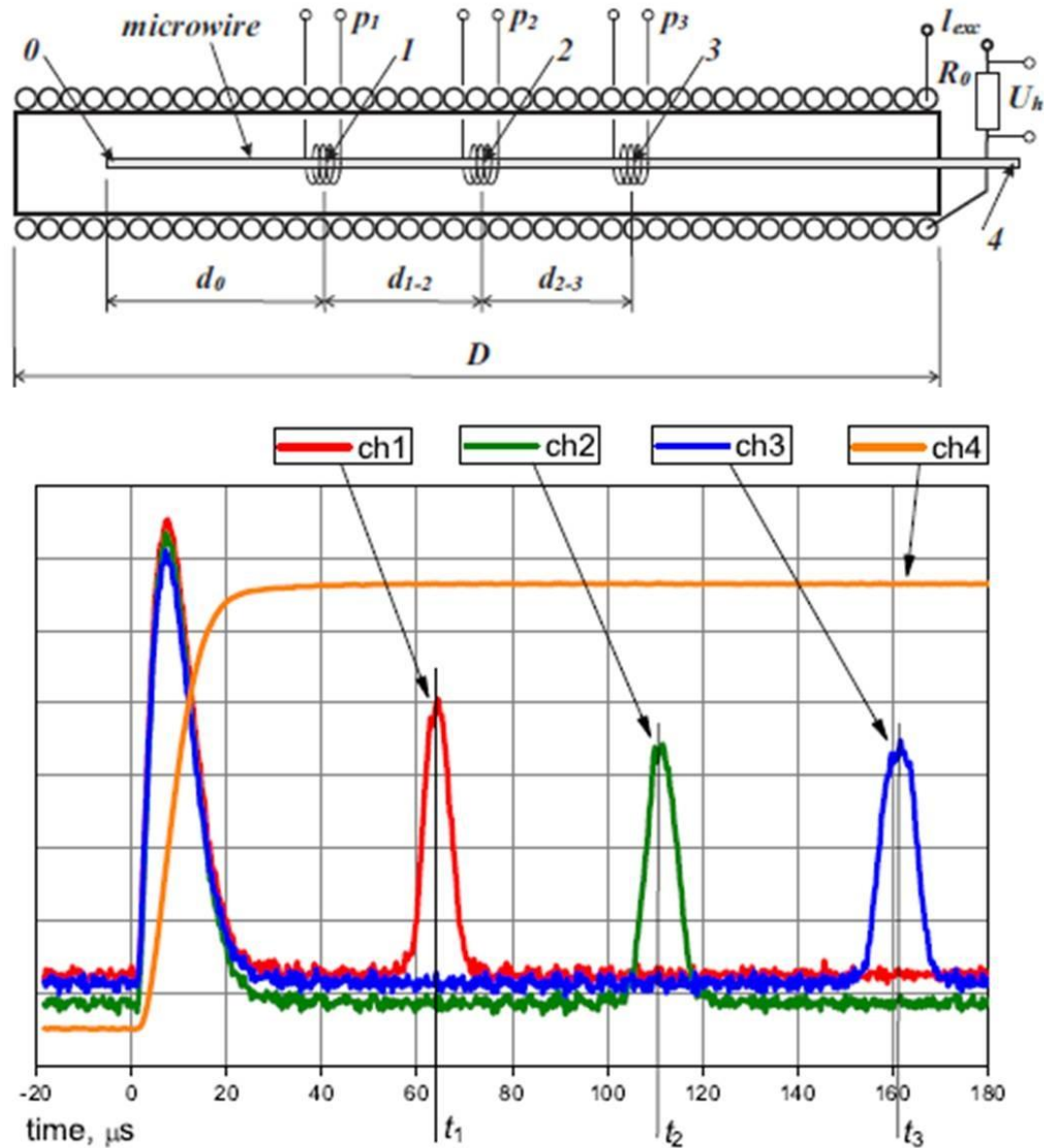


Figure 4.10 Schematic picture of experimental set-up for DW measurements, and signal waveform voltage pulsed captured by the oscilloscope. Pick-up coils  $p_1$ ,  $p_2$  and  $p_3$  are connected to channels 1, 2 and 3 respectively. The voltage  $U_h$  is captured by channel 4



The DW velocity is estimated as:

$$v = \frac{d}{\Delta t} \quad (4.9)$$

where  $d$  is the distance between pick-up coils and  $\Delta t$  is the time difference between the maximum in the induced *emf*.

We have also measured DW velocity under the application of external applied stress. Tensile stresses have been applied during the DW measurements. The loads have been introduced at the end of the microwires, where its placed outside the magnetization solenoid (point number 4 in Fig. 4.10) and the final value of the applied tensile stress within the metallic nucleus and the glass layer has been calculated according to the same algorithms (4.7) described before.

#### 4.3.7 Small angle magnetization rotation (SAMR) for magnetostriction measurements

The magnetostriction coefficient of microwires has been measured using SAMR method [161, 162]. During the measurements the initial tensile stress,  $\sigma_0$ , is created by a weight  $m_0$  attached to the microwire end. An axial magnetic field,  $H_z$ , is created along the microwire  $z$ -axis using the solenoid. In this method the sample is saturated by an axial magnetic field,  $H_z$ , while applying simultaneously a small *ac* transverse field,  $H_y$ , created by an *ac* electric current flowing along the sample. The combination of these fields leads to a reversible rotation of the magnetization within a small angle,  $\theta$ , out of the axial direction. The induction voltage,  $V(2\omega)$ , due to the magnetization rotation is detected by a pick-up coil wound around the microwire. The magnetostriction constant is determined from the measurement of the dependence on axial magnetic field,  $H_z$ , versus on applied stress,  $\sigma$ , at fixed value of induction voltage  $V(2\omega)$  in according to the following expression [163]:

$$\lambda_s = - (\mu_0 M_s / 3) (dH/d\sigma) \quad (4.10)$$

where  $\mu_0 M_s$  is the saturation magnetization

The  $\mu_0 M_s$  values of the investigated microwires obtained from room temperature measurements of the magnetization curves at high magnetic field.

The AC current value,  $i_z$ , flowing through the wire is selected to avoid possible Joule heating of the sample: the current amplitude does not exceed 10-30 mA. As far as the current flows through the wire with frequency,  $f$ , therein the alternating circular magnetic field  $Ht$  occurs. It leads to a periodic deviations of magnetization vector,  $I_s$ , from  $z$ -axis at an angle  $\theta$ . In this case, the component of the magnetization  $I_z$ , coinciding with the direction of the microwire axis, varies in time with double frequency  $2f$ . Due to the temporal change of the magnetization component  $I_z$  with frequency  $2f$ , the electromotive force (*emf*) occurs in compensated measuring coil with a frequency equal to  $2f$ . This *emf* signal is amplified and detected in the measuring block. In this method, it is assumed the constancy of deviation angle  $\theta$  of magnetization vector  $I_z$  from microwire axis (coordinate  $z$ ) during the measurement. The constancy of the angle  $\theta$  at measurements corresponds to a constant value of voltage in the measuring coil (detected during the measurements). Fixing of angle  $\theta$  can be achieved by joint changing of the initial field of the solenoid  $H_{z0}$  (by an amount  $\Delta Hz$ ) and initial stress  $\sigma_0$  (by an amount  $\Delta\sigma$ ). It can be shown that under these conditions ( $\theta = \text{constant}$  and  $Ht = \text{constant}$ ) the value of magnetostriction coefficient, can be clearly obtained by the expression (4.10).

During an experiment, a small mechanical loads were consistently attached to the microwire. Measurement of *emf* signal dependences on the magnetic field of the solenoid  $U_{2h}$  ( $Hz$ ) were carried out for every load by pick-up coils. We evaluated the average magnetostriction coefficient after several measurements of each sample of about 14 cm length.

#### 4.3.8 Magnetic hyperthermia measurements

In order to perform the hyperthermia experiments, the microwires were cut into 5 mm strands. Multiple different configurations of microwire alloy, diameter, orientation, quantity, and separation were examined. Additionally, the sample that demonstrated the best heating was used for additional experiments including orientation, i.e. horizontal versus vertical, and the effects of using multiple microwires.

The single microwire samples were prepared by inserting a single piece of about 5 mm in length into a glass vial filled with 1 mL of deionized water. To test for orientation, the single microwire was placed into a 2% agar solution that would maintain the orientation of the microwire even under high magnetic fields. The orientation was imposed by the use of a small

external permanent magnet and physically aligning it in solution before the agar cooled completely. Multiple microwire testing was done both in water and in agar. The tests in water would demonstrate natural microwire orientation in movement in a random distribution. On the other hand, the tests in agar were specifically done in different distributions or orientations, i.e. in situations where the wires are together, separated, and horizontal. The microwires in the multiple microwire experiments were also 5 mm in length.

In this experiment, we have used an Ambrell Easyheat system that can generate an alternating magnetic field at a frequency between 150–400 KHz. Fig. 4.11 shows an image of the water refrigerated multi-turn helical coil connected to a radio frequency power amplifier. Power to the system is provided by a generator. During the hyperthermia experiments, for each sample, the temperature evolution with time has been monitored while applying an external AC field, between 400 and 800 Oe, at a constant frequency of 310 KHz. The temperature was monitored by using a digital temperature probe which automatically recorded the data to the PC.



Figure 4. 11 Magnetic hyperthermia system employed. Generator on the left and radio frequency amplifier on the right.

The heating efficiency, also known as the specific absorption rate (*SAR*), of the microwires has been estimated following calorimetric methods: the initial slope  $\Delta T/\Delta t$  of the sample has been obtained from the measured curves, and the *SAR* values have been derived from the following formula:

$$SAR = \frac{m_s}{m_w} C_p \frac{\Delta T}{\Delta t} \quad (4.11)$$

where  $C_p$  is the specific heat of the solution,  $m_s$  the mass of the solution,  $m_w$  the mass of the microwires, and  $\Delta T/\Delta t$  the initial slope of the heating curves. The mass for one single piece of microwire was calculated to be 0.24 *mg*.

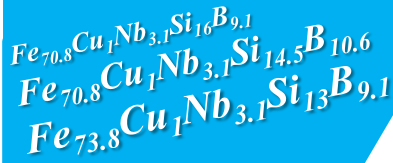
The *SAR* measurements in agar were done in an identical way as it was assumed that the heat capacity change was negligible. In order to remove the heating contribution coming from the coil, we have subtracted the slope measured for the vial without sample from all our measurements. The initial slope was taken shortly after heating began but far before the sample reached temperature saturation, i.e. when the temperature increase was nearly linear.

# Part II

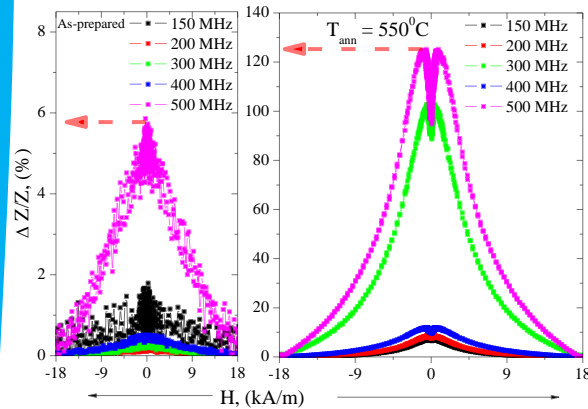
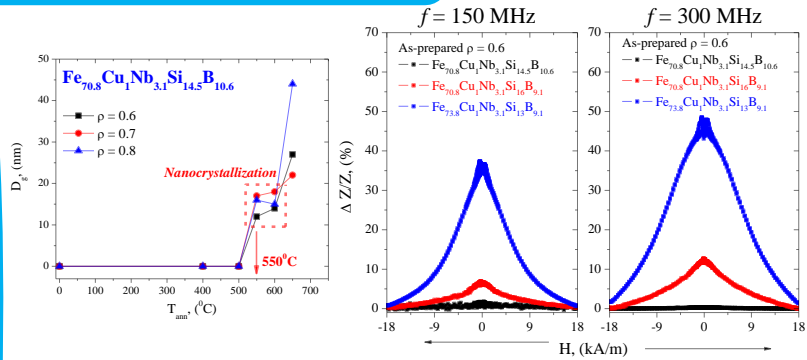
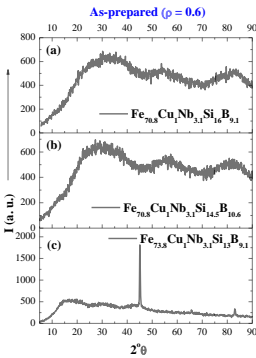
## *Results & discussion*

- 
- Chapter 1: Optimized giant magneto impedance effect (GMI) in thin microwires composed of Finemet-like alloys
  - Chapter 2: Nanocrystalline Hitperm alloys: A structural investigation and magnetization process
  - Chapter 3: Engineering of Co-based amorphous microwires by annealing
  - Chapter 4: Magnetic hyperthermia of Fe-based alloys
  - Chapter 5: Conclusions
-





# Optimized giant magneto impedance effect (GMI) in thin microwires composed of Finemet-like alloys

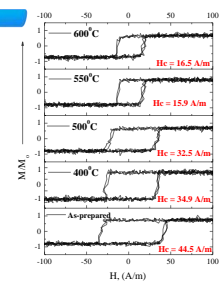
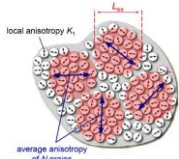


An optimized 125% GMI ratio observed at  $f = 500$  MHz of the poor (1%) response of amorphous Finemet as-prepared microwire samples. GMI values of about 50% for  $f = 300$  MHz are observed for as-prepared microwire samples with nanocrystalline structure.

# 1

# FINEMET

# ALLOY®



## 1.1 Finemet alloys

Chapter 2: glass-coated microwires as a research tool, pointed out the main aspects related to an excellent magnetic softness achieved in nanocrystalline materials. A pioneer alloy composition to accomplish a nanoscale magnetic structure with a unique magnetic softness was found in *Finemet*-like alloys and their derivatives. A feasible instance, on the other hand, to employ such extremely magnetic softness is in connection with oriented applications of GMI discussed as well in chapter 3.

This chapter, therefore, continues with our practical experiences on the investigation of *Finemet*-like glass-coated microwires. A systematic research is beyond the scope of three *Finemet* alloy compositions with either different metallic nucleus diameters or glass thicknesses. We take the somewhat leading perspectives of nanocrystallization phenomena that underlie the technological promise of GMI responses. The major object, herein, combines achieving a remarkable magnetic softness with an ultra fine grain size obtained either through a proper annealing treatment or by controlling the quenching rate and fabrication conditions.

## 1.2 Alloy chemical compositions and microwires dimension

Table 1.1 collects investigated *Finemet* glass-coated microwires with different dimensions and compositions. Internal stresses are arising from either the difference in thermal expansion coefficients of metallic nucleus and glass coating or from rapid solidification from the surface of metallic nucleus. As can be seen in this table, different values of internal stresses are determined by the different dimensions of the metallic core and total diameter. The strength of internal stresses is related to the difference of thermal expansion coefficients is determined by (the geometric ratio,  $\rho$ : the ratio between metallic nucleus diameter,  $d$ , and total diameter,  $D$ ). These stresses together with the magnetostriction coefficient form the major contribution to the magnetoelastic anisotropy. The magnetoelastic anisotropy,  $K_{me}$  (see eq. 2.5 page 18), gives rise to different values of coercive fields. Solid evidences in support of these facts are presented in Fig. 1.1 a-b.

Fig 1.1a supports the fact that the higher internal stresses strength (ascribed by low geometric ratio,  $\rho$ ), the higher the magnetoelastic anisotropy,  $K_{me}$ . Thus, the coercive field



strongly increases as the  $\rho$ -ratio decreases: the coercivity increases from 50 A/m for  $\rho = 0.7$  up to 172 A/m for  $\rho = 0.3$ .

*Table 1.1* Chemical composition, dimensions, and geometric ratios of tested Finemet glass-coated microwires

Chemical composition	Metallic nucleus, $d$ , diameter ( $\mu\text{m}$ )	Total diameter, $D$ , ( $\mu\text{m}$ )	Geometric ratio, $\rho$ , $d/D$
$\text{Fe}_{70.8}\text{Cu}_1\text{Nb}_{3.1}\text{Si}_{16}\text{B}_{9.1}$	14.2	23.0	0.6
	11.4	15.2	0.7
	12.8	15.8	0.8
$\text{Fe}_{70.8}\text{Cu}_1\text{Nb}_{3.1}\text{Si}_{14.5}\text{B}_{10.6}$	10.7	16.4	0.6
	15.6	21.8	0.7
	11.8	14.4	0.8
$\text{Fe}_{73.8}\text{Cu}_1\text{Nb}_{3.1}\text{Si}_{13}\text{B}_{9.1}$	14.6	24.2	0.6

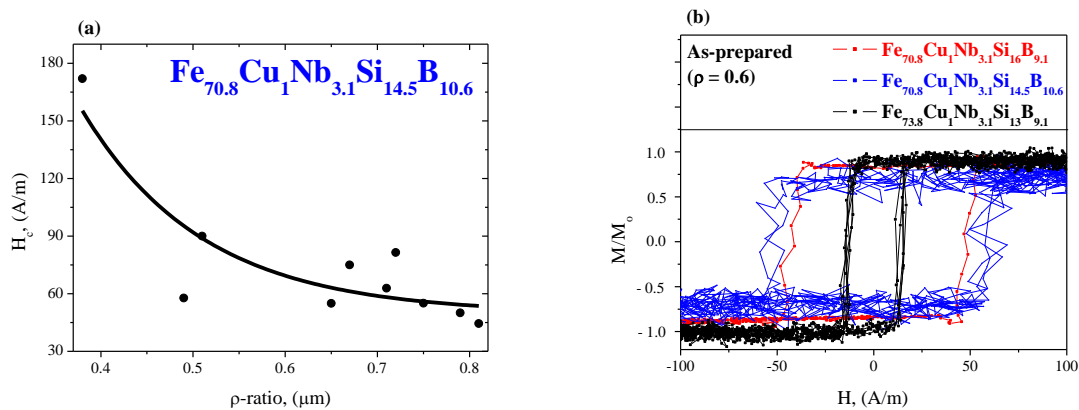


*Figure 1.1* Coercive field dependence on  $\rho$ -ratio for as-prepared  $\text{Fe}_{70.8}\text{Cu}_1\text{Nb}_{3.1}\text{Si}_{14.5}\text{B}_{10.6}$  glass-coated microwires (a), hysteresis loops of as-prepared  $\text{Fe}_{70.8}\text{Cu}_1\text{Nb}_{3.1}\text{Si}_{16}\text{B}_{9.1}$ ,  $\text{Fe}_{70.8}\text{Cu}_1\text{Nb}_{3.1}\text{Si}_{14.5}\text{B}_{10.6}$ , and  $\text{Fe}_{73.8}\text{Cu}_1\text{Nb}_{3.1}\text{Si}_{13}\text{B}_{9.1}$  Finemet glass-coated microwires with the same  $\rho$ -ratio = 0.6 (b).

On the other hand, all studied samples present rectangular hysteresis loops (Fig. 1.1b) typical for all amorphous Fe-based glass-coated microwires. For comparison, we have selected three microwire samples with the same  $\rho$ -ratio = 0.6 as shown in table 1.1 but with different chemical alloy composition. Surprisingly, a rather low coercive field of about 12 A/m is obtained for  $\text{Fe}_{73.8}\text{Cu}_1\text{Nb}_{3.1}\text{Si}_{13}\text{B}_{9.1}$ , while for either  $\text{Fe}_{70.8}\text{Cu}_1\text{Nb}_{3.1}\text{Si}_{16}\text{B}_{9.1}$  or  $\text{Fe}_{70.8}\text{Cu}_1\text{Nb}_{3.1}\text{Si}_{14.5}\text{B}_{10.6}$  the coercivity is much more higher (about 50 A/m) for both compositions. These three microwires differ perhaps more significantly in another way related to the origin of their microstructure. To elucidate these discrepancies of the coercive field behavior, we have performed structural investigation of all studied *Finemet* microwires as will be analyzed in the next section.

### 1.3 Microstructure investigation

Fig. 1.2 shows XRD patterns of three as-prepared *Finemet* glass-coated microwires with different chemical compositions and the same  $\rho$ -ratio = 0.6.

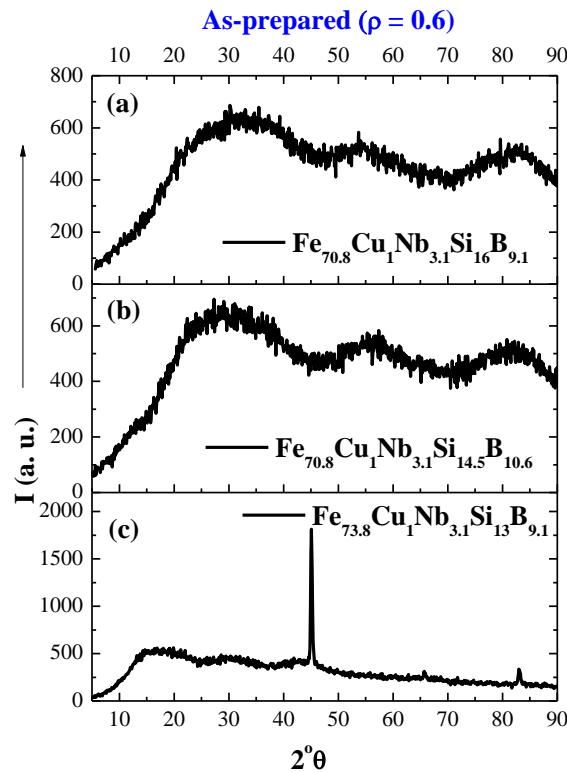


Figure 1.2 XRD of as-prepared  $\text{Fe}_{70.8}\text{Cu}_1\text{Nb}_{3.1}\text{Si}_{16}\text{B}_{9.1}$  (a),  $\text{Fe}_{70.8}\text{Cu}_1\text{Nb}_{3.1}\text{Si}_{14.5}\text{B}_{10.6}$  (b), and  $\text{Fe}_{73.8}\text{Cu}_1\text{Nb}_{3.1}\text{Si}_{13}\text{B}_{9.1}$  *Finemet* glass-coated microwires with the same  $\rho$ -ratio = 0.6.

As clearly shown from XRD in Fig. 1.2, the first two peaks between  $10^\circ$ - $30^\circ$  are corresponding to the glass coating layer, while the third one located between  $40^\circ$ - $60^\circ$  is related to the metallic nucleus, where all our results will be highlighted in this region. Either both as-prepared  $\text{Fe}_{70.8}\text{Cu}_1\text{Nb}_{3.1}\text{Si}_{16}\text{B}_{9.1}$  or  $\text{Fe}_{70.8}\text{Cu}_1\text{Nb}_{3.1}\text{Si}_{14.5}\text{B}_{10.6}$  present wide diffuse amorphous halos exhibiting a complete amorphous structure (Fig. 1.2a-b). In the case of  $\text{Fe}_{73.8}\text{Cu}_1\text{Nb}_{3.1}\text{Si}_{13}\text{B}_{9.1}$  a main crystalline peak appears at a diffraction angle of about  $45^\circ$ . This crystalline peak is well corresponding to BCC  $\alpha$ -Fe-Si crystal structure [164]. By analyzing this peak features (maximum position and width), one can easily estimate the crystalline grain size diameter,  $D_g$ , beyond the well-established Debye-Scherrer correlation [165]:

$$D_g = \frac{K\lambda}{\varepsilon \cos 2\theta} \quad (1.1)$$

where,  $\varepsilon$ , is the half height width of the crystalline peak, and  $2\theta$  is the angular position of the maximum crystalline peak.

Analysis of this crystalline peak (Fig. 1.2c) by eq. 1.1, gave us an average grain size,  $D_g \approx 16 \text{ nm}$ . Therefore, we assume that  $\text{Fe}_{73.8}\text{Cu}_1\text{Nb}_{3.1}\text{Si}_{13}\text{B}_{9.1}$  microwire displays low coercivity (Fig. 1.1b) due to the nanocrystallization achieved directly as-prepared (without annealing).

In principle, as we discussed by the end of chapter 2 (page 31), the crystalline phases embedded in an amorphous metallic matrix (nanocrystalline materials) can be obtained in two different ways either by controlling the crystallization kinetics through optimizing the heat treatment conditions (annealing temperature, annealing time, heating rate, etc.), or by decreasing the quenching rate velocity during the casting process as specifically explained (experimental techniques, pages 49-50). In particular, the decrease in the critical quenching rate leads to a crystal nucleation [166]. It has been also reported that this decrease of quenching velocities usually characterized by the maximum metallic nucleus diameter,  $d$ , at a given glass-coating thickness and thermal exchange coefficient,  $\alpha$ , [34, 35, 143]. This particular assumption matches well with our three selected microwire samples: the thickest metallic diameters ( $d = 14.6$  microns) (see table 1.1) is for the nanocrystalline sample  $\text{Fe}_{73.8}\text{Cu}_1\text{Nb}_{3.1}\text{Si}_{13}\text{B}_{9.1}$ . Moreover the critical quenching rate is related to phase diagram, i.e. liquids temperature. Based on these findings, we outline here that, however, the difference in the chemical alloy composition is rather

small, controlling the fabrication conditions is in a significant importance to attain either amorphous or nanocrystalline structures.

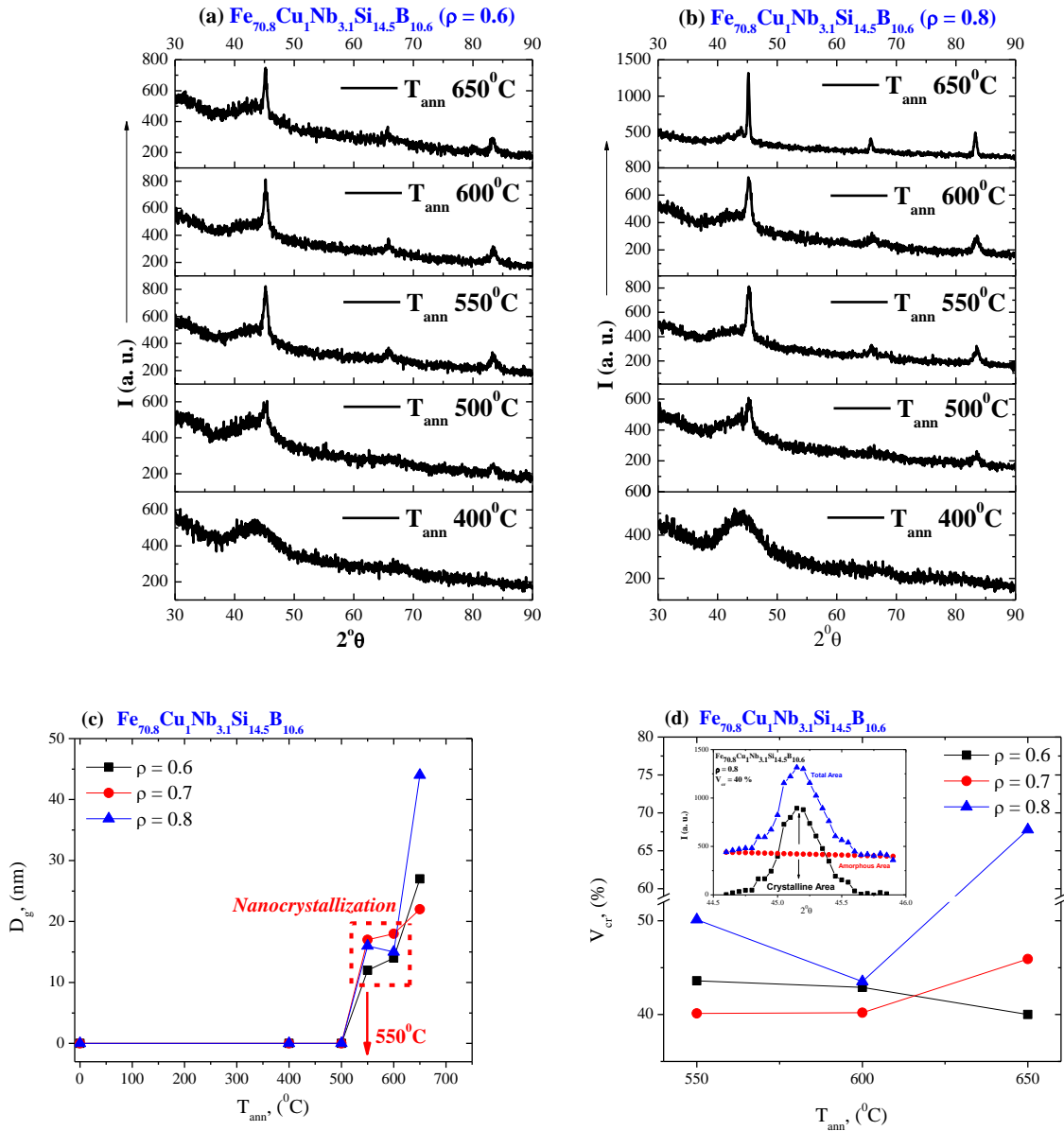


Figure 1.3 XRD patterns of annealed  $Fe_{70.8}Cu_1Nb_{3.1}Si_{14.5}B_{10.6}$  glass-coated microwires at  $T_{ann}$  ranging between 400-650°C for 1 hour for  $\rho$ -ratio = 0.6 (a);  $\rho$ -ratio = 0.8 (b); grain size  $D_g$  dependence on  $T_{ann}$  (c), and crystalline volume fraction  $V_{cr}$  dependence on  $T_{ann}$  of  $Fe_{70.8}Cu_1Nb_{3.1}Si_{14.5}B_{10.6}$  microwires for different  $\rho$ -ratios (d). Inset of (d) shows the determination of  $V_{cr}$  from XRD crystalline peak of annealed  $Fe_{70.8}Cu_1Nb_{3.1}Si_{14.5}B_{10.6}$  at 650°C with  $\rho$ -ratio = 0.8.

On the other hand, in order to accomplish the nanocrystallization of all those samples exhibiting amorphous structure in as-prepared, we carried out a series of conventional annealing for annealing temperature,  $T_{ann}$ , ranging between 400-650°C for 1 hour. XRD patterns of annealed *Finemet* microwire samples are visible in Fig. 1.3a-b. The devitrification processes (Fig. 1.3a-b) are systematically analyzed for annealed  $Fe_{70.8}Cu_1Nb_{3.1}Si_{14.5}B_{10.6}$  microwire samples for two  $\rho$ -ratio = 0.6 and 0.7. Annealing at 400°C results in a decrease in the intensity of the amorphous halo as-compared with the as-prepared microwire samples (Fig. 1.2), this is attributed to the stress relaxation arises from annealing. A real devitrifications process initiates at 500°C, where a noticeable growing in a crystalline peak takes places. In a similar way as the case of as-prepared  $Fe_{73.8}Cu_1Nb_{3.1}Si_{13}B_{9.1}$ , a BCC  $\alpha$ -Fe-Si crystalline peak appears at a diffraction angle of about 45° by reaching  $T_{ann} = 550^\circ C$ . In as much as the annealing temperature,  $T_{ann}$ , increases, such peak are getting higher and narrower indicating an increase of either the grain size growth, or the crystalline volume fraction, respectively. The grain size diameter,  $D_g$ , for each  $Fe_{70.8}Cu_1Nb_{3.1}Si_{14.5}B_{10.6}$  microwires has been calculated following the same aforementioned procedures (eq. 1.1). Fig. 1.3c shows the grain size dependence on annealing temperature. The average grain size,  $D_g$ , is in the range of  $550^\circ C \leq T_{ann} \leq 600^\circ C$  is between 12 and 17 nm, and rapidly increasing at  $T_{ann} \geq 650^\circ C$  reaching a value of about 40 nm. A similar trend of the grain size,  $D_g$ , dependence on  $T_{ann} = 550^\circ C$  for  $Fe_{70.8}Cu_1Nb_{3.1}Si_{16}B_{9.1}$  microwire samples has been also investigated achieving 12, 20, and 16 nm for  $\rho = 0.6, 0.7,$  and 0.8 respectively.

It is interesting to note that not only the average grain size, but also the crystalline volume fraction,  $V_{cr}$ , of the precipitating nanocrystalline phase affects the physical properties of devitrified materials [167, 168]. As a role, several methods for the estimation of the volume fraction have been proposed [167, 168]. For the case of nanocrystalline materials an additional problem arises from the existence of high number of interfaces with random orientation relationships present in the sample, and in consequence, the substantial fraction of atoms lying in the interfaces [169]. Therefore, usually knowledge of the size; the distribution of precipitating grains, and the average thickness of the grain boundary phase are required in a combined way for estimating the accurate crystalline volume fraction,  $V_{cr}$  [167-170]. Such information cannot be correctly estimated only from the XRD (which have been used in the present study). In order to avoid a lack of the necessary experimental information for the correct volume fraction estimation, we paid attention on an useful method for the estimation of the crystalline volume

fraction based on a reported model for mixed *Finemet* amorphous/crystalline materials [171]. This model suggests that a XRD diffraction scan is the sum of the total peak area consisting of the crystalline and amorphous diffractograms together. The true area of the crystalline peaks can be determined from the following equation;

$$V_{cr}(\%) = \frac{\int q^2 I_c dq}{\int q^2 I dq} \approx \frac{\int I_c d(2\theta)}{\int I d(2\theta)} \quad (1.2)$$

where  $q = \frac{4\pi \sin \theta}{\lambda}$ , and  $I = I_{am} + I_C$  being at a given point  $I$  the sum of the amorphous contribution,  $I_{am}$ , and the crystalline contribution,  $I_C$ .

By calculating the total area under the whole peak, taking into account the amorphous portion, finally one can obtain the crystalline phase volume fraction of the sample (see the inset of Fig. 1.3d), which is related to the distribution of the grains inside the crystal. Fig. 1.3d shows the crystalline volume fraction dependence on annealing temperature of  $\text{Fe}_{70.8}\text{Cu}_1\text{Nb}_{3.1}\text{Si}_{14.5}\text{B}_{10.6}$  microwire samples for three different  $\rho$ -ratios. We must take into account that the aforementioned estimation for the crystalline volume fraction is different to that described in [167, 168]. Our estimation can be used only for a first approximation. In other words, the knowledge about the precipitating grains size and their distribution, together with the average thickness of the grain boundary phase will be useful for a further comparison of nanocrystalline microwires with other conventional nanocrystalline materials. For example, the provided estimation does not distinguish the precipitating grains and the grain boundaries. Indeed, the obtained crystalline volume fractions are lower in comparison with those reported for annealed nanocrystalline ribbons at similar conditions [167, 168]. In particular, about 50-60%  $V_{cr}$  values are reported in  $\text{Fe}_{71.1}\text{Cu}_{1.1}\text{Nb}_3\text{Si}_{18.5}\text{B}_{6.3}$  ribbons annealed at 545°C for 1 hour [168]. The obtained  $V_{cr}$ -values are also lower than the 75-80% reported for fully crystallized ribbons indicating that even after annealing at 650°C the nanocrystallization is not yet completed. In addition, the existence of the glass coating in *Finemet* microwire samples might be attributed for these discrepancies. Thus the influence of the glass coating can be correlated to internal stresses distribution as well as to the low thermal conductivity of the glass itself. Notwithstanding of these limitations respect to the crystalline volume fraction, the development of  $\alpha$ -Fe-Si

nanoscaled crystals embedded in a remaining amorphous phase worth continues in a number of appealing characteristics. One of these characteristics is the magnetic behavior of those annealed *Finemet* microwires after achieving the nanocrystallization.

#### 1.4 Beyond the magnetic properties

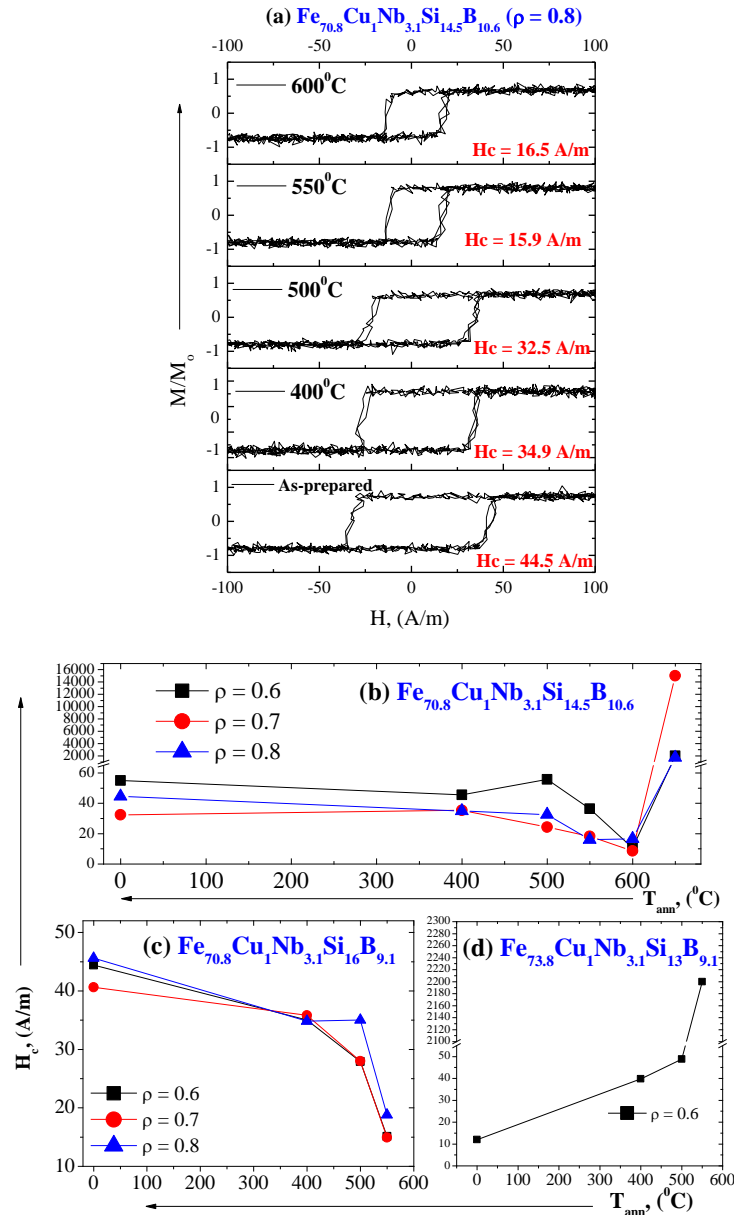


Figure 1.4 Hysteresis loops of as-prepared and annealed  $Fe_{70.8}Cu_1Nb_{3.1}Si_{14.5}B_{10.6}$  microwire samples at  $T_{ann}$  between 400°C-600°C (a); coercive field dependence on  $T_{ann}$  of  $Fe_{70.8}Cu_1Nb_{3.1}Si_{14.5}B_{10.6}$  for different  $\rho$ -ratios (b);  $H_c$  dependence on  $T_{ann}$  of  $Fe_{70.8}Cu_1Nb_{3.1}Si_{16}B_{9.1}$  microwire samples for different  $\rho$ -ratios (c); and of  $Fe_{73.8}Cu_1Nb_{3.1}Si_{13}B_{9.1}$  for  $\rho$ -ratio = 0.6 (d).

Fig. 1.4a presents hysteresis loops of as-prepared and annealed  $\text{Fe}_{70.8}\text{Cu}_1\text{Nb}_{3.1}\text{Si}_{14.5}\text{B}_{10.6}$  microwire samples for  $\rho$ -ratio = 0.8. As can be assumed, the coercive field decreases upon increasing the annealing temperature ( $H_c$  decreases from a value of 44.5 A/m for as-prepared amorphous sample to 15.9 A/m for annealed microwire sample at  $T_{ann} = 550^\circ\text{C}$ ). Meanwhile, the rectangular character of hysteresis loops is observed for either as-prepared or annealed microwires. The coercive field dependence on annealing temperature of  $\text{Fe}_{70.8}\text{Cu}_1\text{Nb}_{3.1}\text{Si}_{14.5}\text{B}_{10.6}$  is shown for different  $\rho$ -ratios in Fig. 1.4b. An optimal magnetic softness with values of coecivities down to 10 A/m is obtained for  $\rho$ -ratio = 0.7 (Fig. 1.4b). A similar tendency has been also observed for different  $\rho$ -ratios of the  $\text{Fe}_{70.8}\text{Cu}_1\text{Nb}_{3.1}\text{Si}_{16}\text{B}_{9.1}$  *Finemet* microwire composition (Fig. 1.4c) reaching  $T_{ann} = 550^\circ\text{C}$ . Whilst increasing the annealing temperature for  $\text{Fe}_{73.8}\text{Cu}_1\text{Nb}_{3.1}\text{Si}_{13}\text{B}_{9.1}$  resulted in an abrupt increase of the coercivity up to 2200 A/m and deterioration of the magnetic softness (Fig. 1.4d). This increase in the coercive field is also observed for  $\text{Fe}_{70.8}\text{Cu}_1\text{Nb}_{3.1}\text{Si}_{14.5}\text{B}_{10.6}$  microwire samples treated at  $T_{ann} = 650^\circ\text{C}$  (Fig. 1.4b), which is interpreted to the precipitation of  $\text{Fe}_2\text{B}$  phase that implies a magnetic hardening character.

It is well-established that there is a direct correlation between the microstructure property and its changes especially upon the nanocrystallization as we specifically detailed in chapter 2 (pages 26-27) through the random anisotropy model which stands herein as a main source of this magnetic softness. Thus a remarkable magnetic softness with the lowest value of coercivity is obtained for all studied  $\text{Fe}_{70.8}\text{Cu}_1\text{Nb}_{3.1}\text{Si}_{16}\text{B}_{9.1}$  and  $\text{Fe}_{70.8}\text{Cu}_1\text{Nb}_{3.1}\text{Si}_{14.5}\text{B}_{10.6}$  *Finemet* microwire samples annealed at  $T_{ann} = 550^\circ\text{C}$ , and as-prepared  $\text{Fe}_{73.8}\text{Cu}_1\text{Nb}_{3.1}\text{Si}_{13}\text{B}_{9.1}$  already nanocrystallized after casting. These findings are ascribed to the fact that the first nanocrystallization stage has been developed, leading to fine  $\alpha$ -Fe-Si nanocrystallites with a grain size,  $D_g$ , of 10-20 nm (Fig. 1.3c). Observed behaviors are in agreement with widely reported *Finemet*-like nanocrystalline materials either ribbons [172], or glass-coated microwires [173].

In a parallel way, upon annealing, a variation of the magnetoelastic anisotropy should be also taken into account. Thus, after the optimum annealing for which nanocrystalline structure is observed, the magnetostriction coefficient of all microwire samples should be diminished among the structural phases present in the nanocrystalline state [174-176]. In a broader sense, the



existence of two different phases gives a good balance of a negative magnetostriction of  $\alpha$ -Fe-Si nanocrystallites of about ( $\lambda_s^{FeSi} \approx -6 \times 10^{-6}$ ) [174] and a positive one for the amorphous matrix of about ( $\lambda_s^{am} \approx 20 \times 10^{-6}$ ) [175] resulting finally in a very low net magnetostriction values, according to [176]:

$$\lambda_s^{eff} \approx V_{cr} \lambda_s^{FeSi} + (1 - V_{cr}) \lambda_s^{am} \quad (1.3)$$

being  $\lambda_s^{eff}$  the saturation magnetostriction coefficient, and  $V_{cr}$  denotes the crystalline volume fraction.

In accordance, the reduced magnetostriction coefficients together with the structural relaxation of the very strong internal stresses achieved by annealing are essentially considered to reduce the total magnetoelastic anisotropy, and therefore achieving such magnetic softness. In addition, we overemphasize these contributions to the magnetostriction by a direct measurement of  $Fe_{73.8}Cu_1Nb_{3.1}Si_{13}B_{9.1}$  microwire exhibiting nanocrystalline structure in as-prepared (Fig. 1.2c) by the help of SAMR method described in (chapter 4, pages 65-66). After several measurements, our sample records three reasonable values equal to either  $0.021 \times 10^{-6}$ ; or  $0.054 \times 10^{-6}$ , and  $0.075 \times 10^{-6}$ , which are pretty much in central support of abovementioned correlations.

## 1.5 Giant magnetoimpedance (GMI)

The preceding part of this chapter has set the experimental basis for the nanocrystallization impact of *Finemet*-like glass-coated microwires on the development of an outstanding magnetic softness. We believe, therefore, that these microwires must present GMI effect as they exhibit a relatively high magnetic permeability and superior magnetic softness. These features are mostly keys factor to obtain GMI response.

Consequently, we have measured dependencies of the diagonal impedance,  $Z_{zz}$ , and GMI ratio on external axial magnetic field,  $H$ , in investigated microwire samples. The magneto impedance ratio,  $\Delta Z/Z$ , is determined by eq. 3.1 (page 35). Fig. 1.5 displays  $\Delta Z/Z(H)$  dependence of as-prepared samples in either amorphous  $Fe_{70.8}Cu_1Nb_{3.1}Si_{16}B_{9.1}$  or  $Fe_{70.8}Cu_1Nb_{3.1}Si_{14.5}B_{10.6}$  and nanocrystalline  $Fe_{73.8}Cu_1Nb_{3.1}Si_{13}B_{9.1}$  having the same  $\rho$ -ratio = 0.6. As was expected, microwire samples with amorphous structure exhibit rather poor GMI responses ( $\approx 1\%$  for  $Fe_{70.8}Cu_1Nb_{3.1}Si_{14.5}B_{10.6}$  and  $\approx 5\%$  for  $Fe_{70.8}Cu_1Nb_{3.1}Si_{16}B_{9.1}$ ) typical for Fe-based glass-coated

microwires with highly positive magnetostriction. In contrast, good GMI values of about 38% for  $f = 150 \text{ MHz}$  and about 50% for  $f = 300 \text{ MHz}$  are observed for as-prepared  $\text{Fe}_{73.8}\text{Cu}_1\text{Nb}_{3.1}\text{Si}_{13}\text{B}_{9.1}$  microwire with nanocrystalline structure. This is definitely, a result of the nanocrystalline structure as well as nearly zero magnetostriction coefficient ( $0.021 \times 10^{-6}$ ).

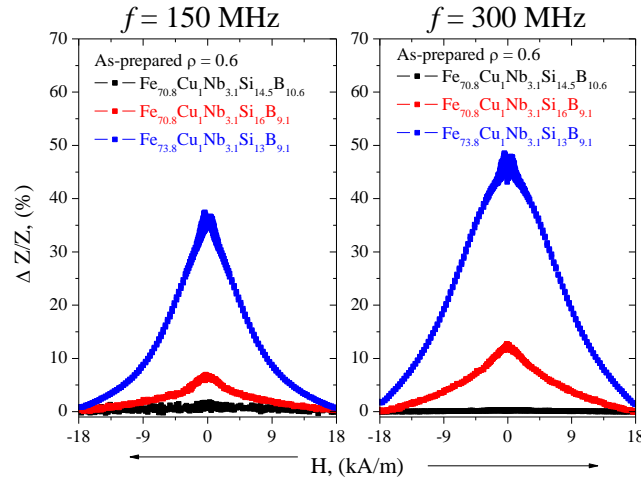


Figure 1.5  $\Delta Z/Z(H)$  dependences of as-prepared  $\text{Fe}_{70.8}\text{Cu}_1\text{Nb}_{3.1}\text{Si}_{16}\text{B}_{9.1}$ ,  $\text{Fe}_{70.8}\text{Cu}_1\text{Nb}_{3.1}\text{Si}_{14.5}\text{B}_{10.6}$ , and  $\text{Fe}_{73.8}\text{Cu}_1\text{Nb}_{3.1}\text{Si}_{13}\text{B}_{9.1}$  Finemet glass-coated microwires with the same  $\rho$ -ratio = 0.6 measured at frequencies of 150 and 300 MHz.

In addition, the stress distribution arising from the coupling between the internal stresses during rapid quenching of the metallic nucleus inside the glass coating and positive magnetostriction coefficient, results in a longitudinal magnetization easy axis for the case of Fe-based alloys. The peculiar domain structure presenting low circular magnetic permeability (see Fig. 2.2 page 20) usually is not favorable to exhibit a GMI effect. Thus, such domain structure impedes the magnetization rotation at low magnetic fields. As a consequence, GMI effect in the as-prepared *Finemet* glass-coated microwires with positive magnetostriction is small. The significant influence of the nanocrystallization on optimizing GMI effect is visible in Fig. 1.6. Interestingly the GMI responses show a remarkable improvement of annealed  $\text{Fe}_{70.8}\text{Cu}_1\text{Nb}_{3.1}\text{Si}_{14.5}\text{B}_{10.6}$  microwire samples at  $T_{\text{ann}} = 550^\circ\text{C}$ : GMI is considerably enhanced from 6% to 125% for  $f = 500 \text{ MHz}$  (Fig. 1.6a). In a similar way as for annealed  $\text{Fe}_{70.8}\text{Cu}_1\text{Nb}_{3.1}\text{Si}_{16}\text{B}_{9.1}$ , GMI increases from 12% up to 90% for  $\rho$ -ratio = 0.7 (Fig. 1.6b) and reaches about 93% for  $\rho$ -ratio = 0.8 (Fig. 1.6c).

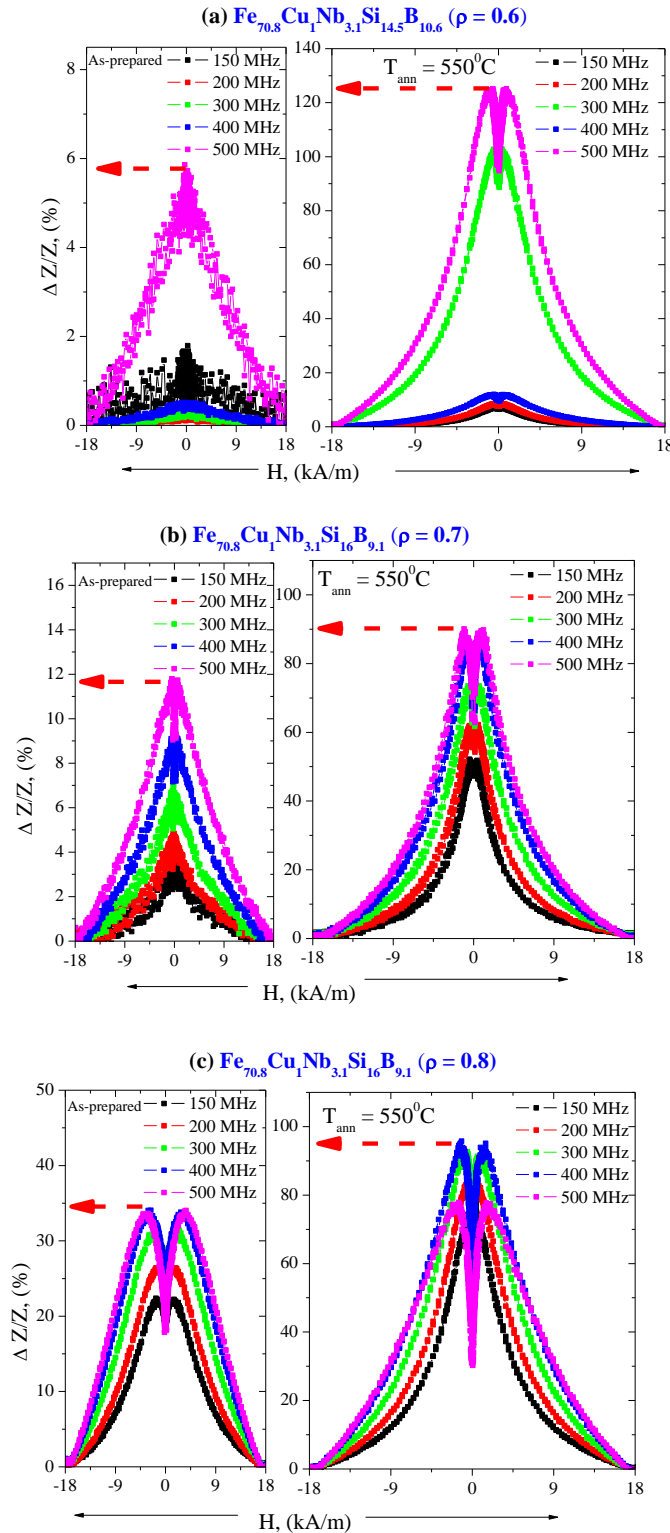


Figure 1.6  $\Delta Z/Z(H)$  dependences of as-prepared and annealed at  $T_{\text{ann}} = 550^\circ\text{C}$  of  $\text{Fe}_{70.8}\text{Cu}_1\text{Nb}_{3.1}\text{Si}_{14.5}\text{B}_{10.6}$  for  $\rho$ -ratio = 0.6 (a);  $\Delta Z/Z(H)$  dependences of  $\text{Fe}_{70.8}\text{Cu}_1\text{Nb}_{3.1}\text{Si}_{16}\text{B}_{9.1}$  for  $\rho$ -ratio = 0.7 (b), and  $\rho$ -ratio = 0.8 (c).

Measuring frequencies are provided in each figure.

These observed experimental results are, indeed, in a practical interest of GMI related-applications. Thus the GMI effect is understood as a skin effect of magnetically soft conductor. As the magnetostriction after nanocrystallization reduces, microwires samples present better magnetic softness, higher permeability, and therefore higher GMI effect. Herein, the GMI effect is mainly due to changes in the resistive component of the impedance, and is basically dominated by the skin effect (eq. 3.6 page 37). According to this equation, the higher the frequency, the shallower the skin depth, that will, consecutively, cause the current to flow nearby the microwire's surface, reducing the effective cross-sectional area along the wire, and therefore, leading to an increase in the GMI responses. Despite this, the frequency at which the GMI profile takes its maximum is strongly dependent on the sample geometry ( $\rho$ -ratio). A comparative results of the frequency dependence on  $\Delta Z/Z_{max}$  based on Fig. 1.6b-c for the case of  $\text{Fe}_{70.8}\text{Cu}_1\text{Nb}_{3.1}\text{Si}_{16}\text{B}_{9.1}$  microwire samples are shown in Fig. 1.7.

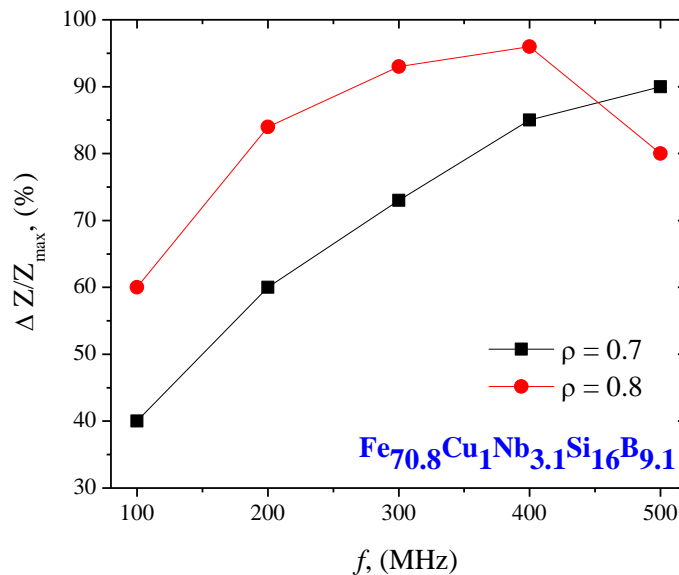


Figure 1.7 Frequency dependence of  $\text{Fe}_{70.8}\text{Cu}_1\text{Nb}_{3.1}\text{Si}_{16}\text{B}_{9.1}$  glass-coated microwires annealed at  $T_{ann} = 550^\circ\text{C}$  for two  $\rho$ -ratios: 0.7 and 0.8.

As can be observed in Fig. 1.7:  $\Delta Z/Z_{max}$  and its frequency dependence are strongly affected by the magnetoelastic anisotropy determined by  $\rho$ -ratio in a similar way as commonly observed in the case for Co-based glass-coated microwires in different frequency dependence of the GMI effect. [104, 177]. A final word is, however, reported GMI ratios for Co-based microwires are

much more higher than currently presented GMI ratios, the affordable commercial cost of *Finemet* alloys are still one of the most desirable prerequisites for GMI applications point of view.

## 1.6 Concluding remarks

Throughout this chapter we have verified experimentally the role of nanocrystallization and its direct correlation to an optimal magnetic softness. A systematic research has been performed in three *Finemet* alloy compositions with either different metallic nucleus diameters or glass thickness.

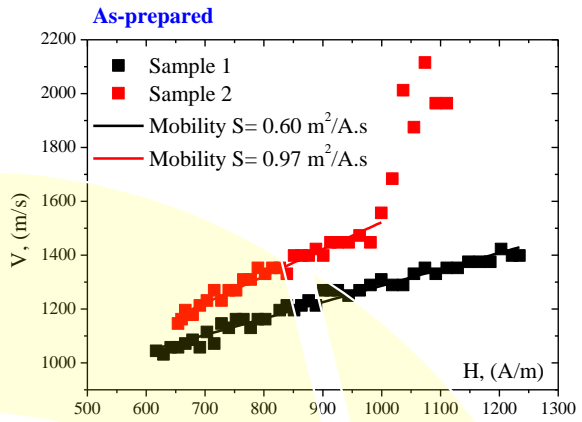
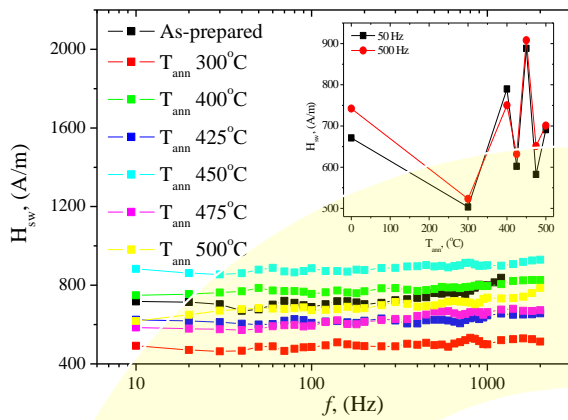
The major findings of our studies combined achieving a remarkable magnetic softness with a coercive field of about 10  $A/m$  and an ultra fine grain size of 11  $nm$  in annealed microwire samples at  $T_{ann} = 550^{\circ}C$ . An optimized 125% GMI ratio observed at  $f = 500 MHz$  of the poor response of amorphous as-prepared microwire samples (1%) has been also achieved. The increase of internal stresses strength is in connection with the magnetoelastic anisotropy: the highest magnetic anisotropy, is corresponding to the lowest  $\rho$ -ratio. Accordingly, the coercive field of either as-prepared or annealed microwire samples results to be very sensitive to the  $\rho$ -ratio. A significant difference in the magnetic softness behavior has been distinguished to the devitification processes either through the participation of  $\alpha$ -Fe-Si crystallites at the first stage of nanocrystallization ( $T_{ann} = 550^{\circ}C$ ) or by the precipitation of  $Fe_2B$  phase with a magnetic hardening character ( $H_c = 2200 A/m$ ).

Controlling the quenching rate during the fabrication process strongly affects the final microstructural of the produced microwires. Consequently, nanocrystalline structure of about 12  $nm$   $\alpha$ -Fe-Si grains and coercive field of 12  $A/m$  obtained in as-prepared microwire samples resulting in an improvement of approximately 50% GMI at frequency of 300  $MHz$ . A drastic change in the magnetostriction coefficients has been presumed upon the nanocrystallization: the magnetostriction values pushed away from highly positive to nearly zero values. A practical instance of these changes in magnetostriction were supported by a direct measurement giving values of about  $0.021 \times 10^{-6}$ . In the light of these findings, noticeable enhancements in the final GMI responses were successfully acquired. Our results provide a good candidate for GMI-oriented applications.

## 1.7 Further reading: Publications related to this chapter

1. A. Talaat, V. Zhukova, M. Ipatov, J. M. Blanco, L. Gonzalez-Legarreta, B. Hernando, J. J. del Val, J. Gonzalez, A. Zhukov. *Optimization of the giant magnetoimpedance effect of Finemet-type microwires through the nanocrystallization*. Journal of Applied Physics 115 (17), 17A313 (2014)
2. A. Talaat, V. Zhukova, M. Ipatov, J. J. Del Val, L. Gonzalez-Legarreta, B. Hernando, J. M. Blanco, A. Zhukov. *Effect of nanocrystallization on giant magnetoimpedance effect of Fe-based microwires*. Intermetallics 51, 59-63 (2014)
3. A. Talaat, M. Ipatov, V. Zhukova, J. M. Blanco, M. Churyukanova, S. Kaloshkin, A. Zhukov. *Giant magneto-impedance effect in thin Finemet nanocrystalline microwires*. physica status solidi (c), 11 (5-6) 1120-1124 (2014)
4. A. Talaat, V. Zhukova, M. Ipatov, J. M. Blanco, M. Churyukanova, S. Kaloshkin, E. Kostitcyna, E. Shuvaeva, L. Gonzalez-Legarreta, B. Hernando, A. Zhukov. *Magnetic properties and giant magnetoimpedance in amorphous and nanocrystalline microwires*. Acta Physica Polonica, A., 126 (1) 146-147 (2014)
5. A. Talaat, V. Zhukova, M. Ipatov, J. M. Blanco, R. Varga, P. Klein, L. Gonzalez-Legarreta, B. Hernando, A. Zhukov. *Magnetic properties of nanocrystalline microwires*. Journal of Electronic Materials DOI: 10.1007/s11664-015-3966-3 (2015)
6. A. P. Zhukov, A. Talaat, M. Ipatov, J. M. Blanco, L. Gonzalez-Legarreta, B. Hernando, V. Zhukova. *Effect of nanocrystallization on magnetic properties and GMI effect of microwires*. IEEE Transactions on Magnetism, 50 (6) 1-4 (2014)
7. V. Zhukova, A. Talaat, M. Ipatov, J. J. del Val, J. M. Blanco, L. Gonzalez-Legarreta, B. Hernando, R. Varga, P. Klein, M. Churyukanova, A. Zhukov. *Optimization of soft magnetic properties in nanocrystalline Fe-rich glass-coated microwires*. Journal of Metals, 67 (9) 2108-2116 (2015)
8. A. Zhukov, A. Talaat, M. Ipatov, J. J. del Val, L. Gonzalez-Legarreta, B. Hernando, A. Chizhik, J. M. Blanco, V. Zhukova. *Optimization of magnetic properties and giant magnetoimpedance effect in nanocrystalline microwires*. Journal of Superconductivity and Novel Magnetism, 28 813-822 (2015)
9. V. Zhukova, A. Talaat, M. Ipatov, J. J. del Val, L. Gonzalez-Legarreta, B. Hernando, A. Zhukov. *Effect of nanocrystallization on magnetic properties and GMI effect of Fe-rich microwires*. Journal of Electronic Materials, 43 (12) 4540-4547 (2014)
10. A. Zhukov, M. Ipatov, A. Talaat, M. Churyukanova, S. Kaloshkin, V. Zhukova. *Giant magnetoimpedance in thin amorphous and nanocrystalline microwires*. Applied Physics A, 115 (2) 547-553 (2014)
11. M. Churyukanova, V. Zhukova, A. Talaat, J. J. del Val, S. Kaloshkin, E. Kostitcyna, E. Shuvaeva, V. Sudarchikova, A. Zhukov. *Studies of thermal and magnetic properties of Fe-based amorphous and nanocrystalline glass coated microwires*. Journal of Alloys and Compounds, 615 S256-S260 (2014)
12. M. Churyukanova, V. Zhukova, A. Talaat, S. Kaloshkin, E. Kostitcyna, E. Shuvaeva, S. Gudoshnikov, V. Sudarchikova, A. Zhukov. *Correlation between thermal and magnetic properties of glass coated microwires*. Journal of Alloys and Compounds, 615 S242-S246 (2014)
13. A. Zhukov, M. Churyukanova, L. Gonzalez-Legarreta, A. Talaat, V. Zhukova, B. Hernando, M. Ilyn, J. González, S. Kaloshkin. *Influence of magnetoelastic anisotropy on properties of nanostructured microwires*. Advanced Materials Research, 646 59-66 (2013)

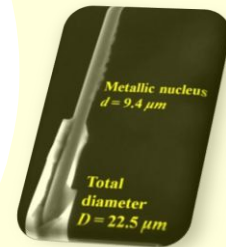
*The chapter deals with magnetic and structural investigations of new  $Fe_{38.5}Co_{38.5}B_{18}Mo_4Cu_1$  Hitperm glass-coated microwires*



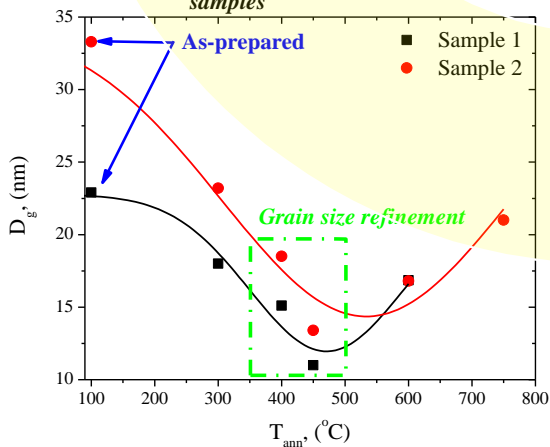
# 2 Nanocrystalline Hitperm alloys:

*A structural investigation and magnetization process*

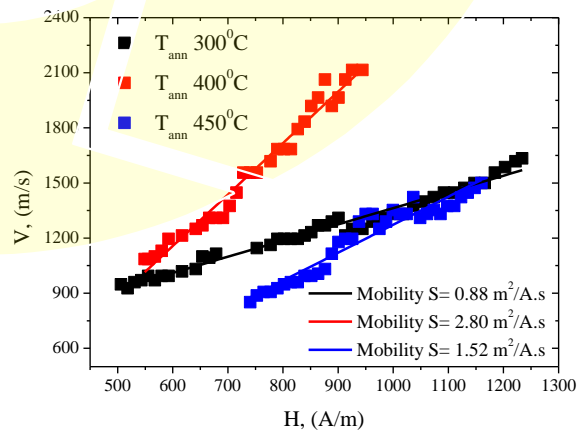
*Fast DW velocities have been recorded for as-prepared samples reaching values as fast as 1.2 Km.s*



*A grain size refinement down to 11 nm has been obtained upon annealing as-prepared microwire samples*



*An enhancement of the DW velocity as well as DW mobility after annealing*



## 2.1 *Hitperm* alloys

*Hitperm* Fe-Co intermetallic alloys are well known to possess a unique combination of high saturation magnetization as well as high Curie temperature. A widespread research and development efforts over the years have initiated by Willard who pointed out that the nanocrystallization achieved in  $\text{Fe}_{44}\text{Co}_{44}\text{Zr}_7\text{B}_4\text{Cu}_1$  chemical alloy system (the first reported instance of *Hitperm* alloy), display high saturation magnetization of about 1.6 to 2.1  $T$  and enhanced Curie temperature up to  $977^\circ\text{C}$  of either the crystalline and the amorphous phases [89]. Later on, a wide variety of partial substitutions of the original *Hitperm* alloy composition has emerged: different selections of the early transition metals (Zr, Nb, Mo, Hf, or Ta) have shown dramatic changes on the crystallization consequences, phase transformations, thermal stabilities, and consecutively the magnetic behavior of the chosen *Hitperm* alloy composition [178, 179]. Among reported *Hitperm* glass-coated microwires, an alloy composed of  $\text{Fe}_{40}\text{Co}_{38}\text{Mo}_4\text{B}_{18}$  has been proposed [180, 181] revealing a BCC  $\alpha$ -FeCo nanocrystalline phase with a grain size of about 19 nm achieved after annealing temperature,  $T_{ann} = 540^\circ\text{C}$  [180]. In addition, due to the positive magnetostriction of  $\alpha$ -FeCo phase, the microwire maintains a bistable behavior in a wide range of temperatures, and as a consequence, quite fast domain wall (DW) velocities up to 3 Km/s were reported [182].

Considering the significant influence of Cu to any nanocrystalline alloy system to obtain finer nanocrystalline structure, this chapter mainly aims to explore the effect of 1% Cu addition to previously reported  $\text{Fe}_{40}\text{Co}_{38}\text{Mo}_4\text{B}_{18}$  alloy composition. We provide two novel  $\text{Fe}_{38.5}\text{Co}_{38.5}\text{B}_{18}\text{Mo}_4\text{Cu}_1$  *Hitperm* glass-coated microwires, having the same metallic nucleus diameter but with different glass thicknesses, paying more attention to elucidate the effect of stress relaxation on the magnetization processes of investigated samples. A comparative research appropriately designates the effect of external parameters such as: the measuring frequency, conventional annealing, and the devitrification processes either on the domain wall dynamics or magnetization switching of *Hitperm* glass-coated microwires.

## 2.2 Samples preparation and microstructure investigation

Ingots of  $\text{Fe}_{38.5}\text{Co}_{38.5}\text{B}_{18}\text{Mo}_4\text{Cu}_1$  were arc melted in an argon atmosphere of purely constituent elements (Fe, Co, B, Mo, Cu), and the microwires have been fabricated by means of



Taylor-Ulitovsky technique as described in the experimental techniques. We produced two *Hitperm* glass-coated microwire samples with the same nominal composition  $\text{Fe}_{38.5}\text{Co}_{38.5}\text{B}_{18}\text{Mo}_4\text{Cu}_1$  as well as almost the same metallic core diameter,  $d$ , but with different total diameters,  $D$ , as shown in table 2.1. For simplicity, each sample has a given number either sample 1 or sample 2, bearing always in mind that sample 1 has higher internal stresses than sample 2 as ascribed by lower  $\rho$ -ratio.

*Table 2.1* Chemical composition, dimensions, and geometric ratios of fabricated *Hitperm* glass-coated microwires

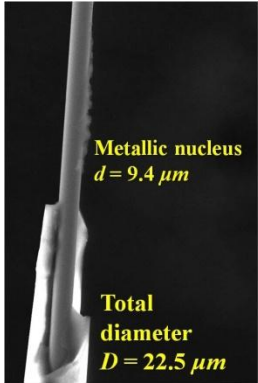
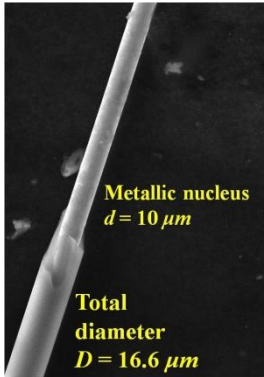
Chemical composition $\text{Fe}_{38.5}\text{Co}_{38.5}\text{B}_{18}\text{Mo}_4\text{Cu}_1$	Metallic nucleus, $d$ , diameter ( $\mu\text{m}$ )	Total diameter, $D$ , ( $\mu\text{m}$ )	Geometric ratio, $\rho$ , $d/D$	SEM pictures
Sample 1	9.4	22.5	0.4	
Sample 2	10	16.6	0.6	

Fig. 2.1a presents XRD diffraction patterns of both as-prepared *Hitperm* glass-coated microwires. As mentioned before for the case of *Finemet*, the first two peaks between  $10^\circ$ - $30^\circ$

are corresponding to the glass coating, while the third one located between  $40^\circ$ - $50^\circ$  is related to the metallic core (see the inset of Fig. 2.1a). As can be deduced, a noticeable peak appears of BCC  $\alpha$ -FeCo B2 ordered phase on a diffraction angle  $45^\circ$  [181, 183] with a grain size of about 23 and 33 nm for sample 1 and 2, respectively. Either the grain size,  $D_g$ , or the crystalline volume fraction,  $V_{cr}$ , of both samples have been analyzed by the same method described in the previous chapter (see eqs 1.1 (page 75) and 1.2 (page 78)) as can be appreciated in Fig. 2.1b for sample 1 and Fig. 2.1c for sample 2.

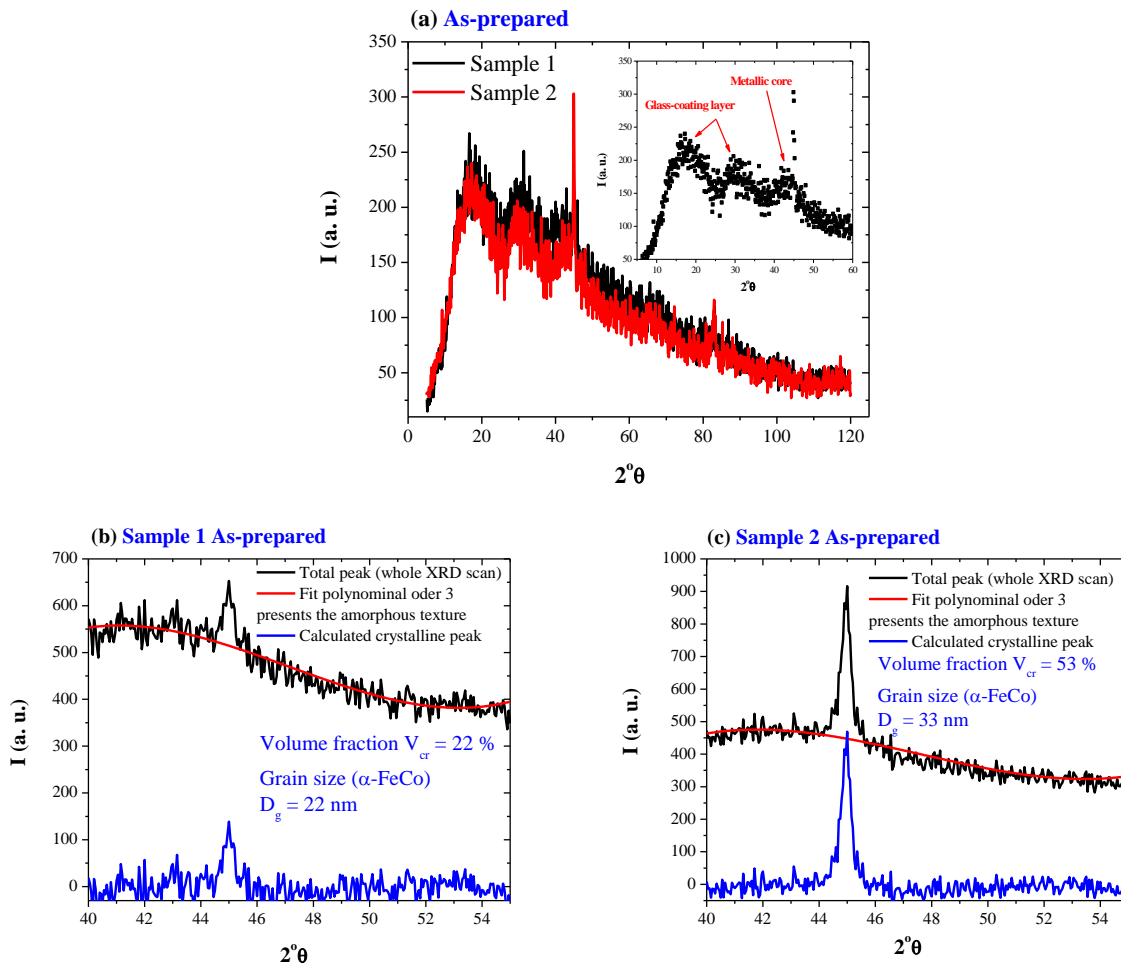


Figure 2.1 XRD patterns of as-prepared  $Fe_{38.5}Co_{38.5}B_{18}Mo_4Cu_1$  Hitperm glass-coated microwires sample 1 and 2 (a), the inset shows a zoom-in of as-prepared microwire sample for the glass layer and metallic core zone, XRD crystalline peak analysis and determination of the average grain size,  $D_g$ , as well as the crystalline volume fraction,  $V_{cr}$ , for sample 1 (b), and sample 2 (c).

As a matter of fact, among any multi-component alloy system: the addition of elements that are chemically and topologically different in their nature, play an important role in the final alloy behavior. In other words, the increment of the number of chemical elements in an alloy will significantly increase the entropy of fusion, leading to an increase in the degree of the dense random packing of atoms [184, 185]. This results in a net decrease in the enthalpy of fusion as well as an increase in the solid–liquid interface energy [185]. In our case, the chosen chemical composition of near equiatomic FeCo alloys is not exactly the one corresponding to the glass-forming alloy, and therefore the solidified phases will not be a homogeneous glassy phase [181]. In addition, as mentioned before (chapter 4 experimental techniques), that the nanocrystallites can be precipitated directly from the melt at somehow moderate quenching speed together with adjusting the chemical alloy composition [143, 166] as shown in the previous chapter for the case of  $\text{Fe}_{73.8}\text{Cu}_1\text{Nb}_{3.1}\text{Si}_{13}\text{B}_{9.1}$  *Finemet* glass-coated microwires. Therefore under these circumstances, a mixed structure consisting of nanocrystallites randomly distributed in an amorphous precursor (Fig. 2.1a) can be obtained especially in the presence of high melting point elements like Mo ( $T_{\text{melting}} = 2617^\circ\text{C}$ ). A similar observation of anomalous polycrystalline structure observed in as-prepared Fe-Mo-B-Cu ribbons has been reported due to insufficient quenching rates [186].

On the other hand, the difference in the grain size of as-prepared samples 1 and 2 correlates with the wires obtained on the initial and final stage during the fabrication process. The latter also manifests the difference between the two sample's intensities presented in Fig. 2.1a, since the bigger grain size (sample 2) is obtained at the initial stage of the fabrication process has higher intensity than sample 1 obtained by the end of the master alloy ingot. Another important factor to be pronounced here is the stress arising from the glass coating, which must also affect the grain size of these two samples (Fig. 2.1b-c).

Likewise *Finemet* alloys in the previous chapter, we carried out a series of conventional annealing at different annealing temperatures,  $T_{\text{ann}}$ , ranging between 300-600°C for 1 hour. Each sample was annealed at a certain temperature, followed by a rapid cooling down to room temperature, and repeatedly annealed for more elevated temperatures. Fig. 2.2a-b shows XRD patterns for all annealed *Hitperm* microwire samples at different annealing temperature for 1 hour.

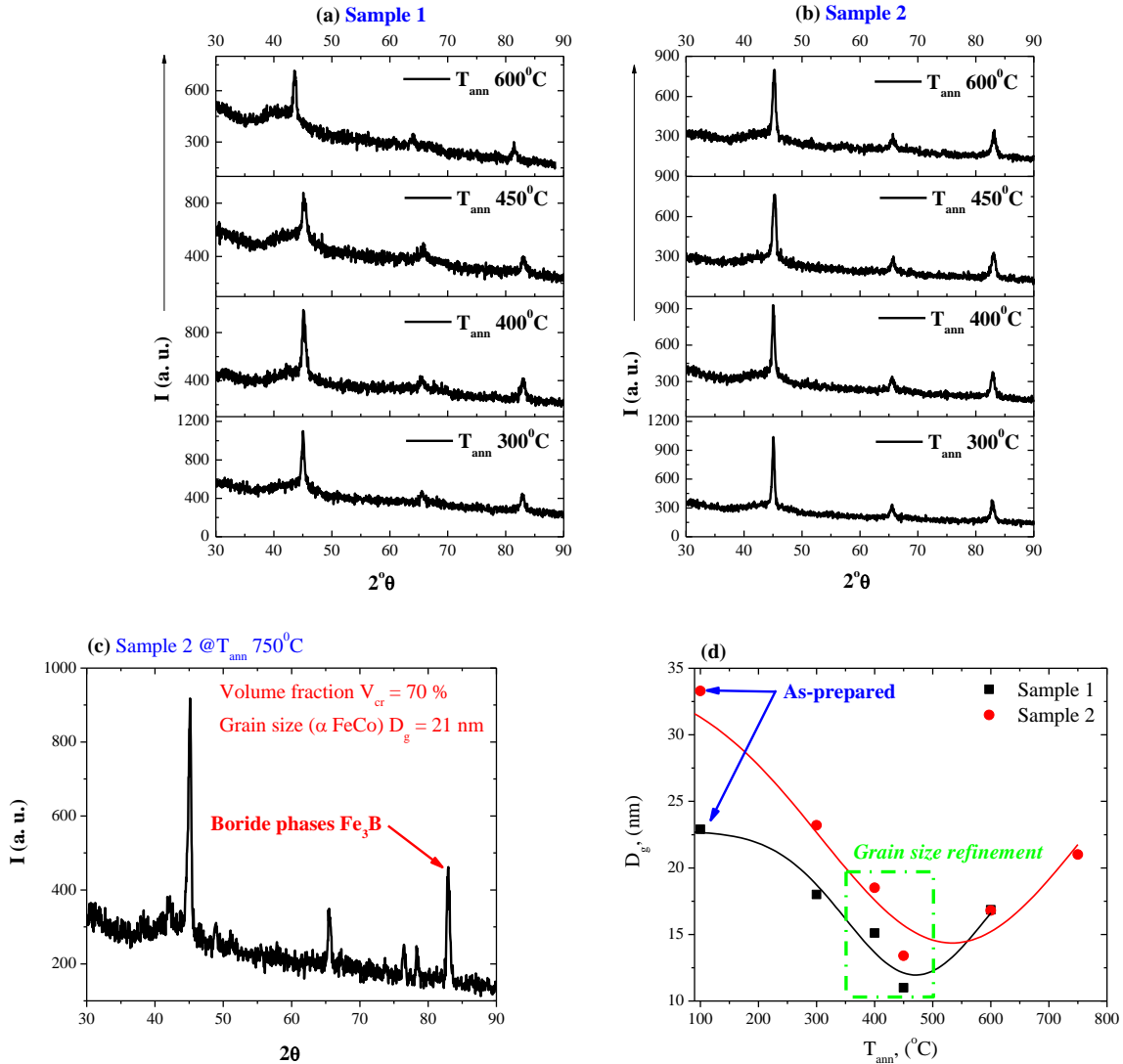


Figure 2.2 XRD patterns of  $Fe_{38.5}Co_{38.5}B_{18}Mo_4Cu_1$  Hitperm glass-coated microwires annealed at different  $T_{ann}$  for sample 1 (a); and sample 2 (b); XRD patterns for sample 2 annealed  $T_{ann} = 750^\circ C$  for 1 hour (c), and grain size dependence on  $T_{ann}$  for sample 1 and sample 2 (d).

Actually quite unusual features are seen in Fig. 2.2a-b. Thus, a sort of peak broadening is observed at  $T_{ann}$  ranging between  $300$ – $450^\circ C$  with somewhat a decrease in the XRD intensities, while at  $T_{ann} = 600^\circ C$  such peak started to grow up again. The latter case indicates an anomalous devitrification processes. In a separate step, we have performed conventional annealing for sample 2 at  $T_{ann} = 750^\circ C$  for 1 hour (Fig. 2.2c) where we observed that the main crystalline peak is getting higher and narrower, indicating an increase of the BCC  $\alpha$ -FeCo crystalline phase. In addition, a noticeable growing of an additional crystalline peak took place at a diffraction angle

of 83° which is likely related to the participation of Fe<sub>3</sub>B boride phases [183]. For all annealed microwire samples, the average grain size as well as the crystalline fraction have been evaluated. A grain size refinement of BCC  $\alpha$ -FeCo grains has been observed for both annealed samples (Fig. 2.2d) with somehow the same crystalline volume fraction: the grain size decreases as the temperature increases then passes through a minimum at  $T_{ann} = 450^{\circ}\text{C}$  (11 nm), and subsequently, increases exhibiting somehow a parabolic shape, while the volume fraction kept constant 54% and 63% for sample 1 and sample 2, respectively.

Basically in the simplest cases, annealing of any nanocrystalline metallic glasses microwires mostly results in an increase of the grain size (like *Finemet* in the previous chapter) due to their nucleation rather than existing of any grain growth itself. In addition, it is well known that the mode of crystallization of most of metallic glasses alloys is primarily crystallization and being as a result of grain's nucleation as we clarified in chapter 2 (page 31). However, the growth of primary crystals, whether they are from liquid, glass, or crystalline solid solution, may be limited by either the rate of atoms transfer across the advancing interface (interface control related to grain growth) or the diffusion rate of the atoms toward or away from the growing phase (diffusion control related to nucleation mechanism) [93, 187]. All the evidences up to date prove that the crystallization of metallic glasses is a diffusion controlled [93, 94, 187, 188].

Similar tendency has been reported for Fe-Si-B alloys about decreasing the grain size upon annealing [187] as a result of the morphology of the primary crystals growth and absence of the interfacial instabilities affirmed by solving the Johnson-Mehl-Avrami equation [187]. Furthermore, a more thoroughly microstructural analysis of Fe<sub>40</sub>Co<sub>38</sub>Mo<sub>4</sub>B<sub>18</sub> *Hitperm* glass-coated microwires has shown a very smooth increase of the grain size by achieving the crystallization onset: the grain size increased from 11 to 13 nm [181]. In the light of these observations, few parallel considerations can be roughly understood. In the case of glass-coated microwires, the crystallization can be count as a stress diffusion growth, basically due to the existence of the glass layer. In order to understand the crystallization under stress one should take into account the nucleation and crystalline growth process related to the atomic diffusion under stress [189]. For the case of glass-coated microwires the influence of internal stresses induced during simultaneous solidification of the metallic nucleus inside the glass has been observed during devitrification of the *Finemet*-type microwires, when the crystallization

temperature and even structure of the nanocrystalline phase has been affected by the glass-coating thickness [173, 190].

As a result, the crystallites growth rate is limited by the diffusivity, i.e. how fast the necessary atoms are transfer from the amorphous matrix to the growing crystalline phase as grains. In general, the rate of diffusion transport falls off very quickly with temperature, thus the decrease of the average grain size (Fig. 2.2d) with proceeding the nanocrystallization may be attributed either to the diffusion of Mo towards the crystallite interface or to the progressive inclusion of regions containing still less Mo atoms [186, 191]. Herein, we must assume the role of Cu as a heterogeneous nucleation site: due to its very limited solubility in Fe, thus, they form small clusters and increase the number of the nucleation sites resulting in a grain refinement. Besides, the low diffusion element (Mo) that will decrease, in turn, the grain growth. Therefore, it can be assumed that either the content or the distribution of the nanocrystalline and amorphous phases change with annealing. Moreover, nanocrystallites obtained after rapid quenching from the melt can present unstable structure at room temperature. As a result, the crystallization process can involve the dissolution of unstable nanocrystallites that will, consecutively, change the crystal composition and thus leads to either the formation or the growing of more stable nanograins [181].

### 2.3 Magnetic characteristics

The magnetization dependencies on temperature of as-prepared microwires are shown in Fig. 2.3a-b. A monotonic magnetization decrease with increasing the temperature up to about 450°C followed by a sharp decrease on the range of 650-700°C is observed. The increase of magnetization above 450°C points to the crystallization onset when the  $\alpha$ -FeCo grains with higher magnetization start to re-crystallize. Observed dependencies assert the presence of two phases (amorphous and nanocrystalline) of both microwire samples with two different Curie temperature of either amorphous texture or  $\alpha$ -FeCo nanocrystallites. On the other hand, rectangular hysteresis loops of both samples (presented in Fig. 2.3a-b insets) typical for amorphous Fe-based glass-coated microwires with positive magnetostriction have been observed with coercivities about 500 and 700 A/m for sample 1 and 2, respectively.

In contrast to the coercive field,  $H_c$ , determined from the hysteresis loops when the magnetization is equal to zero, the switching field,  $H_{sw}$ , is defined as the magnetic field value at which the magnetization switching of microwire samples exhibiting magnetic bistability begins. In fact the characteristic feature of the magnetic bistability is the appearance of a rectangular hysteresis loop. Such behavior is usually observed in amorphous wires when the wire's length and the applied magnetic field are above some of the critical values as we explained in chapter 2 (pages 21-22).

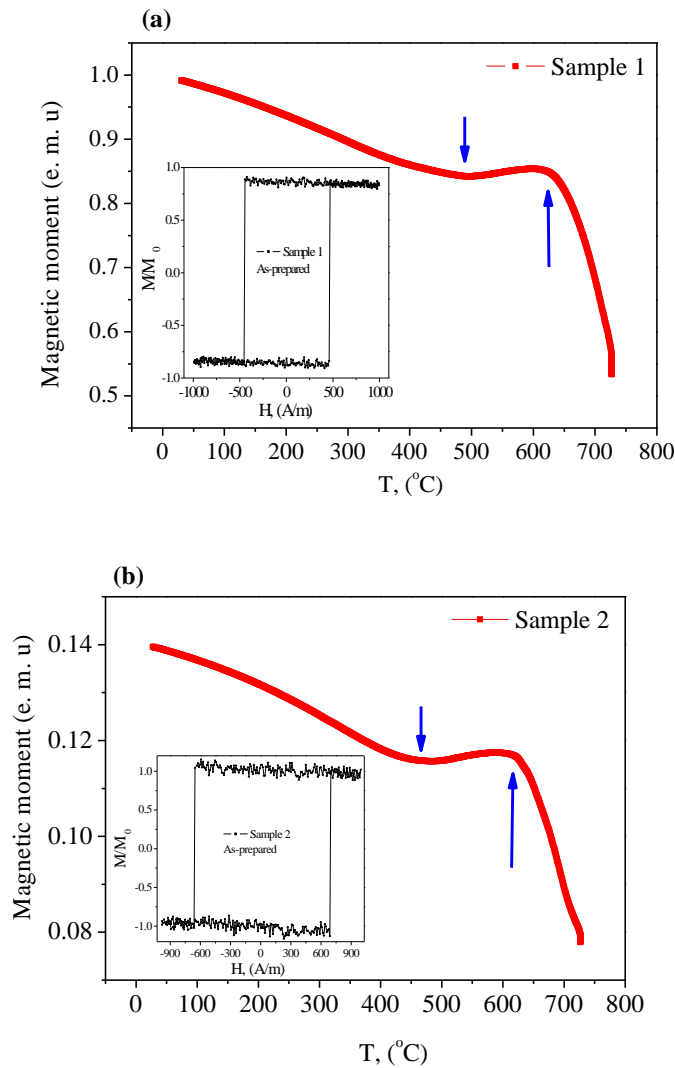


*Figure 2.3 Magnetization dependence on temperature  $M(T)$  of as-prepared  $Fe_{38.5}Co_{38.5}B_{18}Mo_4Cu_1$  Hitperm glass-coated microwires measured at a magnetic field amplitude (1kOe) for sample 1 (a), and sample 2 (b). The inset of both figures shows the corresponding hysteresis loops of as-prepared microwire samples measured at  $f = 50$  Hz.*

Aforementioned magnetic bistable behavior is related to the presence of a single large Barkhausen jump (LBJ), which is commonly interpreted as the magnetization reversal in a large single domain [62]. The value of the switching field can be easily obtained from the hysteresis loops. Usually for low magnetic field frequencies the  $H_{sw}$  and  $H_c$  are very close (see for example insets of Fig. 2.3a-b), but as much as the measuring frequency increases, the overall shape of hysteresis loops changes exhibiting somehow deviation from perfectly rectangular hysteresis loop. This change of hysteresis loop shape has been explained considering the counterbalance between the sweeping rate,  $dH/dt$ , and the switching time related to the time of domain wall propagation through the entire wire [56, 192]. Fig. 2.4 displays the switching field dependence on the measuring frequency of both studied microwire samples.

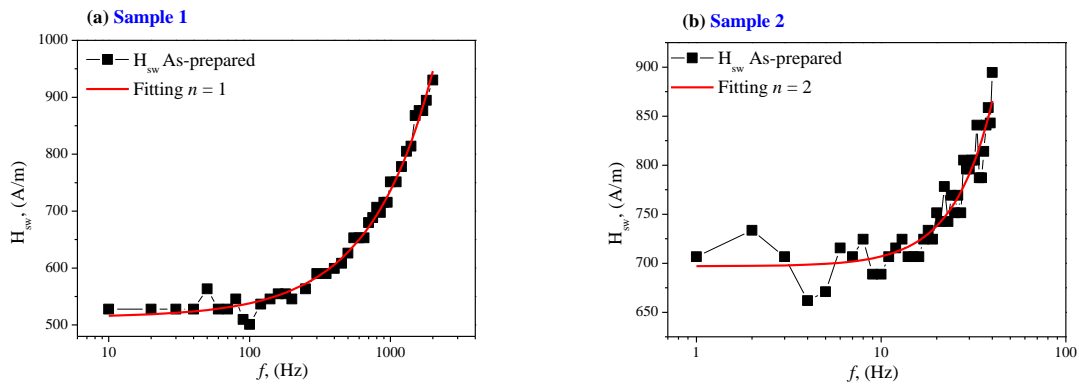


Figure 2.4 Switching field dependence on the measuring frequency  $H_{sw}(f)$  of both as-prepared  $Fe_{38.5}Co_{38.5}B_{18}Mo_4Cu_1$  Hitperm glass-coated microwire sample 1 (a), and sample 2 (b).

The frequency dependence on the switching field as demonstrated in Fig. 2.4 consists of two different regimes. At low frequencies, a slight decrease in the switching field has been observed (Fig. 2.4b), such decrease can be explained based on the magnetic after effect [193]: as the measuring frequency decreases, the measuring time increases and a stabilization of the domain structure through the structural relaxation takes place [194, 195]. At higher frequency, (above 50 Hz) as shown in Fig. 2.4a-b, the switching field is strongly dependent on the frequency [196-198]. Previously, a frequency dependence model of the coercivity in rapidly quenched amorphous materials has been proposed [197]. According to this model, the frequency dependence on the coercivity in various magnetic materials at low enough frequency,  $f$ , can be phenomenologically expressed as:



$$H_{cd} = H_{co} + B (f H_o)^{1/n} \quad (2.1)$$

where  $H_{cd}$  is the dynamic coercivity,  $H_{co}$  is the static coercivity,  $B$  is a coefficient depending on intrinsic parameters of materials, and  $n$  is the coefficient ranging from 1 to 4 depending on sample geometry and the type of the hysteresis loop of the studied materials [197, 198]. In accordance to [197], the coefficient,  $n$ , can take different values as:

- 1 for the case of small domain wall mass,  $m_{DW}$ , and small measuring frequencies.
- 3/2 for the case of small stiffness coefficient,  $\alpha$ , and large measuring frequencies.
- 2 for the case of small stiffness coefficient,  $\alpha$ , and small measuring frequencies.
- 3 for the case of small domain wall mass,  $m_{DW}$ , and large measuring frequencies.

In case of sample 1, the fitting gives parameter  $n = 1$  (Fig. 2.4a). In according to previously published analysis of the frequency dependence on the coercivity [197, 198] this case corresponds to small domain wall mass,  $m_{DW}$ , and low measuring frequencies. Consequently, the frequency dependence on the switching field can be expressed as:

$$H_{sw} = H_{C0} + \frac{4fH_o(L+2M_sA)}{K} \quad (2.2)$$

or,

$$H_{sw} = 3H_{C0} + \frac{fH_o8LM_sA}{K} \quad (2.3)$$

On the other hand, the fitting gives parameter  $n = 2$  for sample 2 (Fig. 2.4b), corresponding to low frequency limits, i.e. when the relaxation time of the domain wall is high. Thus, the frequency dependence of the switching in this case can be expressed as:

$$H_{sw} = H_{C0} + 4A\left(\frac{\chi_{cr}M_s}{L} + 2M_sA\right)f^{1/2} \quad (2.4)$$

being  $\chi_{cr}$  is the critical displacement of the domain wall to be deppined;  $M_s$  is the saturation magnetization, and  $L$  is the damping coefficient. The field from micro-eddy current is proportional to  $AdX/dt$  ( $A$  is a proportionality constant). Accordingly, we can assume that as-prepared nanocrystalline *Hitperm* glass-coated microwires present a strong switching field dependence on the measuring frequency (Fig. 2.4a-b) according to eqs 2.2, 2.3, and 2.4.

Contrary to as-prepared microwire samples, a weak frequency dependence has been observed for either sample 1 or sample 2 annealed at different temperatures. Fig. 2.5 shows the frequency dependence on the switching field for sample 1 (Fig. 2.5a), and for sample 2 (Fig. 2.5b) annealed at various temperatures.

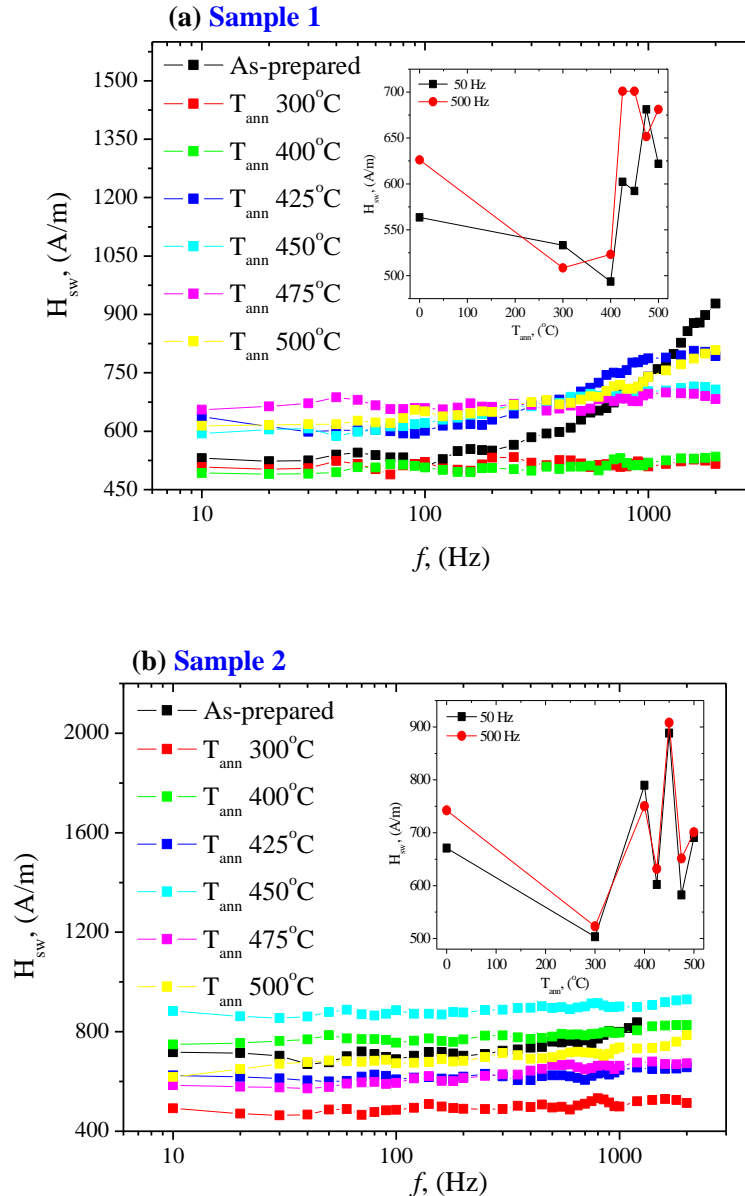


Figure 2.5 Switching field dependence on the measuring frequency  $H_{\text{sw}}(f)$  of as-prepared and annealed  $\text{Fe}_{38.5}\text{Co}_{38.5}\text{B}_{18}\text{Mo}_4\text{Cu}_1$  Hitperm glass-coated microwire at different  $T_{\text{ann}}$  for sample 1 (a), and sample 2 (b). The inset of each figure shows the switching field dependence on  $T_{\text{ann}}$  for samples 1 (a) and 2 (b) measured at  $f = 50$  and  $500$  Hz.

As can be appreciated (Fig. 2.5) only slight changes of the switching field upon increasing the exciting frequency is observed, while depending on the annealing temperature the switching field value changes (insets of Fig. 2.5a-b):  $H_{sw}$  decreases at  $T_{ann}$  ranging between 300-400°C and subsequently increases at higher  $T_{ann}$  either for  $f = 50$  or  $500$  Hz. In a similar way as for  $Fe_{40}Co_{38}Mo_4B_{18}$  Hitperm microwires [199], these variations of the switching field value can be understood in terms of the stress relaxation due to a different thermal expansion coefficient of the metallic nucleus,  $\alpha_m$ , and the glass-coating,  $\alpha_g$ . In addition, grain size refinement (Fig. 2.2) must be taken into account for explanation of the switching field variations after annealing. Therefore, we can conclude that conventional annealing results in a remarkable magnetic softening confirmed by either a decrease in the switching field value (insets of Fig.2.5a-b), or a grain size refinement (Fig. 2.2d).

## 2.4 Domain wall propagation

Usually the rectangular hysteresis loop typical for amorphous wires with positive magnetostriction coefficient is interpreted in terms of nucleation or depinning of the reversed domains inside the internal single domain and the consequent domain wall propagation. Perfectly rectangular shape of the hysteresis loop has been related to a quite fast velocity of such domain wall propagation along the wire. It is noteworthy that the rectangular character of hysteresis loops is due to the highly positive magnetostriction coefficient of  $Fe_{38.5}Co_{38.5}B_{18}Mo_4Cu_1$  Hitperm glass-coated microwires of either both amorphous matrix and the  $\alpha$ -FeCo nanocrystallites ( $\lambda_s \approx 75 \times 10^{-6}$ ) [200]. Consequently, studied  $Fe_{38.5}Co_{38.5}B_{18}Mo_4Cu_1$  Hitperm microwires present DW propagation typical for Fe-based glass-coated microwires. Dependencies of DW velocities on magnetic field of as-prepared and annealed Hitperm microwire samples are visible in Fig. 2.6.

As can be clearly seen (Fig. 2.6a), both samples present rather fast DW velocities (above 1.2 Km/s) and comparable with either other reported Fe-based amorphous [201] or Hitperm nanocrystalline glass-coated microwires [182]. In addition, the DW mobility was also evaluated from  $V(H)$  dependencies according to eq. 3.11 in chapter 3 (page 43). Like the DW velocity, the mobility increases with magnetic field: 0.60, and 0.97  $m^2/A.s$  for sample 1 and sample 2, respectively.

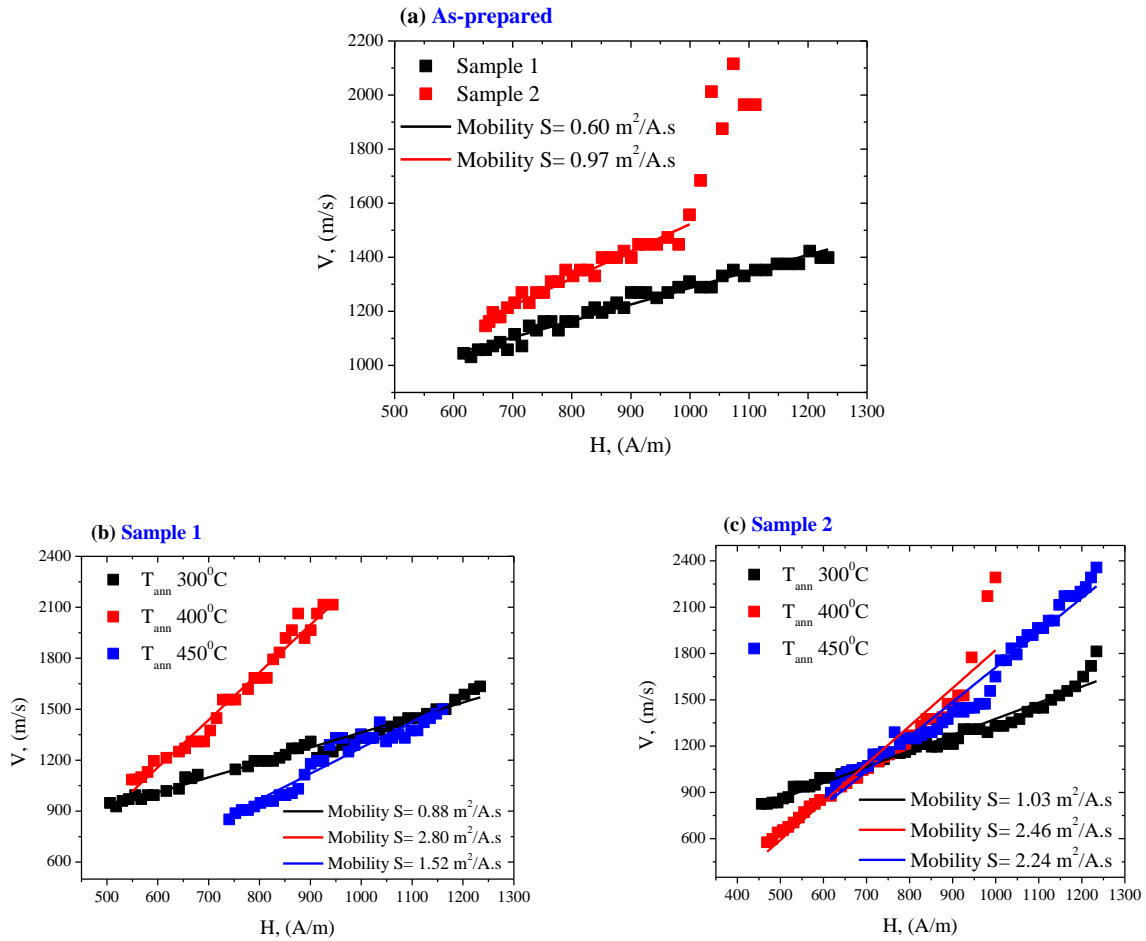


Figure 2.6  $V(H)$  dependencies on magnetic field and calculated mobility for as-prepared  $\text{Fe}_{38.5}\text{Co}_{38.5}\text{B}_{18}\text{Mo}_4\text{Cu}_1$  Hitperm microwire sample 1 and 2 (a);  $V(H)$  dependencies for annealed at different  $T_{\text{ann}}$  for sample 1 (b), and sample 2 (c).

As can be observed (Fig. 2.6 b-c), annealing considerably affects either  $V(H)$  dependencies of both samples or DW mobilities. The common feature of both samples is the extended magnetic field range where linear  $V(H)$  dependencies are observed. In addition, a great enhancement of DW velocities can be appreciated for the sample 1 annealed at  $T_{\text{ann}} = 400^\circ\text{C}$  (Fig. 2.6b) reaching values as fast as 2.1 Km/s, and 2.4 Km/s for sample 2 at  $T_{\text{ann}} = 450^\circ\text{C}$  (Fig. 2.6c). The non-linear  $V(H)$  dependencies observed in both samples (Fig. 2.6 a-c) can be ascribed either to multiple DW nucleation at defects [202, 203] or change the domain structure from transversal to vortex-type [182]. There is also, however, a further point herein to be considered which is related to the magnetoelastic anisotropy,  $K_{me}$ , (see eq. 2.5 page 18) that must affect the DW velocities and mobilities of Hitperm glass-coated microwires. As a result, one can conclude

that the lower magnetoelastic anisotropy (determined by the higher value of  $\rho$ ), the faster domain wall velocity (Fig. 2.6) as well as the higher the DW mobility. In addition, the decrease of the strong internal stresses through annealing results in a total decrease in the magnetoelastic anisotropy. Although the saturation magnetostriction remains highly positive with annealing temperature, the internal stresses sharply decrease from their initial maximum values in the as-prepared to minimal values after annealing. The latter case was confirmed before based on ferromagnetic resonance FMR measurements of  $\text{Fe}_{40}\text{Co}_{38}\text{Mo}_4\text{B}_{18}$  Hitperm microwires: the internal stresses decreased from 800 to 250 MPa after annealing [204]. Finally, this considerable magnetic softens explains the DW velocity enhancement observed after annealing of both Hitperm glass-coated microwire samples.

## 2.5 Concluding remarks

The chapter treated magnetic and structural investigation of new  $\text{Fe}_{38.5}\text{Co}_{38.5}\text{B}_{18}\text{Mo}_4\text{Cu}_1$  Hitperm glass-coated microwires and the effect of 1% addition of Cu. The microstructural analysis of as-prepared samples reveal the presence of nanocrystalline structure consisting of about 23 nm of BCC  $\alpha$ -FeCo B2 ordered crystalline phase and an amorphous precursors formed directly after casting. Quite unusual grains size refinement down to 11 nm has been obtained upon annealing as-prepared microwire samples. Observed microstructural results were discussed in terms of the stress diffusion of limited crystalline growth and the chemical composition. In addition, the devitrification process after conventional annealing might consist of a multiple nucleation of small grains. This massive small grains nucleation resulted in a decrease the average grain size calculated after annealing.

The presence of two structural phases has been confirmed by the magnetization dependence on temperature  $M(T)$  where we observed a noticeable decrease of the magnetization by increasing temperature indicating the existence of two Curie temperatures of either amorphous or nanocrystalline phases. Rectangular hysteresis loops have been observed in as-prepared Hitperm microwire samples, typical for Fe-based glass-coated micowires, which allowed us to investigate the magnetization reversal processes and domain wall dynamics. A strong dependence of the switching field on the measuring frequency of as-prepared samples has been observed. Whereas, a weak dependence has been noticed with annealed microwires. The switching field values have

been drastically changed with annealing: a switching field decrease has been explained due to the structural and stress relaxation of *Hitperm* microwires after annealing.

An overall considerable change of magnetic properties: magnetic softening, change of DW dynamics, and change of the frequency dependence of switching field have been observed after annealing. Observed changes of magnetic properties have been discussed considering structural relaxation of such grains with positive magnetostriction, grains refinement and internal stresses relaxation. Quite fast DW velocities have been recorded for as-prepared samples reaching values as fast as 1.2 *Km.s*. In addition, decreasing the magnetoelastic anisotropy after annealing together with the internal stress relaxations resulted in an enhancement of the DW velocity as well as DW mobility. These structural benefits found in the nanocrystalline *Hitperm* glass-coated microwires are promising for developing outstanding magnetic properties for technological applications in which fast magnetization processes are required.

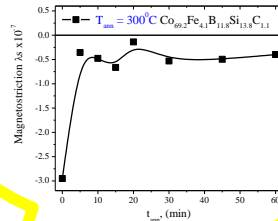
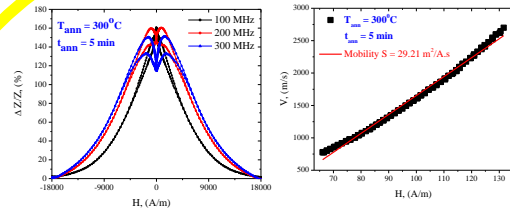
## 2.6 Further reading: Publications related to this chapter

- [1] A. Talaat, J. J. del Val, V. Zhukova, M. Ipatov, P. Klein, R. Varga, J. Gonzalez, M. Zhdanova, M. Zhdanova, M. Churyukanova, A. Zhukov. *Effect of annealing on magnetic properties of nanocrystalline Hitperm-type glass-coated microwires*. Journal of Alloys and Compounds, 660 297-303 (2016)
- [2] A. Talaat, J. J. del Val, V. Zhukova, M. Ipatov, P. Klein, R. Varga, J. Gonzalez, M. Churyukanova, A. Zhukov. *Grain size refinement in nanocrystalline Hitperm-type glass-coated microwires*. Journal of Magnetism and Magnetic Materials (2015) accepted
- [3] A. Talaat, V. Zhukova, M. Ipatov, J. M. Blanco, R. Varga, P. Klein, L. Gonzalez-Legarreta, B. Hernando, A. Zhukov. *Magnetic properties of nanocrystalline microwires*. Journal of Electronic Materials DOI: 10.1007/s11664-015-3966-3 (2015)
- [4] A. Talaat, P. Klein, V. Zhukova, R. Varga, A. Zhukov. *Influence of stress relaxation on the magnetization process of Hitperm-type glass-coated microwires*. International Journal of Advanced Applied Physics Research, 1 (2) 6-13 (2014)
- [5] V. Zhukova, A. Talaat, M. Ipatov, J. J. del Val, J. M. Blanco, L. Gonzalez-Legarreta, B. Hernando, R. Varga, P. Klein, M. Churyukanova, A. Zhukov. *Optimization of soft magnetic properties in nanocrystalline Fe-rich glass-coated microwires*. Journal of Metals, 67 (9) 2108-2116 (2015)

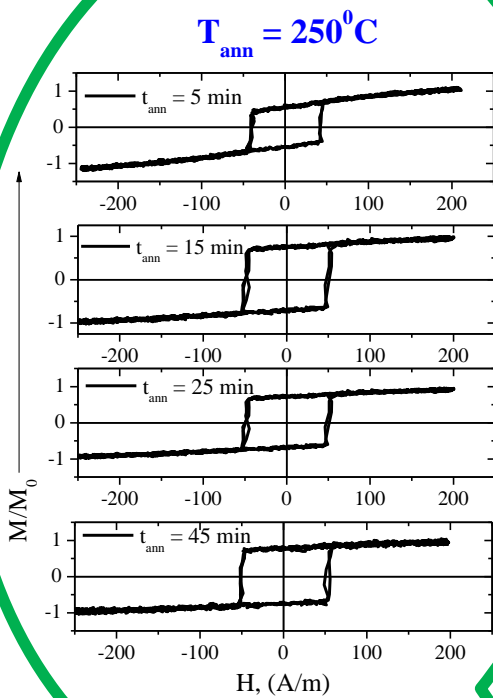
# Engineering of amorphous Co-based microwires by annealing

3

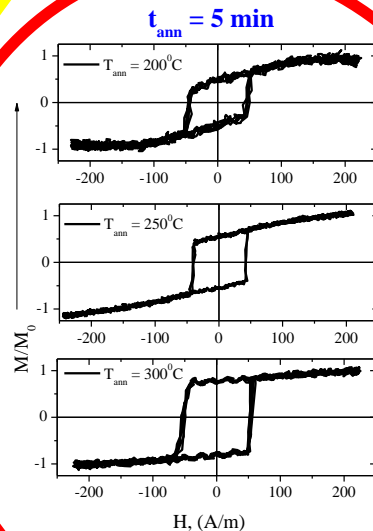
At certain annealing conditions we observed coexistence of high GMI effect and fast DW propagation in the same annealed microwire sample



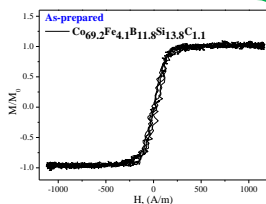
Annealing induces changes in the magnetostriction constant



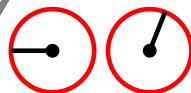
Fixed temperature and different time



Fixed time and different temperatures



Annealing of amorphous Co-based microwires with low negative magnetostriction constant allowed us to tailor their magnetic properties



Conventional and stress annealing

### 3.1 The main objective

The last two chapters have discussed the interesting consequences of the optimization of the magnetic properties by nanocrystallization of either Fe-based glass-coated microwires (*Finemet*-like alloys) or partially substituted Fe% by Co% (*Hitperm*-like alloys). As was demonstrated, in the absence of magnetocrystalline anisotropy, the magnetoelastic anisotropy,  $K_{me}$ , becomes the main factor that affect magnetic properties of these glass-coated microwires. For these concerns, the major possibilities to tailor magnetic properties of amorphous microwires are either the internal stresses or a proper selection of the chemical composition of the metallic nucleus controlling the magnetostriction value of the chosen alloy. The latter found to be negative for amorphous Co-based microwires (see page 19 in chapter 2), positive for Fe-based microwires, and vanishing for  $(\text{Co}_{1-x}\text{Fe}_x)_{75}\text{Si}_{15}\text{B}_{10}$  compositions at  $x > 0.06$  [68, 143]. Around vanishing but still negative magnetostriction compositions, excellent magnetic properties can be achieved by optimizing the heat treatment regime keeping the annealing temperature,  $T_{ann}$ , below the crystallization temperature of the amorphous phase (prior to any participation of additional phases).

Through this chapter, we systematically investigate the effect of either conventional or stress annealing performed at annealing temperature,  $T_{ann}$ , ranging between 200-300°C for annealing time,  $t_{ann}$ , ranging between 5-60 min with the aim to tailor the magnetoelastic anisotropy of low negative magnetostrictive Co-based glass-coated microwires having a nominal composition consisting of  $\text{Co}_{69.2}\text{Fe}_{4.1}\text{B}_{11.8}\text{Si}_{13.8}\text{C}_{1.1}$  with a total diameter,  $D = 30.2$  microns, and metallic nucleus diameter,  $d = 25.6$  microns. At certain annealing conditions we observed coexistence of high GMI effect and fast DW propagation in the same annealed microwire sample.

### 3.2 As-prepared state

Fig. 3.1a shows XRD and hysteresis loops of as-prepared  $\text{Co}_{69.2}\text{Fe}_{4.1}\text{B}_{11.8}\text{Si}_{13.8}\text{C}_{1.1}$  glass-coated microwires. As can be clearly seen,  $\text{Co}_{69.2}\text{Fe}_{4.1}\text{B}_{11.8}\text{Si}_{13.8}\text{C}_{1.1}$  microwires present an amorphous structure confirmed by a diffuse halo without observation of any crystalline peak. Fig. 3.1b shows inclined hysteresis loops of as-prepared microwires exhibiting a very low coercive field of about 8 A/m typical for amorphous Co-based glass-coated microwires with low negative magnetostriction constant. The internal stresses of as-prepared microwires give rise to



an easy magnetization direction perpendicular to the wire axis, leading to an alignment of the magnetic moments in the direction which is perpendicular (circumferential) to the wire axis, as we described in (chapter 2, page 19). As a consequence, only small hysteresis is observed when an axial magnetic field is applied with relatively low coercivities typical for Co-based microwires with low negative magnetostriction.

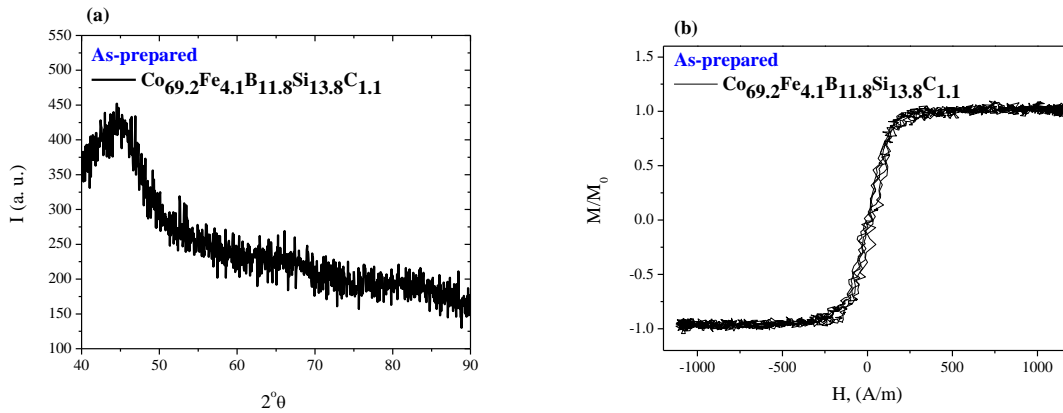


Figure 3.1 XRD patterns for as-prepared  $\text{Co}_{69.2}\text{Fe}_{4.1}\text{B}_{11.8}\text{Si}_{13.8}\text{C}_{1.1}$  glass-coated microwires (a), and hysteresis loops of the same as-prepared sample (b).

### 3.3 Engineering of magnetic properties by heat treatment

#### 3.3.1 Conventional annealing: A manipulation between annealing time and temperature

We performed series of conventional annealing at either different annealing time,  $t_{ann}$ , or annealing temperature,  $T_{ann}$ , as shown in Fig. 3.2. As can be seen, annealing even for a very short annealing time,  $t_{ann} = 5 \text{ min}$  at different annealing temperatures,  $T_{ann}$ , at  $200^\circ\text{C}$ , or  $250^\circ\text{C}$ , and  $300^\circ\text{C}$  induced considerable changes of the hysteresis loops. Effect of annealing temperature,  $T_{ann}$ , on the character of hysteresis loops for a fixed annealing time,  $t_{ann}$ , is shown in Fig. 3.2a. Even 5 minutes annealing at  $T_{ann} = 200^\circ\text{C}$  considerably affects the hysteresis loops: the hysteresis loop transforms from inclined (Fig. 3.1b) to rectangular (Fig. 3.2a). An equally significant parameter affected the magnetic properties of studied  $\text{Co}_{69.2}\text{Fe}_{4.1}\text{B}_{11.8}\text{Si}_{13.8}\text{C}_{1.1}$  microwires is the annealing time,  $t_{ann}$ , at fixed annealing temperature at  $T_{ann} = 250^\circ\text{C}$  as depicted in Fig. 3.2b. As much as the annealing temperature increases (Fig. 3.2a), the hysteresis loop becomes more and more rectangular, in a similar way as the annealing time increases at fixed temperature (Fig. 3.2b). To better clarify the effect of annealing, we represent the evolution of

coercivity,  $H_c$ , (Fig. 3.2c) and reduced remanent magnetization,  $M_r/M_{Hmax}$ , (Fig. 3.2d) versus the annealing time. As can be clearly observed, increasing the annealing temperature as well as the annealing time leads to an increase of either the coercivity or remanent magnetization, being such increase more obvious at higher annealing temperatures, i.e.  $T_{ann} = 300^\circ\text{C}$  (Fig.3.2c).

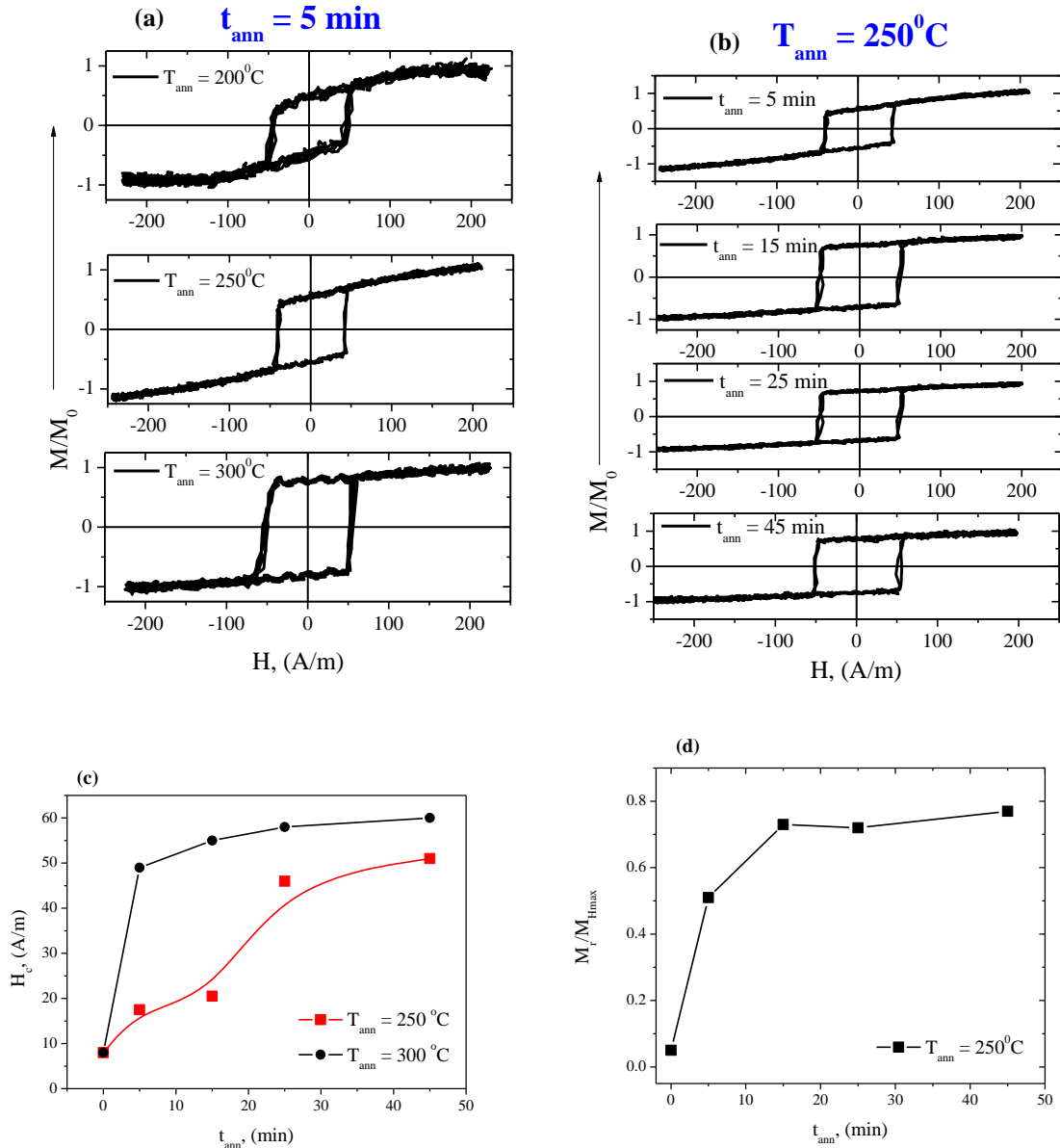


**Figure 3.2** Effect of annealing temperature,  $T_{ann}$  at fixed annealing time,  $t_{ann} = 5$  min on the hysteresis loops of  $\text{Co}_{69.2}\text{Fe}_{4.1}\text{B}_{11.8}\text{Si}_{13.8}\text{C}_{1.1}$  glass-coated microwires (a); effect of annealing time,  $t_{ann}$  at fixed annealing temperature,  $T_{ann} = 250^\circ\text{C}$  on the hysteresis loops of the same microwire sample (b); dependence the coercive field on annealing time at different  $T_{ann}$  (c), and dependence of reduced remanent magnetization on annealing time at  $T_{ann} = 250^\circ\text{C}$  (d).

Usually the inverse tendency: the coercivity decreases with annealing temperatures below the crystallization as we have proved along the previous two chapters for *Finemet* and *Hitperm* glass-coated microwires (due to the stress relaxation). However, herein in order to explain this unusual increase of coercivity after annealing, we must consider not only the stress relaxation but also changing the character of the remagnetization process induced by heat treatment. Considering the effect of stress relaxation on the magnetostriction constant and different character of hysteresis loops of glass-coated microwires with either negative or positive magnetostriction constant, we can assume that the second term of eq. 2.6 (chapter 2, page 18) decreases after annealing. This decrease must be related to the internal stress relaxation (decreasing of  $\sigma_i$ ) and therefore, a total decrease of the magnetostriction value is achieved. Fig. 3.3 shows the magnetostriction values measured for as-prepared and annealed  $\text{Co}_{69.2}\text{Fe}_{4.1}\text{B}_{11.8}\text{Si}_{13.8}\text{C}_{1.1}$  microwire samples at  $T_{\text{ann}} = 300^\circ\text{C}$  for different annealing time.

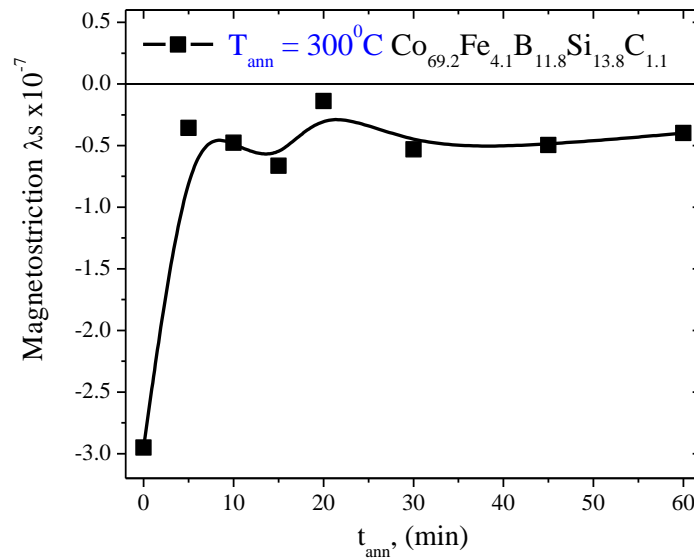


Figure 3.3 Magnetostriction dependence on annealing time for as-prepared and annealed  $\text{Co}_{69.2}\text{Fe}_{4.1}\text{B}_{11.8}\text{Si}_{13.8}\text{C}_{1.1}$  glass-coated microwires at  $T_{\text{ann}} = 300^\circ\text{C}$ .

As can be appreciated, the magnetostriction value changes dramatically with annealing: the magnetostriction shifts from highly negative ( $-2.9 \times 10^{-7}$ ) in as-prepared to low negative ( $-0.3 \times 10^{-7}$ ) after 60 min annealing at  $T_{\text{ann}} = 300^\circ\text{C}$ .

On the other hand, there are various factors affecting the soft magnetic behavior of amorphous materials. At least five pinning effects contributing to the total coercivity have been identified and discussed in details by Kronmuller et al. [205, 206]:

- Intrinsic fluctuations of exchange energies and local anisotropies ( $10^{-3}$ - 1 me),  $H_c(i)$
- Clusters and chemical short ordered regions ( $< 1$  me),  $H_c(SO)$
- Surface irregularities ( $< 5$  me),  $H_c(surf)$
- Relaxation effects due to local structural rearrangements (0.1 - 10 me),  $H_c(rel)$
- Volume pinning of domain walls by defect structures in magnetostrictive alloys (10 - 100 me),  $H_c(\sigma)$

Within the framework of the statistical potential theory, the resultant total coercivity therefore was expressed as following [206]:

$$H_{c\text{total}} = \sqrt{H_c\sigma^2 + H_c\text{sur}^2 + H_cSO^2 + H_ci^2} + H_c\text{rel}^2 \quad (3.1)$$

In the case when the surface irregularities give a largest contribution, the various terms add linearly [2, 3], i.e.:

$$H_{c\text{total}} = H_c\sigma^2 + H_c\text{sur}^2 + H_cSO^2 + H_ci^2 + H_c\text{rel}^2 \quad (3.2)$$

In addition, the induced magnetic anisotropy plays an important role in annealed amorphous materials (especially in the presence of magnetic field or/and applied stress) as we described along chapter 2 (pages 22-25). In the case of glass-coated microwires we must take into account that conventional furnace annealing must be considered as stress annealing in the presence of internal stresses. It is also worth mentioning that the axial internal stresses component induced by glass-coating is the largest one. Therefore applying tensile axial stress during annealing (stress annealing) predicts an enhancement of the induced anisotropy. Consequently we have performed conventional and stress annealing of the samples at the same annealing temperature.

### 3.3.2 Stress annealing

Fig. 3.4a shows hysteresis loops of  $\text{Co}_{69.2}\text{Fe}_{4.1}\text{B}_{11.8}\text{Si}_{13.8}\text{C}_{1.1}$  glass-coated microwires annealed at  $T_{\text{ann}} = 300^\circ\text{C}$  for 45 min without stress and under tensile stress of about 80 MPa.

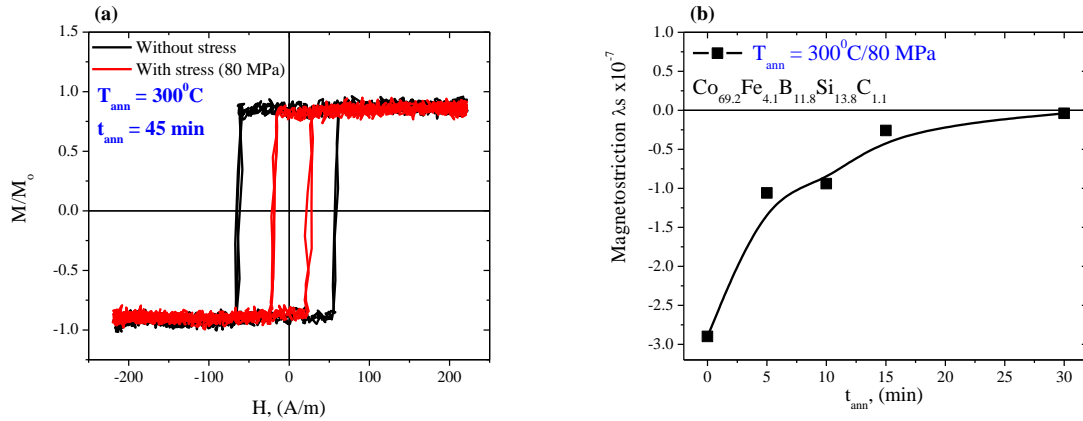


*Figure 3.4* Hysteresis loops of annealed  $\text{Co}_{69.2}\text{Fe}_{4.1}\text{B}_{11.8}\text{Si}_{13.8}\text{C}_{1.1}$  glass-coated microwires at  $T_{ann} = 300^\circ\text{C}$  for 45 min without stress and under tensile stress of about 80 MPa (a), and magnetostriction dependence on on annealing time for stress annealed  $\text{Co}_{69.2}\text{Fe}_{4.1}\text{B}_{11.8}\text{Si}_{13.8}\text{C}_{1.1}$  microwire samples at  $T_{ann} = 300^\circ\text{C}/80\text{ MPa}$  (b).

As can be assumed, stress annealed microwires exhibit lower coercivity as-compared to conventional annealed samples (Fig. 3.4a). Herein, we must consider the back stresses arising during the stress annealing as previously reported for Fe-based amorphous microwires [78] (see Fig. 2.3 chapter 2, page 25). Such back stresses can result in a decrease of the magnetostriction constant according to eq. 2.6 as well as directly recorded values in Fig. 3.4b: the magnetostriction shifts from highly negative in as-prepared to nearly zero for stress annealed  $\text{Co}_{69.2}\text{Fe}_{4.1}\text{B}_{11.8}\text{Si}_{13.8}\text{C}_{1.1}$  microwire samples at  $t_{ann} = 30\text{ min}$ . Consequently, the contribution of two different anisotropies induced by stress annealing, one arises from the mechanical load (longitudinal) and other from annealing (transversal) result in a redistribution of the internal stresses and/or local microstructure of the sample, therefore, the net magnetoelastic energy in the stressed state is minimized. In addition, if the magnetostriction coefficient is low and negative, we must consider two opposite consequences of the internal stresses. The first contribution is an increase of the total magnetoelastic energy. The second one must be related to the stress dependence (either applied or internal stresses:  $\sigma_{total} = \sigma_{applied} + \sigma_{internal}$ ) on magnetostriction coefficient described by eq. 2.6, which is quite relevant for the case of low magnetostriction constant,  $\lambda_{s,0}$ , as described in (see page 24 in chapter 2). In accordance to eq. (2.6) the magnetostriction constant under stress,  $\lambda_{s,\sigma}$ , must decrease (Fig. 3.4b).

Based on the dependencies observed in Figs. 3.2-3.4, the increase of coercivity and rectangular character of hysteresis loops after annealing must be attributed to the stress relaxation and corresponding magnetostriction changes.

On the other hand, undoubtedly, the effect of annealing time,  $t_{ann}$ , for the case of stress annealing on the coercive field behavior is as important as for abovementioned conventional annealing without stress (Fig. 3.2b). Fig. 3.5a displays hysteresis loops of stress annealed  $\text{Co}_{69.2}\text{Fe}_{4.1}\text{B}_{11.8}\text{Si}_{13.8}\text{C}_{1.1}$  microwires performed at fixed annealing temperature,  $T_{ann} = 300^\circ\text{C}$  under 80 MPa for  $t_{ann} = 20$  and 45 min. As can be deduced from this figure (Fig. 3.5a), the coercive field decreases for longer annealing time: the coercive field of stress annealed microwire sample for 20 min is slightly higher than for 45 min (inset of Fig. 3.5a). The reason for such decrease in,  $H_c$ , is also associated with the decrease of the magnetostriction constant with annealing time (Fig. 3.4b).

In addition, we have performed measurements of the DW dynamics considering the rectangular character of hysteresis loops of stress annealed  $\text{Co}_{69.2}\text{Fe}_{4.1}\text{B}_{11.8}\text{Si}_{13.8}\text{C}_{1.1}$  microwires. Thus, due to a rectangular hysteresis loop, the remagnetization of this sample is running through the DW propagation within an inner single-domain core (Fig. 2.2 chapter 2, page 20). As can be appreciated from Fig. 3.5b,  $V(H)$  dependencies on applied magnetic fields present typical linear growth of DW velocity with applied magnetic field. Quite fast either DW velocities or DW mobilities are observed, similarly to other DW velocities for low magnetostrictive glass-coated microwires with magnetic bistability presenting fast DW propagation [201, 207]. In a parallel way as for the coercive fields presented in Fig. 3.5a, stress annealed samples for  $t_{ann} = 45$  min presents either higher DW velocity or mobility than that annealed for  $t_{ann} = 20$  min due to either lower magnetostriction or magnetoelastic anisotropy as discussed before: the DW velocity increases from 1.8 KA/m for  $t_{ann} = 20$  min to 2.1 KA/m for  $t_{ann} = 45$  min giving a corresponding high mobility as much as 25.61 and 22.80  $\text{m}^2/\text{A}\cdot\text{s}$  for 45 and 20 min, respectively.

Interestingly, instead of an usual decrease of DW velocities under the effect of applied stresses [201, 207], we observed considerable enhancements of DW velocity up to 2.5 KA/m at given magnetic field values under applying tensile stresses for either both stress annealed samples (Fig. 3.5c). Such DW enhancement must be attributed to the magnetostriction constant decreasing under effect of applied stress (Fig. 3.4b).

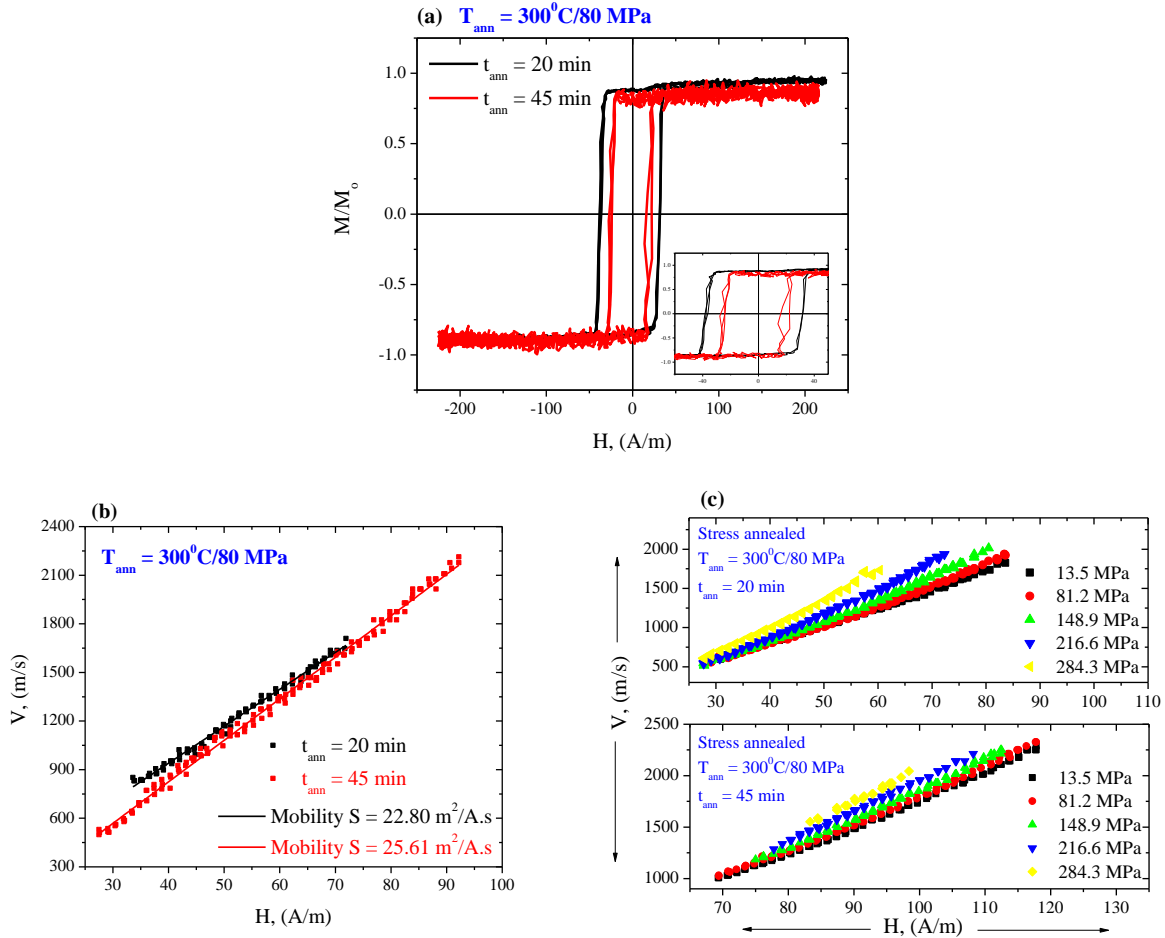


*Figure 3.5* Hysteresis loops of stress annealed  $\text{Co}_{69.2}\text{Fe}_{4.1}\text{B}_{11.8}\text{Si}_{13.8}\text{C}_{1.1}$  microwires performed at fixed annealing temperature,  $T_{\text{ann}} = 300^\circ\text{C}$  under 80 MPa for  $t_{\text{ann}} = 20$  and 45 min (a); the inset shows zoom-in of a narrow magnetic field region (a);  $V(H)$  dependencies on magnetic field and calculated mobility for stress annealed microwire samples at the same conditions for  $t_{\text{ann}} = 20$  and 45 min (b), and dependencies of DW velocity on magnetic field measured for stress annealed microwires at the same conditions for  $t_{\text{ann}} = 20$  and 45 min under different tensile applied stresses (c).

### 3.3.3 Simultaneous detection of DW and GMI in the same annealed microwire samples

Certainly, these versatile properties of studied  $\text{Co}_{69.2}\text{Fe}_{4.1}\text{B}_{11.8}\text{Si}_{13.8}\text{C}_{1.1}$  glass-coated microwires with enhanced and tunable soft magnetic properties make them suitable to design very interesting functional characteristics for technological sensing applications. Similarly to other Co-based amorphous microwires, studied  $\text{Co}_{69.2}\text{Fe}_{4.1}\text{B}_{11.8}\text{Si}_{13.8}\text{C}_{1.1}$  microwire presents quite high GMI ratios at different frequencies. Fig. 3.6a displays  $\Delta Z/Z(H)$  dependence of as-prepared  $\text{Co}_{69.2}\text{Fe}_{4.1}\text{B}_{11.8}\text{Si}_{13.8}\text{C}_{1.1}$  microwire, as can be clearly seen, GMI ratios reaches up to 285%.

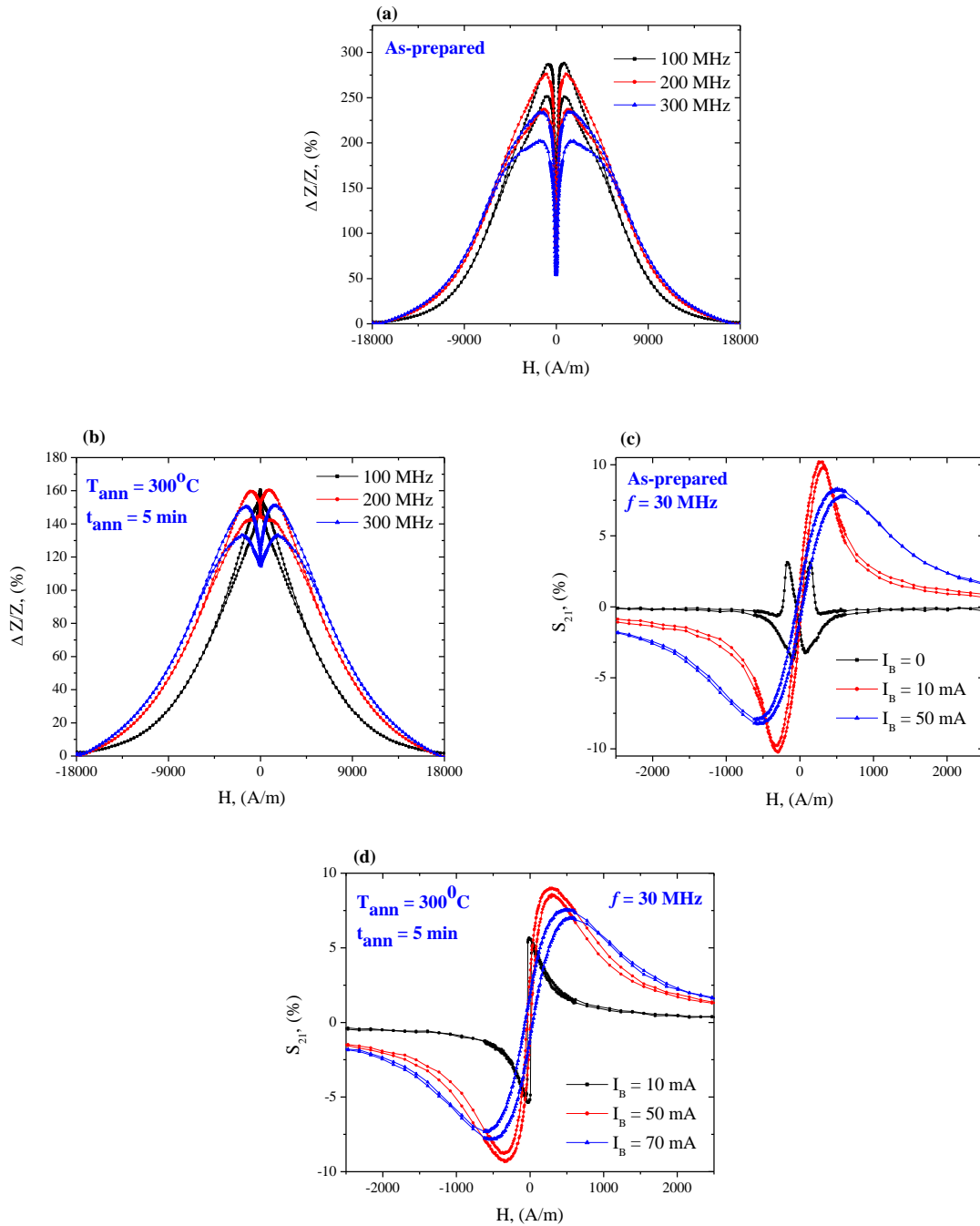


Figure 3.6 Diagonal GMI effect of as-prepared  $\text{Co}_{69.2}\text{Fe}_{4.1}\text{B}_{11.8}\text{Si}_{13.8}\text{C}_{1.1}$  glass-coated microwires (a); diagonal GMI effect of annealed microwire samples at  $T_{ann} = 300^\circ\text{C}$  for  $t_{ann} = 5$  min measured at different frequencies (b); off-diagonal GMI of as-prepared microwires measured at  $f = 30$  MHz for different values of  $I_B$  (c), and off-diagonal GMI for annealed microwire samples at the same conditions (d).



Effect of conventional annealing on GMI is visible in Fig. 3.6b. As can be appreciated, the GMI ratio of annealed microwires at  $T_{ann} = 300^\circ\text{C}$  for  $t_{ann} = 5 \text{ min}$  is lower than in as-prepared microwire:  $\Delta Z/Z$  decreases from 285% in as-prepared state to 160% for annealed microwire sample. In addition, we observed a change of the magnetic field dependence of  $\Delta Z/Z$ : the field of maximum is lower in annealed microwires for all the measured frequencies. As discussed before in chapter 3, the field of maximum corresponds to the magnetic anisotropy field [96]. Moreover magnetic field dependence of GMI ratio is strongly affected by the magnetic anisotropy [177].

It is also interesting to note that either as-prepared or annealed  $\text{Co}_{69.2}\text{Fe}_{4.1}\text{B}_{11.8}\text{Si}_{13.8}\text{C}_{1.1}$  microwires present off-diagonal impedance (Fig. 3.6c-d). The off-diagonal GMI effect represented by  $S_{21}$  without a bias current is rather low (poor) in the as-prepared samples (Fig. 3.6c). Likewise reported before for amorphous Co-based microwires bias field,  $H_B$ , produced by a bias current,  $I_B$ , strongly affects the off-diagonal impedance (Fig. 3.6c-d). Even though under a maximum  $I_B = 70 \text{ mA}$ , (Fig. 3.6d) noticeable hysteresis is observed reflecting a considerable helical magnetic anisotropy of the sample [141, 208]. We have experimentally proved such existence of helical anisotropy of studied sample by means of magneto optical studies [209].

GMI responses of annealed  $\text{Co}_{69.2}\text{Fe}_{4.1}\text{B}_{11.8}\text{Si}_{13.8}\text{C}_{1.1}$  microwires at  $T_{ann} = 300^\circ\text{C}$  for  $t_{ann} = 5 \text{ min}$  are obtained, however, the sample has roughly rectangular hysteresis loop (see Fig.3.2a). Indeed, it is worth mentioning, that the flat regions of the hysteresis loop present a considerable slope, i.e. appreciably high magnetic permeability than those annealed microwires for longer annealing time,  $t_{ann}$ , (see Fig. 3.4a sample annealed for 45 min without stress). We can therefore assume that the outer domain shell presents high magnetic permeability. Simultaneously, the same sample also presents quite fast DW dynamics (Fig. 3.7): we observed typical single DW propagation with nearly-linear  $V(H)$  dependence of DW velocity. A maximum velocity observed in this sample was about 2.7 Km/s having a DW mobility of about  $29.2 \text{ m}^2/\text{A.s}$  as can be appreciated in Fig. 3.7.

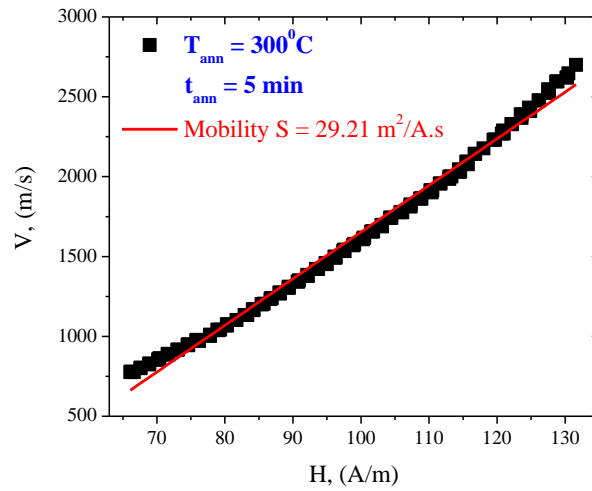


Figure 3.7  $V(H)$  dependencies on magnetic field and calculated mobility of annealed  $\text{Co}_{69.2}\text{Fe}_{4.1}\text{B}_{11.8}\text{Si}_{13.8}\text{C}_{1.1}$  glass-coated microwires at  $T_{\text{ann}} = 300^\circ\text{C}$  for  $t_{\text{ann}} = 5 \text{ min}$ .

We have also aimed to compare between either GMI responses or DW propagation in stress annealed  $\text{Co}_{69.2}\text{Fe}_{4.1}\text{B}_{11.8}\text{Si}_{13.8}\text{C}_{1.1}$  microwire samples as shown in Fig. 3.8. For comparison, we represent conventional and stress annealed microwires performed under the same annealing conditions.

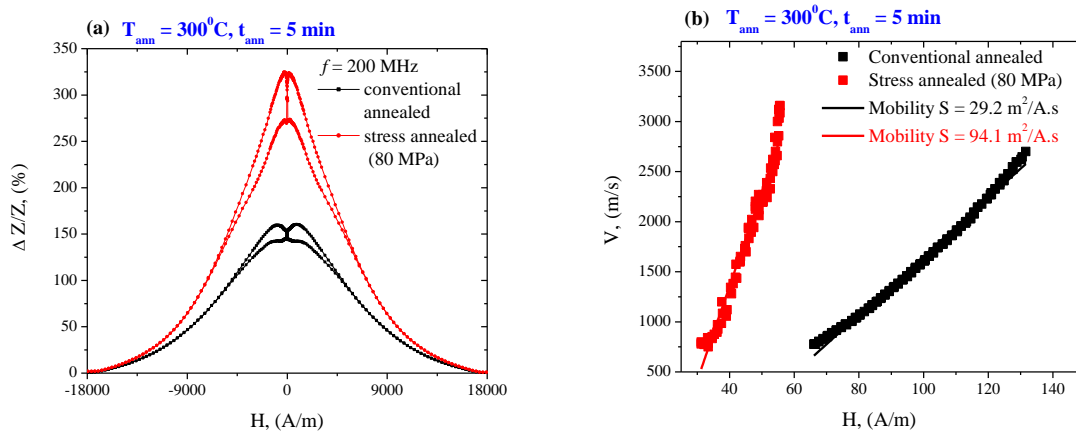


Figure 3.8  $\Delta Z/Z \% (H)$  (a), and  $V (H)$  (b) dependencies on magnetic fields for conventional and stress annealed  $\text{Co}_{69.2}\text{Fe}_{4.1}\text{B}_{11.8}\text{Si}_{13.8}\text{C}_{1.1}$  glass-coated microwires. A Comparison between conventional and stress annealing effect performed at  $T_{\text{ann}} = 300^\circ\text{C}$  for  $t_{\text{ann}} = 5 \text{ min}$ .

As can be observed in Fig. 3.8a, GMI responses likely increase for stress annealed microwire samples:  $\Delta Z/Z_{max}$  (measured at  $f = 200$  MHz) increases from 160% of conventional annealed microwires up to  $\approx 325\%$  for the case of stress annealing. In a similar way, DW velocity and mobility increase for those samples subjected to stress annealing reaching values of about  $3.2$  KA/m (Fig. 3.8b). In addition, stress-annealed microwire samples present fast DW propagation, and magnetic field range for a single DW propagation shifted to the lower field region down to  $30$  A/m. This difference must be attributed to lower coercivity of stress-annealed microwires (similarly to those observed in Fig. 3.4a).

Regarding to experimentally observed dependencies in Figs. 3.1-3.8, there are few parallel connected phenomena must be considered:

In the first instance, we can assume that stress relaxation induced by the annealing either conventional or under stress affects the magnetostriction constant and induces changes in the magnetostriction sign as we have proved in Figs. 3.3 & 3.4b. Therefore, we observe change of the character of hysteresis loops and of the remagnetization process. The application of tensile stresses affects the magnetostriction coefficient allowing reduction of the magnetoelastic energy and achievement of faster DW propagation.

We assume that the outer domain shall of annealed Co-based microwire exhibiting both fast DW propagation and GMI effect (Figs. 3.6-3.8) has high circumferential magnetic permeability. This assumption is deduced by much higher GMI ratio of microwire samples show rectangular hysteresis loop after annealing. These unusual features as well as the rectangular character of hysteresis loop of annealed microwires can be explained considering non-uniformity of the internal stresses distribution induced by glass coating. We can also assume that the internal stresses are distributed inhomogeneously along the metallic nucleus radius, being positive in the inner part and negative in the outer shell. Indeed, in according to previously published calculations: changing of the sign of the internal stresses is reported near the interface between the metallic nucleus and glass-coating [37, 41]. Observed fast DW propagation is related to the fast magnetization switching within the single domain axially magnetized inner core, i.e. related to the remagnetization process of the inner part of the microwire. The GMI effect has completely different origin. The GMI effect is associated with the high circumferential permeability of the surface layer.

Understanding of the processes affecting the formation of magnetic anisotropy and determining the remagnetization process of Co–Fe based microwires with low magnetostriction constant allows us to tailor their magnetic properties as well as to find the annealing conditions where we can simultaneously observe fast DW propagation and considerable GMI effect in the same annealed samples.

### 3.4 Concluding remarks

Along this chapter, it has been experimentally demonstrated that magnetic properties of amorphous  $\text{Co}_{69.2}\text{Fe}_{4.1}\text{B}_{11.8}\text{Si}_{13.8}\text{C}_{1.1}$  glass-coated microwires can be tailored by annealing. Conventional and stress annealing have considerably affected hysteresis loop, GMI effect and DW dynamics of presently studied samples. Observed dependencies have been discussed considering stress relaxation and change of the magnetostriction after samples annealing. At certain annealing conditions we observed coexistence of GMI effect and fast DW propagation in the same annealed microwire sample. Moreover after annealing at certain conditions we observed an increase of DW velocity under applied tensile stress.

The creation of samples exhibiting both aforementioned properties is very attractive, and thus, opens up a new pathway to exploit Co-based wires for dual functional GMI and DW related sensing applications.

### 3.5 Further reading: Publication related to this chapter

- [1] A. Talaat, J. M. Blanco, M. Ipatov, V. Zhukova, A. P. Zhukov. *Domain Wall Propagation in Co-Based Glass-Coated Microwires: Effect of Stress Annealing and Tensile Applied Stresses*. IEEE Transactions on Magnetism, 50 (11) 1-4 (2014)
- [2] A. Talaat, M. Churyukanova, J. M. Blanco, M. Ipatov, V. Zhukova, A. Zhukov. *Simultaneous detection of high giant magnetoimpedance and fast domain wall propagation in Co-based glass-coated microwires*. IEEE Magnetism Letters (2015) accepted. DOI: 10.1109/LMAG.2015.2505242
- [3] A. Talaat, M. Ipatov, V. Zhukova, J. M. Blanco, A. Zhukov. *Manipulation of magnetic and magneto-transport properties of amorphous glass-coated microwires through various annealing processes*. physica status solidi (c), 11 (5-6) 1125-1129 (2014)
- [4] A. Zhukov, A. Talaat, M. Ipatov, J. M. Blanco, V. Zhukova "Tailoring of magnetic properties and GMI effect of Co-rich amorphous microwires by heat treatment" Journal of Alloys and Compounds 615, 610-615 (2014)
- [5] V. Zhukova, A. Talaat, M. Ipatov, J. M. Blanco, M. H. Phan, A. P. Zhukov. *Effect of Annealing on Magnetic Properties and Giant Magnetoimpedance Effect of Amorphous Microwires*. IEEE Transactions on Magnetism, 50 (6) 1-4 (2014)
- [6] A. Zhukov, A. Talaat, J. M. Blanco, M. Ipatov, V. Zhukova. *Tuning of Magnetic Properties and GMI Effect of Co-Based Amorphous Microwires by Annealing*. Journal of Electronic Materials, 43 (12) 4532-4539 (2014)

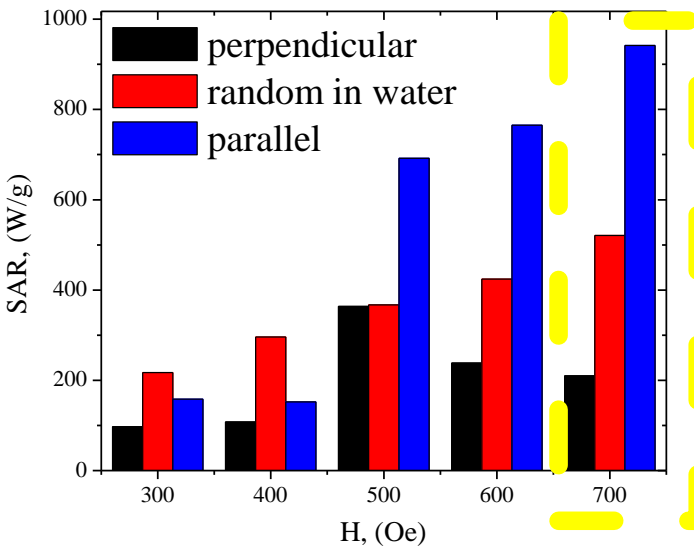
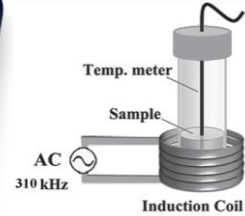
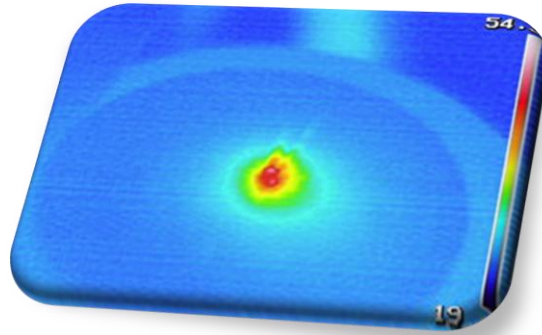
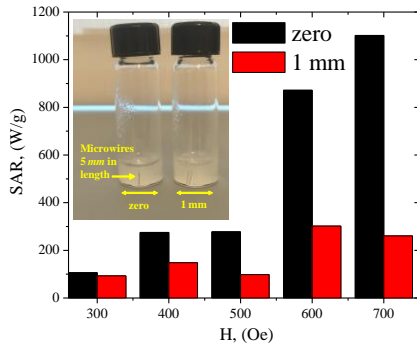
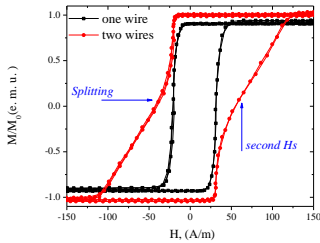
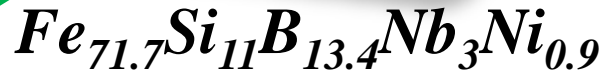
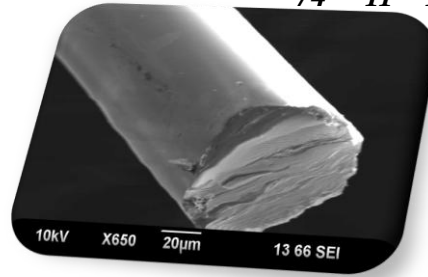
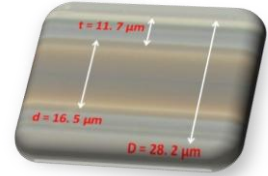
- [7] A. Zhukov, K. Chichay, **A. Talaat**, V. Rodionova, J. M. Blanco, M. Ipatov, V. Zhukova. *Manipulation of magnetic properties of glass-coated microwires by annealing*. Journal of Magnetism and Magnetic Materials, 383 232–236 (2015)
- [8] A. Zhukov, M. Ipatov, **A. Talaat**, J. M. Blanco, V. Zhukova. *Effect of Annealing on Off-Diagonal GMI Effect of Co-Rich Amorphous Microwires*. IEEE Transactions on Magnetics, 50 (11) 1-4 (2014)
- [9] A. Zhukov, A. Chizhik, M. Ipatov, **A. Talaat**, J. M. Blanco, A. Stupakiewicz, V. Zhukova. *Giant magnetoimpedance effect and domain wall dynamics in Co-rich amorphous microwires*. Journal of Applied Physics, 117 (4) 043904 (2015)



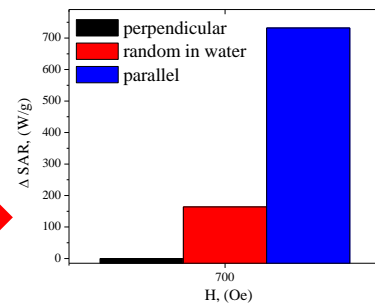
# 4

## Magnetic hyperthermia of Fe-based alloys

The chapter covers the first systematic studies of the inductive heating properties of Fe-based glass-coated microwires for magnetic hyperthermia biomedical application



An optimal profile for the efficient release of heat has been achieved. The shape anisotropy of 5 mm length of a single microwire coupled with the parallel configuration at high applied AC magnetic fields results in SAR values as high as 942 W/g



## 4.1 Magnetic hyperthermia

In chapter 3, part I, we have overviewed the technological importance of glass-coated microwires exhibiting two phenomena as GMI effect and magnetic bistability for sensing technologies. The inspiring characteristics of these microwires broadly create new streams in the application's market. Up to date, there is no use of these microwires for biomedical application, however the glass-coating itself has made them biocompatible. In this chapter, we present the first exploration of glass-coated microwires for applications in clinical hyperthermia. We attempt to elucidate their inductive heating mechanism, knowledge of which is essential to optimize the glass-coated microwires as a foreseeable new candidate for magnetic hyperthermia suitable for cancer therapy.

## 4.2 Fundamental principles

The healing power of heat has been known for a very long time ago, where it was used to cure variety of different diseases. This fact dates back to the important work of Busch et al. [210] who found that tumors cease to grow for temperature above  $42^{\circ}\text{C}$  whilst healthy normal tissue can tolerate even higher temperatures. In more modern studies, the selective damage of tumor tissue by means of a local temperature increase is an approved and established cancer therapy [211, 212]. For this, the so-called "hyperthermia", which alters the function of many structural and enzymatic proteins within biological cells, and hence induces apoptosis, has emerged as one of the most promising approaches [213]. The prospect of using hyperthermia to destroy tumors is appealing because hyperthermia itself is a physical treatment which has a much lesser side effect than chemotherapy or radiotherapy. This would allow for a greater number of repeated treatments without limitations arising from accumulated toxic side effects.

A largely experimental fashion of hyperthermia treatments that have a great potential to address and target tumor tissues has arisen through the use of heating characteristics of ferromagnetic materials. Thus this combination of ferromagnetic materials with hyperthermia is nowadays known as magnetic hyperthermia treatment [214, 215]. Broadly speaking, the technique consists of localizing magnetic particles or seeds within tumor tissue and then applying an external alternating magnetic field to cause heat. In due this process, two main heat



mechanisms are in operation: eddy currents and magnetic hysteresis. This heat then conducts into the surrounding cancerous tissue.

Evidence in support to this concept was first described by Gilchrist et al. [216]. The idea was to treat lymphatic metastases of large bowel cancer with heat by allowing microscopic ferromagnetic particles to be embolized in lymph nodes draining the primary cancer site and then applying an external alternating magnetic field to cause hysteretic heating of the particles. In this study, magnetite particles of diameter 0.02-0.1 microns were injected into the sub-serosa of the intestinal wall of dogs with the expectation that the particles would accumulate in regional lymph nodes. The regional lymph nodes were then dissected out and exposed to an alternating magnetic field of strength in the range between 200-240 *Oe*. It was found that a concentration of 5 *mg* of magnetite per gram of lymph node tissue yielded a temperature increase of 14°C in 3 *min*. Consequently, this early work, based on lymphatic uptake of microscopic ferromagnetic particles, clearly proved that it was possible to selectively heat tumor tissues via magnetic hyperthermia treatment.

Recently, magnetic nanoparticle hyperthermia has shown success in actual clinical trials [217]. The outcome of these clinical trials demonstrated the efficacy of magnetic hyperthermia for prostate cancer, and that patients can tolerate this therapy without discomfort or serious side effects. In the magnetic hyperthermia research community, the heating efficiency of a magnetic material subjected to an alternating magnetic field is often indicated by the specific absorption rate (SAR),  $SAR = A \cdot f$ , where *A* is the area of the AC hysteresis loop and *f* the exciting frequency of the applied magnetic field [215]. Thus, the heating capacity of a magnetic material depends on the hysteresis loop area. The latter is a product of saturation magnetization (the height of the hysteresis loop) and coercive field (the width of the hysteresis loop). Therefore, the majority of research in this field is to create magnetic structures that possess greater inductive heating responses with either high saturation magnetization or coercivity, and undoubtedly, to be biocompatible with the human body. In other words, a compromise between optimal physical and biological properties of the chosen material needs to be reached in order to ensure an efficient patient treatment, and this is will be discussed in detail in the forthcoming section.

### 4.3 Nanostructured magnetic materials for hyperthermia treatment

Different materials often have different optimal sizes for achieving maximum heating capacity around room temperature. At present, an intensive research in magnetic hyperthermia has mostly focused on  $\text{Fe}_3\text{O}_4$  nanoparticles [218] due to an appropriate size that allows the nanoparticle to easily interact with cancer cells toward the tumor site. In particular, most biomedical research has been dealt with small ( $< 20$  nm)  $\gamma\text{-Fe}_3\text{O}_4$  superparamagnetic nanoparticles, however, their relatively small magnetic moment made the temperature rise insufficient throughout the entire volume of the tumor [219]. In addition, if the particles are injected intravenously, they tend to be covered with proteins (opsonized) encouraging their phagocytosis [220]. They can also be recognized as "foreign bodies" and eliminated by the reticuloendothelial system [221]. To avoid the action of the immune system, there is a need for controlling the size of nanoparticles, surface functionalities, aggregation, inhomogeneous distribution, which practically complicates their use in hyperthermia [222]. It has also been reported that once the treatment is finished, the nanoparticles tend to accumulate in the liver and spleen, which possibly cause toxic and side effects [223, 224]. Overall, the use of magnetite nanoparticles has a high risk of severe or persistent side effects and can potentially lead to dire consequences depending on the size of the target region. Thermoablation, on the other hand, may be feasible for some cancer morphologies but as long as one can assure side-effects are reduced to reasonable levels.

For these reasons, alternative approaches of magnetic nanoparticles that exhibit enhanced heating responses for magnetic hyperthermia have been proposed such as ferromagnetic needles [225, 226], chain-like magnetic nanostructures [227], and quite recently magnetic nanowires [228, 229]. Lin et al. [228] reported that Fe nanowires present an order of magnitude improvement in SAR as compared to their Fe nanoparticles counterpart, while Alonso et al. [229] recorded that FeCo nanowires exhibit an enhanced heating efficiency and controllable dimensions for magnetic hyperthermia. However, an important barrier herein for these alternative candidates, is that their surface functionalities need to be optimized in order to make them biocompatible.

A major consideration for enhancing biocompatibility, of any material, is strikingly solved by the use of coating. Earlier findings have shown an improved heating response through the

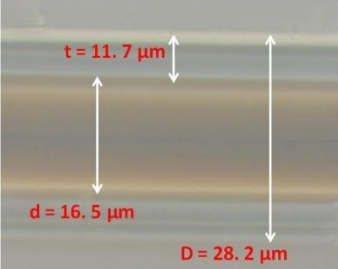
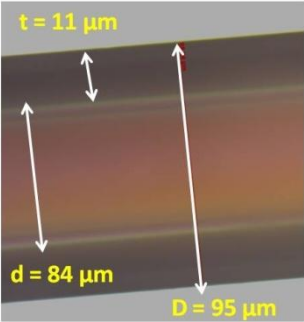
optimization of surface coating on  $\text{Fe}_3\text{O}_4$  nanoparticles for high performance magnetic hyperthermia [230]. In this respect, the glass coating of our microwires has actually made them biocompatible. In addition, their finite length and mechanical flexibility are in support to be incorporated through a guide needle into the tumor area, and after the heating treatment, they can be retracted and recovered. Higher saturation magnetization and well-defined shape anisotropy of these microwires, as we elaborated before, are expected to result greater heating responses or higher SAR values. Although Co-based glass-coated microwires with nearly-zero magnetostriction constant exhibit the best soft magnetic properties and the highest GMI effect, their anhysteretic character and low magnetoelastic anisotropy render them undesirable for use in advanced hyperthermia. Meanwhile, Fe-based ones are characterized by high positive magnetostriction, rectangular hysteresis loops, as well as high saturation magnetization are expected to result in better heating responses.

Inevitably these insights are in practical interest of magnetic hyperthermia treatments. Since the glass-coated microwires have not been previously exploited in hyperthermia, their superior features could advance the existing technology and pave a new pathway for biocompatible hyperthermic treatments without the need for carefully crafted magnetic nanoparticles and nanowires. In addition, their commercial availability, manufacturing flexibility, and cost effectiveness would afford institutions to have for the treatment which can ultimately lower the cost of care for either the health care provider or the patient. Along the rest of this present chapter, we present the first systematic study of the inductive heating properties of glass-coated amorphous microwires, opening up a new opportunity either as a promising alternative for advanced magnetic hyperthermia, or exploring new existing characteristics of these microwires.

#### **4.4 Influence of geometry and varying number of microwires**

Initially, we have tested two Fe-based glass coated microwires with two different dimensions as shown in [table 4.1](#). In the first instance, we have investigated and analyzed the inductive heating properties of the microwire samples with varying wire numbers ( $n = 1$  and 10). Wire pieces of the same length (5 mm) were used for all the experiments. During these hyperthermia experiments, the temperature evolution as a function of time has been recorded while applying different AC magnetic fields at a fixed frequency of 310 KHz, and the results are presented in [Fig. 4.1 a-d](#).

Table 4.1 Chemical composition, dimensions, and optical pictures of tested Fe- based glass-coated microwires

Chemical composition	Metallic nucleus, d, diameter ( $\mu\text{m}$ )	Total diameter, D, ( $\mu\text{m}$ )	Optical pictures
<b><math>\text{Fe}_{74}\text{Si}_{11}\text{B}_{13}\text{C}_2</math></b>			
The mass of single strand of 5 mm length is equal to 0.001 mg/ml	16.5	28.2	
<b><math>\text{Fe}_{71.7}\text{Si}_{11}\text{B}_{13.4}\text{Nb}_3\text{Ni}_{0.9}</math></b>			
The mass of single strand of 5 mm length is equal to 0.243 mg/ml	84	95	

As one can clearly see in this figure, the increase in temperature progressively becomes faster as we increase either the value of AC magnetic field or the number of wires employed. Once the heating curves have been measured, the corresponding SAR values are evaluated from their initial slopes (Fig. 4.1 e-f), following the calorimetric method as has been explained in chapter 4-experimental techniques (page 68). The mass for each microwire sample used either thin or thick was determined as described in table 4.1 under each composition. Fig. 4.1 e-f show SAR values of  $n = 1$  and 10 samples for different AC magnetic fields (300, 500, and 700 Oe). In the case of a single  $\text{Fe}_{74}\text{Si}_{11}\text{B}_{13}\text{C}_2$  microwire, in spite of a temperature change with time as displayed in Fig. 4.1a, the low mass of this thin wire resulted in a negligible heating response (SAR values equal to zero) for all AC magnetic fields. However, the heating response is significant for a system of multi-wires. Evidences in support of this statement can be obviously seen in Fig. 4.1e, where the SAR tends to increase significantly with increasing number of  $\text{Fe}_{74}\text{Si}_{11}\text{B}_{13}\text{C}_2$  microwires. For  $H = 300$  Oe, SAR increases from zero W/g for the  $n = 1$  sample to 118 W/g for the  $n = 10$ , while for  $H = 700$  Oe an increase of about 358 W/g is obtained.

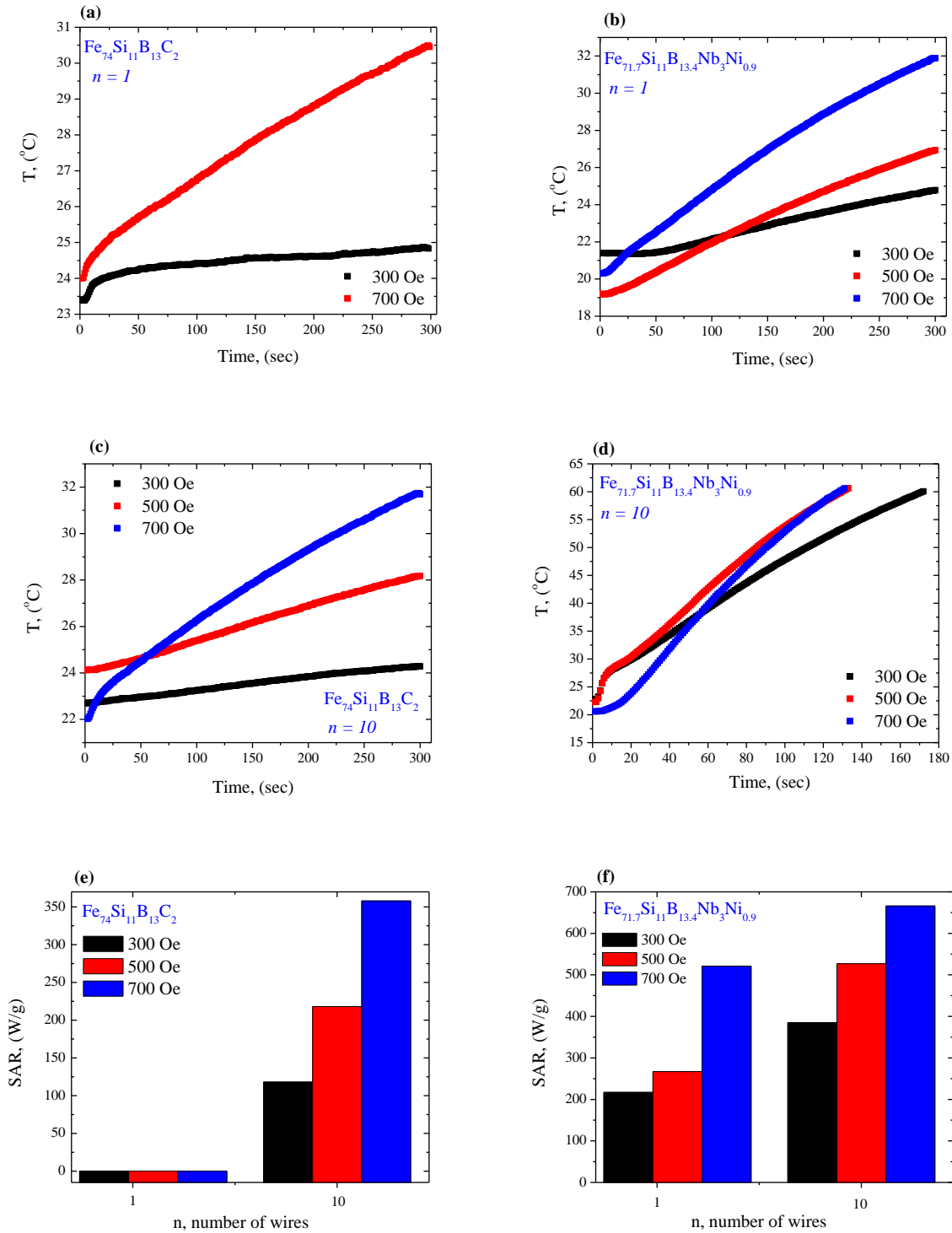


Figure 4.1 Temperature ( $T$ ) as a function of time ( $t$ ) for  $\text{Fe}_{74}\text{Si}_{11}\text{B}_{13}\text{C}_2$  microwires  $n = 1$  (a);  $\text{Fe}_{71.7}\text{Si}_{11}\text{B}_{13.4}\text{Nb}_3\text{Ni}_{0.9}$  microwire  $n = 1$  (b);  $\text{Fe}_{74}\text{Si}_{11}\text{B}_{13}\text{C}_2$  microwires  $n = 10$  (c);  $\text{Fe}_{71.7}\text{Si}_{11}\text{B}_{13.4}\text{Nb}_3\text{Ni}_{0.9}$  microwire  $n = 10$  (d); SAR as a function of the number of microwires for  $\text{Fe}_{74}\text{Si}_{11}\text{B}_{13}\text{C}_2$  (e), and  $\text{Fe}_{71.7}\text{Si}_{11}\text{B}_{13.4}\text{Nb}_3\text{Ni}_{0.9}$  (f).

We note that even for a single  $\text{Fe}_{71.7}\text{Si}_{11}\text{B}_{13.4}\text{Nb}_3\text{Ni}_{0.9}$  microwire ( $n = 1$ ), SAR increases from 217 W/g for  $H = 300$  Oe to 521 W/g for  $H = 700$  Oe. Actually, these values of SAR are larger than either those reported for magnetic nanoparticles (200-400 W/g) [231] or similar magnetic wires of similar composition ( $\approx 100$  W/g) [232] for the same applied AC magnetic fields.

#### 4.5 Heating mechanism of glass-coated microwires

Given this excellent inductive heating properties of these glass-coated microwires as presented in Fig. 4.1, indeed such heating responses are related to several physical mechanisms. Before considering these physical mechanisms, it is important to calculate the actual heating of a single microwire (while the thermal losses to the environment might accrue during the experimental procedure), therefore the measurements were corrected using the modified law of cooling described in [233] as following:

$$\frac{dQ}{dt} = m_{cp} \frac{dT}{dt} + \frac{1}{Rt} (T - T_{inv}) \quad (4.1)$$

where  $Q$  is the thermal energy (heat);  $m_{cp} = m_{cw} c_w + m_{H2O} c_{H2O}$  ( $m_i$  and  $c_i$  mass and specific heat for the entire system of water plus wire, respectively);  $Rt$  is the thermal resistance which in case of radial heat transfer of a cylindrical geometry will be given by; ( $Rt = \ln(r/r_o) / 2\pi LK$ ) being  $L$  the axial length,  $r$  and  $r_o$  are the radial coordinates at  $T$  and  $T_{inv}$  respectively;  $K$  is the thermal conductivity;  $T$  is the measured temperature of the whole solution, and  $T_{inv}$  is the environmental temperature which is around  $22^\circ\text{C}$ .

Thus, the total heat generated by glass-coated microwires can be expressed as that one absorbed by water together with the transferred losses to the environment. If we consider  $T'$  as the theoretical temperature achieved under an ideal adiabatic conditions (zero losses) [234], therefore the previous equation (4.1) can be rewritten as:

$$\frac{dT'}{dt} = \frac{dT}{dt} + \gamma (T - T_{inv}) \quad (4.2)$$

where  $\gamma$  is the time constant equal to  $(1 / Rt m_{cp})$ . Under ideal adiabatic conditions the achieved temperature should linearly increase with time,  $t$ , (the left term in eq. 4.2 will be  $dT' / dt = \text{constant}$ ). Therefore, we assume that the solution of equation (4.2), in turn, will display an

exponential time dependence as ( $A = B = T_{max} - T_{inv}$ ), with  $T_{max}$  being the maximum temperature achieved under the non adiabatic conditions ( $t = \infty$ ) and the time constant ( $C = \gamma$ ).

Table 4.2 summarizes the fitting parameters obtained by fitting the experimental curves of an example of a single  $\text{Fe}_{71.7}\text{Si}_{11}\text{B}_{13.4}\text{Nb}_3\text{Ni}_{0.9}$  microwire (Fig. 4.1b) to an exponential time equation as described above.

Table 4.2 Fitting parameters of the exponential heating curves according to equation (4.2)

AC magnetic field (Oe)	Parameter A (°C)	Parameter B (°C)	Parameter C (s <sup>-1</sup> )
300	13.57	14.56	8.42 x 10 <sup>-4</sup>
500	19.10	22.29	1.53 x 10 <sup>-3</sup>
700	37.00	39.44	1.6 x 10 <sup>-3</sup>

Accordingly, to our understanding each of these theoretical parameters in table 4.2 makes an important contribution to the obtained SAR value. In other words, parameters A and B calculated from the heating curve and its time variation are associated with the actual thermal energy produced by the glass-coated microwires since both values at certain AC magnetic field are approximately equalized. Therefore, we can now believe that the reported SAR values in Fig. 4.1 e-f are corresponding to the actual heating mostly coming from the microwire itself. For a better depiction of the heat transfer, the temperature raise was also recorded during some AC hyperthermia measurements by the help of an employed infra-red thermal camera, where we were able to capture the increase of heating process as depicted in Fig. 4.2.

Regarding the physical mechanism behind a hyperthermia experiment, the induction heating associated with the present case can be classified into two main contributions [235, 236]: eddy-current losses and magnetic hysteresis losses.

The alternating magnetic field generates electrical currents to flow through the microwire, which are well-known as eddy currents. The heating mechanism related to eddy currents can be explained in terms of the power loss dissipation induced by the change in magnetization, which



increases proportionally to the square root of the frequency as long as the flux penetration is complete according to:

$$P_{eddy} \propto \sqrt{\mu\rho f} H_{AC}^2 \quad (4.3)$$

where  $p$  is the power lost per unit mass;  $\mu$  is the effective permeability;  $\rho$  the resistivity, and  $f$  the frequency of AC magnetic field.

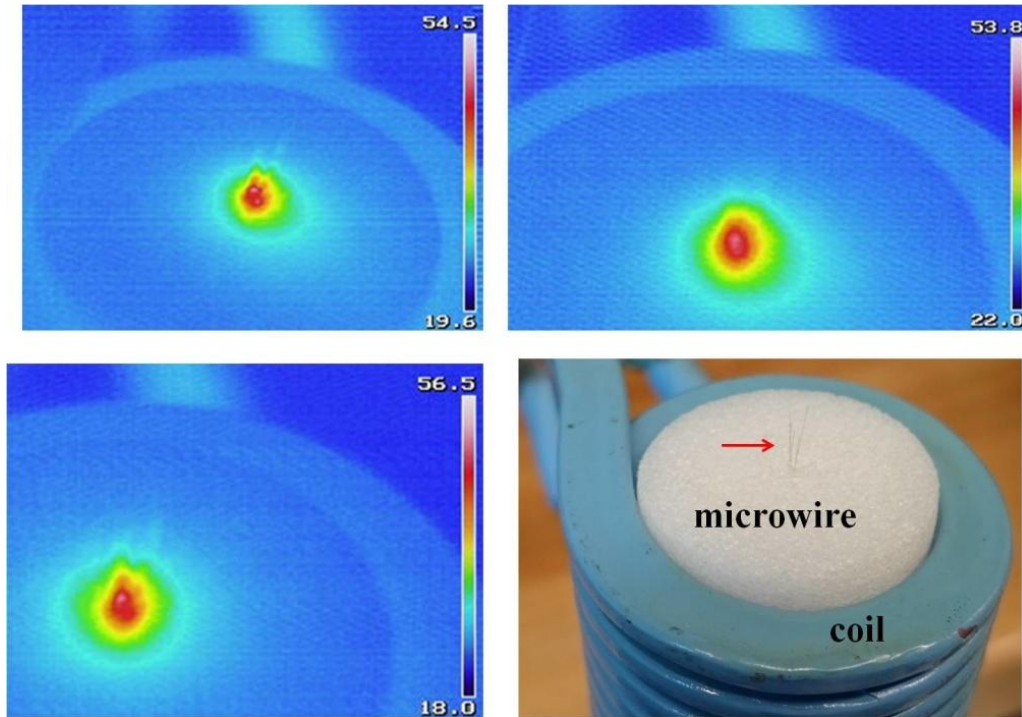


Figure 4.2 Infra-red thermal camera images of  $Fe_{71.7}Si_{11}B_{13.4}Nb_3Ni_{0.9}$  microwire during AC hyperthermia.

Since the magnetic field produced by eddy current always opposes the change in magnetization, so that the latter is damped away inside the microwire. As a consequence, if the frequency is sufficiently high, the eddy current losses become strong enough at the inner core of the microwire and diminish at the surface or the outer shell. In addition, the high frequency used here gives rise to another phenomena associated with the so-called skin depth effect. The higher the operating frequency, the shallower the skin depth. Thus, the skin effect gives rise to an increase in the effective resistance of the metallic core to the passage of large quantities of currents. Therefore it greatly increases the heating efficiency caused by the eddy currents induced into the microwire. The intense alternating magnetic field inside the coil, on the other



hand, repeatedly magnetizes and demagnetizes the microwire. This rapid flipping of the magnetic domains causes a considerable friction and heating inside the microwire sample. In this instance, an equally significant addition to the heating mechanism takes place at the same time as the eddy currents. Heating due to this mechanism is known as a hysteresis loss and it is in a direct correlation with the area of the AC hysteresis loop. The amount of heat generated per cycle, according to [235, 236], is given by:

$$P_{fm} \propto \mu_0 f \int H dM \quad (4.4)$$

where  $f$  is the frequency of an AC applied magnetic field,  $H$  is the magnetic field strength, and  $M$  is the magnetization.

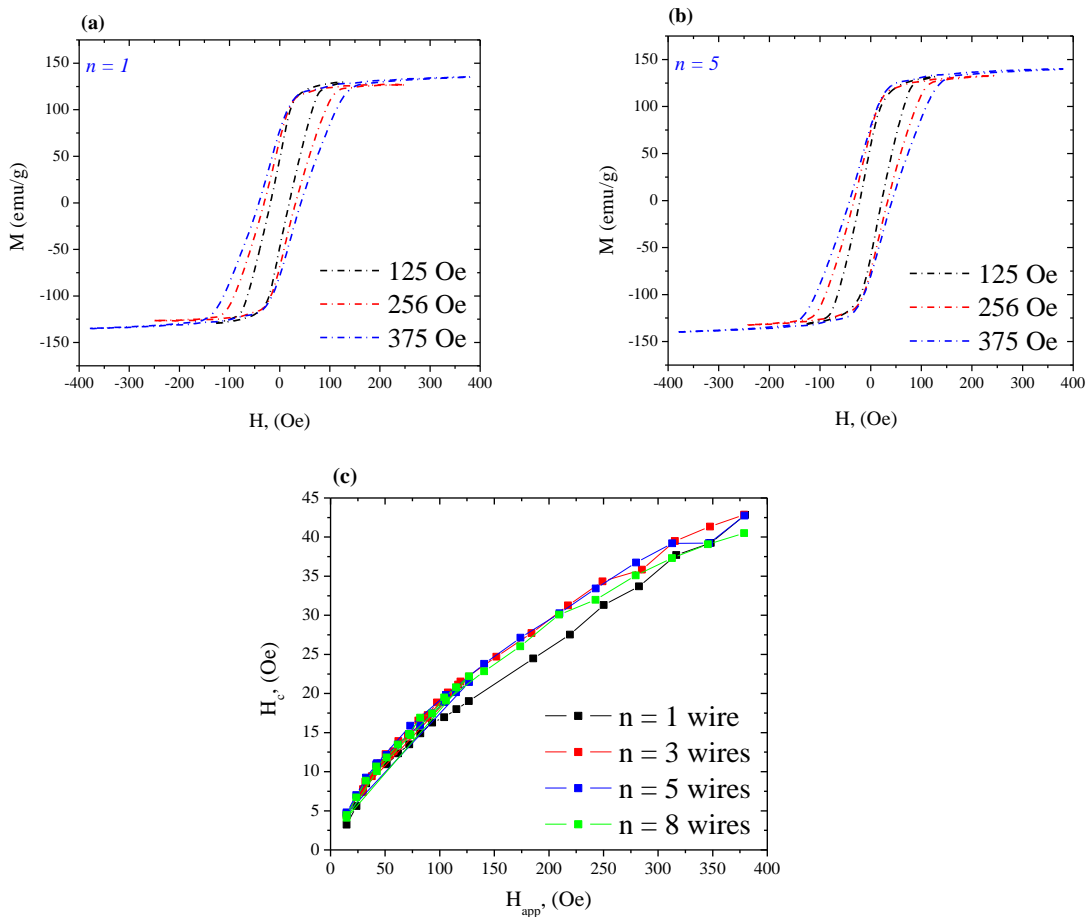


Figure 4.3 AC hysteresis loops of  $n = 1$   $Fe_{71.7}Si_{11}B_{13.4}Nb_3Ni_{0.9}$  glass-coated microwires (a);  $n = 5$  for different AC magnetic field amplitudes (b), and coercive field ( $H_c$ ) as a function of AC magnetic field amplitudes for the  $n = 1, 3, 5, 8$  microwire samples (c).

During remagnetization of the sample, there are two processes contributing to hysteresis losses: first is the displacement of domain walls, while the second is the magnetization rotation process. In accordance, we have performed AC hysteresis loops measurements on microwire samples with varying wires numbers, such as for  $n = 1$  and  $n = 5$  Fe<sub>71.7</sub>Si<sub>11</sub>B<sub>13.4</sub>Nb<sub>3</sub>Ni<sub>0.9</sub> microwires (Fig. 4.3 a-b) using the AC magnetometer for magnetic hyperthermia with a system of three pickup coils, capable of working in a wide range of frequencies 149–1030 KHz with high field intensities up to 22 KA/m at high frequencies [237].

Magnetic field amplitude dependence on the coercive fields,  $H_c$ , are deduced from these loops and plotted in Fig. 4.3c. It is worth noting that values of  $H_c$  are larger for the multi-wire system  $n = 3, 5,$  or  $8$  samples than for the single ( $n = 1$ ) sample (Fig. 4.3c) especially for AC fields exceeding 100 Oe. This difference must be attributed to the important effect of magnetostatic interactions between the microwires. The enhancement of the AC coercivity and hence the SAR in the multi-wire system as-compared to a single microwire can be clearly seen. In addition, as can be observed in Fig. 4.3a-b, the AC hysteresis loops present a rectangular shape for different fields amplitude, which is ideal to maximize the hysteresis losses with high saturation and low coercive fields as it is typical for these amorphous microwires (see Fig. 2.2, page 20 chapter 2). It is interesting to note that the loops tend to saturate even with only  $\approx 100$  Oe, indicating that even at low field values the Fe-based glass-coated microwires give reasonable heating. In other words, by increasing the maximum applied AC magnetic field,  $H_c$  increases (Fig. 4.3c) while the saturation magnetization,  $M_s$ , remains almost the same (Fig. 4.3 a-b), and therefore increasing the heating efficiency of these microwires. Observed dependencies in Fig. 4.3 are actually confirming that the magnetic hysteresis losses are a dominant contributor to the heating of the present microwires.

In all previous experiments, the microwire samples were oriented randomly with respect to the AC magnetic field during hyperthermia measurements. However, like most of the fundamental physical properties of any magnetic material, the position of the material itself apropos the magnetic field plays a crucial role in optimizing their magnetic behavior. The next section is devoted to describing the microwire's behavior versus the AC field direction.

#### 4.6 Effect of microwire orientation respect to the magnetic field direction on SAR

When a physical property of a material present a directional dependence, it has an anisotropy. Chapter 2, part I, covered one of the most dominant anisotropies of this class of materials, which is (in the as-prepared state samples) the shape anisotropy. Once again, in the case of Fe-based glass-coated microwires, the shape anisotropy is determined by a longitudinal easy axis in the metallic core due to a peculiar domain structure (Fig. 2.2 page 20). In light of these considerations, it is therefore important to understand the effect of wire alignment on the SAR of presently investigated microwires.

In this study, hyperthermia measurements on a single  $\text{Fe}_{71.7}\text{Si}_{11}\text{B}_{13.4}\text{Nb}_3\text{Ni}_{0.9}$  glass-coated microwire subject to two AC field directions (namely, the AC field was applied (i) parallel to, and (ii) perpendicular to the length of the wire respect to the field direction) have been performed and analyzed. In order to obtain desirable wire orientations and eliminate effects of physical motion on SAR, the wires were immersed in a 2% agar solution (a viscous material that allowed us to tune the microwires in a controlled way). The results obtained are compared to that of the wire immersed in water oriented randomly as visible in Fig. 4.4a.

A remarkable SAR increase has been obtained upon aligning the microwire along the field direction (parallel), whereas the opposite tendency is observed in case of perpendicular aligning of the microwire with respect the magnetic field. For the parallel orientation, the temperature increases faster than for the perpendicular orientation (Fig. 4.4b). The difference in temperature change is faster by  $7^\circ\text{C}$  when the wire is aligned along the AC magnetic field direction (the parallel case). Such change in wire orientation alters the SAR value by nearly 500 W/g for the parallel orientation (Fig. 4.4c): SAR decreases from 942 W/g for the parallel orientation to 210 W/g for the perpendicular orientation (see Fig. 4.4a). This highlights that the wire alignment with respect to the AC field direction is extremely an important factor in determining the heating efficiency. This effect, however, is less pronounced at lower AC fields (i.e. 300 Oe) but it becomes significant for higher AC fields (i.e. 700 Oe). This might serve in using the microwire alignment effect to exploit a new approach for advanced hyperthermia: it can be considered as a rotating hyperthermia approach, in which one can achieve a temperature rise more faster by simply rotating the wire itself in the presence of a constant AC magnetic field.

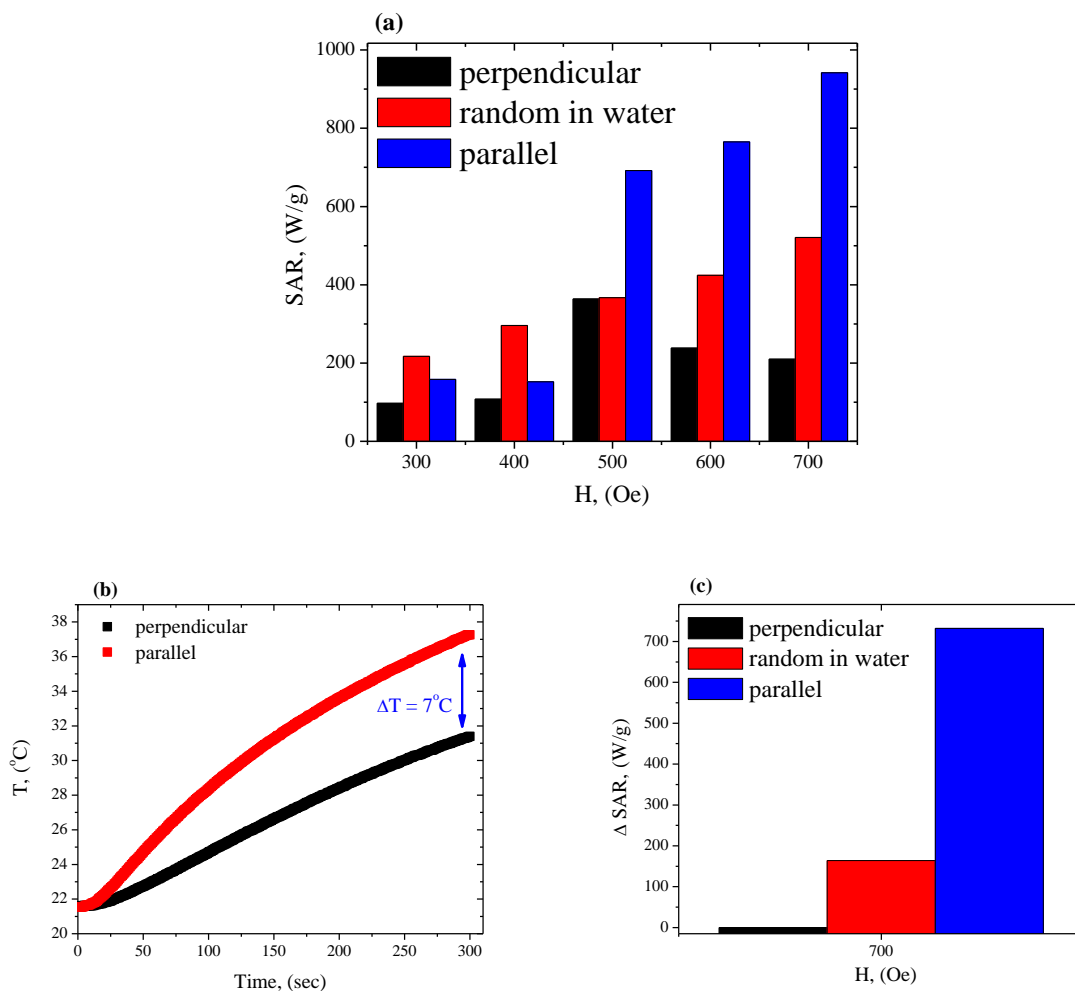


*Figure 4.4 SAR as a function of AC magnetic field for single  $\text{Fe}_{71.7}\text{Si}_{11}\text{B}_{13.4}\text{Nb}_3\text{Ni}_{0.9}$  microwire aligned, in 2% agar; parallel; perpendicular respect to the direction of the applied AC magnetic field, in comparison with that of the single microwire oriented randomly in water (a), the temperature rise change ( $T$ ) as a function of time for two different orientations (b), and subtracted SAR values at 700 Oe respect to the AC field orientation.*

On the other hand, in case of the wire randomly oriented in water, we have observed that the wire tends to align itself with the AC field, but a slight misalignment of the wire with respect to the AC field direction reduces the SAR in comparison to the case of the wire aligned, in agar, perfectly parallel to the direction of the applied AC field. These important findings lead us to conclude that in the case of a single  $\text{Fe}_{71.7}\text{Si}_{11}\text{B}_{13.4}\text{Nb}_3\text{Ni}_{0.9}$  glass-coated microwire, the shape anisotropy coupled with the parallel configuration at high applied AC magnetic fields is an optimal profile for the efficient release of heat. Such profile provides us with a SAR value as

much as 942 W/g which is absolutely much more higher than a system of  $n = 10$  wire samples oriented in a water solution (666 W/g Fig. 4.1f).

Given the current high profile debate with regard to the parallel wire orientation in agar solution, we aimed, therefore, to further enhance the heating efficacy in the case of multi-wires system oriented in agar solution. Herein, the induced magnetostatic anisotropy arising from the stray field and dipolar interaction is quite significant, which will be the final case-study of this chapter.

#### 4.7 Separation between two microwires: Role of magnetostatic anisotropy

One of the advantages of Fe-based glass-coated microwires is their magnetization processes due to a magnetic bistability as discussed chapter 3, part I. This magnetic bistable behavior has shown a potential impact of arrayed multi-wires system in sensing technologies, owing to the plurality of their coercivities. Thus, the distinctive behavior of the switching field,  $H_s$ , and its unusual characteristics, as argued before, is the key factor for Fe-based glass-coated microwires. Now, we move on to smoothly stretch those peculiarities of Fe-based glass-coated microwires on the bases of another interesting phenomena, the so-called "hysteresis loop splitting".

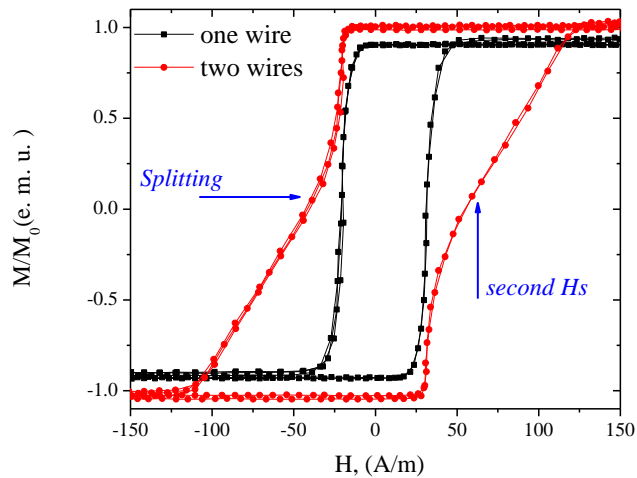


*Figure 4.5* AC hysteresis loops measured at low frequency 115 Hz for one and linear array consisting of two  $Fe_{71.7}Si_{11}B_{13.4}Nb_3Ni_{0.9}$  glass-coated microwires showing the splitting as a result of different values of switching fields.

Hysteresis loop splitting of studied  $\text{Fe}_{71.7}\text{Si}_{11}\text{B}_{13.4}\text{Nb}_3\text{Ni}_{0.9}$  glass-coated microwires, measured by the induction method described in experimental techniques (page 58) at low frequency 115 Hz, is presented in Fig. 4.5.

As can be clearly observed in Fig. 4.5, such phenomena of splitting mainly depends on the value of the switching field ( $H_s$ ) of each glass-coated microwires when they are deposited together. This effect is attributed to the superposition of both the external magnetic field and stray field originated by each microwire magnetized in an axial direction. It is naturally that two microwires do not have the same values of  $H_s$ . In this case, one of the wires delays in switching the magnetization of the other [238]. In other words, after switching the magnetization of a wire with lower  $H_s$ , it produces a stray field in the opposite sense to the external magnetic field, therefore, the total field becomes insufficient to switch the magnetization in the second wire with larger  $H_s$ . Eventually, these features result in splitting, and duly increases the area under the hysteresis loop [238, 239], which in turn is a favorable prerequisite for rising the induction heating (SAR). In addition, the induced magnetostatic anisotropy arising from the stray field and dipolar interaction of two wire samples is indeed quite relevant [239, 240]. This magnetostatic anisotropy is in direct connection with the separation distance between two microwires, increasing by decreasing the distance between employed samples [240, 241]. Accordingly, the inductive heating properties is also well affected by separation between the samples.

To further elucidate this, we have studied the effect of separation between two  $\text{Fe}_{71.7}\text{Si}_{11}\text{B}_{13.4}\text{Nb}_3\text{Ni}_{0.9}$  microwire samples on their heating efficiency (Fig. 4.6). In this study, two identical wire pieces of the same length (5 mm) were embedded in 2% agar solution as depicted in the inset of Fig. 4.6. The wires were separated at (i) zero and (ii) 1 mm for comparison. As one can see clearly in Fig. 4.6, SAR decreases as the distance between the wires increases from 0 to 1 mm. Such change in SAR is especially noticeable at high AC fields: the difference in SAR values respect to the separation distance is 13 W/g for  $H = 300$  Oe, while it is 841 W/g for  $H = 700$  Oe. Interestingly, these results provide a solid evidence that the dipolar interactions (magnetostatic anisotropy) between the wires play an important role in the obtained enhanced SAR values as much 1102 W/g (Fig. 4.6).

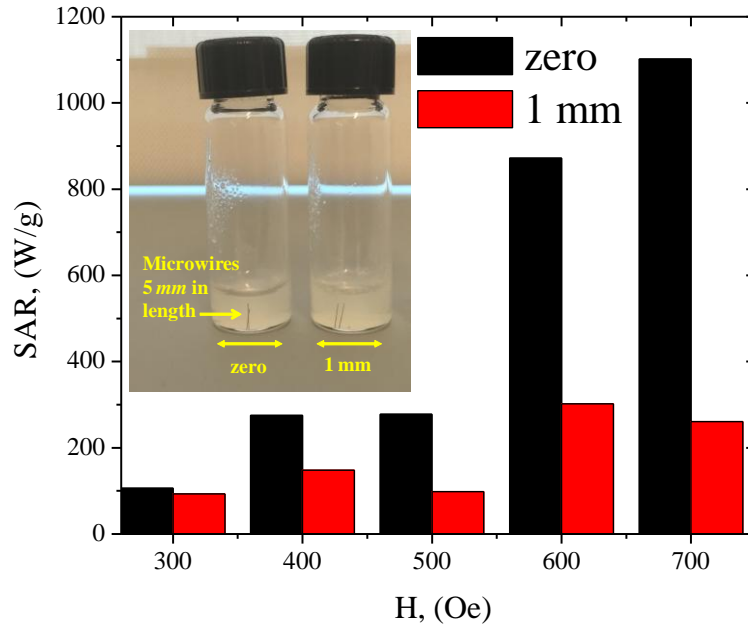


*Figure 4.6 SAR as a function of ac magnetic field for two  $Fe_{71.7}Si_{11}B_{13.4}Nb_3Ni_{0.9}$  glass-coated microwires separated at 0 and 1 mm distance. Inset shows the microwires aligned in 2% agar solution at the 0 and 1 mm distance.*

In summary, the excellent inductive heating properties of Fe-based glass-coated microwires, together with the protective glass-coating layer and cost effectiveness, make them a very promising class of materials for applications in magnetic hyperthermia.

#### 4.8 Concluding remarks

Beyond this chapter, we have systematically analyzed for the first time, the inductive heating properties of Fe-based glass-coated microwires for possible applications in magnetic hyperthermia. We have given remarkable insights for the potential of glass-coated microwires in the foreseeable trends in hyperthermia applications. In detail, we have demonstrated appreciable heating responses in which the therapeutic window (40-45°C) for cancer treatment can be easily reached within a few minutes of heating. We have also indicated optimal conditions, where possible, that permit Fe-glass-coated microwires to perform most efficiently SAR values. Some of those are based on dimensions, orientation, as well as separation effects, in order to develop new glass-coated microwires that balance the best aspects from each of these studies.

We have shown that a single  $\text{Fe}_{71.7}\text{Si}_{11}\text{B}_{13.4}\text{Nb}_3\text{Ni}_{0.9}$  wire sample of 5 mm length is able to produce a sufficient amount of heat, with SAR reaching a value as high as 521 W/g for an AC magnetic field of 700 Oe. Nonetheless, increasing the number of microwires, on one hand, has continued to expand SAR values up to 666 W/g at the highest applied magnetic field, and well improving on the other hand, the zero SAR values of thin (low mass) single  $\text{Fe}_{74}\text{Si}_{11}\text{B}_{13}\text{C}_2$  microwire, achieving a SAR plateau of 358 W/g.

The total heating generated by the studied Fe-based glass-coated microwires has demonstrated an adiabatic process where no heat transfer occurred between the employed system and its surrounding environment, confirming that the Fe-based microwires are very efficient at transferring heat homogenously to the external environment without interfering with each other. The physical induction heating mechanism has been systematically illustrated in the frame of either eddy currents losses or magnetic hysteresis losses. These concerns have also been resolved by the help of direct AC hysteresis loops measurements.

We have critically scoped that, by the use of only single microwire; the shape anisotropy determined by a longitudinal easy axis in the metallic core due to a peculiar domain structure of Fe-based microwires coupled with the parallel configuration at higher applied magnetic field is an optimal profile for the efficient release of heat (942 W/g). While in the case of several microwires, the implementation of two nearby samples does not affect negatively the heat efficiency due to a dipole switching and induced magnetostatic anisotropy reflected by a SAR enhancement up to 1102 W/g. Besides, the protective glass-coating layer itself can be considered as an insulating barrier which enhances the biocompatibility of this family of soft ferromagnetic materials for bio-medical applications.

Our study paves the way for development of low-cost ferromagnetic glass-coated microwires for advanced hyperthermia.



# Chapter 5

## *Conclusions*

## Conclusions and closing remarks

This work has been devoted to the recent advanced studies of glass-coated microwires as a special class of amorphous metallic alloys. These magnetic microwires provide model systems for fundamental studies of a number of physical phenomena not easily accessible in other conventional magnetic materials. The enhanced magnetic softness together with thin dimensions have made them quite promising candidates for many modern technological applications.

Glass-coated microwires investigated in the present research have been all fabricated by the modified Taylor-Ulitovsky technique based on the rapid quenching solidification phenomena. The main difference of glass-coated microwires from other magnetic wires produced by in rotating water method is their composite character. Thus, non-ferromagnetic glass coating necessary for the preparation process affects magnetic properties of the ferromagnetic nucleus though the internal stresses arising during the rapid quenching. The origin of these internal stresses is related to the difference in thermal expansion coefficients of simultaneously solidifying metallic nucleus and glass coating. Therefore by modifying the thickness of glass-coating one can control the strength of internal stresses, and therefore, versatile magnetic characteristics are easily obtainable. In a parallel way, depending on the chemical alloy composition, the magnetostriction value varies and thus opens up pathways to tune either magnetic responses or structural properties of glass-coated microwires having the same dimensions but with different chemical compositions.

Evidences support these facts were given in chapter 1 for the case of *Finemet*-like glass-coated microwires having the same  $\rho$ -ratios and different chemical compositions. On the other hand, the same chemical composition but with different values of internal stresses ( $\rho$ -ratios) has resulted in different magnetic responses as was shown for the case of *Hitperm*-like alloys investigated along chapter 2. In particular, beyond the scope of these two chapters 1 and 2, we have investigated the effect of nanocrystallization on magnetic and structural properties of Fe-based glass-coated microwires in two different alloy families. Therein, we have determined that the nanostructure obtained either after appropriate annealing conditions or in as-prepared microwire samples result in a better magnetic softness owing to randomly distributed nanoscaled crystallites. For this, two different structural consequences based on each chemical compositions have been obtained with two different characteristics as schematically resumed up in [Fig. 5.1](#).

Nanostructures of either  $\alpha$ -FeSi for *Finemet*, or  $\alpha$ -FeCo for the case of *Hitperm* result in nearly zero and highly positive overall magnetostriction sign, respectively. Each of which has been undertaken for two different studies.

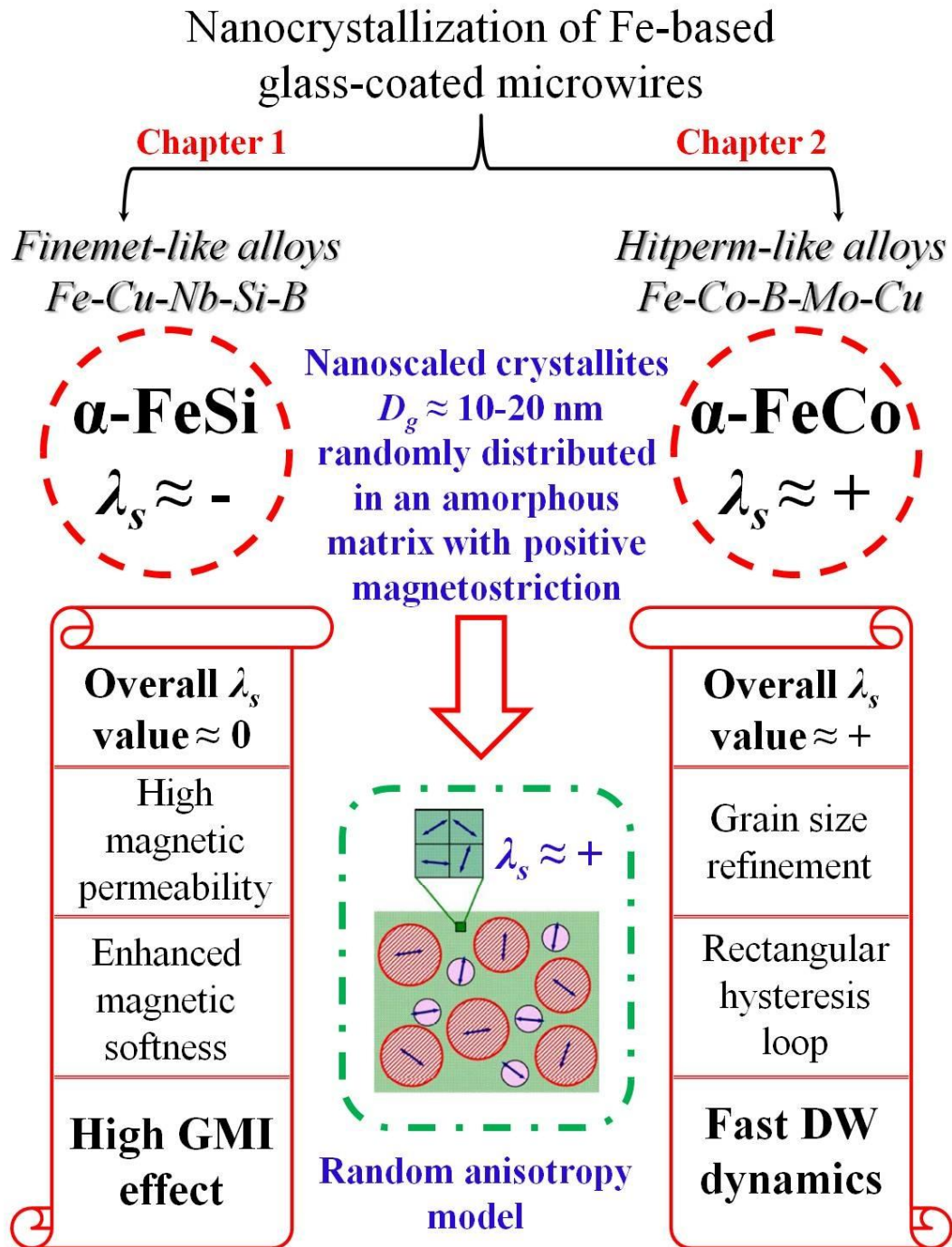


Fig. 5.1 Summary of chapter 1 and chapter 2 through the role of nanocrystallization

The major findings of chapter 1 (left hand side in Fig. 5.1), combined the achievement of a remarkable magnetic softness with low coercive fields of about 10  $A/m$  and an ultra fine grain size down to 11  $nm$  in annealed microwire samples at  $T_{ann} = 550^{\circ}C$ . A drastic change in the magnetostriction coefficients, therefore, has been presumed upon the nanocrystallization: the magnetostriction values pushed away from highly positive to nearly zero values. An optimized 125% GMI ratio observed at  $f = 500 MHz$  of the poor response of amorphous as-prepared microwire samples (1%) has been also achieved. In addition, it has been also demonstrated that controlling the quenching rate during the fabrication process strongly affects the final microstructural of the produced microwires. Consequently, nanocrystalline structure of about 12  $nm$   $\alpha$ -Fe-Si grains and coercive field of 12  $A/m$  obtained in as-prepared microwire sample resulted in an improvement of approximately 50% GMI at frequency of 300  $MHz$ .

In chapter 2 (right hand side in Fig. 5.1), highly positive magnetostriction coefficient of either both amorphous matrix and the  $\alpha$ -FeCo nanocrystallites has been obtained. Rectangular hysteresis loops have been observed in as-prepared microwires which allowed us to investigate the magnetization reversal processes and domain wall dynamics. Quite fast DW velocities have been recorded for as-prepared samples reaching values as fast as 1.2  $Km/s$ . In addition, the decrease the magnetoelastic anisotropy after annealing together with the internal stress relaxations resulted in an enhancement of the DW velocities up to 2.4  $Km/s$ . A curious feature related to the role of Cu addition to *Hitperm*- like alloys resulted in a grain size refinement down to 11  $nm$ . Observed microstructural changes were discussed in terms of the stress diffusion of limited crystalline growth and the alloy chemical composition.

Chapter 3 dealt with the effect of annealing on the magnetic properties of amorphous Co-based glass-coated microwires. Owing to the stress relaxation and changes of the magnetostriction values after annealing (conventional and under stress), remarkable changes in hysteresis loop, GMI effect, and DW dynamics of Co-Fe microwires have been obtained and systematically discussed. At certain annealing conditions we were able to observe coexistence of GMI effect and fast DW propagation in the same annealed microwire.

Chapter 4, on the other hand, has taken the advantage of the magnetic bistability of Fe-based microwires for exploring their inductive heating properties for possible applications in magnetic hyperthermia. Appreciably, these microwires have demonstrated quite good heating responses in

which the therapeutic window (40-45°C) for cancer treatment can be easily reached within a few minutes of heating. Optimal conditions to permit Fe-glass-coated microwires to perform most efficiently SAR values have been highlighted. Some of those conditions found to be dependent on the microwire dimensions, orientation, as well as the separation effects. All these characteristics have been discussed in a combined way in order to develop new glass-coated microwires that balance the best aspects from each of these studies. Actually, this research paves the way for development of cost effectiveness ferromagnetic glass-coated microwires for advanced hyperthermia treatment.

There are still many other opportunities for carrying out innovative lines of investigation for glass-coated microwires.



References

Publications

Resumen

Acknowledgments

## References

- [1] *Soft magnetic materials - technologies, materials, devices, new developments, industry structure and global markets*. Report summary, LONDON (Aug. 26<sup>th</sup>. 2015)
- [2] D. C. Jiles. *Recent advances and future directions in magnetic materials*. Acta Materialia 51, 5907–5939 (2003)
- [3] *Soft magnetic application guide. The magnetic products group of SPS technologies*, 1-36 (The Arnold Engineering Co. 2003)
- [4] *NATURE MATERIALS*, VOL 14 [www.nature.com/naturematerials](http://www.nature.com/naturematerials) (June 2015).
- [5] R. Brill. Z. Kristallogr. (A) 75, 217 (1930)
- [6] A. Brenner, G. Riddell. *Nickel plating on steel by chemical reduction*. Journal of research of the National Bureau of Standards 37, 31-34 (1946)
- [7] W. Buckel, R. Hilsch. *Superconductivity and resistance of Tin with lattice defects*. Z. Phys. 132, 420-442 (1952)
- [8] P. Duwez, R. H. Willens, W. Klement. *Metastable electron compound in Ag-Ge alloys*. J. Appl. Phys. 31, 1136 (1960). [See also, *Metastable solid solutions in the Gallium Antimonide-Germanium pseudo binary system*. Reported by the same authors at the same volume page 1500]
- [9] I. S. Miroshnichenko, I. V. Salli. *A device for the crystallization of alloys at a high cooling rate*. Ind. Lab. 25 1463–1466 (1959).
- [10] W. Klement, R. H. Willens, P. Duwez. *Non-crystalline structure in solidified Gold-Silicon alloys*. Nature 187, 869-870 (1960)
- [11] C. C. Tsuei, P. Duwez. *Metastable amorphous ferromagnetic phases in Palladium-base alloys*. J. appl. phys. 37, 435 (1966)
- [12] P. Duwez, S. C. H. Lin. *Amorphous ferromagnetic phase in Iron-Carbon-Phosphorus alloys*. J. appl. phys 38, 4096 (1967)
- [13] P. Duwez. *Structure and properties of alloys rapidly quenched from the liquid state*. Trans. Am. Soc. Metals, 60 607-633 (1967)
- [14] W. Hume-Rothery, H. M. Powell. Zeitschrift Fur Kristallographie, 91 23-47 (1935)
- [15] R. Pond, R. Maddin. *Method of producing rapidly solidified filamentary castings*. Trans. Met. Soc. AIME, 245 2475-2476 (1969)



- [16] H. H. Liebermann, C. D. Graham. *Production of amorphous alloy ribbons and effects of apparatus parameters on ribbon dimensions*. IEEE Transactions on Magnetics, 12 921-923 (1976)
- [17] R. Roy, A. K. Majumdar. *Thermomagnetic and transport properties of metglas 2605 SC and 2605*. Journal of Magnetism and Magnetic Materials, 25 83–89 (1981)
- [18] I. S. Miroshnichenko, V. F. Bashev, YU. K. Pokrovskiy, E. Z. Spektor. *The structure and properties of cast microwire from Iron-Carbon-Boron alloy*. Russ. Metall. 1, 105 (1980)
- [19] G. F. Taylor. *A method of drawing metallic filaments and a discussion of their properties and uses*. Phys. Rev. , 23 655-660 (1924).
- [20] G. F. Taylor. *Process and apparatus for making filaments*. United States Patent Office 1 793 529 Patented Feb. 24, (1931).
- [21] E. Ya. Badinter, N. R. Berman, I. F. Drabenko, V. I. Zaborovsky, Z. I. Zelikovsky, V. G. Cheban. *Cast microwires and its properties*. Shtinica, Kishinev in Russian (1973)
- [22] A. V. Ulitovsky. *Micro-technology in design of electric devices*. Leningrad, 1951, No.7, p.6. (1951).
- [23] A. V. Ulitovsky, I. M. Maianski, A. I. Avramenco. *Method of continuous casting of glass coated microwire*. Patent No128427 (USSR), 15.05.1960. Bulletin. No10, p.14 (1960).
- [24] A. V. Ulitovsky, N. M. Avernin. *Method of fabrication of metallic microwire*. Patent No161325 (USSR), 19.03.1964. Bulletin No7, p.14 (1964).
- [25] H. Wiesner, J. Schneider. *Magnetic properties of amorphous Fe-P alloys containing Ga, Ge, and As*. Phys. Status Solidi, 26 71-75 (1974)
- [26] J. Nixdorf. *Comparison between whiskers and filaments and their use in fibre-reinforced materials*. Proc. Roy. Soc. Lond., A319 17-32 (1970)
- [27] T. Goto, M. Nagano, N. Wehara. *Mechanical properties of amorphous  $Fe_{80}P_{16}C_3B_1$  filaments produced by glass-coated melt spinning*. Trans. JIM, 18 759-764 (1977)
- [28] T. Goto. *The preparation of fine Ni-Fe-base amorphous filaments using the method of glass-coated melt spinning*. Journal of Materials Science and Engineering, 59, 2 251-256 (1983)
- [29] T. Goto, T. Toyama. *The preparation of ductile high strength Fe-base filaments using the methods of glass-coated melt spinning*. Journal of Materials Science, 20, 5 1883-1888 (1985)
- [30] I. W. Donald. *Review: Production, properties and application of microwire and related products*. J. Materials Science, 22 2661-2679 (1987)

- [31] M. Hagiwara, A. Inoue. *Rapidly Solidified Alloys: Processes, Structures, Properties, Applications*, ed. H. H. Liebermann. Marcel Dekker Inc., New York Chap. 6, p. 139 (1993)
- [32] A. Inoue, T. Masumoto. *Properties and applications of amorphous alloy wire*. Engng Mater., 30 5 47-52 (1982)
- [33] H. Chiriac, T. A. Ovari. *Amorphous glass-covered magnetic wires: preparation, properties, applications*. Progress in Materials Science, 40 333-407 (1996)
- [34] V. S. Larin, A. V. Torcunov, A. Zhukov, J. Gonzalez, M. Vazquez, L. Panina. *Preparation and properties of glass-coated microwires*. J. Magnetism and Magnetic materials, 249 39-45 (2002).
- [35] A. Zhukov, J. Gonzalez, M. Vazquez, V. Larin, A. Torcunov. *Nanocrystalline and amorphous magnetic microwires*. In: H. S. Nalwa Encyclopedia of nanoscience and nanotechnology, Vol. 6, 365-387 (2004)
- [36] S. A. Baranov, V. N. Berzhanski, S. K. Zotov, V. L. Kokoz, V. S. Larin, A.V. Torcunov, Phys. Met. Metall., 67 73 (1989)
- [37] H. Chiriac, T. A. Ovari, Gh. Pop. *Internal stress distribution in glass-coated amorphous magnetic wires*. Phys. Rev. B 52 10104-10113 (1995)
- [38] J. Velazquez, M. Vazquez, A. Zhukov. *Magnetoelastic anisotropy distribution in glass-coated microwires*. J. Mater. Res., 11 2499–2505 (1996)
- [39] A. S. Antonov, V. T. Borisov, O. V. Borisov, A. F. Prokoshin, N. A. Usov. *Residual quenching stresses in glass-coated amorphous ferromagnetic microwires*. J. Phys. D Appl. Phys., 33 1161–1168 (2000)
- [40] M. Vazquez, A. Zhukov. *Magnetic properties of glass-coated amorphous and nanocrystalline microwires*. J. Magn. Magn. Mater., 160 223-228 (1996)
- [41] H. Chiriac, T. A. Ovari, A. Zhukov. *Magnetoelastic anisotropy of amorphous microwires*. J. Magn. Magn. Mater., 254–255, 469–471 (2003)
- [42] A. I. Gubanov. Fiz. Tverd. Tela, 2 502 (1960); Sov. Phys. Solid State, 2 468 (1960)
- [43] S. Chikazumi. *Physics of magnetism*. Robert E. Krieger publishing, New York (1978)
- [44] R. C. O'Handley. *Physics of ferromagnetic amorphous alloys*. J. Appl. Phys., 62, No. 10, R15-R49 (1967)
- [45] R. C. O'Handley. *Modern Magnetic Materials Principles and Applications*. ISBN-13: 978-0471155669 (1999)

- [46] K. Handrich. *A simple model for amorphous and liquid ferromagnets*. Phys. Stat. Sol., 32 K55-K58 (1969)
- [47] F. E. Luborsky. *Amorphous Metallic Alloys*. Chapter 1 in Amorphous Metallic Alloys, Ed. By F. Luborsky Butterworths Monographs in Materials 1-7 (1983)
- [48] R. Alben, J. J. Becker, M. C. Chi. *Random anisotropy in amorphous ferromagnets*. J. Appl. Phys., 49 1653-1658 (1978)
- [49] A. Zhukov, V. Zhukova, J. M. Blanco, A. F. Cobeño, M. Vazquez, J. Gonzalez. *Magnetostriction in glass-coated magnetic microwires*. J. Magn. Magn. Mater., 258–259, 151-157 (2003)
- [50] Y. Konno, K. Mohri. *Magnetostriction measurements for amorphous wires*. IEEE Trans. Magn., 25, 3623–3625 (1989)
- [51] A. Talaat, V. Zhukova, M. Ipatov, J. M. Blanco, L. Gonzalez-Legarreta, B. Hernando, J. J. del Val, J. Gonzalez, A. Zhukov. *Optimization of the giant magnetoimpedance effect of Finemet-type microwires through the nanocrystallization*. J. Appl. Phys. 115, 17A313 (2014)
- [52] A. Talaat, V. Zhukova, M. Ipatov, J. J. del Val, L. Gonzalez-Legarreta, B. Hernando, J. M. Blanco, A. Zhukov. *Effect of nanocrystallization on giant magnetoimpedance effect of Fe based microwires*. Intermetallics 51, 59–63 (2014)
- [53] A. Talaat, J. M. Blanco, M. Ipatov, V. Zhukova, A. P. Zhukov. *Domain wall propagation in Co-Based glass-coated microwires: Effect of stress annealing and tensile applied stresses*. IEEE Transactions on Magnetics, 50 11 2005704 (2014)
- [54] M. Barandiaran, A. Hernando, V. Madurga, O. V. Nielsen, M. Vazquez, M. Vazquez-Lopez. *Temperature, stress, and structural relaxation dependence of the magnetostriction in metallic glasses*. Phys. Rev. B., 35 5066- 5071 (1987)
- [55] J. M. Blanco, P. G. Barbon, J. González, C. Gomez-Polo, M. Vázquez. *Stress induced magnetic anisotropy in non-magnetostrictive amorphous wires*. J. Magn. Magn. Mater., 137-8, 104-107 (1992)
- [56] R. Varga. *Magnetization processes in glass-coated microwires with positive magnetostriction*. Acta. Physica Slovaca, 62 5 411-518 (2012)
- [57] S. A. Gudishnikov, B. Y. Ljubimov, P. S. Pavlanov, Y. V. Prokhorova, V. S. Skomartovski, N. A. Usov, A. V. Torcunov. *Influence of applied tensile stress on the magnetic behaviour of Co-rich amorphous microwires*. Phy. Stat. Solidi A, 206 (4) 625-629 (2009)

- [58] Yu. Kabanov, A. Zhukov, V. Zhukova, J. Gonzalez. *Magnetic domain structure of microwires studied by using the magneto-optical indicator film method*. Appl. Phys. Lett., 87 142507:1-3 (2005)
- [59] A. Chizhik, A. Zhukov, J. M. Blanco, J. Gonzalez. *Magneto-optical investigation of magnetization reversal in nearly zero magnetostrictive Co-rich wire and microwire*. J. Magn. Magn. Mater., 249 27-33 (2002)
- [60] A. P. Zhukov, M. Vazquez, J. Velazquez, H. Chiriac, V. Larin. *The remagnetization process in thin and ultra thin Fe-rich amorphous wires*. J. Magn. Magn. Mat., 151 132-138 (1995)
- [61] A. Zhukov, M. Vazquez, J. Velazquez, A. Hernando, V. Larin. *Magnetic properties of Fe-based glass-coated microwires*. J. Magn. Magn. Mat., 170 323-330 (1997)
- [62] A. Zhukov. *Domain Wall propagation in a Fe-rich glass-coated amorphous microwire*. Applied Physics Letters, 78 3106-3108 (2001)
- [63] R. Varga, K. Richter, A. Zhukov, V. Larin. *Domain wall propagation in thin magnetic wires*. IEEE Trans. Magn., 44 11 3925-3930 (2008)
- [64] M. Vazquez, C. Gomez-Polo, D. X. Chen. *Switching mechanism and domain structure of bistable amorphous wires*. IEEE Trans. Magn., 28, 5 3147-3149 (1992)
- [65] H. S. Chen. *Structural relaxation in metallic glasses*. Chapter 11 in Amorphous Metallic Alloys, Ed. By F. Luborsky Butterworths Monographs in Materials 169-186 (1983)
- [66] A. L. Greer, J. A. Leake. *Structural relaxation and cross-over effect in a metallic glass*. J. Non-Cryst. Solids, 33 291-297 (1979)
- [67] T. Egami. *Magnetic amorphous alloys: physics and technological applications*. Rep. Prog. Phys., 47 1601-1725 (1984)
- [68] A. Zhukov, J. Gonzalez, J. M. Blanco, M. J. Prieto, E. Pina, M. Vazquez. *Induced magnetic anisotropy in Co-Mn-Si-B amorphous microwires*. J. Appl. Phys., 87 1402-1408 (2000)
- [69] A. Zhukov, V. Zhukova, V. Larin, J. M. Blanco, J. Gonzalez. *Tailoring of magnetic anisotropy of Fe-rich microwires by stress induced anisotropy*. Physica B, 384 1-4 (2006)
- [70] H. Fujimori. *Magnetic anisotropy*. Chapter 16 in Amorphous Metallic Alloys, Ed. By F. Luborsky Butterworths Monographs in Materials 300-316 (1983)
- [71] F. E. Luborsky, J. L. Walker. *Magnetic anneal anisotropy in amorphous alloys*. IEEE Trans. Magn. Mag-13, 2 953-956 (1977)

- [72] M. Vázquez, E. Ascasibar, A. Hernando, O. V. Nielsen. *Co-Si-B and Fe-Co-B amorphous alloys: Induced anisotropy and various magnetic properties*. J. Magn. Magn. Mat., 66 37-44 (1987)
- [73] J. González, M. Vázquez, J. M. Barandiarán, V. Madurga, A. Hernando. *Different kinds of anisotropies induced by current annealing in metallic glasses*. J. Magn. Magn. Mat., 68 151-156 (1987)
- [74] T. Miyazaki, M. Takahashi, K. Hisatake. *Magnetic relaxation in amorphous (Fe,Co)<sub>100-x</sub>B<sub>x</sub> alloys*. J. Appl. Phys., 57 3575-3577 (1985)
- [75] M. L. Néel. *Anisotropie magnétique superficielle et surstructures d'orientation*. J. Phys. Radium, 15 225-239 (1954)
- [76] D. X. Chen, L. C. Tai. *Temperature dependence of induced magnetic anisotropies in nearly non-magnetostrictive metallic glasses (Fe<sub>1-x</sub>Co<sub>x</sub>)<sub>78</sub>Si<sub>10</sub>B<sub>12</sub>*. J. Magn. Magn. Mat., 50 329-334 (1985)
- [77] D. X. Chen. *Induced anisotropy and magnetostriction in metallic glasses*. J. Appl. Phys., 61 3781-3783 (1987)
- [78] A. Zhukov. *Design of the magnetic properties of Fe-rich, glass-coated microwires for technical applications*. Adv. Fun. Materials, 16 5 675-680 (2006)
- [79] Y. Yoshizawa, S. Oguma, K. Yamauchi. *New Fe-based soft magnetic alloys composed of ultrafine grain structure*. J. Appl. Phys. 64, 6044 (1988)
- [80] G. Herzer. *Grain structure and magnetism of nanocrystalline ferromagnets*. IEEE Trans. Magn. Mag. 25, 3327-3329 (1989)
- [81] G. Herzer. *Grain size dependence of coercivity and permeability in nanocrystalline ferromagnets*. IEEE Trans. Magn. 26, 1397-1402 (1990)
- [82] G. Herzer. *The random anisotropy model a critical review and update*. In properties and applications of nanocrystalline alloys from amorphous precursors, Kluwer academic publishers 1-21 (2005)
- [83] G. Herzer. *Soft magnetic materials-nanocrystalline alloys*. Handbook of magnetism and advanced magnetic materials, John Wiley and sons, 4 1882 (2007)
- [84] Y. Yoshizawa, K. Yamauchi. *Magnetic properties of Fe-Cu-M-Si-B (M= Cr, V, Mo, Nb, Ta, W) alloys*. Mater. Sci. Eng. A, 133 176-179 (1991)

- [85] M. Muller, N. Mattern. *The influence of refractory element additions on the magnetic properties and on the crystallization behavior of nanocrystalline soft magnetic Fe-B-Si-Cu alloys*. J. Magn. Mater., 136 79-87 (1994)
- [86] N. Kataoka, T. Matsunaga, A. Inoue, T. Masumoto. *Soft magnetic properties of bcc Fe-Au-X-Si-B (X = early transition metal) alloys with fine grain structure*. Mater. Trans. JIM, 30 11 947-950 (1989)
- [87] K. Suzuki, N. Kataoka, A. Inoue, A. Makino, T. Masumoto. *High saturation magnetization and soft magnetic properties of bcc Fe-Zr-B alloys with ultrafine grain structure*. Mater. Trans. JIM, 31 8 743-746 (1990)
- [88] K. Suzuki, A. Makino, N. Kataoka, A. Inoue, T. Masumoto. *High saturation magnetization and soft magnetic properties of bcc Fe-Zr-B and Fe-Zr-B-M (M= transition metal) alloys with nanoscale grain size*. Mater. Trans. JIM., 32 1 93-102 (1991)
- [89] M. A. Willard, D. E. Laughlin, M. E. McHenry, D. Thoma, K. Sickafus, J. O. Cross, V. G. Harris. *Structure and magnetic properties of  $(Fe_{0.5}Co_{0.5})_{88}Zr_7B_4Cu_1$  nanocrystalline alloys*. J. Appl. Phys., 84 12 6773-6777 (1998)
- [90] K. Lu. *Nanocrystalline metals crystallized from amorphous solids*. Materials Science and Engineering, R16 161-221 (1996)
- [91] M. E. McHenry, M. A. Willard, D. E. Laughlin. *Amorphous and nanocrystalline materials for application as soft magnet*. Progress in Materials Science, 44 291-433 (1999)
- [92] T. Kulik. *Nanocrystallization of metallic glasses*. J. non-crystalline solids, 287 145-161 (2001)
- [93] M. G. Scott. *Crystallization*. Chapter 10 in Amorphous Metallic Alloys, Ed. By F. Luborsky Butterworths Monographs in Materials 144-168 (1983)
- [94] A. L. Greer. *Crystallization of amorphous alloy*. Metallurgical and materials transactions A, 27A 549-555 (1996)
- [95] E. P. Harrison, G. L. Turney, H. Rowe. *Electrical properties of wires of high permeability*. Nature, 135 961 (1935)
- [96] L. V. Panina, K. Mohri. *Magneto-impedance effect in amorphous wires*. Appl. Phys. Lett., 65 1189-1191 (1994)
- [97] R. S. Beach, A. E. Berkowitz. *Giant magnetic field dependent impedance of amorphous FeCoSiB wire*. Appl. Phys. Lett., 64 3652 (1994)



- [98] M. H. Phan, H. X. Peng. *Giant magnetoimpedance materials: Fundamentals and applications*. Progress in Materials Science, 53 323–420 (2008)
- [99] M. Knobel, K. R. Pirota. *Giant magnetoimpedance: concepts and recent progress*. J Magn Magn Mater., 242-245 33–40 (2002)
- [100] M. Knobel, M. Vazquez, L. Kraus. *Giant magnetoimpedance*. Chapter 5 in: Buschow KH, editor. Handbook of magnetic materials, vol. 15. Amsterdam: Elsevier Science B.V 1–69 (2003)
- [101] L. Kraus. *GMI modeling and material optimization*. Sens Acta A, 106 187–94 (2003)
- [102] N. A. Usov, A. S. Antonov, A. N. Lagarkov. *Theory of giant magneto-impedance effect in amorphous wires with different types of magnetic anisotropy*. J Magn Magn Mat., 185 159-173 (1998)
- [103] D. Menard, M. Britel, P. Ciureanu, A. Yelon. *Giant magnetoimpedance in a cylindrical conductor*. J. Appl. Phys., 84 2805–2814 (1998)
- [104] A. Zhukov, M. Ipatov, C. Garcia, M. Churyukanova, S. Kaloshkin, V. Zhukova. *From manipulation of giant magnetoimpedance in thin wires to industrial applications*. J. Supercond. Nov. Magn., 26 1045–1054 (2013)
- [105] D. P. Makhnovskiy, L. V. Panina, D. J. Mapps. *Field-dependent surface impedance tensor in amorphous wires with two types of magnetic anisotropy: Helical and circumferential*. Phys Rev B, 63 144424-1:17 (2001)
- [106] S. I. Sandacci, D. P. Makhnovskiy, L. V. Panina, K. Mohri, Y. Honkura. *Off-diagonal impedance in amorphous wires and its application to linear magnetic sensors*. IEEE Trans Magn., 35 3505-3510 (2004)
- [107] M. Ipatov, V. Zhukova, J. M. Blanco, J. Gonzalez, A. Zhukov. *Off-diagonal magneto-impedance in amorphous microwires with diameter 6–10  $\mu\text{m}$  and application to linear magnetic sensors*. phys. stat. sol. (a) 205 No. 8 1779–1782 (2008)
- [108] K. R. Pirota, L. Kraus, H. Chiriac, M. Knobel. *Magnetic properties and GMI in a CoFeSiB glass-covered microwire*. J. Magn. Magn. Mater., 21 L243–L247 (2000)
- [109] V. Zhukova, A. Chizhik, A. Zhukov, A. Torcunov, V. Larin, J. Gonzalez. *Optimization of giant magneto-impedance in Co-rich amorphous microwires*. IEEE Trans. Magn., 38 (5, Part I), 3090–3092 (2002)

- [110] Y. Honkura. *Development of amorphous wire type MI sensors for automobile use*. J. Magn. Magn. Mater., 249 375–381 (2002)
- [111] K. Mohri, T. Uchiyama, L. P. Shen, C. M. Cai, L. V. Panina. *Sensitive micro magnetic sensor family utilizing magneto-impedance (MI) and stress-impedance (SI) effects for intelligent measurements and control*. Sens. Actuat. A, 91 85–90 (2001)
- [112] A. F. Cobeño, A. Zhukov, J. M. Blanco, V. Larin, J. Gonzalez. *Magnetoelastic sensor based on GMI of amorphous microwire*. Sensors and Actuators (A), 91 95-98 (2001)
- [113] K. Mohri, Y. Hankura. *Amorphous wire and CMOS IC based magneto-impedance sensors-origin, topics, and future*. Sens. Lett., 5 267-270 (2007)
- [114] T. Uchiyama, K. Mohri, S. Nakayama. *Measurement of spontaneous oscillatory magnetic field of guinea-pig smooth muscle preparation using pico-tesla resolution amorphous wire magneto-impedance sensor*. IEEE Trans. Magn., 47 (10) 3070-3073 (2011)
- [115] V. Zhukova, M. Ipatov, A. Zhukov. *Thin magnetically soft wires for magnetic microsensors*. Sensors, 9 9216-9240 (2009)
- [116] H. Chiriac, M. Tibu, A. E. Moga, D. D. Herea. *Magnetic GMI sensor for detection of biomolecules*. J. Magn. Magn. Mater., 293 671-676 (2005)
- [117] J. Devkota, T. Luong, J. S. Liu, H. Shen, F. X. Qin, J. F. Sun, P. Mukherjee, H. Srikanth, M. H. Phan. *A soft ferromagnetic multiwire-based inductance coil sensor for sensing applications*. J. of Appl. Phys., 116 234504:1-8 (2014)
- [118] S. Nakayama, T. Uchiyama. *Real-time measurement of biomagnetic vector fields in functional syncytium using amorphous metal*. Sci. Rep. 5, 8837 1-9 DOI:10.1038/srep08837 (2015)
- [119] D. Makhnovskiy, A. Zhukov, V. Zhukova, J. Gonzalez. *Tunable and self-sensing microwave composite materials incorporating ferromagnetic microwires*. Adv. Sci. Technol., 54 201–210 (2008)
- [120] J. R. Wiegand. *Bistable magnetic device*. US Patent 3,820,090, (1974)
- [121] K. Mohri, B. Takeuchi, T. Fujimoto. *Sensitive magnetic sensors using amorphous wiegand-type ribbons*. IEEE Trans. Magn., 17 3370–3372 (1981)
- [122] K. Mohri, S. Takeuchi. *Sensitive bistable magnetic sensors using twisted amorphous magnetostrictive ribbons due to matteucci effect*. J. Appl. Phys., 53 8386–8388 (1982)



- [123] F. B. Humphrey, K. Mohri, J. Yamasaki, H. Kawamura, R. Malmhall, I. Ogasawara. *Reentrant magnetic flux reversal in amorphous wires*. In magnetic properties of amorphous metals; A. Hernando, V. Madurga, M. C. Sanchez-Trujillo, M. Vázquez, Eds.; Elsevier Science: Amsterdam, the Netherlands 110–116 (1987)
- [124] K. Mohri, F. B. Humphrey, K. Kawashima, K. Kimura, M. Muzutani. *Large barkhausen and matteucci effects in FeCoSiB, FeCrSiB, and FeNiSiB amorphous wires*. IEEE Trans. Magn., 26 1789–1791 (1990)
- [125] A. Zhukov, J. González, J. M. Blanco, M. Vázquez, V. Larin. *Microwires coated by glass: a new family of soft and hard magnetic materials*. J. Mat. Res., 15 2107–2113 (2000)
- [126] A. Zhukov, J. Gonzalez, J. M. Blanco, P. Aragoneses, L. Domínguez. *Magnetoelastic sensor of level of the liquid based on magnetoelastic properties of Co-rich microwires*. Sens. Actuat. A-Phys., 81 129–133 (2000)
- [127] A. Zhukov, J. M. Garcia-Beneytez, M. Vázquez. *Magnetoelastic sensor for signature identification based on mechanomagnetic effect in amorphous wires*. J. Phys. IV, 8 Pr2-763–Pr2-766 (1998)
- [128] S. S. P. Parkin, M. Hayashi, L. Thomas. *Magnetic domain-wall racetrack memory*. Science, 320 190–194 (2008)
- [129] D. A. Allwood, G. Xiong, C. C. Faulkner, D. Atkinson, D. Petit, R. P. Cowburn. *Magnetic domain-wall logic*. Science, 309 1688–1692 (2005)
- [130] J. Olivera, R. Varga, P. Vojtanik, V. M. Prida, M. L. Sanchez, B. Hernando, A. Zhukov. *Fast domain wall dynamics in amorphous glass-coated microwires*. J. Magn. Magn. Mater., 320 2534–2537 (2008)
- [131] R. Varga, A. Zhukov, V. Zhukova, J. M. Blanco, J. Gonzalez. *Supersonic domain wall in magnetic microwires*. Phys. Rev. B, 76 132406 (2007)
- [132] D. Atkinson, D. A. Allwood, C. C. Faulkner, G. Xiong, M. D. Cooke, R. P. Cowburn. *Magnetic domain wall dynamics in a permalloy nanowire*. IEEE Trans. Magn., 39 2663–2665 (2003)
- [133] R. Varga, J. Torrejon, Y. Kostyk, K. L. Garcia, G. Infantes, G. Badini, M. Vazquez. *Single-wall dynamics and power law in bistable magnetic microwires*. J. Phys.: Cond. Matter., 20 445215:1-5 (2008)
- [134] C. Kittel, J. K. Galt. Solid State Phys., 3 437 (1956)

- [135] R. P. del Real, C. Prados, D. X. Chen, A. Hernando, M. Vazquez. *Eddy current damping of planar domain wall in bistable amorphous wires*. Appl. Phys. Lett., 63 3518-3520 (1993)
- [136] A. Thiaville, J. M. Garcia, J. Miltat. *Domain wall dynamics in nanowires*. J. Magn. and Magn. Mater., 242–245 1061–1063 (2002)
- [137] L. V. Panina, M. Mizutani, K. Mohri, F. B. Humphrey, I. Ogasawara. *Dynamics and relaxation of large Barkhausen discontinuity in amorphous wires*. IEEE Trans Magn, 27(6):5331–5333 (1991)
- [138] R. Varga, K. L. Garcia, M. Vázquez, P. Vojtaník. *Single-domain wall propagation and damping mechanism during magnetic switching of bistable amorphous microwires*. Phys. Rev. Lett., 94 017201:1-4 (2005)
- [139] G. Infante, R. Varga, G. A. Badini-Confalonieri, M. Vazquez. *Locally induced domain wall damping in a thin magnetic wire*. Appl. Phys. Lett., 95 012503 (2009)
- [140] R. L. Novak, J. P. Sinnecker, H. Chiriac. *Annealing effects on the magnetization reversal and domain wall dynamics in bistable amorphous glass-covered microwires*. J. Phys. D: Appl. Phys. 41 095005 (2008)
- [141] A. Zhukov, V. Zhukova. *Magnetic sensors and applications based on thin magnetically soft wires with tunable magnetic properties*. IFSA Publishing, S. L. Barcelona, Spain. (2014)
- [142] S. Zaporozhan, C. Plotnic, I. Calmicov, V. Larin. *A knowledge-based approach for microwire casting plant control*. Chapter 19 in book: Nanotechnology: Concepts, Methodologies, Tools, and Applications, DOI: 10.4018/978-1-4666-5125-8 419-437 (2014)
- [143] A. Zhukov, V. Zhukova. *Magnetic properties and applications of ferromagnetic microwires with amorphous and nanocrystalline structure*. New York: Nova Science Publishers, ISBN: 978-1-60741-770-5 (2009)
- [144] W. Zhou, R. P. Apkarian, Z. L. Wang, D. Joy. *Fundamentals of Scanning Electron Microscopy*. In Scanning Microscopy for Nanotechnology, W. Zhou and Z. L. Wang, Eds. Springer, (2007)
- [145] M. W. Davidson, M. Abramowitz. *Optical microscopy*. Online PDF source: <http://www.olympusmicro.com/primer/microscopy.pdf> (1999)
- [146] J. R. Connolly. *Introduction to X-ray Powder Diffraction*. Online PDF source: <http://epswww.unm.edu/media/pdf/01-XRD-Intro.pdf> EPS 400 (2007)

- [147] V. K. Pecharsky, P. Y. Zavalij. *Fundamentals of powder diffraction and structural characterization of materials*. Boston: Kluwer Academic Publishers (2003)
- [148] Bruker advanced x-ray solutions user's manual Vol.5 Online PDF source: [https://www.ndsu.edu/chemistry/files/mcl/smart5\\_UserManual.pdf](https://www.ndsu.edu/chemistry/files/mcl/smart5_UserManual.pdf)
- [149] D. B. Cullity. *Elements of x-ray diffraction*. 2-Edition: Addison-Wiley Publishing Company Reading (1978)
- [150] V. Zhukova, V. S. Larin, A. Zhukov. *Stress induced magnetic anisotropy and giant magnetoimpedance in Fe-rich glass-coated magnetic microwires*. J. Appl. Phys, 94 1115-1118 (2003)
- [151] K. Mohri, T. Uchiyama, L. V. Panina. *Recent advances of micromagnetic sensors and sensing application*. Sens. Actuators A, 59 (1-3) 1-8 (1997)
- [152] V. Raposo, M. Vázquez, A. G. Flores, M. Zazo, J. I. Iñiguez. *Giant magnetoimpedance effect enhancement by circuit matching*. Sens. Actuators A, 106 329–332 (2003)
- [153] J. M. Barandiarán, A. Garcia Arribas, J. L. Muñoz, G. V. Kulyanskaya. *Influence of magnetization processes and device geometry on the GMI effect*. IEEE Trans. Magn., 38 3051–3056 (2002)
- [154] Agilent Network Analyzer Basics. Agilent Technologies Online PDF source: <http://cp.literature.agilent.com/litweb/pdf/5965-7917E.pdf>
- [155] S. Lan, L. Shen. *Microwave components based on magnetic wires*. School of Information Science, Computer and Electrical Engineering, Halmstad University, Technical report, IDE1057, November (2010)
- [156] D. de Cos, A. Garcia-Arribas, J. M. Barandiaran. *Analysis of magnetoimpedance measurmenst at thigh frwquency using a microstrip transmission line*. Sensors and Actuators A, 115 368-375 (2004)
- [157] A. Zhukov, A. Talaat, M. Ipatov, V. Zhukova. *Tailoring the High-Frequency Giant Magnetoimpedance Effect of Amorphous Co-Rich Microwires*. Magnetics Letters IEEE, 6 1-4 (2015)
- [158] K. J. Sixtus, L. Tonks. *Propagation of large Barkhausen discontinuities.II*. Phys Rev, 42 419–435 (1932)
- [159] R. Varga, A. Zhukov, J. M. Blanco, M. Ipatov, V. Zhukova, J. Gonzalez, P. Vojtaník. *Fast magnetic domain wall in magnetic microwires*. Phys. Rev. B, 74 212405-1-5 (2006)

- [160] M. Ipatov, V. Zhukova, A. K. Zvezdin, A. Zhukov. *Mechanisms of the ultrafast magnetization switching in bistable amorphous microwires*. J. Appl. Phys., 106 103902:1-5 (2009)
- [161] K. Narita, J. Yamasaki, H. Fukunaga. *Measurements of saturation magnetostriction of a thin amorphous ribbon by means of small-angle-magnetization-rotation*. IEEE Trans. Magn., 16 435-439 (1980)
- [162] A. Siemko, H. Lachowicz. *On indirect measurements of magnetostriction in low magnetostrictive metallic glasses*. IEEE Trans. Magn., 23 2563-2365 (1987)
- [163] S. Gudoshnikov, M. Churyukanova, S. Kaloshkin, A. Zhukov, V. Zhukova, N. A. Usov. *Investigation of the properties of Co-rich amorphous ferromagnetic microwires by means of small angle magnetization rotation method*. J. of Magn. Magn. Mats, 387 53–57 (2015)
- [164] K. Keil, J. L. Berkley, L. H. Fuchs. *Suessite, Fe<sub>3</sub>Si: A new mineral in the North Haig ureilite*. Am. Mineral., 67 126-131 (1982)
- [165] P. Scherrer. *Bestimmung der grösse und der inneren struktur von kolloidteilchen mittels röntgenstrahlen nachrichten von der gesellschaft der wissenschaften göttingen*. Mathematisch-Physikalische Klasse, 2 98-100 (1918)
- [166] A. M. Glezer, I. E. Permyakova. *Melt-quenched nanocrystals*. CRC Press Taylor & Francis Group. ISBN: 978-1-4665-9415-9 (2013)
- [167] H. Okumura, D.E. Laughlin, M.E. McHenry. *Magnetic and structural properties and crystallization behavior of Si-rich FINEMET materials*. J. Magn. Magn. Mater., 267 347-356 (2003).
- [168] C. -Y. Um, F. Johnson, M. Simone, J. Barrow, M. E. McHenry. *Effect of crystal fraction on hardness in FINEMET and NANOPERM nanocomposite alloys*. J. Appl. Phys., 97 10F504:1-3 (2005)
- [169] C. Suryanarayana, C. C. Koch. *Nanocrystalline materials—Current research and future directions*. Hyperfine Interactions, 130 (1) 5-44 (2000)
- [170] M. E. McHenry, F. Johnson, H. Okumura, T. Ohkubo, V.R.V. Ramanan, D.E. Laughlin. *The kinetics of nanocrystallization and microstructural observations in FINEMET, NANOPERM and HITPERM nanocomposite magnetic materials*. Scripta Materialia, 48 881-887 (2003)

- [171] A. G. Ilinsky, V. V. Maslov, V. K. Nozenko, A. P. Brovko. *On determination of volume fraction of crystalline phase in partially crystallized amorphous and nanocrystalline materials*. J. Mat. Sci, 35 4495–4500 (2000)
- [172] H. Q. Guo, H. Kronmüller, T. Dragon, Z. H. Cheng, B. G. Shen. *Influence of nanocrystallization on the evolution of domain patterns and the magnetoimpedance effect in amorphous  $Fe_{73.5}Cu_1Nb_3Si_{13.5}B_9$  ribbons*. J. Appl. Phys., 89 514-520 (2001)
- [173] J. Arcas, C. Gómez-Polo, A. Zhukov, M. Vázquez, V. Larin, A. Hernando. *Magnetic properties of amorphous and devitrified  $FeSiBCuNb$  glass-coated microwires*. Nanostructured Materials, 7 823-834 (1996)
- [174] T. Yamamoto. *The development of Sendust and other ferromagnetic alloys*. Komiyama Printing, Chiba, Japan, Chs, 1-4 26-29 (1980)
- [175] Y. Yoshizawa, K. Yamauchi, S. Oguma. European Patent Application, 0 271 657 (1988)
- [176] G. Herzer. *Magnetization process in nanocrystalline ferromagnets*. Materials Science and Engineering: A, 133 1-5 (1991)
- [177] J. M. Blanco, A. Zhukov, J. Gonzalez. *Asymmetric torsion stress giant magnetoimpedance in nearly-zero magnetostrictive amorphous wires*. J. Appl. Phys., 87 (9) 4813-4815 (2000)
- [178] F. Johnson, P. Hughes, R. Gallagher, D. E. Laughlin, M. E. McHenry, M. A. Willard, V. G. Harris. *Structure and thermomagnetic properties of new  $FeCo$ -based nanocrystalline ferromagnets*. IEEE Trans. Magn., 37 2261–2263 (2001)
- [179] R. S. Sundar, S. C. Deevi. *Soft magnetic  $FeCo$  alloys: alloy development, processing, and properties*. International Materials Reviews, 50 (3) 157-192 (2005)
- [180] P. Klein, R. Varga, P. Vojtanik, J. Kovac, J. Ziman, G. A. Badini-Confalonieri, M. Vazquez. *Bistable  $FeCoMoB$  microwires with nanocrystalline microstructure and increased Curie temperature*. J. Phys. D: Appl. Phys. 43 045002 (6pp) (2010)
- [181] S. Michalik, J. Gamcova, J. Bednarcik, R. Varga. *In situ structural investigation of amorphous and nanocrystalline  $Fe_{40}Co_{38}Mo_4B_{18}$  microwires*. Journal of Alloys and Compounds 509, 3409–3412 (2011)
- [182] P. Klein, R. Varga, M. Vazquez. *Domain wall dynamics in nanocrystalline microwires*. Phys. Status Solidi C, 11 No. 5–6, 1139-1143 (2014)
- [183] JCPDS-ICDD, PCPDFWIN, version 2.0 (1998)

- [184] A. Takeuchi, A. Inoue. *Classification of bulk metallic glasses by atomic size difference, heat of mixing and period of constituent elements and its application to characterization of the main alloying element*. Materials Transactions, 46 (12) 2817-2829 (2005)
- [185] C. Suryanarayana, A. Inoue. *Iron-based bulk metallic glasses*. International Materials Reviews, 58 (3) 131-166 (2013)
- [186] M. Paluga, P. Svec, D. Janickovic, D. Muller, P. Mrafko, M. Miglierini. *Nanocrystallization in rapidly quenched Fe-Mo-Cu-B: surface and volume effects*. Rev. Adv. Mater. Sci., 18 481-493 (2008)
- [187] H. Y. Tong, B. Z. Ding, H. G. Jiang, K. Lu, J. T. Wang, Z. Q. Hu. *Formation kinetics of nanocrystalline FeBSi alloy by crystallization of the metallic glass*. Journal of Applied Physics, 75 654-656 (1994)
- [188] A. V. Serebryakov. *Amorphization reactions and glass to crystal transformations in metallic materials*. J. Non-Crystalline Solids, 156-158 594-597 (1993)
- [189] L. Onsager. *Reciprocal relations in irreversible processes. I*. Physical Review, 37 405-426 (1931)
- [190] J. Gonzalez, A. Zhukov, V. Zhukova, A.F. Cobeño, J. M. Blanco, A. R. de Arellano-Lopez, S. Lopez-Pombero, J. Martinez-Fernandez, V. Larin, A. Torcunov. *High coercivity of partially devitrified glass-coated finemet microwires: effect of geometry and thermal treatment*. IEEE Trans. Magn., 36 (5) 3015-3017 (2000)
- [191] C. F. Conde, J. M. Borrego, J. S. Blázquez, A. Conde, P. Svec, D. Janickovic. *Magnetic and structural characterization of Mo-Hitperm alloys with different Fe/Co ratio*. Journal of Alloys and Compounds, 509 1994–2000 (2011)
- [192] V. Rodionova, M. Ipatov, M. Ilyn, V. Zhukova, N. Perov, J. Gonzalez, A. Zhukov. *Tailoring of magnetic properties of magnetostatically-coupled glass-covered magnetic microwires*. J Supercond Nov Magn., 24 (1-2) 541–547 (2011)
- [193] P. Allia, F. Vinai. *New approach to the study of the magnetic permeability aftereffect of amorphous ferromagnetic alloys*. Phys Rev B, 26 6141-9 (1982)
- [194] R. Varga, K. L. García, A. Zhukov, M. Vázquez, P. Vojtanek. *Temperature dependence of the switching field and its distribution in Fe-rich bistable microwires*. Appl Phys Lett., 83(13) 2620-2 (2003)



- [195] R. Varga, A. Zhukov, J. M. Blanco, J. Gonzalez, V. Zhukova, P. Vojtanik. *Stress dependence of the domain wall potential in amorphous CoFeSiB glass-coated microwires*. Phys. B, 372 230–233 (2006)
- [196] E. Komova, M. Varga, R. Varga, P. Vojtanik, J. Torrejon, M. Provencio, M. Vazquez. *Frequency dependence of the single domain wall switching field in glass-coated microwires*. J. Phys.: Condens. Matter, 19 236229:1-5 (2007)
- [197] A. Zhukov, M. Vázquez, J. Velázquez, C. Garcia, R. Valenzuela, B. Ponomarev, *Frequency dependence of coercivity in rapidly quenched amorphous materials*. J. Mat. Sci. Eng., A226-228 753-756 (1997)
- [198] C. García, V. Zhukova, J. Gonzalez, J. M. Blanco, A. Zhukov. *Effect of magnetic field frequency on coercivity behavior of nanocrystalline  $Fe_{79}Hf_7B_{12}Si_2$  glass-coated microwires*. Physica B, 403 286–288 (2008)
- [199] P. Klein, R. Varga, G. A. Badini-Confalonieri, M. Vazquez. *Study of the switching field in amorphous and nanocrystalline FeCoMoB microwire*. IEEE transactions on magnetics, 46 (2) 357-360 (2010)
- [200] R. C. Hall. *Single crystal anisotropy and magnetostriction constants of several ferromagnetic materials including alloys of NiFe, SiFe, AlFe, CoNi, and CoFe*. Journal of Applied Physics, 30 816-819 (1959)
- [201] A. Zhukov, J. M. Blanco, M. Ipatov, A. Chizhik, V. Zhukova. *Manipulation of domain wall dynamics in amorphous microwires through the magnetoelastic anisotropy*. Nanoscale Research Letters, 7 223:1-8 (2012)
- [202] A. Zhukov, E. Shuvaeva, S. Kaloshkin, M. Churyukanova, E. Kostitcyna, V. Sudarchikova, A. Talaat, M. Ipatov, V. Zhukova. *Influence of the defects on magnetic properties of glass-coated microwires*. Journal of Applied Physics, 115 (17) 17A305 (2014)
- [203] P. A. Ekstrom, A. Zhukov. *Spatial structure of the head-to-head propagating domain wall in glass-covered FeSiB microwire*. J. Phys. D: Appl. Phys., 43 205001 (2010)
- [204] P. Klein, R. Varga, G. Infante, M. Vázquez. *Ferromagnetic resonance study of FeCoMoB microwires during devitrification process*. J. Appl. Phys., 111 053920:1-7 (2012)
- [205] H. Kronmuller, M. Fähnle, M. Domann, H. Grimm, R. Grimm, B. Groger. *Magnetic properties of amorphous ferromagnetic alloys*. J. Magn. Magn. Mat., 13 53-70 (1979)

- [206] H. Kronmuller. *Micromagnetism and microstructure of amorphous alloy*. J. Appl. Phys., 52 1859-1864 (1981)
- [207] A. Zhukov, J. M. Blanco, M. Ipatov, V. Zhukova. *Fast magnetization switching in thin wires: Magnetoelastic and defects contributions*. Sensor Letters, 11 (1) 170-176 (2013)
- [208] M. Ipatov, V. Zhukova, A. Zhukov, J. Gonzalez, A. Zvezdin. *Low-field hysteresis in the magnetoimpedance of amorphous microwires*. Phys. Rev. B., 81 134421:1-8 (2010)
- [209] A. Zhukov, A. Chizhik, M. Ipatov, A. Talaat, J. M. Blanco, A. Stupakiewicz, V. Zhukova. *Giant magnetoimpedance effect and domain wall dynamics in Co-rich amorphous microwires*. Journal of Applied Physics, 117 (4) 043904: 1-7 (2015)
- [210] C. J. Busch. *Einfluss heftiger Erysipeln auf organisierte Neubildungen*. In: Andra, C. J. (Ed.): Verhandlungen Des Naturhistorischen Vereins Der Preussischen Rheinlande und Westphalens (Bonn: Max Cohen und Sohn) 28–33 (1866)
- [211] M. H. Falk, R. D. Issels. *Hyperthermia in oncology*. Int. J. Hyperthermia, 17 (1) 1–18 (2001)
- [212] P. Wust, B. Hildebrandt, G. Sreenivasa, B. Rau, J. Gellermann, H. Riess, R. Felix, P. M. Schlag. *Hyperthermia in combined treatment of cancer*. Lancet Oncol., 3 (8) 487–97 (2002)
- [213] P. Vaupel, F. Kallinowski. *Physiological effects of hyperthermia*. In: hyperthermia and the therapy of malignant tumors, edited by C. Streffer (Springer, Berlin) (1987)
- [214] R. Hergt, W. Andra. *Magnetic hyperthermia and thermoablation*. In magnetism in medicine second edition ed. by W. Andra, H. Nowak WILEY-VCH Verlag GmbH & Co. KGaA, Weinheim, 550-570 (2007)
- [215] D. Ortega, Q. Pankhurst. *Magnetic hyperthermia*. In Nanoscience: volume 1: Nanostructures through Chemistry, Cambridge, Royal Society of Chemistry, 60-88 (2013)
- [216] R. K. Gilchrist, R. Medal, W. D. Shorey, R. C. Hanselman, J. C. Parrott, C. B. Taylor. *Selective inductive heating of lymph nodes*. Ann Surgy, 146 596-606 (1957)
- [217] M. Johannsen, B. Thiesen, P. Wust, A. Jordan. *Magnetic nanoparticle hyperthermia for prostate cancer*. Int. J. Hyperthermia, 26 790–5 (2010)
- [218] C. Binns. *Magnetic nanoparticle hyperthermia treatment of tumours*. In: Nanostructured Materials for Magnetoelectronics, Berlin, Springer-Verlag, 197-215 (2013)



- [219] R. Hergt, S. Dutz, R. Muller, M. Zeisberger. *Magnetic particle hyperthermia: nanoparticle magnetism and materials development for cancer therapy*. J. Phys.: Condens. Matter 18, S2919 (2006)
- [220] M. A. Dobrovolskaia, S. E. McNeil. *Immunological properties of engineered nanomaterials*. Nature Nanotechnology, 2 469-478 (2007)
- [221] T. Neuberger, B. Schopf, H. Hofmann, M. Hofmann, B. Von Rechenberg. *Superparamagnetic nanoparticles for biomedical applications: possibilities and limitations of a new drug delivery system*. Journal of Magnetism and Magnetic Materials, 293(1) 483-496 (2005)
- [222] A. K. Gupta, M. Gupta. *Synthesis and surface engineering of iron oxide nanoparticles for biomedical applications*. Biomaterials, 26 (18) 3995-4021 (2005)
- [223] H. S. Huang, J. F. Hainfeld. *Intravenous magnetic nanoparticle cancer hyperthermia*. Int. J. Nanomedicine, 8 2521–2532 (2013)
- [224] VI. Shubayev, TR. Pisanic, S. Jin. *Magnetic nanoparticles for theragnostics*. Adv Drug Deliver Rev, 61 467–477 (2009)
- [225] K. Sato, Y. Watanabe, A. Horiuchi, S. Yukumi, T. Doi, M. Yoshida, Y. Yamamoto, T. Maehara, T. Naohara, K. Kawachi. *Novel tumor-ablation device for liver tumors utilizing heat energy generated under an alternating magnetic field*. J. Gastroenterol Hepatol, 23 1105–11 (2008)
- [226] R. Zuchini, H. W. Tsai, C. Y. Chen, C. H. Huang, S. C. Huang, G. B. Lee, C. F. Huang, X. Z. Lin. *Electromagnetic thermotherapy using fine needles for hepatoma treatment*. Eur J Surg Oncol, 37 (7) 604-10 (2011)
- [227] C. Martinez-Boubeta, K. Simeonidis, D. Serantes, I. Conde-Leborán, I. Kazakis, G. Stefanou, L. Peña, R. Galceran, L. Balcells, C. Monty, D. Baldomir, M. Mitrakas, M. Angelakeris. *Adjustable hyperthermia response of self-assembled ferromagnetic Fe-MgO core-shell nanoparticles by tuning dipole-dipole interactions*. Adv. Funct. Mater., 22 3737–3744 (2012)
- [228] W. S. Lin, H. M. Lin, H. H. Chen, Y. K. Hwu, Y. J. Chiou. *Shape effects of iron nanowires on hyperthermia treatment*. J. Nanomaterials, 1–6 (2013)
- [229] J. Alonso, H. Khurshid, V. Sankar, Z. Nemat, M. H. Phan, E. Garayo, J. A. García, H. Srikanth. *FeCo nanowires with enhanced heating powers and controllable dimensions for magnetic hyperthermia*. Journal of Applied Physics, 117 17D113 (2015)

- [230] X. L. Liu, H. M. Fan, J. B. Yi, Y. Yang, E. S. G. Choo, J. M. Xue, D. D. Fana, J. Ding. *Optimization of surface coating on Fe<sub>3</sub>O<sub>4</sub> nanoparticles for high performance magnetic hyperthermia agents*. J. Mater. Chem., 22 8235-8244 (2012)
- [231] H. Khurshid, J. Alonso, Z. Nemati, M.-H. Phan, P. Mukherjee, M. L. Fdez-Gubieda, J. M. Barandiarán, H. Srikanth. *Anisotropy effects in magnetic hyperthermia: A comparison between spherical and cubic exchange-coupled FeO/Fe<sub>3</sub>O<sub>4</sub> nanoparticles*. J. Appl. Phys., 117 17A337 (2015)
- [232] C. Gómez-Polo, S. Larumbe, J. I. Pérez-Landazábal, J. M. Pastor. *Analysis of heating effects (magnetic hyperthermia) in FeCrSiBCuNb amorphous and nanocrystalline wires*. J. Appl. Phys., 111 07A314:1-3 (2012)
- [233] A. Chalkidou, K. Simeonidis, M. Angelakeris, T. Samaras, C. Martinez-Boubeta, L. Balcells, K. Papazisis, C. Dendrinou-Samara, O. Kalogirou. *In vitro application of Fe/MgO nanoparticles as magnetically mediated hyperthermia agents for cancer treatment*. Journal of Magnetism and Magnetic Materials, 323 775–780 (2011)
- [234] E. Natividad, M. Castro, A. Mediano. *Adiabatic magnetothermia makes possible the study of the temperature dependence of the heat dissipated by magnetic nanoparticles under alternating magnetic fields*. Appl. Phys. Lett. 98, 243119-1:3 (2011)
- [235] R. Hergt, W. Andra, C. G. d'Ambly, I. Hilger, W. A. Kaiser, U. Richter, H. Schmidt. *Physical limits of hyperthermia using magnetite fine particles*. IEEE transactions on magnetics, 34 (5) 3745-3754 (1998)
- [236] J. Carrey, B. Mehdaoui, M. Respaud. *Simple models for dynamic hysteresis loop calculations of magnetic single-domain nanoparticles: Application to magnetic hyperthermia optimization*. J. Appl. Phys., 109 083921 (2011)
- [237] E. Garaio, J. M. Collantes, F. Plazaola, J. A. Garcia, I. Castellanos-Rubio. *A multifrequency electromagnetic applicator with an integrated AC magnetometer for magnetic hyperthermia experiments*. Meas. Sci. Technol., 25 115702 (10pp) (2014)
- [238] A. Chizhik, A. Zhukov, J. M. Blanco, J. Gonzalez. *Surface and volume hysteresis loops of Fe-rich glass-coated microwires*. Journal of Non-crystalline solids, 287 374-379 (2001)
- [239] V. Rodionova, M. Ipatov, M. Ilyn, V. Zhukova, N. Perov, L. Panina, J. Gonzalez, A. Zhukov. *Magnetostatic interaction of glass-coated magnetic microwires*. J. Apply. Phys., 108 016103 (2010)

- 
- [240] H. Chiriac, S. Corodeanu, T. Óvári. *Dipolar interaction between amorphous microwires*. IEEE transactions on magnetics, 44 (4) 479-484 (2008)
- [241] A. Pereira, J. C. Denardin, J. Escrig. *How do magnetic microwires interact magnetostatically?*. J. Appl. Phys., 105 083903:1-4 (2009)

## Publications

### I. Publications not related to this dissertation

- [1] A. Talaat, M. Ipatov, V Zhukova, A. P. Zhukov, J. González, L. González-Legarreta, V. M. Prida, B. Hernando. *High frequency magnetoimpedance response of stress annealed  $Co_{66.3}Fe_{3.7}Si_{12.0}B_{18.0}$  amorphous alloy ribbons*. Journal of Applied Physics, 114 (2) 023904 (2013)
- [2] S. Kaloshkin, A. Talaat, M. Ipatov, V. Zhukova, J. M. Blanco, M. Churyukanova, K. Chichay, A. Zhukov. *Correlation between the magnetostriction constant and thermal properties of soft magnetic microwires*. physica status solidi (a), 211 (5) 1083-1086 (2014)
- [3] V. Zhukova, A. Talaat, J. J. del Val, M. Ipatov, J. Gonzalez, A. Zhukov. *Preparation and characterization of Fe-Pt and Fe-Pt-M (M=B, Si) microwires*. IEEE Magnetics Letters, 2015. Accepted DOI: 10.1109/LMAG.2015.2506549
- [4] V. Zhukova, M. Ipatov, A. Talaat, A. Zhukov. *Hopkinson effect in Co-rich glass-coated microwires*. physica status solidi (c), 11 (5-6) 1130-1132 (2014)
- [5] K. Chichay, V. Zhukova, V. Rodionova, M. Ipatov, A. Talaat, J. M. Blanco, J. Gonzalez, A. Zhukov. *Tailoring of domain wall dynamics in amorphous microwires by annealing*. Journal of Applied Physics, 113 (17) 17A318 (2013)
- [6] A. Zhukov, M. Churyukanova, S. Kaloshkin, V. Semenkova, S. Gudoshnikov, M. Ipatov, A. Talaat, J. M. Blanco, V. Zhukova. *Effect of annealing on magnetic properties and magnetostriction coefficient of Fe-Ni-based amorphous microwires*. Journal of Alloys and Compounds, 651 718-723 (2015)
- [7] A. Zhukov, E. Kostitcyna, E. Shuvaeva, S. Kaloshkin, M. Churyukanova, V. Sudarchikova, A. Talaat, V. Zhukova. *Effect of composite origin on magnetic properties of glass-coated microwires*. Intermetallics, 44 88-93 (2014)
- [8] A. Zhukov, E. Shuvaeva, S. Kaloshkin, M. Churyukanova, E. Kostitcyna, V. Sudarchikova, A. Talaat, M. Ipatov, V. Zhukova. *Influence of the defects on magnetic properties of glass-coated microwires*. Journal of Applied Physics, 115 (17) 17A305 (2014)

### II. Book chapters

- [1] A. Zhukov, A. Talaat, M. Ipatov, J. J. del Val, L. Gonzalez-Legarreta, B. Hernando, V. Zhukova "Giant Magnetoimpedance Effect of Amorphous and Nanocrystalline Glass-Coated Microwires" Book: Next Generation Sensors and Systems Vol. 16 pp 103-130 DOI: 10.1007/978-3-319-21671-3\_5 (2016)
- [2] L. González-Legarreta, A. Talaat, M. Ipatov, V. Zhukova, A. Zhukov, J. González, B. Hernando "Magnetotransport at High Frequency of Soft Magnetic Amorphous Ribbons" Book: Sensing Technology: Current Status and Future Trends IV Vol. 12 Chapter 12 pp 235-251(2015)
- [3] A. Zhukov, M. Ipatov, A. Talaat, J. M. Blanco, V. Zhukova "Tailoring of Magnetic Properties and GMI Effect of Amorphous Microwires by Annealing" Book: Sensing Technology: Current Status and Future Trends III Vol. 11 Chapter 20 pp 399-423 (2015)

### III. Conference proceeding

- [1] A. Talaat, V. Zhukova, M. Ipatov, J. M. Blanco, P. Klein, R. Varga, L. Gonzalez-Legarreta, B. Hernando A. Zhukov "Magnetic properties of nanocrystalline microwires" Energy

technology (2015) carbon dioxide management and other technologies, TMS (The minerals, metals & materials society 2015), Ch. 31 pp 283-289

[2] **A. Talaat**, V. Zhukova, M. Ipatov, L. Gonzalez-Legarreta, B. Hernando, A. Zhukov "Effect of nanocrystallization on giant magnetoimpedance effect of microwires" Proceedings of the International Conference on Sensing Technology, 2013, ICST pp 922-926, ISBN: 978-1-4673-5221-5, doi: 10.1109/ICSensT.2013.6727784

[3] **A. Talaat**, V. Zhukova, M. Ipatov, J. M. Blanco, A. Zhukov "Effect of annealing on magnetic properties and giant magnetoimpedance effect of amorphous microwires" Proceedings of the International Conference on Sensing Technology, 2013, ICST pp 916-921, ISBN: 978-1-4673-5221-5, doi: 10.1109/ICSensT.2013.6727783

[4] **A. Talaat**, M. Ipatov, V. Zhukova, J. Gonzalez, L. Gonzalez-Legarreta, V. M. Prida, B. Hernando, A. Zhukov "Soft magnetic amorphous ribbons with high frequency magnetoimpedance for sensors" Proceedings of the International Conference on Sensing Technology, 2013, ICST pp 927-932, ISBN: 978-1-4673-5221-5, doi: 10.1109/ICSensT.2013.6727785

[5] **A. Talaat**, V. Zhukova, M. Ipatov, J. M. Blanco, M. Churyukanova, S. Kaloshkin, E. Kostitcyna, A. Zhukov "Giant magnetoimpedance effect in nanocrystalline microwires" Progress in Electromagnetics Research Symposium, PIERS 2013, pp 1246-1249

[6] A. Zhukov, **A. Talaat**, M. Ipatov, V. Zhukova "High frequency giant magnetoimpedance effect of amorphous microwires for magnetic sensors applications" Proceeding of the 8th International Conference on Sensing Technology, 2014, ICST pp 624-629

[7] V. Zhukova, **A. Talaat**, M. Ipatov, J. M. Blanco, M. Churyukanova, S. Kaloshkin, E. Kostitcyna, E. Shuvaeva, L. Gonzalez Legarreta, B. Hernando, A. Zhukov "Magnetic properties and giant magnetoimpedance effect in nanocrystalline microwires" TMS-2014-Annual meeting supplemental proceedings, TMS (The minerals, Metals & Materials Society), USA, ISBN: 978-1-118-88972-5, pp 793-798.

[8] V. Zhukova, **A. Talaat**, M. Ipatov, J. J. del Val, J. M. Blanco, L. Gonzalez-Legarreta, B. Hernando, A. Zhukov "Optimization of soft magnetic properties in nanocrystalline glass-coated microwires" Proceeding of the TMS Middle East - Mediterranean Materials Congress on Energy and Infrastructure Systems (MEMA 2015), ISBN: 978-1-119-06527-2, pp 157-164.

[9] A. Zhukov, M. Ipatov, **A. Talaat**, V. Zhukov "Design of magnetic properties of glass-coated microwires for magnetic sensors applications" 7th ECCOMAS Thematic Conference on Smart Structures and Materials SMART 2015.

[10] A. Zhukov, M. Ipatov, **A. Talaat**, J. M. Blanco, V. Zhukova "Tailoring of magnetic properties and GMI effect in thin amorphous wires" TMS-2014-Annual meeting supplemental proceedings, TMS (The minerals, Metals & Materials Society), USA, ISBN: 978-1-118-88972-5, pp 785-792.

[11] V. Zhukova, E. Shuvaeva, E. Kostytsyna, M. Churyukanova, S. Kaloshkin, **A. Talaat**, M. Ipatov, A. Zhukov "Influence of the inhomogeneities on magnetic properties of glass-coated microwires" 7th ECCOMAS Thematic Conference on Smart Structures and Materials SMART 2015.

[12] A. Zhukov, M. Churyukanova, V. Sudarchikova, S. Gudoshnikov, M. Ipatov, **A. Talaat**, J. M. Blanco, V. Zhukova "Magnetostriction of Co-Fe-based amorphous soft magnetic microwires" Energy technology (2015) carbon dioxide management and other technologies, TMS (The minerals, metals & materials society 2015), Ch. 29 pp 265-271

#### IV. Conference participation

##### 2015:

- (1-4 September) Donostia international workshop on Energy, Materials, and Nanotechnology (DINEMN), San Sebastian, Spain.

**Oral talk:** A. Talaat, J. Alonso, V. Zhukova, A. Zhukov, M. H. Phan "Exploiting the inductive heating properties of Fe-based glass-coated microwires for advanced magnetic hyperthermia".

**Poster presentation:** A. Talaat, J. J. del Val, P. Klein, M. Ipatov, V. Zhukova, R. Varga, J. Gonzalez, A. Zhukov "Microstructural impact on the magnetization process of Hitperm glass-coated microwires"

- (1-3 July) 7<sup>th</sup> International workshop on magnetic wires (IWMW), Ordizia, Spain.

**Oral talk:** A. Talaat, J. J. del Val, P. Klein, M. Ipatov, V. Zhukova, R. Varga, A. Zhukov "Effect of nanocrystallization on structural and magnetic properties of Hitperm-type glass-coated microwires".

**Poster presentation:** A. Talaat, S. Gudoshnikov, J. M. Blanco, M. Ipatov, V. Zhukova, A. Zhukov "Comparative magnetic studies of amorphous glass-coated microwires manipulated by annealing".

##### 2014:

- (4-8 May) IEEE International Magnetics Conference (Intermag Europe), Dresden, Germany.

**Poster presentation:** A. Talaat, J. M. Blanco, M. Ipatov, V. Zhukova, A. Zhukov "Domain wall propagation in amorphous Co-based glass-coated microwires: Effect of stress annealing and tensile applied stresses".

##### 2013:

- (22-25 September) Recent advances in nanoscience and nanotechnology conference (NANOSMAT), Granada, Spain.

**Poster presentation:** A. Talaat, M. Ipatov, V. Zhukov, J. M. Blanco, M. Churyukanova, S. Kaloshkin L.Gonzalez-Legarreta, B. Hernando, J. J. del Val, A. Zhukov "Magnetic properties of amorphous and devitrified Finemet glass-coated microwires".

- (9-13 September) Donostia International Conference on Nanoscaled Magnetism and Applications (DICNMA), San Sebastian, Spain.

**Poster presentation:** A. Talaat, M. Ipatov, V. Zhukova, J. M. Blanco, A. Zhukov "Off-diagonal magneto impedance in Co-Fe rich amorphous microwires".

**Poster presentation:** A. Talaat, M. Ipatov, V. Zhukova, J. M. Blanco, M. Churyukanova, S. Kaloshkin, A. Zhukov "Giant magneto-impedance in thin Finemet nanocrystalline microwires".

**Poster presentation:** V. Zhukova, M. Ipatov, A. Talaat, A. Zhukov "Hopkinson effect in Co-rich glass-coated microwires".

- (6-10 May) Spring workshop school entitled "Spring school on Magnetic Materials and Application, held in the Basque center of materials, applications and nanostructures, Bilbao, Spain.

### **V. Scholar fellowships**

**2015:** (March 1<sup>st</sup>-June 1<sup>st</sup>) Spanish fellowship for three-month stay realized at Functional Materials Laboratory (FML), Department of Physics, University of South Florida, Tampa, Florida, USA.

**2014:** (March 1<sup>st</sup>-June 1<sup>st</sup>) Spanish fellowship for three-month stay realized at ferromagnetism laboratory, Institute of Physics, Faculty of Science, University of Pavol Jozef Safarik-UPJS, Kosice, Slovakia.

## Resumen

Esta tesis doctoral se ha dedicado a los modernos avances en los estudios de microhilos con recubrimiento de capa vítrea que representen una clase especial de vidrios metálicos. Estos microhilos magnéticos proporcionan un amplio campo para estudios fundamentales de muchos fenómenos físicos, que no serían fáciles de estudiar en otro tipo de materiales magnéticos convencionales. Sus propiedades magnéticas junto con su pequeño diámetro, los hacen candidatos muy prometedores para nuevas aplicaciones.

Los microhilos con recubrimiento de capa vítrea, fabricados mediante la técnica modificada de Taylor-Ulitovsky basada en un enfriamiento rápido de la aleación fundida, se definen como un material compuesto de un núcleo metálico cubierto por una capa de vidrio. Una de las características más atractivas de estos microhilos es la técnica de fabricación. Esta técnica consiste en la obtención por solidificación ultrarrápida de un microhilo compuesto simultáneamente de un núcleo ferro-magnético metálico de la aleación fundida recubierto con una capa vítrea mediante un enfriamiento ultrarrápido desde el estado fundido. Por lo tanto, las diferencias entre los coeficientes de dilatación térmica del núcleo metálico y del vidrio dan como resultado la aparición de grandes tensiones internas, lo cual influye en las características magnéticas de estos materiales. Por otro lado, debido a la ausencia de anisotropía magnetocristalina, las propiedades magnéticas de un microhilo totalmente amorfo se determinan predominantemente por la energía magnetoelástica determinada por la magnetización espontánea (momentos magnéticos locales) y las tensiones internas. En consecuencia, la atención principal para controlar las propiedades magnéticas de los microhilos se orienta a su anisotropía magnetoelástica,  $K_{me}$ . A este respecto, las principales posibilidades para modificar las propiedades magnéticas de microhilos amorfos son a través de la manipulación entre las tensiones internas y la selección adecuada de la composición química del núcleo metálico (controlar la magnetostricción).

Por lo tanto, modificando el espesor del vidrio, se podría controlar las tensiones internas, y correspondientemente, las características magnéticas variarían en función de la relación entre los diámetros del núcleo y de la capa vítrea del microhilo. De forma paralela, dependiendo de la composición de la aleación química el valor de la magnetostricción varía, y por lo tanto, se abren



líneas de investigaciones para sintonizar las respuestas magnéticas o las propiedades estructurales de microhilos que tienen las mismas dimensiones pero con diferentes composiciones químicas.

Esta tesis doctoral estudia las novedosas características de los microhilos magnéticamente blandos desde el punto de vista de tres perspectivas: (i) controlar los valores de la tensión interna a través de la modificación del diámetro del núcleo metálico y/o el espesor de la capa vítrea. (ii) obtener un estado nanocristalino de dos fases: una de pequeños cristales de tamaño nano incrustadas en una matriz amorfa. (iii) el control de las condiciones del tratamiento térmico antes de la formación de fases cristalinas, es decir, cuando se relajan las tensiones internas después del proceso de fabricación.

El desarrollo del trabajo realizado se divide en dos partes de 4 capítulos cada una. La primera parte, comienza con una introducción general y la historia de los vidrios metálicos hasta llegar a los microhilos. El capítulo 2 de la primera parte se exponen los parámetros que determinan el comportamiento magnético/estructural de los microhilos. A continuación, en los capítulos 3 y 4, se describe el interés tecnológico y las técnicas experimentales que han sido utilizadas para estudiar las propiedades de los microhilos magnéticos. Por último, en la segunda parte, se describen, los principales resultados que se han obtenido a lo largo de 4 capítulos.

## Parte II

### Capítulo 1

A lo largo del primer capítulo, hemos comprobado experimentalmente la correlación directa entre el efecto de nanocristalización y las propiedades magnéticas. Para ello, se ha realizado una investigación sistemática en tres composiciones de aleación de tipo FINEMET con diferentes diámetros de núcleo metálico o espesor del vidrio. Principalmente de nuestros estudios se ha logrado optimizar un campo coercitivo alrededor de  $10 \text{ A/m}$  correspondiente a un tamaño de grano ultrafino de  $11 \text{ nm}$  en muestras recocidas a  $T_{ann} = 550^\circ\text{C}$ . Además, hemos detectado un valor de 125% de GMI observado a  $f = 500 \text{ MHz}$  lo que supone una gran mejora respecto a la pobre respuesta de las muestras amorfas (as-cast) (1% de GMI).

El aumento del valor las tensiones internas está en conexión con la anisotropía magnetoelástica: un alto valor de la anisotropía, se corresponde con la  $\rho$ -proporción más baja. En consecuencia, el campo coercitivo de los microhilos, tanto sean muestras as-cast como recocidas, resulta de ser muy sensible a la relación- $\rho$ .

Por otro lado, se ha observado una diferencia significativa en el comportamiento magnético en los procesos de desvitrificación debido a la formación de pequeños cristales de fase  $\alpha$ -Fe-Si en la primera etapa de nanocrystalización ( $T_{ann} = 550^{\circ}\text{C}$ ) o por la precipitación de la fase Fe<sub>2</sub>B a altas temperaturas (más de  $650^{\circ}\text{C}$ ). También, hemos observado, que el control de la velocidad de enfriamiento rápido durante el proceso de fabricación afecta fuertemente a la estructura final de los microhilos producidos. Consecuentemente, una estructura nanocrystalina de aproximadamente  $12\text{ nm}$  de tamaño grano con una fase  $\alpha$ -Fe-Si y un campo coercitivo de  $12\text{ A/m}$  se han obtenido a partir del tratamiento de muestras as-cast lo que ha dado lugar a un considerable aumento del valor de GMI de hasta 50%. Además, se produce un cambio drástico en los coeficientes de la magnetostricción después de la nanocrystalización: los valores de magnetostricción cambian de positivas a casi nulas. Estos resultados hacen de estos microhilos unos buenos candidatos para aplicaciones basadas en el efecto GMI.

## Capítulo 2

El capítulo 2 incluye la investigación magnética y estructural de nuevos microhilos de aleación de tipo HITPERM y el efecto de añadir 1% de Cu. El análisis estructural de las muestras as-cast resulta muestra la presencia de una estructura nanocrystalina que consiste en granos de aproximadamente  $23\text{ nm}$  de la fase BCC  $\alpha$ -FeCo B2 ordenada y una fase amorfa, obtenidos directamente sin tratamientos térmicos. Se ha observado un comportamiento bastante anómalo tras el tratamiento térmico: el tamaño de grano bajó hasta  $11\text{ nm}$  en lugar de subir. Hemos explicado este comportamiento teniendo en cuenta el crecimiento cristalino limitado por la composición química. Además, después del recocido podría consistir en un proceso de nucleación múltiple con la formación pequeños granos. Esta misma masiva nucleación de pequeños granos dio como resultado una disminución del tamaño de grano promedio calculado después del recocido. La presencia de dos fases estructurales ha sido confirmado por la dependencia de la imanación  $M(T)$  con la temperatura, donde se observó una disminución

notable de la imanación al aumentar la temperatura lo que indica la existencia de dos temperaturas de Curie, una de la fase amorfa y otra de la fase nanocristalina.

Los ciclos de histéresis de todas las muestras presentan forma rectangular, tanto as-cast como recocidas, lo que nos permitió investigar los procesos de inversión de la magnetización y la dinámica de la pared de dominio. Un cambio drástico de las propiedades magnéticas: cambio de la dinámica de la pared, y de la dependencia de la frecuencia del campo switching se han observado después del recocido. Los cambios observados en las propiedades magnéticas se han justificado teniendo en cuenta la relajación estructural de dichos granos con magnetostricción alta positiva. Unas velocidades bastante rápidas de la pared magnética han sido observadas en muestras as-cast alcanzando valores tan rápidos como  $1.2 \text{ Km/s}$ . Además, la disminución de la anisotropía magnetoelástica después del recocido junto con la relajación de la tensión interna dio como resultado una mejorara de la velocidad de la pared así como de su movilidad. El desarrollo de las propiedades magnéticas de los microhilos de tipo HITPERM puede servir para aplicaciones tecnológicas en las que se requieren procesos de magnetización rápida.

### Capítulo 3

El capítulo 3 se ha demostrado, experimentalmente, que las propiedades magnéticas de los microhilos amorfos ricos en Co, pueden ser modificadas después del tratamiento térmico adecuado. Recocidos convencionales, sin tensión y con tensión, han afectado considerablemente a los ciclos de histéresis, al efecto GMI, y a la dinámica de la pared magnética. Todas las dependencias observadas han sido justificadas considerando la relajación de las tensiones internas y el cambio de la magnetostricción después del tratamiento. Además, en ciertas condiciones de recocido observamos coexistencia de efecto GMI y rápida propagación de la pared en la misma muestra recocida. Por otra parte, después del recocido, para ciertas condiciones, se observó un aumento de la velocidad de pared al aplicar una tensión externa.

### Capítulo 4

Por primera vez, se ha llevado a cabo un estudio sistemático de la eficiencia de los microhilos amorfos ricos en Fe para terapia de hipertermia magnética. Hemos aportado notables ideas para desarrollar el potencial de estos microhilos en las previsible tendencias en aplicaciones de hipertermia. Concretamente, hemos demostrado respuestas de calentamiento

apreciables en el que el intervalo terapéutico (40-45°C) para el tratamiento del cáncer se puede alcanzar fácilmente a los pocos minutos de calentamiento.

Hemos encontrado que estos microhilos presentan una alta eficiencia de calentamiento cuando se exponen a un campo magnético alterno. Solamente un trozo de 5 mm de longitud es capaz de alcanzar un valor de SAR considerablemente elevado de hasta 553 W/g, gracias a su ciclo de histéresis rectangular y a su característica estructura de dominios magnéticos. La interacción entre dos microhilos da lugar a un mejor calentamiento, alcanzándose valores de SAR de hasta 950 W/g. Además, hemos encontrado una fuerte correlación entre el número de microhilos y la eficiencia de calentamiento de las muestras estudiadas. A este respecto, hemos observado que reduciendo la separación entre microhilos mejora significativamente los valores de SAR debido a la interacción magnetostática entre los mismos. También, hemos analizado el efecto de la alineación del microhilo con respecto a la dirección del campo magnético aplicado. En estas ocasiones, hemos determinado que la orientación paralela a la dirección del campo magnético es la mejor disposición para aumentar el valor de SAR.

Por otro lado, el calentamiento total generado por los microhilos estudiados, ha demostrado un proceso adiabático donde no ocurrió ninguna transferencia de calor entre el sistema empleado y su entorno, lo que confirma que los microhilos a base de Fe son muy eficientes en la transferencia de calor de forma homogénea. Además, la capa vítrea se puede considerar como una barrera aislante, y por lo tanto, mejora la compatibilidad de esta familia de materiales para aplicaciones biomédicas. A tenor de estos resultados, podemos afirmar que nuestro estudio pone de relieve la importancia de investigar nuevos materiales para tratamientos de hipertermia magnética.

## Acknowledgments

First, I would like to declare that much of the materials presented here have appeared elsewhere. The idea, selection, search, arrangement, and presentation all are, for better or worse, my own. I apologize to those whose important contributions to these scientific approaches, along years, have been overlooked herein because of my own unfamiliarity with them or my insufficient ability to appreciate their significance.

So many inputs from numerous friends and colleagues, through direct or indirect help, have inspired me to carry on this track. I would like to begin by thanking my dissertation advisors, the two Zhukovs: Arcady and Valentina who tirelessly worked on improving the quality of this research and shared with me the riches of their magnetic experiences. I deeply appreciate their generous support and the time they have dedicated to improve the treatment of various aspects and search out errors. Many sincere thanks go to the three J of our group: Julian Gonzalez, Juan Jose del Val, and Juan Maria Blanco for their enormous help and mostly for their friendship shared with me along 4 years. This friendship would be incomplete without mentioning Blanca Hernando and Oviedo's group. Sincere heartfelt thanks for all of them for their kindness and emotional support.

I am truly grateful for valuable experiences I acquired through two research visits one in Kosice, and another in Tampa. Namely would like to thank Rastislav Varga for hosting me in his group and his guidance during my stay in Slovakia. In Tampa, I have been privileged and was extremely fortunate to work with Manh-Huong Phan, the formidable young scientist who taught me how to handle experimental results and how to write up more fancy manuscripts rather than traditional ones. He has also applied his own professional writing skills to editing my drafts, helping out to remove my awkward and incorrect constrictions.

There are also many debts of gratitude owed to great many individuals. Particular gratitude goes to coworkers and postdocs I dealt with. Thanks to Mihail Ipatov, Peter Klein for their comfortable silence, and most notably to Javier Alonso who helped me to learn various experimental aspects and Origin's-program secrets. There are however so many names to acknowledge, most of them actually are high caliber individuals and expect to make a very brilliant scientific future. Thank you so much all.

Finally, I would like to dedicate this dissertation to Veronika, Soraya, and Talaat, who cared and shared much of their time for too many days, nights, and weekends. Their love and encouragement made it easier to persevere when the task grew bigger than I ever would have imagined.



Ahmed Talaat

Fall 2015